# Elucidating the cellular and molecular mechanisms that govern filovirus pathogenesis within ferrets with emphasis on Marburg virus

By: Zachary Schiffman

A thesis submitted to the Faculty of Graduate Studies of The University of Manitoba in partial fulfillment of the requirements of the degree of

DOCTOR OF PHILOSOPHY

Department of Medical Microbiology and Infectious Diseases
University of Manitoba
Winnipeg

Copyright © 2024 by Zachary Schiffman

# DEDICATION

This thesis is dedicated to my parents, Barry and Grazia Schiffman. Mom and Dad, you always supported me through every endeavour. No matter what I wanted to pursue in life, you always supported me without question. Even when following my dreams meant moving away from home and being far away from family. Your constant visits over the years gave me a much-needed recharge to allow me to push through and finish up my grad studies. I couldn't have done it without you!

# ACKNOWLEDGEMENTS

I would like to express my sincere gratitude to my Ph.D supervisor, Dr. Jim Strong, for his endless support throughout my graduate studies. Jim, you took me into your lab during a challenging time during my graduate studies, and it made me feel as if I were part of our little lab family. You have shared valuable wisdom with me throughout the years and taught me many valuable lessons that I will carry with me for the remainder of my career.

I would also like to express my sincere gratitude to Dr. Logan Banadyga. You have been an influential mentor to me since the day I started my graduate studies. I still remember constantly bugging you during my first couple of weeks because our desks were side by side in the library, and you never once got annoyed. Even today, you still allow me to bug you with endless science questions. I attribute most of my success as a scientist to you and your endless dedication to teaching me and helping me improve every step of the way.

To Kaylie Doan, my mom away from home. No matter what hardships I was faced with, you always encouraged me and helped me see the brighter side of things. There were many situations where I was discouraged, but you always helped me get through each and every one. You taught me many valuable skills throughout my degree that I will carry for the rest of my career, whether training me in CL4 or teaching me "Kaylie tricks" that would save me tons of time. To Lauren Garnett, my sister away from home. You helped me much throughout my graduate studies, whether helping me with my unnecessarily large growth kinetics studies or endless $TCID_{50}$ reads in CL4. You were always willing to help me and never asked for anything in return. I will miss your constant reminders that you are a few months younger than me and that I will turn 30 first. Kaylie and Lauren, I couldn't have done it without you, and I will never forget everything you've done for me.

To my committee members, Drs. Xiao-Jian Yao, Jason Kindrachuck, and Sam Kung thank you for always showing interest in me and my project. Your support and suggestions throughout the years allowed me to grow as a scientist and helped keep me on track throughout my degree. Special thanks to Mrs. Angela Nelson within the Department of Medical Microbiology and Infectious Diseases. Since the day I joined the program, you were always very kind to me and helped me with any program-related questions I may have had. You made going through graduate studies much easier for me.

To everyone within the Special Pathogens Program at the National Microbiology Laboratory. Throughout the years, many of you have played an instrumental role in my degree. Notable thanks to Dr. Jonathan Audet, who taught me everything I know about sequencing, and Anders Leung, who helped train me for CL4 and shared insight on many aspects of my project.

Finally, a shout-out to my dog Apollo. I couldn't have written my thesis without the endless echoes of your snoring in the background.

# ABSTRACT

Recently, the ferret has gained attention as a novel animal model for studying filoviruses. Ferrets are highly susceptible to several orthoebolaviruses, including Ebola virus (EBOV), yet refractory to infection with orthomarburgviruses, namely Marburg virus (MARV) and Ravn virus. The fact that ferrets are uniformly susceptible to infection with most orthoebolaviruses but not orthomarburgviruses suggests that these viruses differ fundamentally in their pathogenic mechanisms.

This thesis explored two main hypotheses. Firstly, it was hypothesized that this lack of susceptibility by ferrets to lethal infection with orthomarburgviruses resulted from a block in glycoprotein (GP) mediated viral entry. The results demonstrate that while MARV-GP can mediate entry into ferret cells, the efficiency is lower than that of EBOV-GP, particularly during the early stages of infection. While MARV can replicate within ferret cells, replication is attenuated compared to EBOV. Lastly, rEBOV-mGP is uniformly lethal in ferrets. However, the onset of disease and viremia was delayed compared to EBOV. These data demonstrate that GP may represent one probable factor accounting for the lack of disease among MARV-challenged ferrets.

Secondly, it was hypothesized that this lack of susceptibility by ferrets to lethal infection with orthomarburgviruses but not orthoebolaviruses is the result of mechanistic differences in the innate immune evasion tactics of these two viruses. The results demonstrated that inhibition of type I IFN production using drugs has a negligible impact on the replication of MARV within ferret cells. In contrast, inhibition of type I IFN signalling using drugs targeting the JAK/STAT pathway positively enhanced viral replication of MARV within ferret cells. Together, these data emphasize the potential contribution of MARV VP40 toward the viral replication of MARV within ferret cells. Challenge with guinea pig-adapted Marburg virus (GPA-MARV) resulted in uniform

lethality among ferrets, whereas challenge with mouse-adapted (MA)-MARV resulted in only partial lethality. High levels of viral replication, a dysregulated immune response and hematological perturbations in biochemistry and blood counts were also observed among GPA-MARV-challenged ferrets. Lastly, several genome mutations appeared following challenge with GPA-MARV. This is the first report of a lethal orthomarburgvirus ferret model, and these data provide insight into the pathogenesis of orthomarburgviruses.

# Table of Contents

DEDICATION ..... II

ACKNOWLEDGEMENTS ..... III

ABSTRACT ..... V

LIST OF TABLES ..... XI

LIST OF FIGURES ..... XII

LIST OF ABBREVIATIONS ..... XIV

AUTHOR CONTRIBUTIONS ..... XIX

1. CHAPTER 1: INTRODUCTION ..... 1

1.1. HISTORY OF FILOVIRUSES ..... 1

1.1.1. Discovery and Emergence ..... 1

1.1.2. Taxonomy of Filoviruses ..... 1

1.1.2.1. Mammalian hosts ..... 3

1.1.2.2. Piscine and reptilian hosts ..... 3

1.1.3. Historical Filovirus Outbreaks ..... 4

1.1.3.1. Orthomarburgviruses ..... 4

1.1.3.2. Orthoebolaviruses ..... 6

1.1.4. Ecology and geographical distribution of filoviruses ..... 9

1.2. FILOVIRUS BIOLOGY ..... 12

1.2.1. Virion Structure ..... 12

1.2.2. Genome Organization ..... 13

1.2.3. Genome Expression Products ..... 15

1.2.4. GP Expression Products ..... 17

1.3. FILOVIRUS LIFE CYCLE ..... 19

1.3.1. Attachment and Entry ..... 19

1.3.2. Genome Replication and Transcription ..... 22

1.3.3. Assembly and Budding ..... 23

1.4. FILOVIRUS PATHOGENESIS AND PATHOLOGY ..... 23

1.4.1. Transmission and Clinical Course of Disease ..... 24

1.4.2. Virus Dissemination, Cellular Tropism, and Pathophysiology ..... 26

1.4.3. The Role of Cytokines and Chemokines in Filovirus Pathogenesis ..... 27

1.5. IMMUNITY TO INFECTION AND EVASION TACTICS OF FILOVIRUSES ..... 30

1.5.1. Innate Immune Response ..... 31

1.5.2. Adaptive Immune Response ..... 33

1.6. Classical Animal Models ..... 35
1.6.1. Rodents ..... 35
1.6.1.1. Immunocompetent Mice (Mus musculus) ..... 35
1.6.1.2. Immunocompromised Mice (Mus musculus) ..... 42
1.6.1.3. Syrian Golden Hamsters (Mesocricetus auratus) ..... 43
1.6.1.4. Guinea Pigs (Cavia porcellus) ..... 48
1.6.2. Non-Human Primates ..... 53
1.7. The Domestic Ferret (Mustela putorius furo) ..... 58
1.7.1. The Ferret as A Model for Orthoebolaviruses ..... 59
1.7.2. The Ferret as A Model for Orthomarburgviruses ..... 65
1.7.3. Ferret and Countermeasure Evaluation ..... 67
1.7.3.1. Monoclonal Antibodies ..... 67
1.7.3.2. Vaccines ..... 71
1.8. Gaps in Knowledge ..... 72
1.9. Central Hypotheses and Aims ..... 73
1.9.1. Aim 1: Evaluate the influence of GP-mediated viral entry on the infectivity of ferret cell lines in vitro and viral pathogenesis in vivo ..... 73
1.9.2. Aim 2: Determine if inhibitors of the type I IFN response promote MARV replication in vitro within ferret cell lines ..... 73
1.9.3. Aim 3: Evaluate the pathogenicity of rodent-adapted filoviruses in vivo within ferrets ..... 74
2. CHAPTER 2. MATERIALS AND METHODS ..... 75
2.1. Development and Characterization of Immortalized Ferret Cell Lines ..... 75
2.1.1. Establishment of Primary Cell Culture ..... 75
2.1.2. Immortalization of Primary Ferret Cells ..... 76
2.1.3. Characterization of Immortalized Ferret Cell Lines By 10X Genomics ..... 76
2.2. Evaluation of GP-mediated Entry Using VSV Pseudotypes ..... 77
2.2.1. Cells and Viruses ..... 77
2.2.2. Infection of Immortalized Ferret Cells with VSV Pseudotypes ..... 77
2.3. Infection of Ferret Cell Lines with EBOV and MARV Viruses ..... 78
2.3.1. Cells and Viruses ..... 78
2.3.2. Next Generation Sequencing of Stock Viruses ..... 79
2.3.3. Growth Kinetics on Ferret Cell Lines ..... 80
2.3.4. Quantification of viral RNA by RT-qPCR ..... 80
2.3.5. Quantification of Infectious Virus by $TCID_{50}$ ..... 81
2.4. Infection of Ferrets with EBOV-mGP ..... 81
2.4.1. Viruses ..... 81
2.4.2. Rescue of Recombinant Chimeric EBOV-mGP ..... 81

2.4.3. Ethics Statement ..... 82
2.4.4. Animals ..... 82
2.4.5. Quantification of Viral RNA by RT-qPCR ..... 83
2.4.6. Quantification of Infectious Virus by $TCID_{50}$ ..... 83
2.5. In vitro Evaluation of Type I IFN Response Inhibitors on Filovirus Infected Ferret Cell Lines 84
2.5.1. Cells ..... 84
2.5.2. Viruses ..... 84
2.5.3. Growth Kinetics of Various Filoviruses on Ferret Cell Lines ..... 85
2.5.4. Drugs ..... 86
2.5.5. Ruxolitonib Pilot Study ..... 86
2.5.5.1. Immunofluorescence Assay and Plate Read ..... 86
2.5.6. Testing of Type I IFN Response Inhibitors on MARV Infected Ferret Cell Lines ..... 87
2.6. Evaluate the Pathogenicity of Rodent-Adapted Filoviruses In vivo Within Ferrets ..... 88
2.6.1. Viruses ..... 88
2.6.2. Ethics Statement ..... 88
2.6.3. Animals ..... 88
2.6.4. Hematology ..... 89
2.6.5. Quantification of viral RNA by RT-qPCR ..... 89
2.6.6. Quantification of Infectious Virus by $TCID_{50}$ ..... 90
2.6.7. Next-Generation Sequencing of RNA Extracted From Blood and Tissues ..... 90
2.6.8. 12-Plex Ferret Cytokine Luminex Assay ..... 90
2.7. Evaluate the Pathogenicity of Taï Forest Virus In vivo Within Ferrets ..... 91
2.7.1. Ethics Statement ..... 91
2.7.2. Viruses ..... 91
2.7.3. Animals ..... 91
2.7.4. Hematology ..... 92
2.7.5. Quantification of viral RNA by RT-qPCR ..... 92
2.7.6. Generation and Purification of TAFV GP ..... 92
2.7.7. Evaluation of Humoral Immune Response by ELISA ..... 93
2.7.8. Data Analysis ..... 94
3. CHAPTER 3: THE INABILITY OF MARBURG VIRUS TO CAUSE DISEASE IN FERRETS IS NOT SOLELY LINKED TO THE VIRUS GLYCOPROTEIN ..... 95
3.1. Background ..... 95
3.2. Results: Ferret spleen Cells Are Permissible to MARV GP-mediated Entry ..... 96
3.3. Results: MARV is Capable of Replicating in Ferret Cells ..... 97
3.4. Results: EBOV-mGP is Uniformly Lethal Among Infected Ferrets ..... 99

3.5. Discussion: Key Findings, Significance, and Limitations ..... 104

4. CHAPTER 4: INHIBITORS OF THE INTERFERON RESPONSE ENHANCE MARBURG VIRUS REPLICATION WITHIN FERRET CELL LINES TO VARYING DEGREES ..... 109

4.1. Background ..... 109
4.2. Results: Orthoebolaviruses Replicate Efficiently Within Ferret Cell Lines Whereas Replication of Orthomarburgviruses is Modest ..... 113
4.3. Results: Ruxolitinib Enhances Replication of EBOV-GFP ..... 120
4.4. Results: Inhibitors of Type I IFN Production Do Not Enhance Replication of MARV in Ferret Cells 123
4.5. Results: Select Inhibitors of Type I IFN Signaling Enhance Replication of MARV In Ferret Cells 126
4.6. Discussion: Key Findings, Significance, and Limitations ..... 133

5. CHAPTER 5: RODENT-ADAPTED ORTHOMARBURGVIRUSES ARE LETHAL IN FERRETS ..... 138

5.1. Background ..... 138
5.2. Results: GPA-MARV is Uniformly Lethal in Ferrets ..... 140
5.3. Results: GPA-MARV Infected Ferrets Support High Levels of Viral Replication ..... 143
5.4. Results: GPA-MARV Causes Deviations in Baseline Hematology Characteristic of FVD ... 147
5.5. Results: Infected Ferrets Demonstrate A Cytokine Storm Characteristic Of FVD ..... 153
5.6. Results: Several Mutations Reach Consensus Threshold Following Challenge With GPA-MARV 159
5.7. Discussion: Key Findings, Significance, and Limitations ..... 162

6. CHAPTER 6: FINAL DISCUSSION, CONCLUSIONS AND FUTURE DIRECTIONS ..... 168

6.1. Summary of Key Findings ..... 168
6.2. Concluding Remarks ..... 176

7. REFERENCES ..... 180

8. APPENDIX 1: TAÏ FOREST VIRUS DOES NOT CAUSE LETHAL DISEASE IN FERRETS ..... 210

8.1. Background ..... 210
8.2. Results: Ferrets Did Not Develop Lethal Disease Following TAFV Infection ..... 212
8.3. Results: Transient Viremia Early After Infection ..... 213
8.4. Results: No Major Perturbations in Hematology or biochemistry ..... 215
8.5. Results: High Titers of TAFV GP-Specific IgG Detectable as Early as 14 dpi ..... 217
8.6. Discussion: Key Findings, Significance, and Limitations ..... 218

9. APPENDIX 2: CHARACTERIZATION OF IMMORTALIZED FERRET CELL LINES BY 10X GENOMICS 223

# List of Tables

Table 1. Filoviridae Taxonomy ..... 2
Table 2. Historical outbreaks linked to orthomarburgviruses ..... 6
Table 3. Historical outbreaks linked to orthoebolaviruses ..... 8
Table 4. RT-qPCR Primer and Probe Sequences for VSV ..... 78
Table 5. RT-qPCR Primer and Probe Sequences for EBOV/MARV ..... 81
Table 6. Summary of consensus mutations present in blood and tissues of GPA-MARV challenged ferrets ..... 162
Table 7. Viral RNA load in blood of ferrets infected with TAFV ..... 214
Table 8.Viral RNA load in tissues of ferrets (tissues) infected with TAFV ..... 215

# List of Figures

Figure 1. Schematic representation of the filovirus virion ..... 13
Figure 2. Filovirus genome organization ..... 14
Figure 3. Filovirus life cycle ..... 21
Figure 4. Depiction of non-synonymous mutations in mouse-adapted (MA) filoviruses. ..... 39
Figure 5. Depiction of non-synonymous mutations in hamster-adapted Marburg virus ..... 46
Figure 6. Depiction of non-synonymous mutations in Guinea pig-adapted (GPA) filoviruses.... 50
Figure 7. Hallmarks of pathogenesis for different filoviruses in ferrets. ..... 62
Figure 8. Quantification of viral RNA in supernatant of cells inoculated with VSV pseudotypes. ..... 97
Figure 9. Replication kinetics of EBOV and MARV in ferret cell lines. ..... 98
Figure 10. Replication kinetics of EBOV-mGP and EBOV in ferret cell lines. ..... 100
Figure 11. Clinical parameters of infected ferrets. ..... 101
Figure 12. Viral RNA levels in blood, oral/rectal swabs and nasal washes of infected ferrets. . 102
Figure 13. Viral load in tissues of infected ferrets. ..... 103
Figure 14. Alignment of ferret and human NPC1 Domain C. ..... 105
Figure 15. Depiction of the Type I IFN production pathway and the targets of various drug inhibitors. ..... 110
Figure 16. Depiction of Type I, II and III IFN signaling via the JAK/STAT pathway and the targets of various drug inhibitors. ..... 111
Figure 17. Genome replication kinetics of orthomarburgviruses in ferret cell lines ..... 114
Figure 18. Infectious virus replication kinetics of Orthomarburgviruses on ferret cell lines ..... 116
Figure 19. Impact that washing cells post virus adsorption has on replication kinetics. ..... 117
Figure 20. Replication Kinetics of Orthoebolaviruses on ferret cell lines ..... 119
Figure 21. Treatment of mpfSpleen cells with ruxolitinib enhances replication of EBOV-GFP 121
Figure 22. Quantification of EBOV-GFP infected mpfSpleen cell populations in the presence of 2.5 μM ruxolitinib ..... 122
Figure 23.Quantification of MARV-ZsG infected mpfSpleen cell populations in the presence of ruxolitinib ..... 123
Figure 24. Impact of TPCA-1 treatment on replication of MARV in ferret cell lines ..... 125
Figure 25. Impact of BX795 treatment on replication of MARV in ferret cell lines ..... 126

Figure 26. Impact of ruxolitinib treatment on replication of MARV in ferret cell lines ..... 128
Figure 27. Impact of tofacitinib treatment on replication of MARV in ferret cell lines..... 130
Figure 28. Impact of AZD1480 treatment on replication of MARV in ferret cell lines..... 131
Figure 29. Impact of CYT-387 treatment on replication of MARV in ferret cell lines..... 133
Figure 30. Clinical parameters of ferrets inoculated with rodent-adapted filoviruses..... 141
Figure 31. Rash and gross pathology observed among ferrets infected with rodent-adapted filoviruses..... 142
Figure 32. Viral load in blood and tissues of ferrets infected with Guinea pig adapted filoviruses. ..... 144
Figure 33. Levels of viral RNA in oral, rectal and nasal swabs of ferrets infected with Guinea pig adapted filoviruses. ..... 146
Figure 34. Viral load in blood and tissues of ferrets infected with MA-MARV. ..... 147
Figure 35. Select biochemistries and blood counts of rodent adapted filovirus infected ferrets. 150
Figure 36. Serum biochemistry of ferrets challenged with rodent-adapted filoviruses. ..... 152
Figure 37. Hematology of ferrets challenged with rodent-adapted filoviruses. ..... 153
Figure 38. The cytokine/chemokine response in ferrets challenged with rodent-adapted filoviruses ..... 156
Figure 39. The cytokine/chemokine response in ferrets challenged with rodent-adapted filoviruses (Extended.)..... 158
Figure 40. Heatmap depicting mutations that meet consensus threshold in the blood of ferrets challenged with GPA-MARV..... 160
Figure 41. Mutations that meet consensus threshold within tissues. ..... 161
Figure 42.Clinical parameters of TAFV-infected ferrets..... 213
Figure 43.Biochemical parameters of TAFV-infected ferrets. ..... 216
Figure 44.Complete blood counts of TAFV-infected ferrets..... 217
Figure 45. Endpoint Titers of TAFV GP-specific IgG ..... 218
Figure 46. UMAP of immortalized ferret spleen cells (mpfSpleen)..... 224
Figure 47. UMAP of immortalized ferret heart cells (mpfHeart)..... 225
Figure 48. UMAP of immortalized ferret lung cells (mpfLung) ..... 226

# List of Abbreviations

| Abbreviation | Definition |
|---|---|
| ADCC | antibody-dependent cellular cytotoxicity |
| ALB | albumin |
| ALP | alkaline phosphatase |
| ALP | alkaline phosphatase |
| ALT | alanine transaminase |
| AMY | amylase |
| aPTT | activated partial thromboplastin time |
| ASGPRI | asialoglycoprotein receptor 1 |
| AST | aspartate transaminase |
| AXL | tyrosine-protein kinase receptor |
| BAT | Brown adipose tissue |
| BDBV | Bundibugyo virus |
| BOMV | Bomabali virus |
| BUN | blood urea nitrogen |
| BVD | Bundibugyo virus disease |
| $Ca^{2+}$ | calcium |
| CBC | complete blood counts |
| CFR | Case Fatality Rate |
| CL4 | Containment level 4 |
| CLRs | C-type lectin receptors |
| CMC | complement-mediated cytotoxicity |
| CNS | central nervous system |
| CR | Conserved region |
| CRE | creatinine |
| CSCHAH | Canadian Science Center for Human and Animal Health |
| DC-SIGN | dendritic cell-specific ICAM-3-grabbing non-integrin |
| DCs | dendritic cells |
| DIC | disseminated intravascular coagulation |
| DMEM | Dulbecco's Modified Eagle Medium |
| DPBS | Dulbecco's Phosphate Buffered Saline |
| dpi | days post-infection |
| dpi | days-post infection |
| DRC | Democratic Republic of Congo |
| dsRNA | double-stranded RNA |
| EBOD | Ebola disease |
| EBOV | Ebola virus |
| EVD | Ebola virus disease |
| EXT1 | exostosin 1 |
| FFU | focus forming units |
| FIWIV | Fiwi virus |
| FVD | Filovirus disease |
| FVIIa | factor VIIa |
| GE | gene end |

| Abbreviation | Definition |
|---|---|
| GGT | gamma-glutamyl transferase |
| GLOB | globulin |
| GLU | glucose |
| $GP_{1,2\Delta}$ | shed glycoprotein |
| GPA | Guinea Pig Adapted |
| GS | gene start |
| GWAT | gonadal white adipose tissue |
| HA | Hamster-adapted |
| HGB | hemoglobin |
| HI-FBS | heat inactivated fetal bovine serum |
| hMGL | human macrophage galactose- and acetylgalactosamine-specific C-type lectin |
| hpi | hours-post-infection |
| HPIV3 | human parainfluenza virus type 3 |
| Hr | hours |
| HUJV | Huángjiāo virus |
| IB | inclusion bodies |
| IFN | interferon |
| IFNAR | type I IFN receptor |
| $IFNAR^{-/-}$ | IFN-α/β receptor knockout mice |
| IFNα | interferon-alpha |
| IgG | immunoglobulin G |
| IID | IFN inhibitory domain |
| IKKε | IκB kinase-ε |
| IL | interleukin |
| IM | intramuscular |
| IN | Intranasal |
| IP | intraperitoneal |
| IP-10 | interferon gamma-induced protein 10 |
| IR | intergenic regions |
| IRF | IFN regulatory factor |
| ISGs | IFN-stimulated genes |
| ISRE | IFN-stimulated response elements |
| JAK | Janus kinase |
| $K^+$ | potassium |
| KNDV | Kander virus |
| KPNA | karyopherin alpha |
| L-SIGN | liver/lymph node-specific ICAM-3 grabbing non-integrin |
| $LD_{50}$ | median lethal dose |
| LLOV | Lloviu virus |
| LSECTin | lymph node sinusoidal endothelial cell C-type lectin |
| LYM | lymphocytes |
| MA | Mouse-Adapted |
| mAbs | monoclonal antibodies |
| MARD | Marburg disease |

| Abbreviation | Definition |
|---|---|
| MARV | Marburg virus |
| MCP-1 | monocyte chemoattractant protein-1 |
| MCP1 | monocyte chemoattractant protein 1 |
| MDA5 | melanoma differentiation associated gene 5 |
| MES | mesenteric white adipose tissue |
| MHC | major histocompatibility complex |
| MIP-1 | macrophage inflammatory protein-1 |
| MIP-1B | macrophage inflammatory protein-1 beta |
| MLAV | Měnglà virus |
| MODS | multiple organ dysfunction syndrome |
| MOI | multiplicity of infection |
| MON | Monocytes |
| *mpf* | *mustela putorius furo* |
| *mpf*Heart | immortalized ferret heart cells |
| *mpf*Lung | immortalized ferret lung cells |
| *mpf*Spleen | immortalized ferret spleen cells |
| MPV | mean platelet volume |
| mRNA | messenger RNA |
| MVD | Marburg virus disease |
| $Na^+$ | sodium |
| NAbs | neutralizing antibodies |
| NEU | Neutrophils |
| NGS | Next-Generation Sequencing |
| NHP | Non-human Primate |
| NK | natural killer |
| NO | nitric oxide |
| NP | nucleoprotein |
| NPC1 | Niemann-Pick C1 |
| OBLV | Oberland virus |
| ORF | open reading frames |
| Ova | ovaries |
| PAMPs | pathogen-associated molecular patterns |
| PBS | phosphate-buffered saline |
| PDW | platelet distribution width |
| PFU | plaque-forming units |
| PHAC | Public Health Agency of Canada |
| PHOS | phosphorous |
| PKR | protein kinase R |
| PLT | platelet |
| Pre-GP | precursor GP |
| Pre-sGP | precursor sGP |
| Pre-ssGP | precursor ssGP |
| PRR | pathogen by pattern recognition receptors |
| PT | prothrombin time |
| R.T | room temperature |

| Abbreviation | Definition |
|---|---|
| RANTES | regulated on activation, normal T cell expressed and secreted |
| RAVV | Ravn Virus |
| RBS | receptor-binding site |
| RdRP | RNA dependent RNA polymerase |
| RESTV | Reston virus |
| RIG-I | retinoic acid-inducible gene-I |
| RLR | RIG-I-like receptors |
| RNA | ribonucleic acid |
| RNA-dependent-RNA polymerase | RdRp (L) |
| RNP | ribonucleoprotein |
| ROS | reactive oxygen species |
| RWAT | retroperitoneal white adipose tissue |
| SARS | severe acute respiratory syndrome |
| SARS-CoV | severe acute respiratory syndrome coronavirus |
| SC | subcutaneous |
| SCID | severe combined immunodeficient |
| sGP | secreted glycoprotein |
| SHF | Simian hemorrhagic fever |
| ssGP | secondary secreted glycoprotein |
| STAT | signal transducers and activators of transcription |
| $STAT1^{-/-}$ | STAT-1 knockout mice |
| $STAT2^{-/-}$ | STAT2 knockout |
| SUBQ | subcutaneous white adipose tissue |
| SUDV | Sudan virus |
| SVD | Sudan virus disease |
| TAFV | Tai Forest virus |
| TAPV | Tapajós virus |
| TBIL | total bilirubin |
| TBK1 | TANK-binding kinase 1 |
| $TCID_{50}$ | median tissue culture infectious dose |
| Th | T helper |
| TIM-1 | T cell immunoglobulin mucin domain receptor-1 |
| TLR | toll-like receptors |
| TNF | tumour necrosis factor |
| TNFα | tumor necrosis factor alpha |
| TP | Total protein |
| tPA | tissue-type plasminogen activator antigen |
| TT | thrombin time |
| TTS | testes |
| TYK2 | tyrosine kinase 2 |
| uPA | urokinase-type plasminogen activator |
| UTMB | University of Texas Medical Branch |
| UTR | untranslated region |
| ULOQ | upper limit of quantification |

| Abbreviation | Definition |
|---|---|
| VP24 | nucleocapsid protein (VP24) |
| VP30 | polymerase cofactor (VP30) |
| VP35 | polymerase cofactor (VP35) |
| VP40 | matrix protein (VP40) |
| VSV | Vesicular stomatitis virus |
| WBC | white blood cells |
| XILV | Xīlǎng virus |

# AUTHOR CONTRIBUTIONS

1. Schiffman Z, Liu G, Cao W, et al. The Ferret as a Model for Filovirus Pathogenesis and Countermeasure Evaluation. ILAR Journal [Internet]. 2021 [cited 2021 Dec 5]; (ilab011). Available from: https://doi.org/10.1093/ilar/ilab011
    - The material from this publication is used in *Chapter 1.7* of this thesis and is unmodified except to match the formatting style of this thesis
    - Author contributions are as follows: ZS wrote the introduction, LB wrote the section "filovirus animal models", ZS and WC wrote the section "filovirus pathogenesis in ferrets", WZ and GL wrote the section "ferrets and countermeasure evaluation", LB wrote the section "perspective on ferrets as a filovirus animal model and KE prepared all the figures. XQ was an honorary author. All authors participated in review and editing of the manuscript.
2. Schiffman Z, Garnett L, Tran KN, et al. The Inability of Marburg Virus to Cause Disease in Ferrets Is Not Solely Linked to the Virus Glycoprotein. The Journal of Infectious Diseases. 2023; 28(Supplement_7):S594–S603
    - The material from this publication is used in *Chapter 3* of this thesis and is unmodified except to match the formatting style of this thesis
    - Author contributions are as follows: ZS, LB, and WC conceptualized and designed the study. ZS, LG, KNT, LB, JES, SH, and WC conducted *in vivo* experiments in containment level (CL)-4. KT and KA conducted animal husbandry. WC cloned and rescued EBOV-mGP. ZS developed ferret cell lines and conducted vesicular stomatitis virus experiments in CL-2. ZS, LG, KNT, and KE conducted sample processing. ZS and LB conducted data

analysis. ZS wrote and prepared the original manuscript draft. All authors participated in review and editing of the manuscript.

3. Schiffman Z, Yan F, He S, et al. Taï Forest Virus Does Not Cause Lethal Disease in Ferrets. Microorganisms. 2021; 9(2).

- The material from this publication is used in *Appendix 1* of this thesis and is unmodified except to match the formatting style of this thesis
- Author contributions are as follows: XQ conceptualized and designed the study. ZS and LB conducted formal analysis. ZS, FY, SH, KT, WZ, KE and LB conducted the experiments. HZ provided reagents and resources. ZS wrote the original manuscript draft and ZS and LB reviewed and edited the manuscript. ZS prepared all figures. All authors participated in review and editing of the manuscript.

# 1. Chapter 1: INTRODUCTION

## 1.1. History of Filoviruses

### 1.1.1. Discovery and Emergence

In August 1967, a severe disease of unknown etiology emerged among laboratory workers in two centers in Germany, namely Marburg and Frankfurt, as well as in Belgrade, Serbia (formerly Yugoslavia) [1]. The source of infection was traced back to African green monkeys (*Chlorocebus aethiops*), which were imported to all three locations (Marburg, Frankfurt and Belgrade) from Uganda, East Africa [2]. In total, 31 individuals contracted the disease consisting of 25 primary and six secondary infections, with seven patients having a fatal outcome corresponding to an overall case fatality rate (CFR) of 22.5% [3]. All 25 primary infections were acquired following necropsies of the non-human primates (NHPs) for the purpose of obtaining kidney cells for the culture of poliomyelitis vaccine strains [3]. The remaining six secondary infections were acquired via secondary transmission among colleagues or nosocomial transmission during clinical treatment of patients [3]. The patients who contracted the disease presented with fever, headache, myalgia and malaise, followed by conjunctival injection, photophobia and a generalized skin rash [1,3]. In most fatal cases, these symptoms progressed to severe hemorrhagic shock with a mean time of death of nine days [3]. The incubation period was retrospectively determined to be 5-9 days with a mean of eight days. Within three months, the unknown etiological agent was isolated, characterized, and identified as Marburg virus (MARV), named after the city with the most cases representing the first isolation of a filovirus [2,4,5]. The details regarding the emergence of MARV are comprehensively reviewed in [6,7].

### 1.1.2. Taxonomy of Filoviruses

Belonging to the order *Mononegavirales,* the family *Filoviridae* is subdivided into eight distinct genera, namely *Orthoebolavirus, Orthomarburgvirus, Cuevavirus, Dianlovirus,*

*Oblavirus, Striavirus, Thamnovirus* and *Tapjovirus* [8]. Filovirus genus assignment is based on nine determinants 1) pairwise genome sequence similarities, 2) phylogenetic distance of coding-complete genomes, 3) large protein (L) sequences, 4) RNA (ribonucleic acid)-dependent RNA polymerase (RdRp), 5) number and location of open reading frames (ORFs), 6) the presence or absence of cotranscriptional editing sites, 7) geographical distribution, 8) host tropism and 9) pathogenic potential [9,10]. Filovirus genera can be further classified according to their host tropism, with *Orthoebolavirus, Orthomarburgvirus, Cuevavirus* and *Dianlovirus* affecting mammalian hosts, *Oblavirus, Striavirus* and *Thamnovirus* affecting piscine hosts and *Tapjovirus* affecting reptilian hosts [11]. Each genus can be further subdivided into one or more species (Table 1).

**Table 1.** Filoviridae Taxonomy

| Genus | Species | Virus | Degree of Pathogenicity in Humans* |
|---|---|---|---|
| *Orthoebolavirus* | *Orthoebolavirus zairense* | Ebola virus (EBOV) | ++++ |
| | *Orthoebolavirus sudanese* | Sudan virus (SUDV) | ++++ |
| | *Orthoebolavirus bundibugyoense* | Bundibugyo virus (BDBV) | +++ |
| | *Orthoebolavirus taiense* | Tai Forest virus (TAFV) | + |
| | *Orthoebolavirus restonense* | Reston virus (RESTV) | - |
| | *Orthoebolavirus bombaliense* | Bomabali virus (BOMV) | ? |
| *Orthomarburgvirus* | *Orthomarburgvirus marburgense* | Marburg virus (MARV) | +++ |
| | | Ravn Virus (RAVV) | +++ |
| *Cuevavirus* | *Cuevavirus lloviuense* | Lloviu virus (LLOV) | ? |
| *Dianlovirus* | *Dianolvirus menglaense* | Měnglà virus (MLAV) | ? |
| *Oblavirus* | *Oblavirus percae* | Oberland virus (OBLV) | - |
| *Striavirus* | *Striavirus antennarii* | Xīlǎng virus (XILV) | - |
| *Thamnovirus* | *Thamnovirus kanderense* | Kander virus (KNDV) | - |
| | *Thamnovirus percae* | Fiwi virus (FIWIV) | - |
| | *Thamnovirus thamnaconi* | Huángjiāo virus (HUJV) | - |
| *Tapjovirus* | *Tapjovirus bothropis* | Tapajós virus (TAPV) | - |

* Virulence is estimated based on a variety of factors, including case fatality rates, outbreak sizes, and virulence in nonhuman primates, with "++++" highly virulent and "−" not virulent.

#### 1.1.2.1. Mammalian hosts

Four filovirus genera affect mammalian hosts, including *Orthoebolavirus, Orthomarburgvirus, Cuevavirus* and *Dianlovirus,* each of which can be further subdivided into one or more species (Table 1) [8]. The genus *Orthoebolavirus* consists of six species, each containing a single type virus: *Orthoebolavirus zairense* (Ebola virus, EBOV), *Orthoebolavirus sudanese* (Sudan virus, SUDV), *Orthoebolavirus bundibugyoense* (Bundibugyo virus, BDBV), *Orthoebolavirus restonense* (Reston virus, RESTV), *Orthoebolavirus taiense* (Taï Forest virus, TAFV) and *Orthoebolavirus bombaliense* (Bombali virus, BOMV) [8]. The genus *Orthomarburgvirus* consists of a single species, *Orthomarburgvirus marburgense,* consisting of two type viruses, namely Marburg virus (MARV) and Ravn virus (RAVV) [8]. The genus *Cuevavirus* consists of a single species *Cuevavirus lloviuense* consisting of a single virus (Lloviu virus, LLOV) [8]. The genus *Dianlovirus* consists of a single species, *Dianolvirus menglaense,* consisting of a single virus (Měnglà virus, MLAV) [8].

#### 1.1.2.2. Piscine and reptilian hosts

Three filovirus genera affect piscine (fish) hosts, including *Oblavirus, Striavirus* and *Thamnovirus,* each which can be further subdivided into one or more species (Table 1) [8]. The genus *Oblavirus* consists of a single species *Oblavirus percae* consisting of a single virus (Oberland virus, OBLV) [8]. The genus *Striavirus* consists of a single species *Striavirus antennarii* consisting of a single virus (Xīlǎng virus, XILV) [8]. The genus *Thamnovirus* consists of three species, each containing a single type virus: *Thamnovirus kanderense (*Kander virus, KNDV), *Thamnovirus percae* (Fiwi virus, FIWIV) and *Thamnovirus thamnaconi* (Huángjiāo virus, HUJV) [8].

The filovirus genera *Tapjovirus* is the sole genera known to harbour a filovirus affecting reptilian hosts (Table 1). The genus *Tapjovirus* consists of a single species *Tapjovirus bothropis*

consisting of a single virus (Tapajós virus, TAPV) [8]. Filovirus genera affecting piscine and reptilian hosts are beyond the scope of this thesis and will not be discussed beyond what is mentioned in this subsection.

### 1.1.3. Historical Filovirus Outbreaks

Since their first discovery in 1967, filoviruses have continued to pose a threat to global public health and have been responsible for causing numerous sporadic outbreaks over the decades. Since 1967, there have been a total of 22 outbreaks linked to orthomarburgviruses, with a total of 537 cases and 431 deaths, corresponding to an overall case fatality rate of 80% (Table 2). In contrast, 46 outbreaks have been linked to orthoebolaviruses since 1976, with 34,947 cases and 15,406 deaths (Table 3).

#### 1.1.3.1. Orthomarburgviruses

As described in *Section 1.1.1*, MARV first emerged in 1967, resulting in concurrent outbreaks across three centres located in Germany (Marburg and Frankfurt) and Serbia, representing the first occurrence of filovirus disease (FVD), more specifically Marburg disease (MARD) (Table 2). Eight years after its initial discovery, MARV re-emerged in 1975 in Johannesburg, South Africa, after an Australian with a travel history to Zimbabwe was admitted to the Johannesburg hospital [12]. At the time of his death, the traveller had transmitted the disease to two additional individuals, both of whom made a full recovery, and the outbreak was contained [12]. Five years later, MARV emerged in Kenya, causing a small outbreak among two individuals, one of whom recently visited Kitum Cave, Mount Elgon National Park, known to harbour large bat populations [13]. Two laboratory-acquired MARV infections were reported in Russia (formerly the Soviet Union) in 1988 and 1990 [14,15].

In 1998, MARV re-emerged in the Democratic Republic of Congo (DRC), causing the second-largest outbreak to date, with a total of 154 cases and 128 deaths [16]. This outbreak, which

spanned two years and ended in September 2000, was sustained by sporadic cases and short chains of human-to-human transmission spanning two main villages, namely Durba and Watsa [16]. Durba is a known mining village, with ~52% of the cases occurring among miners, suggesting the source of infection originated from caves [16]. The primary contacts subsequently transmitted the disease to their family members, with 21% of cases occurring among housewives and 10% among infants [16]. Interestingly, sequencing identified at least nine genetic lineages of MARV during the Durba outbreak with a low incidence of nosocomial infection [16]. Given the high genetic diversity and sporadic appearance of irregular intervals over the two-year outbreak, it is suspected that there were multiple potential spillover events [16].

Four years later, MARV re-emerged in the Uige Province in northern Angola, causing the largest recorded MARV outbreak spanning 2004-2005 with 252 cases and 227 deaths and an overall case fatality rate of 90% [17]. The index case for this outbreak could never be identified, and unlike the Durba outbreak, there was very little genetic diversity among the sequenced isolates [17]. Following this outbreak, MARV continued to cause sporadic outbreaks in 2007, 2012, 2014 and 2017 across Uganda. In 2008, imported cases of MARV were detected in Colorado, USA and Leiden, Netherlands, both of which were traced back to Uganda following a visit to Python Cave in Maramagambo Forest [18,19]. MARV continues to emerge, with recent outbreaks in 2021 in Guinea and 2022 in Ghana, the first-ever reports of MARV in these regions. As recently as 2023, MARV resulted in two concurrent outbreaks in Equatorial Guinea and Tanzania, further emphasizing the risk to global public health posed by MARV.

RAVV was first identified in 1987 after a 15-year-old Danish boy succumbed to infection during a vacation trip in Kenya [20]. Since 1987, at least two outbreaks have been linked to RAVV, including one during the 1998-2000 Kenya outbreak and one during the 2007 Uganda outbreak

[16,21]. While there have only been three outbreaks linked to RAVV, many cases have likely been missed, given that MARV and RAVV have identical clinical presentations and can only be differentiated by sequencing, which was not readily available during earlier outbreaks.

**Table 2.** Historical outbreaks linked to orthomarburgviruses

| Virus | Year | Location | Number of Cases | Deaths | Case Fatality Rate (%) | References |
|---|---|---|---|---|---|---|
| MARV | 1967 | Germany (Marburg) | 24 | 5 | 21 | [3] |
| | 1967 | Germany (Frankfurt) | 6 | 2 | 33 | [3] |
| | 1967 | Serbia | 2 | 0 | 0 | [3] |
| | 1975 | South Africa | 3 | 1 | 33 | [12,22] |
| | 1980 | Kenya | 2 | 1 | 50 | [13] |
| | 1988 | Russia (USSR) | 1 | 1 | 100 | [14] |
| | 1990 | Russia (USSR) | 1 | 0 | 0 | [15] |
| | 1998-2000 | DRC | 154 | 128 | 83 | [16] |
| | 2004-2005 | Angola | 252 | 227 | 90 | [17] |
| | 2007 | Uganda | 4 | 1 | 25 | [21] |
| | 2008 | USA | 1 | 0 | 0 | [18] |
| | 2008 | Netherlands | 1 | 1 | 100 | [19] |
| | 2012 | Uganda | 26 | 15 | 58 | [23] |
| | 2014 | Uganda | 1 | 1 | 100 | [24] |
| | 2017 | Uganda | 4 | 3 | 75 | [25] |
| | 2021 | Guinea | 1 | 1 | 100 | [26] |
| | 2022 | Ghana | 3 | 2 | 66 | [27] |
| | 2023 | Equatorial Guinea | 40 | 35 | 88 | [28] |
| | 2023 | Tanzania | 8 | 5 | 62.5 | [29] |
| | **Total (n=19)** | | **534** | **429** | **80%** | |
| RAVV | 1987 | Kenya | 1 | 1 | 100 | [20] |
| | 1998-2000 | DRC | 1 | 1 | 100 | [16] |
| | 2007 | Uganda | 1 | 0 | 0 | [21] |
| | **Total (n=3)** | | **3** | **2** | **66%** | |

#### 1.1.3.2. Orthoebolaviruses

In 1976, two outbreaks of hemorrhagic fever with exceptionally high mortality rates occurred simultaneously in southern Sudan and the northern region of the DRC (formerly Zaire) [30]. The clinical presentation of the disease closely resembled that observed during two previous

MARV outbreaks in 1967 and 1975, and as such, MARV was initially believed to be the etiological agent causing these 1976 outbreaks. Upon isolation and characterization, this virus was determined to be distinct from MARV and was named Ebola virus after the Ebola River in Zaire [30]. Initially, it was thought that both the outbreak in Sudan and DRC were caused by the same virus, identified as EBOV; however, seven years later, in 1983, it was determined that these simultaneous outbreaks were caused by discrete viruses [31]. The 1976 outbreak in DRC was caused by EBOV and resulted in 318 cases with 280 deaths, corresponding to a case fatality rate of 88%, whereas the 1976 outbreak in Sudan was caused by SUDV and resulted in 284 cases with 151 deaths, corresponding to a case fatality rate of 53%. Since their discovery and emergence in 1976, there have been 25 outbreaks linked to EBOV and eight linked to SUDV (Table 3).

In 1989 at a NHP facility in Reston, Virginia, there was an epizootic outbreak among NHPs (*Macaca fascicularis*) recently imported from the Philippines [32]. These NHPs presented with clinical signs typical of simian hemorrhagic fever (SHF) and were culled upon confirmation of SHF [32]. Following the culling, additional NHPs began developing disease that resembled SHF. Upon isolation and characterization, the causative agent was identified as a novel filovirus named Reston virus after the location of the outbreak [32]. Indeed, four individuals were confirmed to be infected with RESTV, with none presenting with clinical signs of disease [33]. Three additional cases of RESTV were identified in the Philippines in 1989, none of which were lethal [34]. It was only 19 years later, in 2008, when six more asymptomatic cases of RESTV were declared in the Philippines [34], and since then, no additional human cases have been reported.

In 1994, a 34-year-old female veterinarian became ill in Côte d'Ivoire after performing an autopsy on a wild chimpanzee found in the Taï Forest [36,37]. The patient initially presented with dengue-like symptoms but later made a full recovery, and the causative agent was later identified

as a novel filovirus named Taï Forest Virus after the region where it was discovered [36,37]. Since 1994 no additional cases of TAFV have been reported.

In 2007, a hemorrhagic fever outbreak of unknown etiology was declared in Bundibugyo, Uganda, and later confirmation determined that the causative agent was a novel filovirus named Bundibugyo virus after the region it was discovered [38]. This represented the largest recorded BDBV outbreak, with a total of 131 cases and 42 fatalities, corresponding to a case fatality rate of 32%. The second and last recorded BDBV outbreak occurred seven years later, in 2012, in the DRC, with a total of 38 cases and 13 fatalities, corresponding to a case fatality rate of 34% [39]. No additional human cases have been reported since 2012.

**Table 3.** Historical outbreaks linked to orthoebolaviruses

| Virus | Year | Location | Number of Cases | Deaths | Case Fatality Rate (%) | References |
|---|---|---|---|---|---|---|
| EBOV | 1976 | Zaire | 318 | 280 | 88 | [30,40] |
| | 1977 | DRC | 1 | 1 | 100 | [40] |
| | 1994 | Gabon | 52 | 31 | 61 | [41] |
| | 1995 | DRC (Kikwit) | 315 | 254 | 81 | [42] |
| | 1996 | Gabon | 31 | 21 | 68 | [41] |
| | 1996 | Gabon | 60 | 45 | 75 | [41] |
| | 1996 | South Africa | 2 | 1 | 50 | [43] |
| | 2001-2002 | DRC | 59 | 44 | 75 | [44] |
| | 2001 | Gabon | 65 | 53 | 81 | [44] |
| | 2003 | DRC (Mbomo district) | 35 | 29 | 83 | [45] |
| | 2003 | DRC | 143 | 128 | 89 | [46] |
| | 2005 | DRC | 12 | 10 | 83 | [47] |
| | 2007 | DRC (Etoumbi district) | 264 | 187 | 71 | [48] |
| | 2008-2009 | DRC (Kasaï Occidental) | 32 | 15 | 47 | [49] |
| | 2013-2016 | Guinea, Liberia, Sierra Leone | 28,652 | 11,325 | 39 | [50] |
| | | Italy | 1 | 0 | 0 | [51] |
| | | Mali | 8 | 6 | 75 | [50] |
| | | Nigeria | 20 | 8 | 40 | [50] |
| | | Senegal | 1 | 0 | 0 | [50] |
| | | Spain | 1 | 0 | 0 | [52] |
| | | United Kingdom | 1 | 0 | 0 | [53] |
| | | United States of America | 4 | 1 | 25 | [50] |
| | 2014 | DRC (Équateur Province) | 69 | 49 | 71 | [54] |
| | 2017 | DRC (Bas Uélé District) | 8 | 4 | 50 | [55] |
| | 2018-2020 | DRC, Uganda | 3470 | 2287 | 66 | [56] |

| Virus | Year | Location | Number of Cases | Deaths | Case Fatality Rate (%) | References |
|---|---|---|---|---|---|---|
| | 2018 | DRC (Équateur Province) | 54 | 33 | 61 | [57] |
| | 2020 | DRC (Équateur Province) | 130 | 55 | 42 | [58] |
| | 2021 | DRC (North Kivu Province) | 11 | 6 | 55 | [59] |
| | 2021 | DRC (North Kivu Province) | 12 | 6 | 50 | [59] |
| | 2021 | Guinea | 23 | 12 | 52 | [60] |
| | 2022 | DRC (Équateur Province) | 5 | 5 | 100 | [61] |
| | 2022 | DRC (North Kivu Province) | 5 | 5 | 100 | [59] |
| | **Total** | | **33,822** | **14,884** | **44%** | |
| **SUDV** | 1976 | Sudan | 284 | 151 | 53 | [30,62] |
| | 1979 | Sudan | 34 | 22 | 65 | [63] |
| | 2000 | Uganda | 425 | 224 | 53 | [64] |
| | 2004 | Sudan | 17 | 7 | 41 | [65] |
| | 2011 | Uganda | 1 | 1 | 100 | [66] |
| | 2012 | Uganda | 6 | 3 | 50 | [67] |
| | 2012 | Uganda | 11 | 4 | 36 | [67] |
| | 2022 | Uganda | 164 | 55 | 34 | [68] |
| | **Total** | | **942** | **467** | **54%** | |
| **RESTV** | 1989 | Philippines | 3 | 0 | 0 | [34,69] |
| | 1989 | United States of America | 4 | 0 | 0 | [33] |
| | 2008 | Philippines | 6 | 0 | 0 | [35] |
| | **Total** | | **13** | **0** | **0%** | |
| **BUDV** | 2007 | Uganda | 131 | 42 | 32 | [38] |
| | 2012 | DRC (Orientale Province) | 38 | 13 | 34 | [39] |
| | **Total** | | **169** | **55** | **33%** | |
| **TAFV** | 1994 | Côte D'Ivoire | 1 | 0 | 0 | [36,37] |
| | **Total** | | **1** | **0** | **0%** | |

### 1.1.4. Ecology and geographical distribution of filoviruses

As described in *Section 1.1.3*, filoviruses have been responsible for a multitude of sporadic outbreaks, primarily across Africa, since their discovery and emergence in 1967. While both EBOV and MARV are endemic to Africa, ecological niche modelling along with analysis of epidemiological patterns demonstrate that EBOV is endemic to rain forests of Central and Western Africa while MARV is more prevalent among open, dry areas of eastern and south-central Africa [70–72].

The search for the natural reservoir of filoviruses began almost immediately following their first emergence, with little success during the late 1990s and early 2000s [73–75]. Early search into the natural reservoir focused on hosts with the potential to sustain virus populations within the environment without succumbing to disease. Humans and NHPs are thought to represent incidental hosts with acquired infections typically resulting in fatal outcomes and, as such, were not considered reservoir hosts. However, the debate about primates (especially humans) as potential reservoir hosts has been reinvigorated recently, with increasing evidence that EBOV can persist among human survivors. More specifically, it has been demonstrated that EBOV viral RNA can persist among recovering patients within breast milk, sweat, urine, vaginal secretions, ocular aqueous humour, conjunctival fluid and semen [76]. As such, persistence in these immune-privileged niches poses the risk of either asymptomatic or symptomatic transmission. Indeed, Den Boon et al. identified 13 possible events of viral persistence-derived transmission of EBOV during the 2014-2016 EBOV outbreak [77]. Additionally, genetic evidence suggests that the recent 2021 EBOV outbreak in Guinea was not linked to a zoonotic spillover event but rather re-emergence from a persistently infected human [60].

Bats have long been suspected of playing a pivotal role in the transmission cycle of filoviruses, and indeed, early MARV outbreaks had a high incidence of index cases linked to human entry into caves inhabited by bats [16,70]. In 2005, Leroy et al. provided the first direct evidence from field studies that bats represent potential reservoir hosts for EBOV [78]. More specifically, during three trapping expeditions across the DRC and Gabon, Leroy et al. successfully detected anti-EBOV immunoglobulin G (IgG) and EBOV viral RNA in three fruit bat species, namely *Hypsignathus monstrosus*, *Epomops franqueti* and *Myonycteris torquate* [78]. Shortly after, in 2007, researchers detected MARV-specific RNA and IgG among *Rousettus*

*aegyptiacus* bats sampled across the DRC and Gabon; however, no infectious virus could be recovered [79,80]. It was only in 2009 that infectious MARV was isolated from *Rousettus aegyptiacus* bats found within Kitaka mine in Uganda [81]. This marked the first instance a filovirus had been isolated from bats. Since then, MARV has repeatedly been isolated from *Rousettus aegyptiacus* bats, providing definitive evidence of these bat species as the natural reservoir host for MARV [82–84].

In 2002, roughly around the same time, Leroy et al. were conducting their expeditions, researchers began investigating die-off events of Schreiber's bats (*Miniopterus schreibersii*) in the Iberian Peninsula [85]. This investigation resulted in the discovery of a novel filovirus named Lloviu virus that was genetically and antigenically distinct from previously discovered filovirus and was assigned to a novel genus *Cuevavirus* [86,87]. Not only did this represent the first instance a filovirus had been detected in Europe, but also the first time a novel filovirus belonging to a novel genus had been detected since the emergence of EBOV in 1976. More than a decade later, in 2016, LLOV was detected again in Schreiber's bats carcasses, this time in Hungary, confirming LLOV was more widespread across Europe than previously thought [88]. Nearly 20 years after its discovery in Spain, LLOV was successfully isolated from Schreiber's bats in Hungary and then shortly after in Italy, representing only the second filovirus isolated from a reservoir host [89,90].

More recently, in 2018, evidence of a novel *Orthoebolavirus* named Bombali virus was detected in Sierra Leone among free-tailed bats, namely *Chaerephon pumilus* and *Mops condylurus* [91]. This represented the first instance where a previously unknown filovirus genome belonging to the *Orthoebolavirus* genus had been identified among bats [91]. Since its discovery in 2018, BOMV has been detected in *Mops condylurus* bats sampled in Kenya and Guinea [92,93]. Despite repeated detection of viral genomes, infectious BOMV has yet to be isolated. Even more

recently, in 2019, researchers discovered genomic evidence of a novel filovirus named Měnglà virus (MLAV) among *Rousettus leschenaultia* bats in Southern China [94]. Sequencing of the viral genome revealed MLAV to be genetically distinct from previously discovered filoviruses and was assigned to a novel genus named *Dianlovirus* [94]. Since then, genetic evidence of *Dianloviruses* have been detected in *Rousettus* bats sampled in Vietnam [95].

Since the initial discovery by Leroy et al. in 2005, serological evidence of EBOV has been detected in several additional bat species, namely *Eidolon helvum*, *Epomophorus gambianus*, *Micropteropus pusillus*, *Mops condylurus*, *Rousettus aegyptiacus* and *Rousettus leschenaultia* [96–99]. Despite sampling thousands of bats and repeatedly detecting anit-EBOV IgG and EBOV viral RNA in numerous bats, infectious EBOV has yet to be isolated [100,101]. Other than EBOV, serological evidence of RESTV has also been detected in a variety of bat species sampled in China [102,103], the Philippines [104] and Bangladesh [96]. However, like EBOV, no infectious RESTV has ever been isolated from bats. EBOV, RESTV and BOMV remain the sole members of the *Orthoebolaviurus* genus that have been detected in bats.

## 1.2. Filovirus Biology

*For the purpose of this thesis, filovirus biology will only be discussed for orthoebolaviruses and orthomarburgviruses.*

### 1.2.1. Virion Structure

The taxonomy of the family *Filoviridae* was defined in 1982, with the name *filoviridae* being derived from the Latin noun *filum,* which means "threadlike structure," alluding to the filamentous morphology of filovirions [105]. Indeed, filovirions are among the most recognizable virions due to their characteristic filamentous morphology, as observed in electron micrographs. While filovirions typically appear as long filamentous particles, they can assume pleomorphic morphologies with additional forms, including branched, toroid, U-shaped or 6-shaped "shepherd's

crook" (Figure 1) [10,106,107]. The diameter of filovirions are quite uniform and range in size from ~91-98 nm, whereas their length can vary depending on the form, with lengths ranging from 1-20µm [10]. *Orthoebola and Orthomarburg* virions contain a central core corresponding to the helically arranged ribonucleoprotein (RNP) complex [10]. The RNP complex is ~30-41 nm in diameter with a pitch of 7-7.5 nm and is embedded in a matrix layer surrounded by a lipid envelope [10].

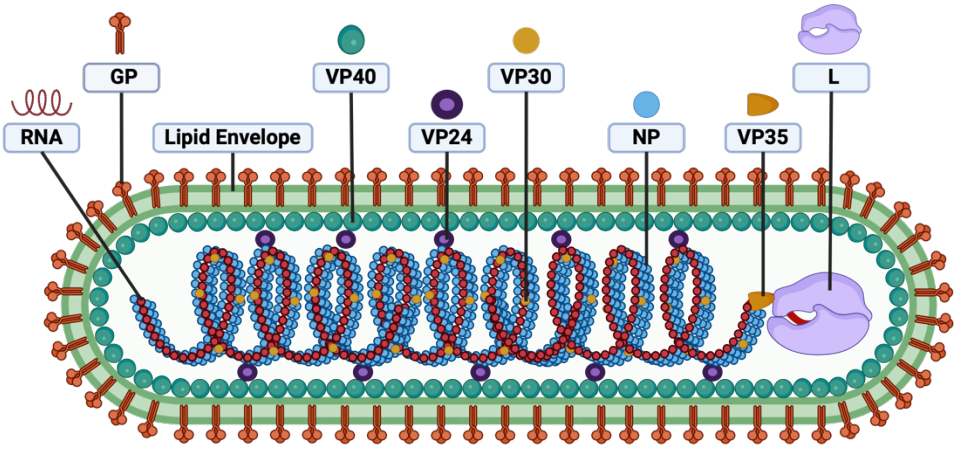


**Figure 1. Schematic representation of the filovirus virion**

Filovirions exhibit a characteristic morphology appearing as long filamentous particles often with pleomorphic morphologies that can range in size from 1-20 µm. Virions are composed of a central ribonucleoprotein (RNP) complex consisting of genomic RNA encased by nucleoprotein (NP), viral protein (VP)-35, VP30 and RNA-dependent RNA polymerase (L). The RNP complex is surrounded by a matrix composed of the VP40 and VP24 proteins and an outer lipid envelope derived from the host cellular plasma membrane. Spikes of the GP protein protrude from the envelope surface. Figure created on Biorender.com

### 1.2.2. Genome Organization

Filovirus genomes are linear, nonsegmented, negative-sense RNA molecules that encode a variable number of genes inserted at various locations throughout the genome depending on the genus affiliation (Figure 2) [10,108–110]. Filovirus genomes are consistent in length but can vary depending on the genus affiliation, with mammalian filoviruses having a length of ~19 kb, whereas piscine filoviruses are shorter with lengths of ~15-17 kb [10,109]. Genomes for both

orthoebolaviruses and orthomarburgviruses consist of seven genes, namely nucleoprotein (NP), polymerase cofactor (VP35), matrix protein (VP40), surface glycoprotein (GP), polymerase cofactor (VP30), nucleocapsid protein (VP24) and RdRp (L) (Figure 2) [10,108,109]. Unlike orthomarburgviruses, the GP gene of orthoebolaviruses encodes several GP products, which will be discussed further in *Section 1.2.4*. Filovirus genes are flanked by conserved gene start (GS) and gene end (GE) signals, which either overlap or are separated by short intergenic regions (IR) [108]. Upstream of the GS signal of the first gene is the 3' leader sequence, and downstream of the GE signal of the last gene is the 5' trailer sequence, both of which contain important regulatory elements for replication and transcription of messenger RNA(mRNA) [108,111]. Including the 3'leader and 5' trailer, both orthoebolaviruses and orthomarburgviruses have the following gene order: 3'-NP-VP35-VP40-GP-VP30-VP24-L-5' (Figure 2).

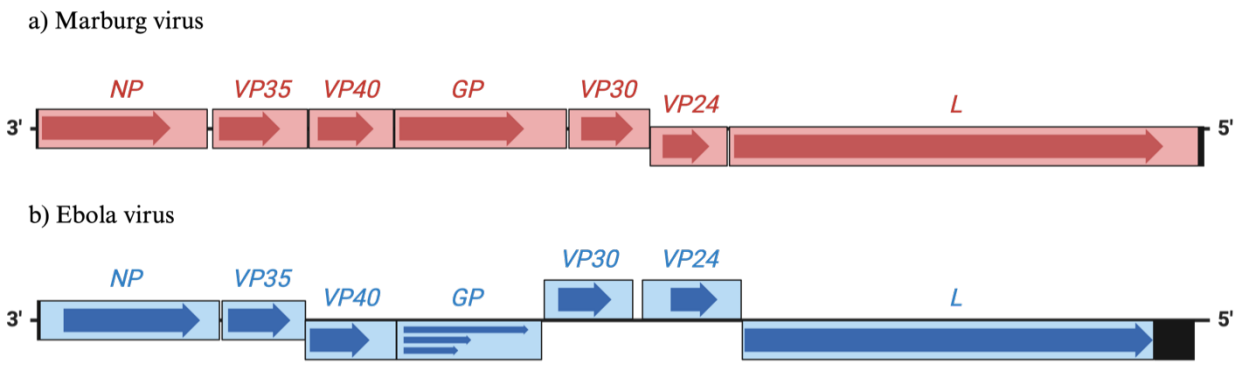


**Figure 2. Filovirus genome organization**

The genome of mammalian filoviruses encoded a total of seven genes which, depending on the genus, can encode 6-10 proteins. (**a**) The genome of orthomarburgviruses contain seven genes which encode seven proteins, namely NP, VP35, VP40, GP, VP30, VP24 and L. (**b**) Orthoebolaviruses contain the same seven genes; however, due to cotranscriptional editing, they give rise to 10 expression products instead of seven. Unlike orthomarburgviruses, the GP gene of orthoebolaviruses is subject to cotranscriptional editing, yielding a total of four expression products, namely GP, secreted glycoprotein (sGP), secondary secreted glycoprotein (ssGP). Arrows depict the coding sequences and black shading represent 3' and 5 'untranslated regions (UTRs). Figure created on Biorender.com

### 1.2.3. Genome Expression Products

Seven genes are encoded within the genome of mammalian filoviruses, which, depending on the genus, can encode 6-10 proteins. In the case of orthomarburgviruses, these seven genes encode seven proteins, namely NP, VP35, VP40, GP, VP30, VP24 and L (Figure 2) [10,109]. By comparison, orthoebolaviruses contain the same seven genes; however, due to cotranscriptional editing, they give rise to 10 expression products instead of seven (Figure 2) [10,109]. This is because unlike orthomarburgviruses, the GP gene of orthoebolaviruses is subject to cotranscriptional editing, yielding a total of four expression products, namely GP, secreted glycoprotein (sGP), secondary secreted glycoprotein (ssGP) and Δ-peptide [10,109]. Filovirus GP expression products will be discussed further in *Section 1.2.4*.

NP represents the first gene encoded in the negative-sense genome of filoviruses (Figure 2) and gives rise to a protein ~692-749 amino acids long [109]. NP monomers associate to form long, left-handed helical polymers which encapsulate the viral RNA genome, forming NP-RNA complexes [112]. These NP-RNA complexes act as functional templates for transcription and replication performed by L and VP35 [10,109,112]. NP does not interact directly with L; instead, these interactions are mediated by VP30 and VP35, which are essential for RNA synthesis [113,114].

VP35 represents the second gene encoded in the negative-sense genome of filoviruses (Figure 2) and gives rise to a protein ~320-341 amino acids long [109]. VP35 acts as a polymerase cofactor interacting with both L and NP and is essential for virus transcription and replication [109,112]. In addition to its role as a polymerase cofactor, VP35 also plays a critical role as an immunomodulator, which antagonizes the host innate immune response by binding double-stranded RNA (dsRNA) [115]. The role of filovirus VP35 as an antagonist of the host innate immune response will be discussed further in *Section 1.5.1*.

VP40 represents the third gene encoded in the negative-sense genome of filoviruses (Figure 2) and gives rise to a protein 326 amino acids long in the case of orthoebolaviruses and 303 amino acids long in the case of orthomarburgviruses [109]. VP40 is the main structural component of the filovirus matrix and polymerizes to form protein filaments from which the virion matrix is constructed, giving rise to the characteristic filamentous shape of the virion [116,117]. More specifically, VP40 recruits the nucleocapsid to the virion as well as has critical interactions with GP and the cell membrane during budding [118,119]. Additionally, VP40 has been shown to be critical for transcriptional control [120]. Lastly, VP40 has been shown to function as an antagonist of host interferon signaling, a function unique to orthomarburgviruses and will be discussed further in *Section 1.5.1*. [121–123]. The multifunctionality of VP40 is believed to be attributed to the ability of the VP40 polypeptide to adopt different structures [109].

GP represents the fourth gene encoded in the negative-sense genome of filoviruses (Figure 2) and gives rise to a protein 676-681 amino acids in length [109]. GP is the viral surface glycoprotein and represents the sole protein expressed on the virion surface and plays a critical role in mediating entry into the host cell. The details surrounding GP and its expression products will be discussed further in *Section 1.2.4*.

VP30 represents the fifth gene encoded in the negative-sense genome of filoviruses (Figure 2) and gives rise to a protein 281-289 amino acids in length [109]. The role of VP30 has been well studied for orthoebolaviruses and functions as a transcriptional activator and regulator of RNA synthesis [124,125]. Furthermore, VP30 facilitates reading by L through RNA hairpin structures located in the 5' untranslated region (UTR) [126]. VP30 is also believed to promote L transcription reinitiation during the sequential transcription of Orthoebolavirus genes as well as regulate cotranscriptional GP gene editing [127,128]. In fact, VP30 is unique to filoviruses and is absent

having no homolog in the nucleocapsid of other mononegaviruses and represents a critical component needed for the filovirus life cycle [109]. The activity of VP30 is regulated by phosphorylation (transcriptional repression) and dephosphorylation (transcriptional activation) by cellular kinases and phosphatases. [10,109]

VP24 represents the sixth gene encoded in the negative-sense genome of filoviruses (Figure 2) and gives rise to a protein 233-241 amino acids in length [109]. VP24 adopts a pyramidal α/β fold and plays an important role in the assembly and function of the viral RNP complex [129]. More specifically, VP24 interacts with NP, and this interaction inhibiting transcription and replication while facilitating the translocation of the RNP to budding sites for packaging into virions [130]. Lastly, VP24 of orthoebolaviruses but not orthomarburgviruses also functions as an inhibitor of interferon signalling and will be discussed further in *Section 1.5.1* [131].

L represents the seventh and largest gene encoded in the negative-sense genome of filoviruses (Figure 2) and gives rise to a protein 2196-2331 amino acids in length [109]. L functions as an RdRp and is expressed as a single polypeptide responsible for all enzymatic activities required from RNA synthesis [109]. L contains six highly conserved regions, namely conserved region (CR) I-VI mediating nucleotide triphosphate binding (CRI), RNA template recognition (CRII), RNA polymerization (CRIII), polyadenylation (CRIII), mRNA capping/polyribonucleotidyl transfer (CRIV/CRV) and methylation (CRVI) [10]. L also mediates cotranscriptional mRNA editing in the case of orthoebolaviruses [132]. Unfortunately, little remains known about the structure of L due to difficulties associated with gathering sufficient amounts of protein for analysis.

### 1.2.4. GP Expression Products

The GP gene of orthomarburgviruses contain a single ORF without editing sites, ultimately giving rise to a single GP expression product (Figure 2) [133]. In contrast, the GP gene of

orthoebolaviruses contain three ORFs which are subject to cotranscriptional editing and following post-translational modifications yield a total of five GP expression products, namely GP, sGP, ssGP, shed glycoprotein ($GP_{1,2\Delta}$) and Δ-peptide [10,134] .

Preceding the 0 frame is a Kozak sequence consisting of seven consecutive uridine residues (7U), which is transcribed by the filovirus polymerase (L+VP30), giving rise to mRNA transcripts consisting of a stretch of seven adenosine residues (7A) [10]. Two additional ORFs begin at the -1 and +1 reading frames at the 7U site, which are subject to cotranscriptional polymerase stuttering [10]. As a result of this cotranscriptional polymerase stuttering, these -1 and +1 ORFs give rise to mRNA transcripts consisting of a stretch of eight (8A) and (9A) adenosine residues, respectively [10]. As such, three transcripts result from the GP gene, namely 7A (70%), 8A (25%) and 9A (5%), which are subsequently translated into three expression products, namely precursor sGP (pre-sGP), precursor GP (pre-GP) and precursor ssGP (pre-ssGP) [135,136]. All three proteins are expressed in various isoforms, given that multiple adenosine residues can be inserted/skipped during cotranscriptional editing. This cotranscriptional editing is regulated by *cis*-acting sequences located nine nucleotides upstream and downstream of the editing site and by VP30, which functions as a *trans-acting* factor.

Pre-sGP is proteolytically cleaved by furin-like endoproteases yielding two products, namely sGP (11kDa) and Δ-peptide (5kDa) [137,138]. The exact function of sGP remains largely unknown, but is thought to function as an antibody decoy [139,140]. This is because sGP contains the identical residues of $GP_{1,}$ which are critical for receptor binding and, as such, is a prominent target of the host adaptive immune response. As such, sGP, being the major GP product, is present at high concentrations, ultimately providing a target for host antibodies. The Δ-peptide is secreted

from infected cells and has been shown to inhibit replication *in vitro* and is thought to function as a means of regulating superinfection of host cells [138].

Pre-GP is glycosylated, dimerized via disulfide bonds, and subsequently cleaved by furin-like endoproteases yielding $GP_1$ and $GP_2$ subunits [10,134]. The $GP_1$ subunit represents the surface-exposed moiety of mature GP and plays an essential role in mediating cell-surface attachment to host cell receptors via its receptor-binding site (RBS) [141]. The $GP_2$ subunit is a class I fusion protein that plays an important role in the fusion of viral and host cell membranes [133]. These two heterodimers trimerized into mature $GP_{1,2}$ prior to being transported to the cell membrane for incorporation into virions. Little is known about shed glycoprotein ($GP_{1,2\Delta}$) and ssGP, but like sGP is thought to act as an antibody decoy [143]

## 1.3. Filovirus Life Cycle

The filovirus life cycle consists of three stages, namely 1) virion attachment and entry into the host cell, 2) genome replication, transcription and translation and 3) assembly and budding of progeny virions (Figure 3).

### 1.3.1. Attachment and Entry

The first stage in the filovirus life cycle is the attachment of the virion to the host cell (Figure 3 #1). Attachment of the virion to the host cell is mediated through at least two types of alternative surface receptor interactions, namely binding of GP to carbohydrate-binding receptors and binding of the virion outer leaflet lipid envelope to phosphatidylserine receptors [109].

Filovirus GP will bind via its *N*- and *O*-linked glycans to two groups of carbohydrate-binding receptors, namely C-type lectin receptors (CLRs) and glycosaminoglycans [109]. CLRs that have been shown to bind filovirus GP include dendritic cell-specific ICAM-3-grabbing non-integrin (DC-SIGN) [144,145], liver/lymph node-specific ICAM-3 grabbing non-integrin (L-SIGN) [144,145], lymph node sinusoidal endothelial cell C-type lectin (LSECTin) [146],

asialoglycoprotein receptor 1 (ASGPRI) [147] and human macrophage galactose- and acetylgalactosamine-specific C-type lectin (hMGL) [148].

An example of a glycosaminoglycan found to bind filovirus GP is exostosin 1 (EXT1) [149]. Phosphatidylserine embedded within the virion outer leaflet lipid envelope will bind a variety of phosphatidylserine receptors independent of the presence of the viral glycoprotein. More specifically, phosphatidylserine has been shown to bind a variety of TIM receptors, such as T cell immunoglobulin mucin domain receptor-1 (TIM-1) [150] and TIM-4, as well as a variety of TAM receptors, including AXL [151]. While TIMs and TAMs have been shown to enhance filovirus attachment, the exact mechanism by which they induce internalization remains unknown. Furthermore, these attachment factors are also thought to be a mechanism for concentrating virions at the cell surface, facilitating uptake.

Following attachment, the virion is internalized to the host cell by micropinocytosis (Figure 3 #2), a process which involves the large-scale rearrangement of the host plasma membrane to engulf the virion into the endo/lysosomal pathway (Figure 3 #3) [152,153]. Acidification of the early endosome leads to cleavage of GP by the cysteine proteases cathepsin B and L, exposing the receptor binding domain of $GP_1$ and permitting interaction with intracellular receptor Niemann-Pick C1 (NPC1) in the late endosome (Figure 3 #4) [154,155]. Although cysteine proteases, namely cathepsin B and L, are required for entry, requirements of exact proteases can vary depending on the filovirus [156–158]. The interaction between GP and NPC1 triggers fusion of the viral and host membranes (Figure 3 #5) and the subsequent release of the RNP complex into the cytosol, where viral replication occurs (Figure 3 #6).

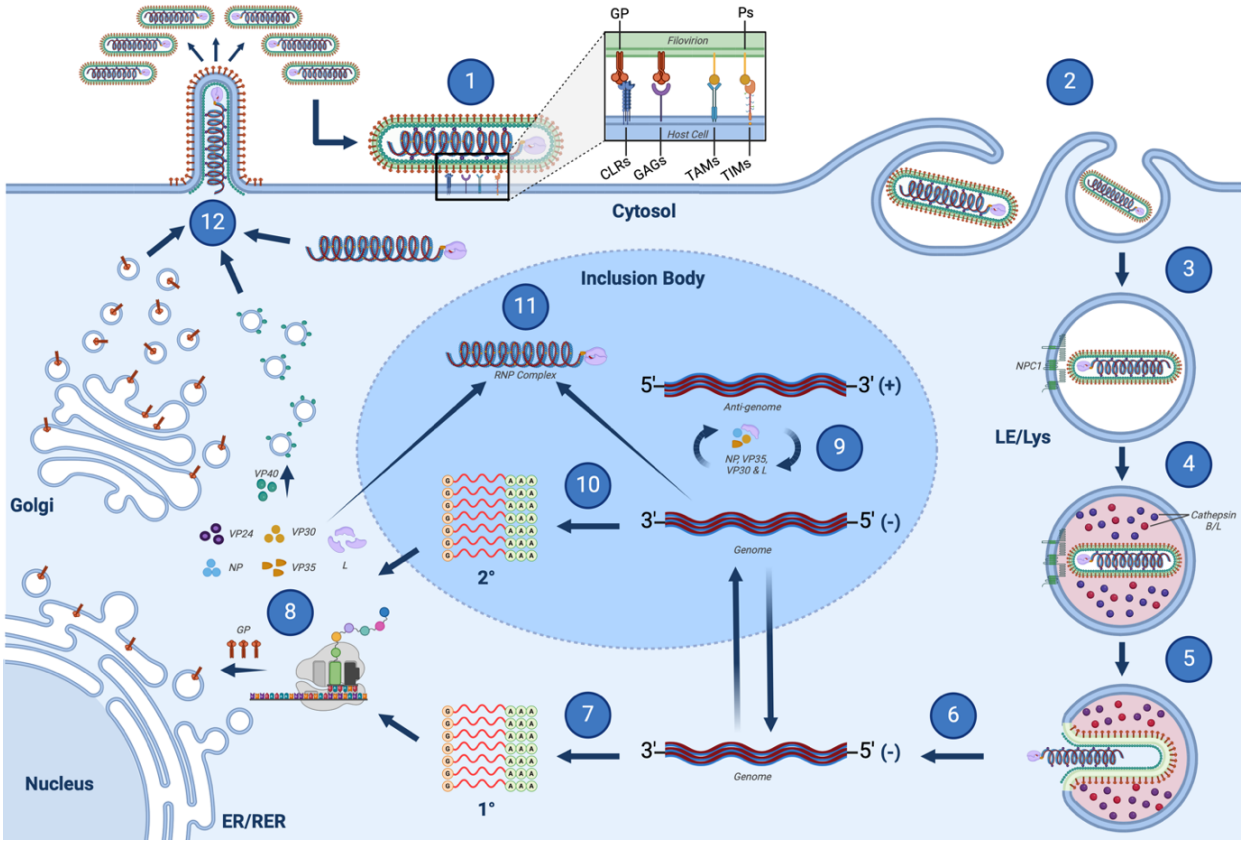


**Figure 3. Filovirus life cycle**

The filovirus life cycle begins with (**1**) attachment of the virion to the host-cell membrane via interaction between GP with attachment factors namely C-type lectin receptors (CLRs) and glycosaminoglycans (GAGs) or phosphatidylserine (Ps) with TIM and TAM receptors. (**2**) Following attachment, the virion is internalized to the host cell by micropinocytosis. (**3**) This process involves the large-scale rearrangement of the host plasma membrane to engulf the virion into the endo/lysosomal pathway. (**4**) Acidification of the early endosome leads to cleavage of GP by the cysteine proteases cathepsin B and L, exposing the receptor binding domain of $GP_1$ and permitting interaction with intracellular receptor NPC1 in the late endosome. (**5**) The interaction between GP and NPC1 triggers fusion of the viral and host membranes followed by (**6**) the release of the RNP complex into the cytosol, where unwinds into a uncondensed helical state. (**7**) Upon release, the single-stranded, nonsegmented RNA genome undergoes primary transcription by L into seven monocistronic mRNA species which are subsequently capped and polyadenylated. (**8**) The resulting mRNAs are translated, yielding the viral proteins NP, VP35, VP40, GP, VP30, VP24 and L. (**9**) As these viral proteins are expressed, a switch occurs, transitioning from transcription to replication. The replication process involves synthesizing the antigenome, a positive-sense replicative intermediate (5'-3') and reverse complement of the RNA genome. (**10**) The negative sense genome (3'-5') then undergoes secondary transcription, a process analogous to step #7. Replication and translation lead to the accumulation of viral proteins and copies of genomic RNA, which are concentrated within inclusion bodies (IB), regions where replication and translation occur. (**11**) As these viral proteins and genomic RNA accumulate, they coalesce into mature RNP which are (**12**) transported to budding sites via actin-dependent mechanisms, resulting in the release of progeny virions. Figure created on Biorender.com

### 1.3.2. Genome Replication and Transcription

Upon release of the RNP complex into the cytosol, the single-stranded, nonsegmented RNA genome is transcribed by L into seven monocistronic mRNA species (Figure 3 #7) [111]. The mRNA species are subsequently capped and polyadenylated [159]. Transcription of the RNA template involves a process of "starting" and "stopping" as the polymerase encounters conserved GS and GE signals, which flank filovirus genes [108]. More specifically, transcription begins with binding of the polymerase to a highly conserved 3' leader sequence. Upon binding, the polymerase proceeds along the RNA template until a GE signal is encountered, at which point the polymerase will "fall off" the template [111]. The polymerase then reinitiates at the GS signal downstream, allowing for the sequential transcription of the individual genes in their 3' to 5' order [111]. Reinitiation at genes located downstream is attenuated, resulting in a transcriptional gradient [111]. As such, genes located at the 3' end, such as NP, are transcribed at the highest levels, and those at the 5' end, such as L, are transcribed to the lowest levels [111]. Viral proteins present in the RNP complex, including NP, VP35 and L, are sufficient to drive transcription of orthomarburgviruses; however, orthoebolaviruses require VP30 in addition to NP, VP35 and L [160,161]. Following transcription, the resulting mRNAs are translated, yielding the viral proteins NP, VP35, VP40, GP, VP30, VP24 and L (Figure 3 #8). As these viral proteins are expressed, a switch occurs, transitioning from transcription to replication (Figure 3 #9), a process which remains unclear and is thought to be driven by the accumulation of NP [10].

The replication process involves synthesizing the antigenome, a positive-sense replicative intermediate (5'-3') and reverse complement of the RNA genome (Figure 3 #9). Given the high degree of sequence complementarity, stem-loop structures are predicted to form at the genomic and antigenomic RNAs' 3' and 5' ends [162]. Both the genomes and antigenomes are encapsidated by nucleocapsid protein (Figure 3 #11) [160,161].

### 1.3.3. Assembly and Budding

Filovirion morphogenesis is driven by NP, VP35, VP40 and VP24, which initiate and regulate several processes, including RNP transport and envelopment, as well as virion budding. Replication and translation lead to the accumulation of viral proteins and copies of genomic RNA, which are concentrated within inclusion bodies (IB), regions where replication and translation occur (Figure 3 #11). As these viral proteins and genomic RNA accumulate, they coalesce into mature RNP complexes (Figure 3 #11). Mature RNP complexes are transported to budding sites via actin-dependent mechanisms, a process that involves the polymerization of branched actin filaments (Figure 3 #12). [163–165] In addition to actin-dependent mechanisms, RNP transport is mediated in part by late budding motifs with VP40 [10]. GP is the sole protein translated at endoplasmic reticulum (ER) bound ribosomes and are transported to the plasma membrane via the classical secretory pathway (Figure 3 #12) [166]

## 1.4. Filovirus Pathogenesis and Pathology

Filovirus disease is the primary disease category and refers to the disease caused by all filoviruses [167]. In contrast, Ebola disease (EBOD) is the first disease subcategory corresponding to disease caused by all viruses within the *Orthoebolavirus* genus [167]. Ebola virus disease (EVD) is the second disease subcategory, which reflects disease caused explicitly by EBOV [167]. This can also be applied to SUDV and BDBV, for which the second disease subcategory is Sudan virus disease (SVD) and Bundibugyo virus disease (BVD) [167]. Likewise, MARD is the first disease subcategory corresponding to disease caused by all viruses within the *orthomarburgvirus* genus [167]. Lastly, Marburg virus disease (MVD) is the second disease subcategory, which reflects disease caused explicitly by MARV [167].

### 1.4.1. Transmission and Clinical Course of Disease

Human filovirus infections are acquired by direct contact with infectious fluid, which allows for virus entry into the body via breaks in the skin or mucosal membranes [10,110,115,168,169]. Infection can also occur via fomite-to-human transmission, such as contact with contaminated biological or non-biological materials, needlestick or contact with deceased bodies [169]. Examples of infectious bodily fluids include blood, stool, semen, breast milk, saliva, sweat, and tears [169–171]. While human-acquired infections can occur via many possible situations, the most common means of infections include care of infected patients [172], preparation of bodies for burial [173] and butchering of infectious bushmeat [174]. While rare, sexual transmission of filoviruses can occur and has been documented for both EBOV [175] and MARV [176] (Comprehensively reviewed in [170]). Although a likely occurrence, there are no confirmed cases of human EBOV spillover via direct or indirect contact with bats [177]. In contrast, direct or indirect contact with bats has been strongly implicated in MARV human spillover events and linked to several outbreaks [21,84].

Following acquired infection, filoviruses have an incubation period ranging from 2-21 days, with a mean incubation period of 6.22 ± 1.57 days [178]. The clinical course of FVD consists of several phases, namely incubation, nonspecific prodrome phase, gastrointestinal phase, and peak illness followed by death or slow recovery. The nonspecific prodrome phase generally consists of influenza-like symptoms, including abdominal pain, fever, anorexia, fatigue, myalgia and headache [179]. FVD patients presenting with these nonspecific symptoms are often misdiagnosed with malaria or typhoid fever, given their co-endemicity in these regions, and are often not suspected of having FVD unless associated with a known chain of transmission [179]. Progression to the gastrointestinal phase typically occurs on or around day five post-infection. The gastrointestinal phase typically consists of diarrhea, nausea, and vomiting and is often

accompanied by the dramatic loss of gastrointestinal fluid, hypotension, edema and rhabdomyolysis [10,110,179]. During this gastrointestinal stage, patients may begin to present with hemorrhagic manifestations typically associated with clotting factor deficiency or thrombocytopenia. Patients may also present with less common signs, including hiccups, dyspnea and cough [10,110,179]. This gastrointestinal phase generally occurs from day 5-12 post-infection and is the precursor to the peak phase of the disease. During peak illness, severely ill patients present with symptoms of hypovolemic or septic shock, which is often accompanied by metabolic acidosis and severe electrolyte abnormalities [10,110,179]. In fatal cases, this phase leads to the progression to multiple organ dysfunction syndrome (MODS), which involves multiple organ failure such as acute liver and kidney injury, respiratory failure and central nervous system (CNS) dysfunction, followed by death [10,110,179]. This CNS dysfunction can be characterized by altered mental status, seizures, meningoencephalitis, and CNS hypoperfusion, among others (reviewed in [110]). Those who survive the peak phase progress into the recovery phase, typically including viral clearance and resolution, allowing for the transition from tissue injury to repair [110]. Many survivors can experience sequelae and viral persistence.

While the clinical course of FVD among humans is relatively similar, the outcomes can vary depending on filovirus species. Some filovirus species, such as EBOV, are highly lethal among humans, whereas others, such as RESTV and TAFV, are otherwise non-lethal and cause only mild or asymptomatic disease. It remains unknown why certain filoviruses are more lethal than others; however, it is likely the result of subtle differences among these viruses and their ability to interact with critical host proteins, such as those responsible for viral entry and those essential for the host's innate immune response. Further investigation is required to fully elucidate the root causes responsible for these differences in disease outcomes among filovirus species

### 1.4.2. Virus Dissemination, Cellular Tropism, and Pathophysiology

Upon entry into the body, filoviruses will target resident tissue macrophages, monocytes and dendritic cells (DCs) located near or at the site of exposure [180–182]. These infected mononuclear cells, in turn, migrate through the bloodstream to the lymphatics and enter regional lymph nodes, a prominent site of filoviral replication. While filoviruses preferentially infect mononuclear cells, including macrophages, monocytes and DCs, they exhibit a broad cell tropism infecting Kupffer cells, fibroblasts, hepatocytes, endothelial and epithelial cells [10,168]. Nonetheless, filoviruses preferentially infect mononuclear cells, particularly during the early stages of infection, and are thought to be a mechanism for disseminating throughout the body [180–182]. This mechanism of dissemination is a common strategy for many viruses, including severe acute respiratory syndrome (SARS) coronavirus [183], Toscana virus [184] and meseales virus [185]. Infected macrophages become activated following binding of GP, which in turn stimulates the secretion of pro-inflammatory cytokines, including interleukin (IL)-1β, IL-6, IL-8, IL-10, monocyte chemoattractant protein 1 (MCP1), macrophage inflammatory protein-1α (MIP1α), MIP1β and tumour necrosis factor (TNF)-α [186–191]. In addition to pro-inflammatory cytokines and chemokine, activated macrophages also lead to the production of reactive oxygen species (ROS) and nitric oxide (NO) [192]. The contribution of pro-inflammatory cytokines and chemokines towards dysregulation of the host immune response will be discussed further in *Section 1.4.3*. In contrast, infection of DCs inhibits their maturation, which prevents antigen presentation to T-cells, a mechanism thought to be linked to the suppression of innate immune signalling pathways. While lymphocytes, including natural killer (NK) cells and T lymphocytes, are not targets of infection for filoviruses, they are subject to apoptosis early during the disease, resulting in lymphopenia [193–195].

The systematic spread of filoviruses throughout the bloodstream results in dissemination to several tissues, with the liver representing the primary target organ of filoviruses. Infection of hepatocytes and Kupffer cells results in acute liver degeneration, which is accompanied by significant increases in alanine transaminase (ALT) and aspartate transaminase (AST), a hallmark feature of FVD [196,197]. The kidney represents another prominent target of filoviruses with renal damage and impaired functioning associated with increased concentrations of blood urea nitrogen (BUN) and creatinine (CRE) [196,198]. Lastly, the spleen, rich in lymphocytes, represents yet another prominent target of filoviruses with considerable lymphoid depletion, apoptosis and necrosis as a result of infection [199].

With respect to hematology, thrombocytopenia is a hallmark feature of FVD, with decreases in platelet (PLT) counts to near zero during peak disease [196]. This decrease in PLT, along with vascular permeability as a result of macrophage activation, contributes to the hemorrhagic manifestation of FVD [196]. Lymphopenia and leukocytosis are also commonly observed in FVD. In addition, coagulation abnormalities are also prominent during FVD, with increases in coagulation factor III expression levels along with fibrinogen concentrations resulting in disruptions in homeostasis [196]. These coagulation abnormalities ultimately result in increased clotting times, contributing to disseminated intravascular coagulation (DIC) [200].

### 1.4.3. The Role of Cytokines and Chemokines in Filovirus Pathogenesis

Cytokines are small proteins <20 kDa essential in regulating various biological and immune processes and can be subdivided into interleukins, growth factors, chemokines, and interferons. Often referred to as a 'cytokine storm,' the overzealous cytokine response to filovirus infection represents a hallmark feature of FVD and a strong contributor toward viral pathogenesis [201]. This cytokine storm in response to filovirus infection is characterized by the production of

high levels of pro-inflammatory cytokines and chemokines, the vast majority of which are produced by infected monocytes and macrophages [201].

Type I interferons (IFN), including IFN-β and several IFN-α isoforms, are produced by infected cells following the recognition of a pathogen by pattern recognition receptors (PRRs) and toll-like receptors (TLRs) [201]. Among the TLRs, the RIG-I-like receptors (RLR), namely retinoic acid-inducible gene-I (RIG-I) and melanoma differentiation associated gene 5 (MDA5), are most relevant to filoviruses [202]. More specifically, RIG-I and MDA5 are cytoplasmic receptors which detect and signal in response to dsRNA products generated during virus replication [202]. These type I IFNs play an essential role in triggering a plethora of antiviral signalling pathways, most notably the Janus kinase/signal transducers and activators of transcription (JAK/STAT) signalling pathway, which is essential for the expression of IFN-stimulated genes (ISGs) that, in turn, induce an antiviral state, rendering cells refractory to viral infection [202,203]. Filoviruses have evolved various mechanisms to counteract and evade these antiviral responses and promote infection and will be discussed further *in* *Section 1.5.1*. The IFN family includes the type II IFN-γ, which, unlike type I IFNs, which most cell types can produce, are only produced by immune cells, most notably T-cells and NK cells [204]. IFN-γ production is a crucial feature of T helper (Th) 1 response and induces upregulation of major histocompatibility complex (MHC) I and II, promoting the effector functions of CD4+ and CD8+ T-cells [204]. Indeed, elevated levels of IFN-γ have been found among humans and NHPs infected with MARV and EBOV [191,205,206].

Chemokines are small cytokines that play an important role in chemotaxis and cell trafficking and function to attract immune cells, such as monocytes and neutrophils, to the site of infection in response to stimulation or other cytokines. Chemokines which are upregulated in

filovirus infection include MCP-1, MIP-1α, MIP-1β, regulated on activation, normal T cell expressed and secreted (RANTES), eotaxin, gro-α, IL-8 and Interferon gamma-induced protein 10 (IP-10). With respect to EBOV, increased levels of IL-8, MCP-1 and IP-10 have been associated with EBOV patients and fatal cases associated with high levels of IL-8, MCP-1, MIP-1α, MIP-1β, IP-10, gro-α, and eotaxin [193]. Similarly, upregulation of IL-8, MIP-1α, MIP-1β, and MCP-1 has been observed among MARV-infected NHPs [205,207–209]. Human SUDV infections were characterized by elevated levels of IP-10 and RANTES as well as IL-8 and MIP-1β, which were higher among fatal cases than survivors [210]. High levels of these chemokines result in the recruitment of inflammatory cells to the site of infection, including monocytes and macrophages, which contribute to tissue damage and pathology of filovirus infection and recruit additional cell targets for infection [194,201].

Interleukins (IL) are cytokines primarily produced by leukocytes and lymphocytes, among many other cell types. They are critical for the host immune response and can be pro-inflammatory or anti-inflammatory. Filovirus infections profoundly affect lymphocyte responses, with both EBOV and MARV inducing lymphocyte apoptosis. Correlated with this are low levels of important T-cell cytokines such as IL-2, IL-3, IL-4, IL-5, IL-9 and IL-13, which have been observed among fatal human EBOV cases [193] and in MARV-infected NHPs [205]. In contrast, asymptomatic EBOV patients exhibit elevated levels of IL-2 and IL-4, cytokines important for T-cell activation [211]. Similarly, high levels of IL-6 and IL-1β are associated with lethal human EBOV [193] and SUDV [210] infections as well as in MARV-infected NHPs [212]. Both IL-6 and IL-1β function as pro-inflammatory cytokines and have several overlapping functions serving as direct stimulants of the coagulation system and thus play a critical role in the coagulopathy associated with FVD [213]. More specifically, IL-6 serves as a transition cytokine, bridging innate

and adapted immune responses and recruitment and activation of monocytes and differentiation of T-cells [213]. IL-1β stimulates vasodilation and expression of adhesion molecules on endothelial cells, contributing to increased endothelial cell permeability and vascular leakage [213].

Indeed, the overzealous "cytokine storm" resulting from filovirus infection strongly correlates to fatal outcomes. In particular, inflammatory cytokines have been associated with increased mortality and are considered a key component of filovirus pathogenesis. Evidence has shown that the induction of cytokines and chemokines can vary depending on filovirus species and strains, potentially accounting for differences in their pathogenicity. For example, patients who survived SUDV infection were shown to have elevated levels of IFNα [210]. In contrast, in the case of EBOV, these elevated levels of IFNα were associated with fatal outcomes[191]. Similarly, lower TNFα and IFNγ expression among SUDV infections correlates with a longer time to death than that observed for EBOV [210]. Nonetheless, much remains unknown regarding cytokine levels in various tissue compartments during infection and a more detailed analysis is needed to provide insight into filovirus immunopathogenesis.

## 1.5. Immunity to Infection and Evasion Tactics of Filoviruses

Innate and adaptive immune responses, including both humoral and cell-mediated immune responses, play a critical role in combating filovirus infections. Filoviruses have evolved several mechanisms to counteract and evade these antiviral responses and promote infection. As described above, a characteristic feature of FVD is the "cytokine storm" characterized by the excessive production of pro-inflammatory cytokines and chemokines contributing to the immunopathogenesis of filoviruses. Much remains to be learned about innate and adaptive immune responses' contribution to the immunopathogenesis of filovirus infections. Indeed, the massive production of pro-inflammatory mediators during FVD results from the infection of macrophages

and monocytes, representing prominent sources of these molecules. While these cytokines comprise an essential component of the innate and adaptive immune responses to viral infections, their uncontrolled production plays a significant role in the clinical and pathological features of FVD. Nonetheless, the balance between pro-inflammatory and anti-inflammatory mediators, including cytokines and chemokines, heavily influences the outcome of infection, whether acute or chronic. The amalgamation of factors that influence this balance is a bottomless pit and remains to be fully elucidated and an active area of research. The factors influencing immunity and immunopathology and their impact on disease outcomes are comprehensively reviewed for select pathogens in [214].

### 1.5.1. Innate Immune Response

As described in *Section 1.4.3* , the host innate immune response, particularly the type I IFN response (IFN-α and IFN-β), plays a pivotal role in combatting filovirus infection by triggering a plethora of antiviral signalling pathways establishing an antiviral state and restricting viral replication. RIG-I and MDA5 are cytoplasmic RNA helicases that detect viral RNAs and induce IFN-response. Upon recognition of 5'triphosphates and dsRNA, RIG-1 and MDA5 become activated and, in turn, activate serine/threonine kinases, namely TANK-binding kinase 1 (TBK1) and IκB kinase-ε (IKKε) [215]. Upon activation, TBK1 and IKKε phosphorylate IFN regulatory factor (IRF)-3 and IRF7, transcription factors which, upon accumulation, engage IFN-stimulated response elements (ISREs), triggering the expression of type I IFNs [215].

Indeed, EBOV and MARV encode VP35, which functions as an antagonist of the innate immune response critical for inhibiting different stages of the IFN response. More specifically, VP35, via its C-terminal IFN inhibitory domain (IID), forms a novel fold that recognizes and binds dsRNA intermediates in a sequence-independent manner [216,217]. This, in turn, prevents the recognition of dsRNA intermediates by RIG-I and MDA-5, ultimately preventing the detection of

the pathogen-associated molecular patterns (PAMPs) [216,217]. Moreover, EBOV VP35 has also been demonstrated to block the phosphorylation of IRF3, a transcription factor essential for the induction of the IFN-β promoter [218]. Further to its role in suppressing IFN-α and IFN-β production, EBOV VP35 has also been shown to inhibit the activation of protein kinase R (PKR), an IFN-induced dsRNA activated kinase with well-characterized antiviral activity [219,220]. Lastly, VP35 has also been demonstrated to disrupt the maturation of DCs, a process that represents a critical link between innate and adaptive immune responses [221]. Much of what is known regarding VP35 as an antagonist of the innate immune response has been elucidated for EBOV; however, MARV VP35 is thought to behave similarly.

While both EBOV and MARV, through the activity of VP35, inhibit the production of type I IFNs, they also encode proteins, namely VP24 and VP40, which act to inhibit downstream signalling of ISGs via inhibition of the JAK/STAT pathway. The JAK/STAT pathway is composed of three components, namely the cell receptor, JAK and STAT proteins. Together, these components of the JAK/STAT pathway are essential for transmitting extracellular chemical signals (IFNs) to the nucleus, facilitating transcription and expression of specific effector genes known as ISGs [222]. Once secreted, type I IFNs bind a common cell-surface receptor referred to as the type I IFN receptor, composed of two distinct subunits: interferon alpha and beta receptor subunit (IFNAR)-1 and 2 [223,224]. Each subunit interacts with a member of the JAK family. Specifically, IFNAR1 interacts with tyrosine kinase 2 (TYK2) and IFNAR2 with JAK1 [223,224]. Binding of type I IFNs to IFNAR results in the rapid autophosphorylation and activation of TYK2 and JAK1, which in turn promotes the phosphorylation and activation of STATs, namely STAT1, STAT2, STAT3 and STAT5 [223,224]. In turn, these activated STATs form homo- or heterodimers, which translocate to the nucleus and, through binding to promoters, initiates the transcription of ISGs

[223,224]. These ISGs, among which there are >500, result in the expression of a plethora of proteins whose effector functions aim to combat infection through various mechanisms. Unfortunately, of the hundreds of ISGs, very few have been characterized *in vivo* to identify their contribution to antiviral immune responses [215]

Indeed, EBOV and MARV interfere with type I IFN signalling via the JAK/STAT pathway, albeit through different mechanisms. Particularly, this subversion is mediated by VP24 in the case of EBOV, which acts as a competitive inhibitor of pSTAT1. In contrast, in the case of MARV, this subversion is mediated by VP40, which blocks the activation and function of JAK1 [115]. More specifically, EBOV VP24 interacts with select karyopherin alpha (KPNA) proteins, which represent important nuclear import factors for transporting molecules from the cell cytoplasm into the nucleus through nuclear pores [225]. As such, EBOV VP24 competitively binds the pSTAT1 binding site of KPNA, ultimately impairing the nuclear entry of pSTAT1 into the nucleus [131,226]. As a result of this competitive inhibition, pSTAT1 translocation to the nucleus is impeded, preventing binding to ISG promoters effectively preventing their expression [131,226]. In contrast, MARV VP24 does not bind KPNAs or significantly alter IFN-induced gene expression [121]. Instead, inhibition of IFN signalling by MARV is mediated by VP40, which blocks the activation and function of JAK1 [121,122]. While JAK1 function is inhibited by MARV VP40, the underlying mechanism by which this is accomplished remains unknown, with a direct interaction between MARV VP40 and JAK1 having yet to be demonstrated.

### 1.5.2. Adaptive Immune Response

While innate immune responses play a vital role in controlling filovirus replication during the early stages of infection, adaptive immune responses, including both humoral and cell-mediated responses, are pivotal for viral clearance and recovery [227,228].

Indeed, humoral immune responses are correlated with positive human outcomes of FVD and are characterized by the early development of IgM and isotype switching to IgG, with fatal cases being associated with a lack of IgM [229–233]. Antibodies generated from the humoral immune response can have several effector functions, including neutralization and antibody-dependent cellular cytotoxicity (ADCC) or complement-mediated cytotoxicity (CMC). Neutralizing antibodies (NAbs) are antibodies which protect a cell from a pathogen by neutralizing the ability of the pathogen to infect a cell. In the case of filoviruses, NAbs exhibit their effector function by binding multiple epitopes of the surface-expressed glycoprotein, which, upon binding, cannot interreact with their intracellular receptor NPC1. Indeed, long-term survivors of EVD have been shown to develop effective NAbs against several epitopes of EBOV GP to appreciable titters [234,235]. Most of these NAbs appear to target the GP glycan cap and the region bridging GP1 and GP2 [236]. While NAbs produced among EVD survivors appear to be capable of effectively neutralizing EBOV, they likely play a small role in recovery from acute EVD, given that they are not detectable until weeks or months after recovery [237]. Like EBOV, humans infected with MARV also develop NAbs, primarily targeting the surface-exposed glycoprotein [238–240]. Indeed, filovirus GP represents the primary antigenic target of many post-exposure therapeutics, predominantly monoclonal antibodies (mAbs) such as ZMapp [241], Mab114 [242] and REGN-EB3 [243] for EBOV and MR191-N [244] for MARV. Unfortunately, few studies have evaluated the host-humoral immune response in humans diagnosed with FVD, given the difficulties associated with accessing samples. As such, the majority of what is known about the host humoral immune response has been deduced using NHPs as models. As mentioned previously, fatal cases of EBOD are associated with severe depletion of T cells, including both CD4+ and CD8+ T cells, whereas in the case of survivors, this depletion is less pronounced [193].

## 1.6. Classical Animal Models

Animal models represent critical tools for studying many aspects of filoviruses, most notably viral pathogenesis and the efficacy of candidate countermeasures or therapeutics. Indeed, several animal models have been developed and utilized to date, including rodents such as immunocompetent and immunocompromised mice, hamsters, and guinea pigs. These rodent models are classical small animal models, each providing their own unique advantage. More recently, ferrets have become popular as intermediate-sized animals of higher sentient order than rodents, and they represent a novel, non-classical animal model for filoviruses. Lastly, NHPs are considered the gold-standard animal model as they share many physiological and anatomical features with humans and often represent the final animal for investigating the efficacy of candidate countermeasures *in vivo*.

*Animal models will only be discussed for EBOV, MARV and RAVV*

### 1.6.1. Rodents

Rodents offer several advantages as models for studying filoviruses, most notably their small size, low cost and ease of use in high containment. Unfortunately, most rodent models, except for immunocompromised mice, are not susceptible to wild-type filoviruses, making them less ideal for pathogenic evaluations. This section will discuss classical rodent models, including immunocompetent and immunocompromised mice, hamsters, and guinea pigs.

#### 1.6.1.1. Immunocompetent Mice (*Mus musculus*)

Immunocompetent BALB/c mice are resistant to disease caused by WT-EBOV [245], WT-MARV and WT-RAVV [246,247] regardless of challenge route and dose [248,249]. More specifically, these animals do not demonstrate any deviations in weight or temperature following infection or exhibit any other clinical manifestations of disease [245,247]. While these animals do not develop disease, they support the replication of WT-EBOV and WT-MARV with

dissemination to the tissues before being cleared from the host [245,247]. Additionally, WT-MARV inoculated mice do not demonstrate any significant deviations from baseline hematology concerning plasma biochemistry or complete blood counts (CBC) [247].

To establish a uniformly lethal EBOV, WT-EBOV$_{Mayinga}$ was sequentially passaged nine times in progressively older suckling mice [250]. The resulting plaque-purified mouse-adapted (MA)-EBOV was lethal in adult BALB/C, CD-1 and C57BL/6 mice at infectious doses of 1-100 plaque-forming units (PFU) or 30-3,000 median lethal dose ($LD_{50}$) via the intraperitoneal route (IP) [250]. Surprisingly, inoculation with MA-EBOV at a dose of $10^6$ PFU via the subcutaneous (SC) or intramuscular (IM) route was non-lethal among mice with no symptoms of disease [250,251]. Inoculation with MA-EBOV via the IP route results in uniform lethality between 4-7 days post-infection (dpi) [250,251]. The clinical course of disease among mice infected with MA-EBOV$_{Mayinga}$ closely resembles what is observed in NHPs, including significant weight loss observable as early as 3 dpi [250]. Additionally, infected BALB/c mice supported high levels of viral replication with viral titers in the liver and spleen exceeding $10^7$ PFU/g at 2 dpi and peak serum virus titers of 7.5 x $10^7$ PFU/mL reached at 3 dpi [250]. By comparison, BALB/c mice inoculated with WT-EBOV supported low levels of replication with viral titers in the spleen ranging from 3 x $10^3$ – 1.2 x $10^5$ PFU/g and liver from 4 x $10^3$ – 1.5 x $10^4$ PFU/g [250]. Moreover, histopathological data demonstrate extensive necrosis of the liver, spleen and kidney, similar to what is seen in NHPs [250,252]. Infected mice demonstrated disruptions in blood biochemistry with highly elevated levels of AST and ALT, mildly elevated levels of alkaline phosphatase (ALP), gamma-glutamyl transferase (GGT) and bilirubin, decreased levels of BUN and stable levels of CRE [253]. These animals also show widespread lymphocyte apoptosis, a hallmark feature of EBOD observed in humans and NHPs [250–252,254]. Production of pro-inflammatory cytokines,

namely TNF-α, IFN-γ, IL-8, MIP-1α, MIP-1β and MCP-1, also closely resembled that seen in NHPs infected with EBOV [251,255]. Interestingly, BALB/C and C57BL/6 mice exhibit little to no coagulopathy or hemorrhagic manifestations, including tissue fibrin deposition, DIC or maculopapular/petechial rash, a hallmark feature of EBOD in NHPs.

More recently, using reverse genetics, Kobasa et al. developed MA-EBOV derived from the Makona isolate responsible for the 2014 West African Ebola epidemic [256]. To generate MA-$EBOV_{Makona}$, seven mutations from MA-$EBOV_{Mayinga}$ were inserted into the Makona genome, and the resulting rescued virus serially passaged in suckling mice until a uniformly lethal virus was achieved after eight passages [256]. The resulting MA-$EBOV_{Mayinga}$ was uniformly lethal in BALB/c mice, with the time of death ranging from 6-9 dpi and an $LD_{50}$ of 0.004 PFU [256]. Similar to MA-$EBOV_{Mayinga}$, MA-$EBOV_{Makona}$ replicated to high titres in BALB/c mice with mean titers in the blood ranging from 6.8-8.7 $Log_{10}$ $TCID_{50}$/mL at 5 dpi [256]. Likewise, the virus disseminated to several tissues, including the liver, spleen, kidney, lung and intestine, to moderate-high titers [256]. The brain was the sole tissue where the virus could not be detected [256]. Moreover, MA-$EBOV_{Makona}$ animals also exhibited lymphopenia along with elevated levels of monocytes (MON) and neutrophils (NEU) and, like MA-$EBOV_{Mayinga}$, showed no significant changes in PLT [256]. Blood biochemistry for MA-$EBOV_{Makona}$ revealed minimal changes to ALP and ALT in contrast to MA-$EBOV_{Mayinga}$, which showed significantly elevated levels of ALP at 5 dpi [256]. Lastly, animals challenged with MA-$EBOV_{Makona}$ demonstrate a robust pro-inflammatory cytokine and chemokine response through 5 dpi [256].

With respect to genotype, MA-$EBOV_{Mayinga}$ contained a total of 13 mutations, with four mutations present prior to host adaptation [257]. Among these nine mutations, five resulted in non-synonymous amino acid substitutions, with only two of these mutations, namely S72G in NP and

T50I in VP24, required to confer virulence (Figure 4A) [257]. While the exact molecular function of these two mutations remains unknown, it is thought that they may play an important role in the mouse IFN response [257]. In contrast, the MA-EBOV$_{Makona}$ contained the same mutations as MA-EBOV$_{Mayinga}$ plus an additional two mutations, namely H630N in NP and K212M in VP24, with only the K212M being critical for virulence (Figure 4A)[256].

Like EBOV, WT-MARV and WT-RAVV do not cause disease in immunocompetent mice regardless of challenge route and dose [246,247]. To overcome this, Warfield et al. serially passaged WT-MARV isolates Ci67 and Musoke and WT-RAVV in severe combined immunodeficient (SCID) BALB/c mice [258]. To achieve this, groups of mice (n=10) were inoculated via the IP route with 1000 PFU of either WT-MARV isolates Ci67 and Musoke and WT-RAVV, and two animals from each group euthanized at 7 dpi for subsequent infection of a new group of SCID mice with liver homogenates [258]. This serial passaging was continued until uniform lethality was achieved with a mean time to death of <10 days. Generation of MA-MARV$_{Ci67}$ required 15 passages in SCID mice followed by 14 passages in BALB/c mice, whereas generation of MA-RAVV required 10 passages in SCID mice followed by 14 passages in BALB/c mice [247,259].

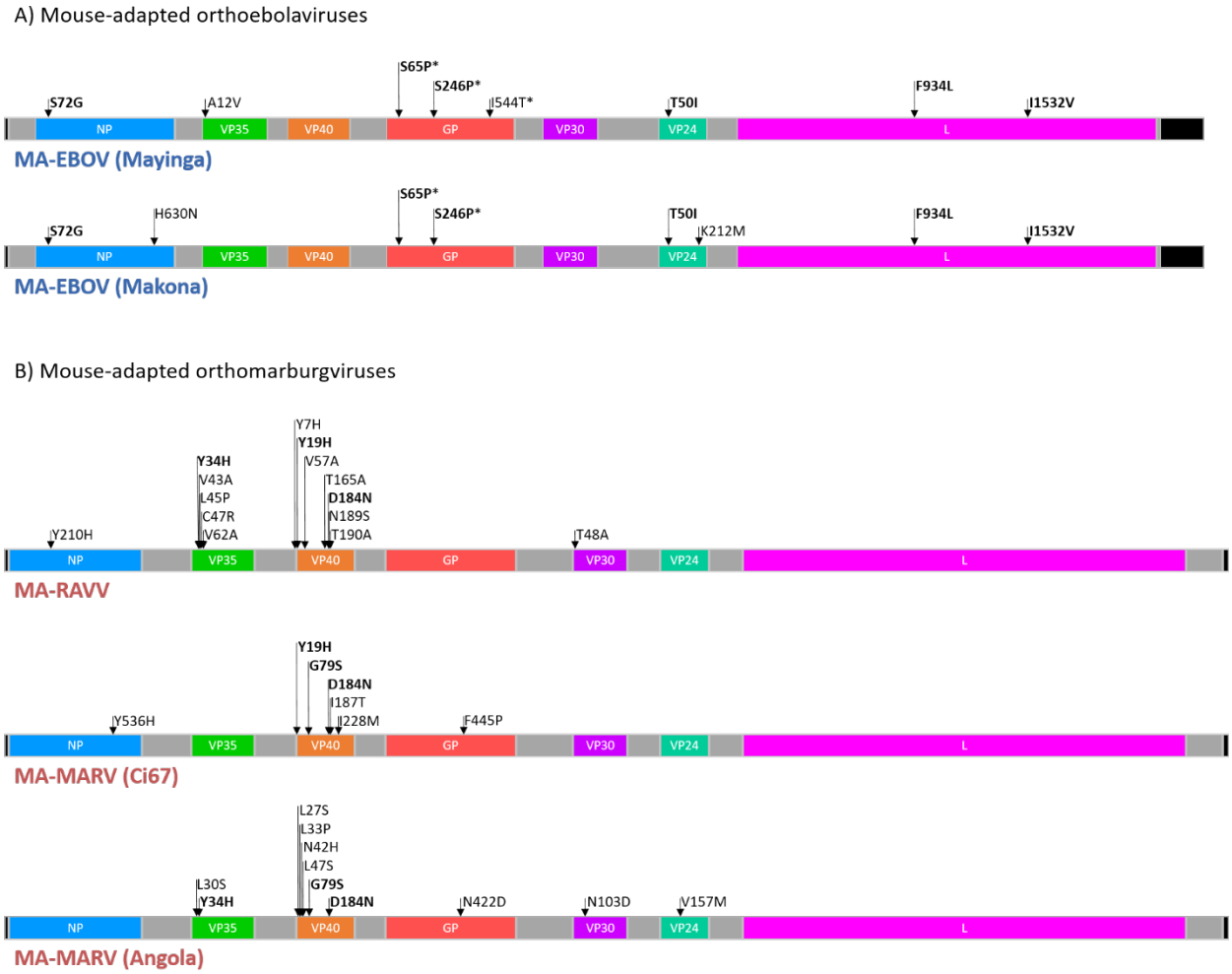


**Figure 4. Depiction of non-synonymous mutations in mouse-adapted (MA) filoviruses.**

Non-synonymous mutations are indicated with arrows along the length of the (**A**) Orthoebolavirus or (**B**) orthomarburgvirus genomes. Amino acid mutations are denoted using the one-letter amino acid code and the number of the residue mutated in each particular protein. Mutations in bold text are those which appear in more than one adapted virus. Listed mutations are relative to the wild type isolate from which the adapted virus is derived.

The resulting MA-MARV$_{Ci67}$ was only partially lethal in BALB/c, with 80% of animals succumbing to disease by 10 dpi and 60% of C57BL/6 mice by 12 dpi following IP inoculation [259]. In contrast, MA-RAVV is uniformly lethal in BALB/c and C57BL/6 mice, with all animals succumbing to disease at 8 and 12 dpi, respectively [259]. In 2014, Qiu et al. serially passaged WT-MARV$_{Angola}$ in SCID mice with a uniformly lethal MA-MARV$_{Angola}$ achieved after 24 passages [260]. The resulting MA-MARV$_{Angola}$ was determined to have an $LD_{50}$ of 0.05 $TCID_{50}$ in

BALB/c mice for the IP route [260]. Moreover, MA-MARV$_{Angola}$ was uniformly lethal in BALB/c and C57BL/6 mice, with all animals succumbing to disease by 7 and 8 dpi, respectively, following IP inoculation with 2000 x $LD_{50}$ [260]. Interestingly, MA-MARV$_{Angola}$ was also partially lethal in BALB/c following intranasal (IN) inoculation, with 80% of animals succumbing to diseases by 10 dpi [260]. MA-MARV$_{Angola}$ was non-lethal in BALB/c mice inoculated via the IM route [260]. None of the mouse-adapted orthomarburgviruses cause disease following SC inoculation, similar to what is observed for MA-EBOV. Other routes tested for MA-RAVV include tail, footpad and IM, all of which were non-lethal in BALB/c mice [247]

All viruses, namely MA-RAVV, MA-MARV$_{Angola}$ and MA-MARV$_{Ci67}$, replicated to high titers within blood and disseminated to multiple tissues, including spleen, liver and kidney as well as immune privilege niches including brain and gonads [247,259,260]. Interestingly, WT-RAVV was capable of replicating within the blood of inoculated BALB/c mice and disseminating to several tissues, although levels were significantly lower than those observed for MA-RAVV [247]. While WT-MARV$_{Angola}$ was capable of replicating within the blood of inoculated BALB/c mice, the virus was unable to spread systemically to the tissues, unlike what is observed for MA-MARV$_{Angola}$ [260]. Pathological features among infected mice infected with MA-RAVV or MA-MARV$_{Angola}$ are similar, with antigen detectable 3-5 dpi in the spleen and liver with prominent hepatocellular degeneration and necrosis [247,260]. Regarding biochemistry, an increase in AST and ALT can be observed throughout the course of disease, indicative of decreased liver function among mice infected with MA-RAVV and MA-MARV$_{Angola}$ [247,260]. CBC analysis revealed a decrease in white blood cells (WBC) and lymphocytes (LYM) among MA-RAVV and MA-MARV$_{Angola}$ infected mice as well as a reduction in PLT observable 3-5 dpi [247,260]. Lastly, both MA-RAVV and MA-MARV$_{Angola}$ inoculated mice demonstrated increased levels of several

cytokines and chemokines, including TNF-α, IFN-γ, IL-6, IL-5 and MCP-1, among others indicating a dysregulated immune response [247,260]. In contrast, none of the cytokines and chemokines demonstrated significant changes following inoculation with WT-RAVV and WT-$MARV_{Angola}$ [247,260].

Concerning genotype, MA-RAVV, MA-$MARV_{Ci67}$ and MA-$MARV_{Angola}$ contain a total of 14, seven and 11 non-synonymous mutations, respectively (Figure 4B) [248]. Among these mutations, MA-RAVV contains one mutation in NP, five in VP35, seven in VP40 and one in VP30; MA-$MARV_{Ci67}$ contains one mutation in NP, five in VP40 and one in GP; MA-$MARV_{Angola}$ contains two mutations in VP35, six in VP40, one in GP, one in VP30 and one in VP24 [248]. MA-RAVV, MA-$MARV_{Ci67}$ and MA-$MARV_{Angola}$ contain seven, five and six amino acid mutations, respectively, within VP40, with all three viruses sharing a single common mutation, namely D184N (Figure 4B) [248]. A higher number of mutations within VP40 suggests potential adaptations to enhance VP40's ability to subvert the host's innate immune response. Indeed, the mutations V57A and T165A found VP40 of MA-RAVV have been shown to be critical for inhibiting the IFN response in both human and mouse cells by preventing JAK1 phosphorylation [122]. Interestingly, both MA-$MARV_{Ci67}$ and MA-$MARV_{Angola}$ lack these two mutations yet are still capable of countering the IFN in response in mouse cells, an ability linked to the G79S mutation [261]. Additionally, both MA-RAVV and MA-$MARV_{Ci67}$ share a common Y19H mutation in VP40, whereas MA-$MARV_{Ci67}$ and MA-$MARV_{Angola}$ share the G79S mutation (Figure 4B)[248].

In short, this adaptation process involving the serial passaging of the virus within a given host forces the virus to adapt in response to selective pressures applied by the host organism, including both innate and adaptive immune responses. As a result of these selective forces,

pressure is applied to the virus, driving changes to the virus genotype, many of which result in changes to the protein-coding sequences to proteins essential for immune evasion and viral replication, such as VP35, VP40 and VP24. The amalgamation of these mutations to VPs effectively orchestrates together, augmenting several aspects of the virus life cycle, such as immune evasion and viral replication. This coordination ultimately enhances the virus's pathogenesis within an otherwise refractive host species.

#### 1.6.1.2. Immunocompromised Mice (*Mus musculus*)

Commercially available IFN-α/β receptor knockout ($IFNAR^{-/-}$) mice are susceptible to infection with WT-EBOV, WT-RAVV and WT-MARV following IP inoculation, each of which are non-lethal in immunocompetent BALB/c mice [245–247]. Interestingly, these mice are also susceptible to SC infection with MA-EBOV, unlike immunocompetent mice, which are not susceptible to infection via the SC route [245]. While $WT\text{-}EBOV_{Mayinga}$ is lethal in $IFNAR^{-/-}$ mice, $WT\text{-}EBOV_{Kikwit}$ is non-lethal despite both isolates causing similar virulence in NHPs [245]. Unlike immunocompetent BALB/c mice, which are only susceptible to MA-EBOV and MA-RAVV via the IP route, $IFNAR^{-/-}$ mice are susceptible to infection via other routes, including aerosol exposure [262]. These $IFNAR^{-/-}$ mice support viral replication within the blood and dissemination to tissues, notably the liver and spleen. Like $IFNAR^{-/-}$ mice, STAT-1 knockout mice ($STAT1^{-/-}$) are also susceptible to WT-EBOV and WT-MARV, which following 1000 PFU IP inoculation results in lethal disease within 7 dpi [263]. As expected, $STAT1^{-/-}$ mice are also susceptible to lethal infection with MA-EBOV, with disease onset being more rapid and severe than that observed for WT-EBOV [263]. Taken together, $IFNAR^{-/-}$ mice defective in type I IFN singling and $STAT1^{-/-}$ mice defective in type I, II and III IFN signalling are suspectable to WT-EBOV and WT-MARV, unlike immunocompetent mice, further emphasizing the importance of the host IFN response at combatting filovirus infection. SCID mice lack B and T-cells and are uniformly

susceptible to infection with WT-EBOV, WT-MARV (Musoke and Ci67), and RAVV [245,258]. The disease course in these mice is considerably longer, with lethality achieved only 3-8 weeks after inoculation [258]. These immunocompromised mouse models support high viremia and dissemination to the tissues and exhibit characteristic features of FVD, including lymphopenia, thrombocytopenia, neutrophilia, kidney dysfunction and liver damage [245,258]. Additional disease features include fever, huddling, weight loss, dehydration and diarrhea, and alterations in serum biochemistry from baseline [245,258]. Together, these immunocompromised mouse models are ideal for evaluating the virulence and pathogenesis of filoviruses for which no rodent-adapted viruses exist.

#### 1.6.1.3. Syrian Golden Hamsters (*Mesocricetus auratus*)

Similar to mice, Syrian golden hamsters are not suspectable to infection with WT-EBOV or WT-MARV, with inoculated animals exhibiting no clinical signs of disease [264–267]. Although these animals do not develop disease, they support the replication of WT-EBOV and WT-MARV with dissemination to tissues, including the liver and spleen, albeit to low levels [265,266].

Although WT-EBOV does not cause disease in hamsters, inoculation with 1000 focus forming units (FFU) of MA-EBOV$_{Mayinga}$ via the IP route results in uniform lethality 4-5 dpi [265]. Like mice, inoculation with MA-EBOV$_{Mayinga}$ via the SC route with doses ranging from 10 to $10^5$ FFU fails to produce lethal disease [265]. Hamsters infected with MA-EBOV begin manifesting clinical signs of disease as early as 3 dpi, with the most notable signs being ruffled fur and decreased activity [265]. MA-EBOV-infected hamsters also demonstrated significantly prolonged prothrombin time (PT), activated partial thromboplastin time (aPTT) and thrombin time (TT) values during late stages of infection, suggesting severe coagulopathy in fatally infected animals [265]. This severe coagulopathy is not observed in hamsters infected with WT-EBOV [265].

Fibrinogen levels among MA-EBOV-infected hamsters were elevated at 3 dpi, with peak levels at 4 dpi before dropping just before death [265]. WT-EBOV inoculated animals also demonstrated elevated levels of fibrinogen that peaked at 5 dpi before returning to normal at 8 dpi [265]. Unlike WT-EBOV, MA-EBOV replicated to high titers with systemic spread to all tested organs, including the spleen, liver, kidney, heart, lung and brain [265]. Lymphocytopenia and thrombocytopenia could also be observed among MA-EBOV-infected hamsters and absent among WT-EBOV-challenged animals [265]. Quantitative real-time RT-PCR (RT-qPCR) analysis of the spleen, liver and blood demonstrated significant activation of pro-inflammatory and anti-inflammatory responses following infection with MA-EBOV [265]. However, this response was weak following inoculation with WT-EBOV [265]. Proinflammatory cytokines and chemokines, including IL-1β, IL-6, and IL-10, were upregulated in the spleen and IL-1β, IL-6, TNF-α, IL-12p35, IP-10 in the liver [265]. All tested cytokines were strongly upregulated in terminal blood samples, mirroring what is observed in humans and NHPs.

As with WT-EBOV, WT-MARV does not cause disease in Syrian golden hamsters. To overcome this, Marzi et al. developed a hamster-adapted (HA)-MARV based on the variant Angola [266]. To establish HA-$MARV_{Angola}$, WT-$MARV_{Angola}$ was serially passaged three times in Hartley guinea pigs (*Cavia porcellus*) until uniform lethality was achieved, followed by five passages of the resulting guinea pig adapted (GPA)-MARV in Syrian golden hamsters yielding HA-$MARV_{Angola}$ [266]. Inoculation with 0.1 to 1000 PFU via the IP route results in uniform lethality, with hamsters succumbing to disease between 7 and 11 dpi [266]. The $LD_{50}$ of HA-$MARV_{Angola}$ in hamsters was calculated to be 0.01 PFU [266]. Hamsters inoculated with HA-$MARV_{Angola}$ demonstrate decreased activity with significant weight loss observable at 5 dpi, with this trend continuing until time of euthanasia at 8 dpi [266]. Moreover, these animals exhibited a significant

spike in body temperature at 6 dpi, followed by a dramatic drop during the terminal stages of the disease [266]. In contrast, animals challenged with WT-MARV$_{Angola}$ are clinically healthy following inoculation with increases in weight and no change in body temperature throughout the study [266]. Remarkably, by 7 dpi, all hamsters developed a maculopapular rash with visible petechiae on the face, chest, abdomen and limbs [266]. Additionally, hamsters demonstrate severe coagulopathy similar to what is observed in humans and NHPs with significantly elevated PT, aPTT and TT during the late stages of the disease, indicating delays in blood clot formation [266]. Hematological analysis was consistent with other rodent models, including leukocytosis, neutrophilia and lymphopenia, and elevated levels of liver enzymes, including ALT, AST, and ALP [266]. Viral replication was systemic and robust, with peak titers reaching $10^8$ TCID$_{50}$/mL in the blood and $10^6$-$10^7$ TCID$_{50}$/mL in the liver and spleen at time of euthanasia at 8 dpi [266]. mRNA transcript levels for many cytokines and chemokines were analyzed from the liver, spleen and blood to investigate innate immune response mounted following infection. In the blood, IP-10, IL-6, TNF-α, and IL-4 transcripts were all significantly higher in WT-MARV-infected animals compared to HA-MARV at 4 dpi [266]. IL-6 and IL-4 increased significantly among HA-MARV-infected animals during the terminal stage of infection at 6 dpi [266]. Other gene transcripts, including pro-inflammatory cytokines TNF-α and IL-6, Th2 cytokines IL-4 and IL-5 and Th1 cytokines IL-12, were all elevated early on in infection before decreasing throughout the disease [266]. Concerning genotype, the established HA-MARV$_{Angola}$ had 61 mutations; however, only three were non-synonymous, namely L33P in VP35 and G106D and D184N in VP40 (Figure 5) [266]. Among these mutations, D184N in VP40 has previously been identified in MA-RAVV [247], MA-MARV (Ci67 & Angola) [259,260] and GPA-MARV$_{Musoke}$ [268] and has been found to promote nucleocapsid recruitment and virion budding [269]. How VP35 L33P and VP40 G106D

affect IFN antagonism remains unknown but are thought to contribute to the virulence of HA-MARV$_{Angola}$ in some manner [266].




**Figure 5. Depiction of non-synonymous mutations in hamster-adapted Marburg virus**

Non-synonymous mutations are indicated with arrows along the length of the Orthomarburgvirus genomes. Amino acid mutations are denoted using the one-letter amino acid code and the number of the residue mutated in each particular protein. Mutations in bold text are those which appear in more than one adapted virus. Listed mutations are relative to the wild-type isolate from which the adapted virus is derived.

More recently, Cross et al. conducted a study to model MARD in Syrian golden hamsters, contrasting the virulence of the Angola and Ci67 strains of MARV [270]. In this study, Cross et al. developed a HA-MARV$_{Ci67}$ through the serial passaging of GPA-MARV$_{Ci67}$ in hamsters until uniform lethality was achieved after three passages [270]. Moreover, they investigated the pathogenesis of previously established GPA-MARV strains Ci67 and Angola and GPA-RAVV within hamsters [270,271]. Inoculation of hamsters with 1000 PFU of GPA-MARV$_{Angola}$ via the IP route results in uniformly lethal disease with a mean time of death of 7.5 dpi [270]. In contrast, GPA-MARV$_{Ci67}$ was only partially lethal, with 50% of animals succumbing to disease, and this lethality increased to 66% after a single passage. Similarly, GPA-RAVV was also partially lethal, with 75% of animals succumbing to disease following four passages in hamsters [270]. The established HA-MARV$_{Ci67}$ resulted in uniformly lethal disease with a mean time of death of 8.5 dpi [270]. HA-MARV$_{Ci67}$ hamsters demonstrated weight loss at 3 dpi, which continued throughout the duration until endpoint, whereas in the case of GPA-MARV$_{Angola}$, this weight loss was less pronounced [270]. Both GPA-MARV$_{Angola}$ and HA-MARV$_{Ci67}$ animals were viremic as early as 3 dpi with peak viral titers in the blood of ~ 1 x $10^{6.5}$ PFU/mL [270]. Overall, viral titers in the liver, spleen and kidney were higher among GPA-MARV$_{Angola}$ challenged hamsters compared to HA-

$MARV_{Ci67}$ [270]. GPA-$MARV_{Angola}$ and HA-$MARV_{Ci67}$ both demonstrated perturbations in CBC, including lymphocytopenia, neutrophilia and late-stage thrombosis, as well as elevated ALP, suggesting impaired liver function [270]. While both GPA-$MARV_{Angola}$ and HA-$MARV_{Ci67}$ resulted in severe coagulopathy, GPA-$MARV_{Angola}$ challenged hamsters have prolonged PT and aPTT at 7 dpi compared to HA-$MARV_{Ci67}$ [270]. Additionally, GPA-$MARV_{Angola}$ and HA-$MARV_{Ci67}$ both developed severe petechial rash following infection [270]. Sequencing of HA-$MARV_{Ci67}$ has yet to be published, and as such, no comment can be made regarding mutations resulting in host adaptation.

Further to immunocompetent hamsters, an immunodeficient hamster model has also been described for orthomarburgviruses using STAT2 knockout ($STAT2^{-/-}$) hamsters deficient in STAT2 signalling [272]. These STAT2 knockout (KO) hamsters are uniformly susceptible to IP infection with $10^5$ PFU WT-MARV variant Musoke and Voege, with all animals succumbing to disease by 12 dpi [272]. In contrast, inoculation with WT-RAVV was non-lethal, whereas infection with WT-$MARV_{Angola}$ was partially lethal, with 80% of animals reaching euthanasia criteria by 20 dpi [272]. Animals infected with WT-MARV variant Musoke and Voege manifested signs of disease, including ruffled fur, lethargy and weight loss by 5 dpi [272]. In the case of WT-$MARV_{Angola}$, the onset of the disease was delayed. Similarly, WT-RAVV-challenged hamsters demonstrated weight loss that peaked at 16 dpi, followed by recovery and weight gain until the study endpoint at 28 dpi [272]. The $LD_{50}$ for WT-$MARV_{Musoke}$ was calculated to be 10 PFU, with 50% of animals succumbing to disease between 9 and 11 dpi [272]. STAT2 KO hamsters became viremic at 4 dpi with peak titers in the blood of $10^8$ PFU/mL reached by 5 dpi [272]. Dissemination to all tested tissues was observable between 4 and 8 dpi with infectious titers ranging from $10^5$-$10^6$ PFU/mL in liver, spleen, lung, heart and kidney [272]. The virus was also delectable in lymph

nodes and the brain to moderate titers [272]. None of the animals had observable maculopapular or petechial rash throughout the study [272]. Hematological analysis revealed no significant changes in analyzed parameters among infected animals, particularly PLT counts [272]. Analysis of mRNA transcripts revealed increased levels of several cytokines and chemokines throughout the disease. More specifically, MIP-1α and IP-10 were elevated within the liver, with peak levels reached at 6 dpi [272]. Similarly, pro-inflammatory cytokines IL-6, TNF-α and IL-1β peaked at 2,4 and 6 dpi respectively [272]. Additional cytokines and chemokines, including IL-2 and IL10, as well as Th1 cytokine IL-12 and Th2 cytokines IL-5 and IL-12, were all elevated at various times throughout the disease across several tissues [272].

#### 1.6.1.4. Guinea Pigs (*Cavia porcellus)*

Like other rodent models, infection of adult oatbread Hartley guinea pigs with WT-EBOV results in febrile illness, whereas infection of inbred strain 13 guinea pigs results in 20% lethality [273–275]. Nonetheless, evidence of viral infection can be detected in the liver of guinea pigs infected with WT-EBOV with viral titres of 1.1-1.3 x $10^5$ PFU/mL at 7-8 dpi [274]. Likewise, infection of Hartley guinea pigs with WT-MARV results in mild febrile illness approximately 4-10 dpi with manifestations of disease including weight loss, decreased activity, ruffled fur and diarrhea lasting 4-6 days [1,264,274].

To overcome this, several groups have developed GPA-EBOV through serial passaging in Guinea pigs. Indeed, several GPA-EBOV derived from the Mayinga isolate have been developed, including GPA-EBOV$_{8mc}$ [276], GPA-EBOV$_{P7}$ [277], GPA-EBOV$_{USAMRIID}$ [273], GPA-EBOV$_{UTMB}$ [278] and GPA-EBOV$_{K5}$ [279]. Generation of GPA-EBOV$_{K5}$ required a total of 24 passages on Vero E6 cells, three passages in NHPs, 15 passages in L68 cells, followed by five passages in Hartley guinea pigs [279]. Only the VP24 coding sequence was sequenced for GPA-EBOV$_{K5}$ and contained two non-synonymous mutations, namely H186Y and D165G, which were

present prior to adaptation (Figure 6A) [276]. Generation GPA-EBOV$_{8mc}$ required a total of 24 passages on Vero E6 cells followed by eight passages in Hartley Guinea pigs with the resulting GPA-EBOV$_{8mc}$ containing a total of six non-synonymous mutations, namely F648L in NP, D397G in GP, M71I, L147P and T187I in VP24 and T820A in L (Figure 6A) [276]. Generation of GPA-EBOV$_{P7}$ required a total seven passages in Hartley guinea pigs, with the resulting GPA-EBOV$_{P7}$ containing a total of 10 non-synonymous mutations namely N438H, R525K, L544P, N566S, S598P, and S647F in NP, M71I, L147P and R154L in VP24 and V236I in L (Figure 6A) [277]. Mutations N438H, R525K and S647F were present before adaptation [277]. Generation of GPA-EBOV$_{USAMRIID}$ required seven passages in strain 13 guinea pigs to achieve uniform lethality [273]. The sequence of GPA-EBOV$_{USAMRIID}$ has yet to be published. Lastly, the generation of GPA-EBOV$_{UTMB}$ required a total of four passages in strain 13 guinea pigs, with the resulting GPA-EBOV$_{UTMB}$ containing a total of five non-synonymous mutations, namely A575T and S647Y in NP, I544T in GP and L26F and K142E in VP24 (Figure 6A) [278]. Overall, infection of guinea pigs with the aforementioned GPA-EBOVs results in uniform lethality at 8-12 dpi, with onset of febrile illness observable at 4-7 dpi [253,273,277,278]. The most thorough characterization and modelling have been done for GPA-EBOV$_{USAMRIID}$ and will be the focus of this section.




**Figure 6. Depiction of non-synonymous mutations in Guinea pig-adapted (GPA) filoviruses**

Non-synonymous mutations are indicated with arrows along the length of the (**A**) Orthoebolavirus or (**B**) orthomarburgvirus genomes. Amino acid mutations are denoted using the one-letter amino acid code and the number of the residue mutated in each particular protein. Mutations in bold text are those which appear in more than one adapted virus. Listed mutations are relative to the wild type isolate from which the adapted virus is derived.

Inoculation of strain 13 guinea pigs with $10^{3.8}$ pfu of GPA-EBOV$_{USAMRIID}$ via the SC route results in uniform lethality with a mean time of death of 9.05 dpi [273]. Clinical signs of disease were minimal, up to 7 dpi, after which animals began exhibiting signs of febrile illness accompanied by dehydration with no signs of hemorrhage at the time of euthanasia, around 9 dpi [273]. The onset of viremia occurred within 48 h post-infection with mean levels of 1.8 $\log_{10}$ PFU/mL, with peak levels observed at 7 dpi with a mean value of 5.2 $\log_{10}$ PFU/mL [273]. Infectious virus within the tissues was first detectable within the spleen and liver at 2 dpi, followed by the kidney, adrenal, lung and pancreas at 3 dpi [273]. Peak titers were reached within tissues at

9 dpi with mean levels ranging from 4.8-6.4 $log_{10}$ PFU/g [273]. Regarding CBC, all animals exhibited leukocytosis due to increasing neutrophilia and observable lymphopenia at the time of death at 9 dpi and thrombocytopenia as early as 7 dpi [273]. Serum biochemistry demonstrated elevated levels of BUN, AST and ALT characteristic of EBOD in humans [273]. Moreover, infected animals demonstrated signs of coagulation abnormalities characterized by prolonged PT and aPTT, decreased protein C activity, and elevated levels of inflammatory mediators, including TNF-α, IL-6 and nitric oxide [278].

Like EBOV, WT-MARV does not cause lethal disease in guinea pigs [1,264]. To overcome this, several groups have developed guinea pig-adapted viruses, namely GPA-$RAVV_{USAMRID}$ and GPA-$RAVV_{UTMB,}$ as well as GPA-MARVs derived from Ci67, Musoke and Angola variants [268,271].

Generation of GPA-$RAVV_{USAMRID}$ required only 1-2 passages in strain 13 guinea pigs, with the resulting adapted virus containing a total of five non-synonymous mutations, namely T14S in NP, L27S, L33P and F53S in VP40 and G435A in GP (Figure 6B) [271]. In contrast, the generation of GPA-$RAVV_{UTMB}$ required two passages in strain 13 guinea pigs followed by two passages in Hartley guinea pigs with the resulting adapted virus containing the identical non-synonymous mutations as GPA-$RAVV_{USAMRID}$ except for the mutation in GP, which was N283H rather than the G435A present in GPA-$RAVV_{UTMB}$ [268]. Generation of GPA-$MARV_{Ci67}$ required 1-2 passages in strain 13 guinea pigs, with the resulting adapted virus containing a total of two non-synonymous mutations, namely C50R in VP35 and D184N in VP40 (Figure 6B) [268]. By comparison, the generation of GPA-$MARV_{Musoke}$ required eight passages in strain 13 guinea pigs with the resulting adapted virus containing a total of four non-synonymous mutations, namely D184N in VP40 and S742C, D759A and A760D in L (Figure 6B) [268]. Lastly, the generation of

GPA-MARV$_{Angola}$ required only three passages in Hartley guinea pigs, with the resulting adapted virus containing a total of three non-synonymous mutations, namely N56K in VP40 and V66I and L216S in VP24 (Figure 6B) [271].

While survival rates were not reported for GPA-RAVV$_{USAMRID,}$ inoculation of outbred Hartley guinea pigs with 5000 PFU GPA-RAVV$_{UTMB}$ via the IP route results in uniform lethality by 10 dpi [271]. By comparison, inoculation with $10^3$ PFU of GPA-MARV$_{Musoke}$ results in a mortality rate of 95% for strain 13 guinea pigs and 91% for Hartley guinea pigs with a mean time of death of 10 days [268]. By comparison, GPA-MARV$_{Angola}$ was only partially lethal in Hartley guinea pigs inoculated with 5000 PFU via the IP route, with 75% of animals succumbing to disease by study endpoint at 10 dpi [271]. Animals infected with GPA-RAVV$_{UTMB}$ or GPA-MARV$_{Angola}$ become viremic as early as 3 dpi with peak titers of 7.9 $\log_{10}$ PFU/mL reached by 7 dpi for GPA-MARV$_{Angola}$ compared to only 6.4 $\log_{10}$ PFU/mL for GPA-RAVV$_{UTMB}$ [271]. Viremia among Hartley and strain 13 guinea pigs infected with GPA-MARV$_{Musoke}$ was lower, with mean levels of 4.9 $\log_{10}$ PFU/mL at 7 dpi [268]. Additionally, virus dissemination for GPA-RAVV$_{UTMB}$ and GPA-MARV$_{Angola}$ was observed as early as 3 dpi within the spleen, lung and liver, with increasing titers observed throughout terminal time point [271]. Clinical manifestations of disease included weight loss and elevated temperatures, with weight loss most prominent among GPA-RAVV$_{UTMB}$ compared to GPA-MARV$_{Angola}$ [271]. With respect to hematology, both GPA-RAVV$_{UTMB}$ and GPA-MARV$_{Angola}$ challenged animals developed leukocytosis due to increasing neutrophilia, lymphocytopenia and thrombocytopenia consistent with that is observed in other animal models, including the EBOV guinea pig model [271]. Moreover, animals demonstrated elevations in several biochemistry analytes, including AST, ALT and ALP, with peak levels observed during the late stage of disease for both GPA-RAVV$_{UTMB}$ and GPA-MARV$_{Angola}$ [271]. Additionally, both

GPA-RAVV$_{UTMB}$ and GPA-MARV$_{Angola}$ challenged animals demonstrated coagulation abnormalities, including prolonged PT and aPTT and increased levels of plasminogen activator inhibitor 1 and von Willebrand factor during the late stages of the disease [271].

### 1.6.2. Non-Human Primates

Indeed, NHPs represent the gold standard animal model for filovirus as they recapitulate many hallmark features of human FVD. To date, several studies have shown African green monkeys (*Chlorocebus aethiops*), cynomolgus macaques (*Macaca fascicularis*) and rhesus macaques (*Macaca mulatta*) to be excellent models for EBOV [200,280–286] and MARV [20,205,208,246,264,287–291]. Additional, less traditional species of NHPs that have been used to model FVD include common marmosets (*Callithrix jacchus*) [292–294] and hamadryas baboons (*Papio hamadryas*) [282,295–298]

The vast majority of NHP infection with EBOV is done via the IM route [280,281,299–301] using a standard dose of 1000 PFU; however, several alternative routes have been explored, including oral and conjunctival [285,302,303] and aerosol [208,209,304–306] exposure. Although 1000 PFU is the most common challenged dose, doses as low as 0.01 PFU via the IM route have been shown to result in lethal disease [299]. Rhesus macaques infected IM with EBOV become febrile with elevated temperatures beginning at 2-4 dpi followed by mild anorexia, dehydration and decreased activity 1-2 days after onset of fever [280]. Additionally, a petechial rash is observable at roughly 4-7 dpi, with most animals succumbing to disease around 5-9 dpi with a mean time of death of 6.5 dpi [280,307]. In addition, some animals, but not all, may demonstrate other clinical manifestations of disease, including diarrhea, epistaxis and bleeding from various sites, including venipuncture sites, gums, rectum and vagina [280]. The course of disease in cynomolgus macaques is nearly indistinguishable from that observed in rhesus macaques, with the exception that the disease course is compressed compared to rhesus macaques with the normal

disease course ranging from 6-7 dpi [301]. Like rhesus macaques, the onset of disease in cynomolgus macaques is apparent as early as 3 dpi, with animals exhibiting elevated temperatures followed by anorexia, dehydration and decreased activity around 4-5 dpi [301]. Likewise, infected animals manifest macular cutaneous rashes on the arms and groins as early as 4 dpi, with select animals exhibiting nasal and rectal bleeding by 6 dpi [301]. Rhesus macaques challenged with 1000 PFU EBOV via the IM route become viremic as early as 3 dpi with peak levels of ~6.5 $\log_{10}$ PFU/mL reached at terminal time point at 10 dpi [308]. Similarly, cynomolgus macaques challenged with 1000 PFU EBOV via the IM route also become viremic as early as 3 dpi with mean titres of 2.5 $\log_{10}$ PFU/mL, which peak at 6 dpi with mean levels of 6.9 $\log_{10}$ PFU/mL [301]. Virus could be detected in select tissues, including the spleen, inguinal and mesenteric lymph nodes, as early as 2 dpi and by 3 dpi in the liver, lung and bone marrow of infected cynomolgus macaques [301]. Viral titers in the organs increased progressively throughout the disease, with peak levels reached at 6 dpi ranging from 5.5-8.6 $\log_{10}$ PFU/mL, with the highest titers found in the spleen and liver [301].

Characteristic hematological features of EBOV infection in rhesus and cynomolgus macaques are leukocytosis due to increasing neutrophilia with concomitant lymphopenia and thrombocytopenia by 6 dpi [301]. More specifically, lymphopenia is characterized by the depletion of CD4 and CD8 lymphocytes, with a 45% reduction in CD8 lymphocytes as early as 3 dpi [301]. Furthermore, NK populations showed a dramatic decrease of 75% by 4 dpi [301]. Additionally, hemoglobin, hematocrit, and erythrocyte counts decreased post-infection, with the most significant decrease observed between 4 and 5 dpi [301]. Notably, biochemistry remained stable during the early stages of the disease but was elevated during the late stages. In particular, AST, ALT, BUN, ALP, CRE and GGT all peaked at 6 dpi, while total serum proteins did not fluctuate during the

course of infection, with a decrease in ALB noticeable at 4 dpi [301]. Moreover, several cytokines and chemokines, including IL-6, IFN-α, MIP-1α, IL-2, MIP-1β, and IFNγ, were elevated at various times throughout the course of disease [301]. Other cytokines and chemokines, including IL-1β, IL-4, IL-8, IL-10 and IL-12, remained unchanged across all animals [301]. Interestingly, nitric oxide levels were increased at 3 dpi, with these levels increasing throughout disease, with peak levels of >550 mmol/L observed at 5 dpi.

Lastly, both rhesus and cynomolgus macaques demonstrate coagulation abnormalities as a result of EBOV infection characteristic of human EBOD [200]. A rapid decrease in plasma levels of protein C is observed during the early stages of disease as early as 2 dpi with decreases of 60% compared to preinfection levels at 6 dpi [200]. A sharp increase in tissue-type plasminogen activator antigen (tPA) of ~5.5 fold over preinfection levels can be observed at 4 dpi with no detectable difference a day earlier at 3 dpi [200]. tPA levels continued to increase 14- and 18-fold relative to preinfection levels through days 5 and 6 post-infection, respectively [200]. Likewise, levels of urokinase-type plasminogen activator (uPA) increased in a similar manner with 2-, 4.5 and 8-fold increases over preinfection levels at days 4, 5 and 6 post-infection [200]. Levels of factor VIIa (FVIIa) decreased throughout the course of disease with >2-fold decreases at days 1 and 2 post-infection and >3-fold decreases by days 5 and 6 post-infection [200]. Development of fibrin degradation products (D-dimers) demonstrated rapid increases of 45- and 55-fold by day 5 and 5 post-infection, respectively [200]. Furthermore, PT and PTT were also shown to increase throughout the course of disease approximately 2-3-fold relative to baseline values [309]

With respect to MARV, both cynomolgus and rhesus macaque models have been extensively characterized with respect to the course of disease of MARD [205,310–312]. Cynomolgus macaques challenged with 1000 PFU or FFU $MARV_{Angola}$ via the IM route develop

uniformly lethal disease, with animals succumbing to disease anywhere between 7 and 10 dpi [310–313]. By comparison, infection of rhesus macaques with 1000 FFU $MARV_{Angola}$ via the IM route also resulted in uniform lethality, with all animals succumbing to disease by 8 dpi [299]. Interestingly, infection of cynomolgus macaques with 1000 FFU $MARV_{Musoke}$ was only partially lethal, with 50% of animals (1/2) succumbing to disease by 8 dpi [313]. In contrast, 1000 FFU $MARV_{Musoke}$ was uniformly lethal in rhesus macaques, with all animals succumbing to disease by 16 dpi [313]. Remarkably, IM challenged with 1000 FFU $MARV_{ozoline}$ is non-lethal in both cynomolgus and rhesus macaques, with minimal clinical manifestations of disease [313]. Astonishingly, IM challenged with 1000 FFU RAVV is uniformly lethal in cynomolgus macaques, with all animals succumbing to disease at 9 dpi, whereas infection of rhesus macaques is non-lethal [313]. Despite not succumbing to disease, RAVV-challenged rhesus macaques did seroconvert [313]. Cynomolgus and rhesus macaques challenged with MARV all developed severe disease characteristic of MARD, including anorexia, hunched posture, decreased activity and elevated temperatures, all of which became observable as early as 3 dpi for most animals [310–313]. Furthermore, challenged animals developed rashes ranging from petechial to macular, a hallmark feature of MARD in humans [310–313]. Manifestations for rhesus macaques challenged with $MARV_{Musoke}$ as well as RAVV paralleled what was observed from $MARV_{Angola}$ challenged cynomolgus macaques [313]. Surprisingly, NHPs challenged with $MARV_{ozoline}$ only began manifesting mild signs of disease around 7 dpi, including mild fever, hunched posture and mild anorexia, but made a full recovery and survived [313].

Concerning viremia, select cynomolgus macaques challenged with $MARV_{Angola}$ were qRT-PCR positive for MARV RNA within serum as early as 3 dpi with all animals positive by 5 dpi with mean titers of $5.72 \times 10^6$ GEQ/μL and $8.59 \times 10^6$ GEQ/μL at 5 and 7 dpi respectively which

increased to 8.13 x $10^8$ GEQ/µL at terminal time point [311]. While only select animals were qRT-PCR positive for MARV RNA in serum at 3 dpi, all animals were positive for infectious virus at 3 dpi with mean tiers of 1.48 x $10^3$ PFU/mL, which increased to 6.35 × $10^7$, 8.06 × $10^7$ and 8.81 × $10^7$ PFU/mL at days 5 and 7 post-infection and terminal time point respectively [311]. In a serial sacrifice study involving cynomolgus macaques, infectious virus could be detected in the spleen, right axillary lymph node and lung as early as 2 dpi and all tested tissues were positive for infectious virus beyond 5 dpi [310]. Cynomolgus and rhesus macaques lethally infected with $MARV_{Musoke}$ and $MARV_{Angola}$ demonstrate viremia levels ranging between $10^6$-$10^9$ $TCID_{50}$/mL at the time of death around 6-9 dpi with viral titers of ≥ $10^5$ $TCID_{50}$/g in many target tissues including liver and spleen [313]. Although cynomolgus and rhesus macaques did survive challenge with $MARV_{ozoline,}$ these animals showed viral titers in the blood that peaked around $10^3$ $TCID_{50}$/mL at 6 dpi, followed by rapid clearance [313]. Animals challenged with $MARV_{ozoline}$ seroconverted with MARV GP IgG-specific titers ≥ 1:25,600 at study endpoint at 21 dpi [313]. Cynomolgus macaques lethally infected with RAVV demonstrate peak viral titers in the blood of ≥ $10^7$ $TCID_{50}$/mL at time of euthanasia at 9 dpi with titers of ≥ $10^6$ $TCID_{50}$/g in multiple tissues, including liver and spleen [313]. In contrast, rhesus macaques, which do not develop disease following challenge with RAVV, demonstrated viremia in only 1/2 animals with titres of $10^3$ $TCID_{50}$/mL at 6 dpi with no tissues positive for infectious virus at time of euthanasia at study endpoint at 21 dpi [313].

With respect to hematology, cynomolgus and rhesus macaques lethally infected with $MARV_{Angola}$ demonstrated moderate to severely elevated levels of ALT, BUN and CRE at terminal timepoint where levels of ALP were severely elevated for cynomolgus macaques but only mildly elevated for rhesus macaques [313]. These findings are consistent with what has been observed

previously in cynomolgus macaques [310–312]. Cytokine analysis demonstrated up-regulation of several proinflammatory cytokines such as IFN-γ, IL-6, MCP-1 and TNFα among nonsurvivors [313]. In contrast, up-regulation of proinflammatory cytokines was mild among survivors early following challenge, followed by a down-regulation with no changes in TNF-α throughout infection [313]. These findings are consistent with what has been observed among $MARV_{Angola}$ challenged cynomolgus macaques with increased levels of IFN-γ, IL-2, IL-10, IL-15, IL-17, IL-1Ra, IL-13, IL-4, IL-6, MIP-1α, MCP-1, MIP-1β, IL-12 observable on days 5 through 9 post-challenge [310]. Furthermore, $MARV_{Angola}$ infected cynomolgus macaques demonstrated transient neutrophilia and lymphopenia following challenge [297]. Additionally, $MARV_{Angola}$ challenged cynomolgus macaques demonstrate coagulation abnormalities consistent with MARD. More specifically, decreases in PLT levels were observable as early as 5 dpi, with prolonged clotting times beginning at 7 dpi [310]. Increases in aPTT were observed at 7 dpi and terminal timepoint and PTT at days 7 and 9 post-infection and decreases in fibrinogen at 4 and 5 dpi [310,312].

## 1.7. The Domestic Ferret (*Mustela putorius furo*)

*The material in this section has been published previously in Schiffman, Z. et al. The Ferret as a Model for Filovirus Pathogenesis and Countermeasure Evaluation. ILAR Journal 61, 62–71 (2020)* [314] *and is unmodified except for formatting to match the style of this thesis.*

The domestic ferret (*Mustela putorius furo*) is a small carnivore belonging to the Mustelidae family, members of which can be found across the globe in a number of highly diverse ecosystems ranging from arctic tundra to tropical rainforests [315]. These animals, thought to have been domesticated from the European polecat more than 2000 years ago [316], share many anatomical, metabolic, and physiological features with humans, which has long made them appealing models for infectious disease research. The utility of the ferret as an animal model in

virus research first became apparent in the early 1930s following the discovery of their susceptibility to influenza virus [317]. To this day, the ferret remains one of the best animal models for evaluating viral pathogenesis and transmission of influenza viruses, as well as efficacy testing of candidate countermeasures [318]. Their suitability as an animal model for influenza virus research is, in most part, due to their susceptibility to wild-type viruses without the need for host adaptation, their ability to efficiently transmit the virus, and their recapitulation of many aspects of human disease. Although the ferret has proven to be an exceptional model for influenza viruses, it has also been shown to be a valuable model for a number of other respiratory viruses, such as human respiratory syncytial virus [319,320], severe acute respiratory syndrome coronavirus (SARS-CoV) [321–323], and, more recently, SARS-CoV-2 [324,325]. Furthermore, as the natural host of canine distemper virus, ferrets also represent a suitable model for many morbilliviruses [326]. For example, canine distemper virus infection in ferrets reproduces many of the clinical manifestations associated with measles virus in humans, serving as a surrogate model system for evaluating the pathogenesis and efficacy of candidate countermeasures. A number of additional viruses have also been evaluated in the ferret model with varying degrees of success, including Middle East respiratory syndrome coronavirus [327], rabies virus [328–330], Hendra virus [331,332], Nipah virus [333], mumps virus [334–336], simian virus 5 [337] and canine [338] and human parainfluenza viruses [339].

### 1.7.1. The Ferret as A Model for Orthoebolaviruses

*The material in this section has been published previously in Schiffman, Z. et al. The Ferret as a Model for Filovirus Pathogenesis and Countermeasure Evaluation. ILAR Journal 61, 62–71 (2020)* [314] *and is unmodified except for formatting to match the style of this thesis.*

Ferret models for ebolavirus infections have been developed primarily by two different research groups: one at the University of Texas Medical Branch (UTMB) and one at the Public Health Agency of Canada (PHAC). At UTMB, Cross and colleagues established models for EBOV (variant Kikwit), BDBV (variant Uganda 2007), and SUDV (variant Gulu) in 2016 [340], while at PHAC, Kozak et al and Kroeker et al developed similar models for EBOV (variant Makona-C07) and BDBV (variant Uganda 2007) in 2016 [341] as well as SUDV (variant Boneface) in 2017 (Figure 7) [342]. Additionally, in 2019, Yan and colleagues, also at PHAC, established a model for RESTV (variant AZ-1435) [343]. Remarkably, in all cases, ferrets were susceptible to wild-type viruses without the requirement of virus adaptation. In general, all animals developed disease that recapitulated many of the significant hallmarks of Ebola disease (EBOD) that have been observed in NHPs and humans, including fever, weight loss, vascular leakage, dysregulated immune response, uncontrolled systemic virus replication, multi-organ failure, and coagulopathy. Disease was lethal in all cases, although the time to death varied, possibly reflecting differences in virulence inherent to each virus. Notably, animals were uniformly susceptible to both IN and IM challenge, with a range of inoculation doses from 159 $TCID_{50}$ to 1000 PFU. Indeed, a separate study demonstrated that doses as low as 0.1 PFU of reverse genetics-derived EBOV (variant Makona-C07) caused 100% lethality, with a median lethal dose calculated to be 0.015 PFU [344].

Regardless of the inoculation dose or route, disease caused by all ebolaviruses followed a similar course but with species specific variances. Ferrets infected either IM or IN with EBOV succumbed to disease at 5 to 6 dpi with viremia first detected at 4 dpi and peaking at the terminal time point (5–6 dpi) [340,341]. Ferrets infected with SUDV succumbed to infection at 7 or 8 dpi, depending on the variant used, with viremia first observed at 4 dpi [340,342]. In BDBV-infected animals, viremia was first detected at 4 dpi and peaked at 8 dpi, and the animals died between 8

and 9 dpi [340]. Animals survived the longest after infection with RESTV between 9 to 11 days, and the viremia increased slowly following detection at 3 and 5 dpi for IM- and IN-inoculated groups, respectively [343]. Fever was usually the first sign of disease observed in all the models, beginning at 3 to 6 dpi, depending on the virus. Marked weight loss was also observed from 4 to 7 dpi in all animals, although the decrease was not as pronounced in animals infected with EBOV variant Makona-C07 [340]. Other common clinical signs observed in the ferrets throughout infection included progressively worsening depression, diarrhea, dehydration, and laboured breathing. In addition, a petechial rash—an important feature of EBOD seen in humans and NHPs—was observed in all animals except for those infected with SUDV variant Gulu [340]. Systemic viral spread was identified in all cases, with high virus titers found in the liver, spleen, kidney, and lung at terminal time points, regardless of the virus or route of infection. In addition, EBOV, BDBV, and SUDV were detected in the brain and heart. Virus shedding from the oral, nasal, and rectal mucosae was observed in all animals, regardless of virus, and a separate study demonstrated the capacity for both direct and indirect EBOV transmission among ferrets [345].

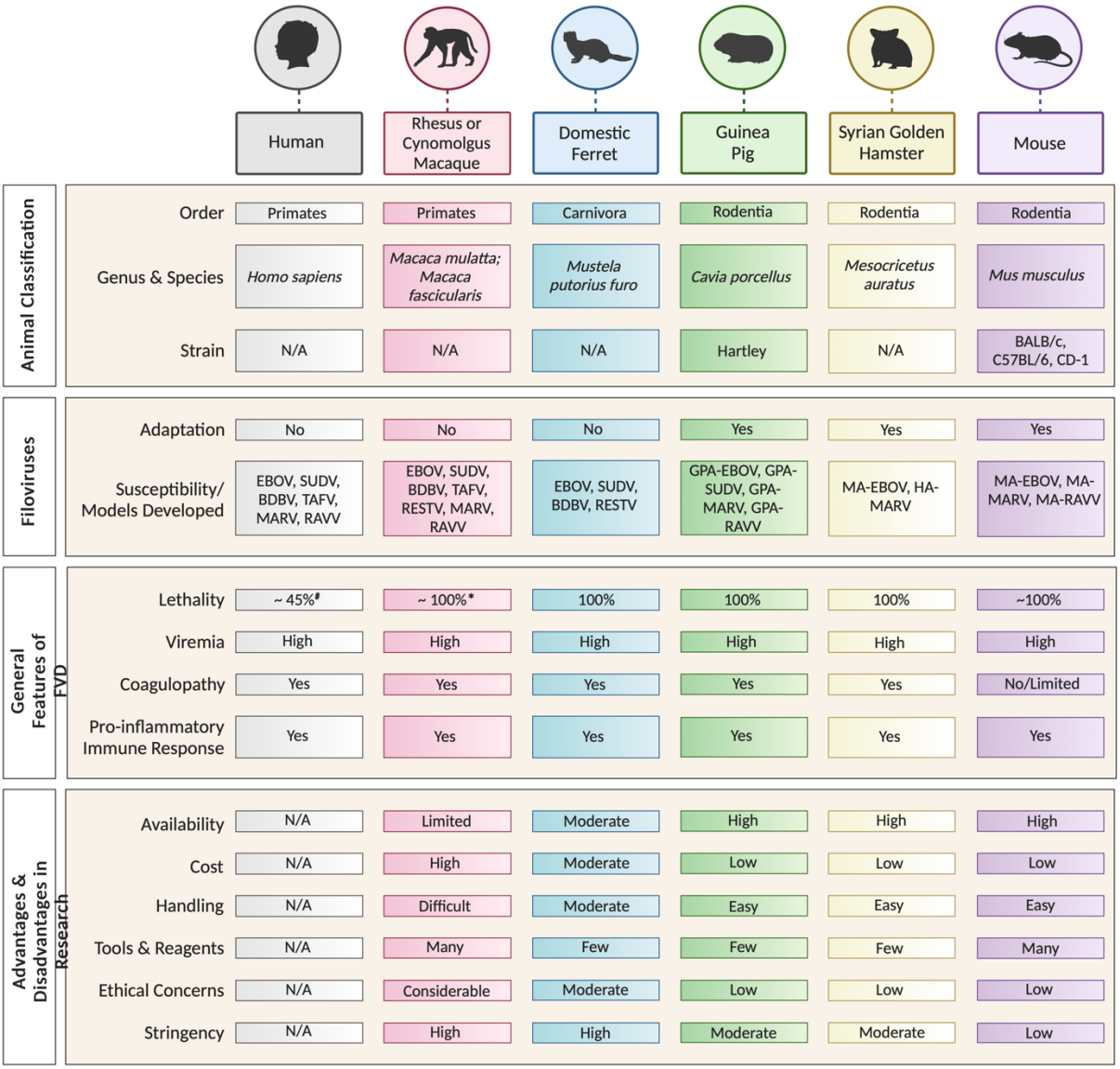


**Figure 7. Hallmarks of pathogenesis for different filoviruses in ferrets.**

Comparison of filovirus animal models. General features of filovirus disease (FVD) and various elements affecting research use are compared among humans, non-human primates (rhesus or cynomolgus macaques), domestic ferrets, guinea pigs, hamsters, and mice. #, Indicates average lethality of all filoviruses from all outbreaks; virus-specific lethality ranges from 0% to approximately 81%. *, Indicates uniform lethality is commonly observed, but may be lower depending on the virus or virus variant. GPA = guinea pig adapted; HA = hamster adapted; MA = mouse adapted; A = not applicable. Figure and caption obtained from [314]. Figure created on Biorender.com

Dysregulation of the immune system, including depletion of immune cells, is another hallmark of FVD in humans, and evidence for these processes was observed in ferrets. Although the magnitude varied among studies, most animals infected with EBOV, BDBV, SUDV, or RESTV showed some degree of reduction in white blood cells and/or lymphocytes, with disturbances in monocytes, eosinophils, and basophils observed by the UTMB group [340]. Increased levels of circulating TNF-α and nitric oxide were also found beginning around 4 dpi in the UTMB-developed models for EBOV, BDBV, and SUDV, suggesting a pro-inflammatory response [340]. Moreover, transcriptomic analyses of the blood of ferrets infected with EBOV revealed a dramatic upregulation in a number of pro-inflammatory cytokines, chemokines, and interferon-stimulated genes, suggestive of a dysregulated immune response and similar to what is observed in humans and NHPs [346]. Disruption of the coagulation pathway was a consistent finding in all animals infected with the ebolaviruses. A dramatic reduction in platelet levels, indicating thrombocytopenia, was observed in all animals. Moreover, serum biochemical analyses in animals infected with EBOV, BDBV, or SUDV indicated prolonged activated partial thromboplastin times, prothrombin time, and thrombin time, as well as the increased level of fibrinogen (although the latter was not significant in BDBV-infected animals). Together, these data are suggestive of consumptive coagulopathy [340,341].

Abnormalities in the levels of certain enzymes and biomarkers in the serum of infected ferrets were indicative of multiorgan failure. Liver damage was consistently found in all animals, indicated by increased levels of alanine aminotransferase, alkaline phosphatase, and total bilirubin and decreased levels of albumin. Renal failure was also indicated by increases in blood urea nitrogen and creatinine. The organ damage suggested by the serum biochemical analyses was further confirmed by histopathology. The most significant lesions reported by the UTMB group

for EBOV, SUDV, and BDBV infection were marked lymphohistiocytic and neutrophilic necrotizing hepatitis and necrotizing splenitis [340]. In addition, increased lymphocyte apoptosis in the spleen was observed in all infected ferrets. Accordingly, viral antigens were detected in hepatic sinusoidal mononuclear cells, hepatocytes, and mononuclear cells within the red and white pulp of the spleen. Similar histological lesions were also observed in the other ferret models developed by the PHAC research group [341–343]. Moderate to severe pathology was observed in the liver, including diffuse or multifocal vacuolar degeneration and loss of hepatocytes that led to disruption of normal structure as well as penetration of inflammatory cells into the portal area. In addition, viral inclusion bodies were observed in some animals. Lesions observed in the spleens of many animals included red pulp hyperplasia, increased macrophages, and multifocal necrotic areas, as well as lymphocytosis, although an increase in macrophages was not found for SUDV-infected animals [342]. Kidney lesions were less common, but interstitial nephritis associated with necrotic cells was found in RESTV- and SUDV-infected animals, and scattered epithelial tubular degeneration was mostly seen in animals infected with EBOV, BDBV, or RESTV. In contrast, pathology in the lung was usually mild to moderate, with the most consistent lesion being the expansion of alveolar walls by inflammatory cells and edema. Notably, however, severe necrotizing pneumonia, bronchiolitis, and perivasculitis was observed in ferrets inoculated IN with EBOV, and severe bronchointerstitial pneumonia was observed in animals inoculated IN with SUDV. Importantly, all of these histological changes were associated with the detection of virus antigen, suggesting the presence of replicating virus.

Together, these four studies provide a thorough characterization of ferret models for EBOV, SUDV, BDBV, and RESTV, and they are particularly notable for introducing the first, and so far only, small animal model for BDBV infection. Nonetheless, some outstanding issues remain

unresolved. Firstly, some caution may be required in making direct comparisons between results from the UTMB and PHAC studies, because both groups used different virus variants and inoculation doses. Secondly, with the exception of the RESTV study, all other studies that characterized ebolavirus pathogenesis in ferrets used exclusively female animals. It is, therefore, unclear whether significant differences exist in disease presentation between male and female ferrets but considering that many subsequent papers assessing transmission or evaluating countermeasures use both males and females, it may be important to better understand this issue. Finally, it is worth noting that, to date, ferret models for TAFV and BOMV have not been published. Although public health and research interest in these viruses is relatively low, a ferret model for either virus may provide additional insight into the biology and pathogenesis of ebolaviruses in general.

### 1.7.2. The Ferret as A Model for Orthomarburgviruses

*The material in this section has been published previously in Schiffman, Z. et al. The Ferret as a Model for Filovirus Pathogenesis and Countermeasure Evaluation. ILAR Journal 61, 62–71 (2020)* [314] *and is unmodified except for formatting to match the style of this thesis.*

The same two research groups at UTMB and PHAC responsible for developing the ferret models of ebolavirus infection also evaluated the pathogenesis of marburgviruses in ferrets. In two separate studies, male and female ferrets were challenged with MARV (variant Angola or Musoke) or RAVV via a number of different routes (IM, IN, or IP) and doses (317 $TCID_{50}$ –100,000 PFU) in an attempt to establish a lethal model (Figure 7) [347,348]. Surprisingly, however, regardless of challenge dose, route, or virus/variant, ferrets were found to be not susceptible to infection with marburgviruses. Among the 36 ferrets challenged across both studies, none displayed any of the disease signs—such as weight loss, fever, or decreased food/water intake that are observed in

ferrets infected with ebolaviruses. Furthermore, no significant changes from baseline hematology or serum biochemistry were observed at any point, nor could any infectious virus be detected in the blood or tissues. Interestingly, viral RNA ($8.35 \times 10^6$ GEQ/mL) was detected in the blood of a single animal at 6 dpi; however, no additional details on this animal were available [347]. Despite the lack of viremia, all animals seroconverted and demonstrated moderate neutralizing antibody titers at endpoint.

Taken together, the findings from these two studies demonstrate that, in contrast to ebolaviruses, the domestic ferret is not susceptible to lethal infection with marburgviruses. While the lack of detectable viral RNA and infectious virus in both blood and tissues indicates that inoculation with marburgviruses does not lead to a productive infection, the presence of MARV-specific IgG and moderate neutralizing antibody titers indicates that the animals did mount a humoral immune response. Although it remains unclear as to why ferrets are refractory to infection with marburgviruses yet susceptible to ebolaviruses, it is reasonable to speculate that differences in the immune response to infection, including differences in innate immune evasion between ebolaviruses and marburgviruses may be at least partly responsible [115]. Additionally, ferret cells themselves may differ in their permissiveness to filovirus infection, with species-specific differences in viral entry and/or replication possibly affecting the development (or not) of FVD. Further investigations are required to fully elucidate the molecular determinants of filovirus virulence in ferrets, and future directions could involve the establishment of a ferret-adapted virus that could prove critical for the identification of mutations responsible for the avirulence of marburgviruses in these animals.

### 1.7.3. Ferret and Countermeasure Evaluation

*The material in this section has been published previously in Schiffman, Z. et al. The Ferret as a Model for Filovirus Pathogenesis and Countermeasure Evaluation. ILAR Journal 61, 62–71 (2020)* [314] *and is unmodified except for formatting to match the style of this thesis.*

Candidate countermeasures against filoviruses are typically screened for efficacy in rodents before confirmatory evaluation in NHPs; however, the recent success in recapitulating ebolavirus infection in ferrets has offered a potential alternative model. The apparent stringency of the ferret ebolavirus model, along with the ability to use wild-type viruses, may position the ferret as an intermediate model system to be used after primary evaluation in rodents and prior to evaluation in NHPs. However, to date, there are still relatively few efficacy studies involving ferrets and, therefore little understanding of the predictive value of this model. Moreover, the majority of efficacy studies that have been performed have been limited to the evaluation of mAbs against BDBV infection, for which the ferret is the only small animal model available.

#### 1.7.3.1. Monoclonal Antibodies

*The material in this section has been published previously in Schiffman, Z. et al. The Ferret as a Model for Filovirus Pathogenesis and Countermeasure Evaluation. ILAR Journal 61, 62–71 (2020)* [314] *and is unmodified except for formatting to match the style of this thesis.*

The past decade has witnessed remarkable progress in the development of therapeutics against filoviruses [349]. Among them, mAbs targeting the surface GP of ebolaviruses have shown exceptional efficacy in several pre-clinical evaluations. Indeed, a clinical trial conducted during the recent outbreak in the Democratic Republic of the Congo demonstrated that a single mAb known as Mab114, as well as a cocktail of three mAbs known as REGN-EB3, conferred a significant survival advantage in patients [350]. Although these mAbs solely target EBOV, the

therapeutic promise of mAbs in general has generated great interest in developing broadly cross-reactive mAbs capable of protecting against multiple ebolaviruses or filoviruses.

Ferrets have played a key role in the pre-clinical development of many of these candidate mAb therapeutics, primarily because they offer a suitable model in which to test efficacy against BDBV. Among the first mAbs to be evaluated in the ferret model were ADI-15878 and ADI-15742 [351]. These mAbs were isolated from a human survivor and shown to bind a GP base region spanning both GP1 and GP2, which includes the conserved internal fusion loop that is essential for the fusion of viral and cellular membranes. The two mAbs each recognize multiple ebolavirus GPs and strongly neutralize recombinant vesicular stomatitis viruses pseudotyped with GPs of the five human-pathogenic ebolaviruses as well as authentic EBOV, SUDV, and BDBV. Both mAbs were highly protective against MA-EBOV and MA-SUDV in mice, and thanks to the recently developed ferret model of BDBV infection, they were also tested for their efficacies against BDBV. Ferrets were infected with a target dose of 1000 $TCID_{50}$ wild-type BDBV via IM injection and treated IP with 15 mg of ADI-15878 or ADI-15742 on 3 dpi, followed by a second dose of 10 mg at 6 dpi. Control animals who received phosphate-buffered saline (PBS) post-challenge all succumbed to infection within 10 days. By contrast, significant survival rates were observed among the treated animals, with ADI-15878 and ADI15742 resulting in 75% and 50% survival, respectively. Both mAbs clearly delayed and/or significantly reduced peak viral loads in the blood; however, among the survivors, animals treated with ADI-15878 showed lower viral loads and earlier virus clearance than those treated with ADI-15742. Interestingly, this discrepancy has been linked to possible escape mutation (G528S) in the BDBV GP found in animals treated with ADI-15742.

CA45 is another broadly neutralizing antibody, this time isolated from memory B cells of a cynomolgus macaque immunized with recombinant GPs of EBOV, SUDV, and MARV, that shows strong binding activity against multiple ebolaviruses [352]. Similar to ADI-15878, CA45 also targets the GP1-GP2 interface at the GP base but in a distinct region with major contacts predominantly in and around the internal fusion loop stem. In concordance with its GP binding profile, CA45 is a strong neutralizer of EBOV, BDBV, and SUDV in both GP-pseudotyping and authentic systems and a moderate neutralizer of RESTV GP-mediated infection. CA45 was highly protective against MA-EBOV in mice and both MA and guinea pig-adapted GPA-SUDV in mice and guinea pigs, respectively, but it was only partially protective against GPA-EBOV in guinea pigs. When combined with another NHP-derived mAb, known as FVM04, which targets the receptor binding region of GP, the cocktail provided full protection against GPA-EBOV and GPA-SUDV in guinea pigs. The authors then decided to test the cocktail for efficacy against BDBV in ferrets. Equal numbers of male and female ferrets challenged via the IM route with a lethal dose (253 $TCID_{50}$) of BDBV followed by IP treatment with PBS or the antibody cocktail (20 mg of each mAb) at 3 and 6 dpi. The control animals treated with PBS died at 7 dpi, whereas the animals treated with the cocktail all survived without clinical signs of diseases or weight loss. The control animals exhibited high viral loads in the blood, peaking at nearly $10^{10}$ GEQ/mL on the day of death, whereas, in contrast, viral RNA was undetectable in the treated male animals and only transiently detected at low levels (approximately $10^4$ GEQ/mL) in the females on 6 dpi. No viral RNA was detected in the oral, nasal, or rectal mucosa of the treated animals, suggesting the absence of virus shedding in the treated animals, while up to approximately $10^6$ GEQ/mL of viral RNA was detected in the control animals. Blood chemistry features associated with organ damage, including dramatic elevation in ALT and ALP levels, were observed in the control animals but not

in the treated animals. In addition, lymphopenia and thrombocytopenia were at least partially reversed in all treated animals, which was not the case in the controls. Thus, the rodent studies combined with the ferret study indicate that CA45, particularly when combined with FVM04, is highly potent against the three most pathogenic ebolaviruses.

In 2018, two studies from the same group were published describing broadly neutralizing mAbs isolated from human survivors of ebolavirus infection [353,354]. The first study, by Flyak et al., identified three cross-neutralizing mAbs (termed BDBV223, BDBV317, and BDBV340) from human survivors of BDBV [354]. All three mAbs targeted the canonical heptad repeat 2 region close to the membrane-proximal external region in GP and showed neutralizing activity against BDBV as well as EBOV, RESTV, and SUDV. BDBV223 completely protected mice from MA-EBOV infection and partially protected guinea pigs from GPA-EBOV infection. To assess the protective efficacy of BDBV223 against BDBV, male and female ferrets were IM-inoculated with a target dose of 1000 PFU BDBV and treated with 20 mg of antibody on 3 and 6 dpi. While the control animals treated with an irrelevant mAb died at 7 dpi, 2 of the 4 animals treated with BDBV223 survived, having exhibited no weight loss or clinical signs of illness. In the second study, the same group reported the protective efficacy of EBOV-520, a mAb isolated from a human survivor of EBOV [353]. EBOV-520 exhibited neutralizing activity against EBOV, SUDV, and BDBV *in vitro*, as well as *in vivo* efficacy against MA-EBOV, MA-SUDV, and GPA-SUDV. To assess the antibody's protective efficacy against BDBV, male and female ferrets were IM-inoculated with a target dose of 1000 PFU virus and treated IP with 18 mg EBOV-520 on 3 and 6 dpi. Surprisingly, 3/4 animals treated with EBOV-520 succumbed by 10 dpi even though all animals had undetectable viremia in the blood at 6 dpi, just prior to the second treatment. Only 1/3 ferrets that succumbed to disease showed evidence of viremia, with virus levels peaking on 10 dpi,

the terminal time point. Unlike the animal that survived, all three ferrets that succumbed showed disturbances in clinical chemistry parameters, including ALP and ALT, suggesting organ damage. However, the presence of virus in tissues at the time of death was not investigated.

To date, only a single study has evaluated mAb efficacy against an ebolavirus other than BDBV in the ferret model [355]. The mAb cocktail known as MBP134$^{AF}$ consists of 2 broadly neutralizing mAbs, ADI-15878 (discussed above) and ADI-23774, which have individually been shown to neutralize GP and protect from disease in small animal models[351,356]. In ferrets, MBP134$^{AF}$ successfully protected all animals (female) from EBOV, SUDV, and BDBV (1000 PFU delivered IN) following two 15-mg doses of antibody given IP on 2 and 5 dpi (EBOV) or 3 and 6 dpi (SUDV, BDBV). None of the animals infected with EBOV or SUDV showed evidence of viremia, and only one animal infected with BDBV exhibited low levels of viral RNA and infectious virus in the blood. Interestingly, a lower dose of 5-mg MBP134$^{AF}$, given via the same regimen, did not protect against SUDV infection, offered partial protection against BDBV, and was not tested against EBOV. Notably, the efficacy of MBP134$^{AF}$ was also evaluated against EBOV and SUDV in rhesus macaques—in which it provided full protection—and against BDBV in cynomolgus macaques— in which it offered near-complete protection. Thus, this study is the only one to date that provides a direct comparison between the virus-specific efficacy of a therapeutic in ferrets and in NHPs, providing some idea of the predictive value of the ferret model.

#### 1.7.3.2. Vaccines

*The material in this section has been published previously in Schiffman, Z. et al. The Ferret as a Model for Filovirus Pathogenesis and Countermeasure Evaluation. ILAR Journal 61, 62–71 (2020) [314] and is unmodified except for formatting to match the style of this thesis.*

Recently, a study evaluated the protective efficacy of a vaccine cocktail against BDBV infection in ferrets [357]. This trivalent cocktail is composed of three vaccines, each expressing EBOV, BDBV, or SUDV GP in a human parainfluenza virus type 3 (HPIV3) vector. The cocktail demonstrated potent protective efficacy against GPA-EBOV and GPA-SUDV infection in guinea pigs. To evaluate its efficacy against BDBV, female ferrets were vaccinated with $1 \times 10^7$ PFU of the monovalent HPIV3-BDBV vaccine or the cocktail containing $1 \times 10^7$ PFU of each vaccine through IN inoculation and challenged 4 weeks later with a target dose of 1 × 103 PFU BDBV via IM injection. The vaccine cocktail induced a strong antibody response against BDBV, with GP binding capacity and neutralizing activity comparable with that elicited by the BDBV monovalent vaccine and weaker responses against EBOV and SUDV. The BDBV challenge (1000 PFU) was uniformly lethal among the control animals, which experienced continuous weight loss starting at 3 dpi and suffered rapid disease progression, with signs of disease appearing on or 1 day before the day of death at 7 dpi. By contrast, both the vaccine cocktail and the monovalent HPIV3-BDBV provided full protection, with all vaccinated animals testing negative for viremia and no animals exhibiting weight loss or showing signs of disease. The successful evaluation of the efficacy of these vaccines against BDBV in ferrets suggests that this animal model may be useful for testing vaccines against other pathogenic ebolaviruses.

## 1.8. Gaps in Knowledge

Although previous studies have demonstrated that ferrets are highly susceptible to lethal infection with certain orthoebolaviruses but not orthomarburgviruses, it remains largely unknown why this is. Indeed, no studies have been published investigating possible mechanisms responsible for this lack of disease among ferrets infected with orthomarburgviruses but not orthoebolaviruses.

## 1.9. Central Hypotheses and Aims

Overall, this thesis explores two main hypotheses. Firstly, it is hypothesized that this lack of susceptibility by ferrets to lethal infection with orthomarburgviruses but not orthoebolaviruses is due to a block in GP-mediated viral entry, which functions to either interfere or inhibit viral entry and/or replication. Secondly, it is hypothesized that this lack of susceptibility by ferrets to lethal infection with orthomarburgviruses but not orthoebolaviruses is the result of mechanistic differences in the innate immune evasion tactics of these two viruses.

### 1.9.1. Aim 1: Evaluate the influence of GP-mediated viral entry on the infectivity of ferret cell lines *in vitro* and viral pathogenesis *in vivo*

This aim is related to the first hypothesis and investigates the role of GP-mediate entry towards infectivity of ferret cell lines *in vitro* and viral pathogenesis *in vivo*. Evaluating this involves the establishment of immortalized ferret cell lines to be used as an *in vitro* cell model. Next, this aim investigates the permissibility of these ferret cell lines to GP-mediated entry using vesicular stomatitis virus (VSV) pseudotyped with either EBOV or MARV GP and their ability to support replication of authentic filoviruses. Lastly, this aim investigates the role that MARV GP has on viral pathogenesis *in vivo* within ferrets using a recombinant chimeric EBOV expressing MARV GP in place of EBOV GP (EBOV-mGP). The results from this aim are presented in *Section 3*.

### 1.9.2. Aim 2: Determine if inhibitors of the type I IFN response promote MARV replication *in vitro* within ferret cell lines

This aim is related to the second hypothesis. It investigates whether inhibitors of the type I IFN response, including production and signalling via the JAK/STAT pathway, promote replication of MARV *in vitro* within ferret cell lines. The results from this aim are presented in *Section 4*.

### 1.9.3. Aim 3: Evaluate the pathogenicity of rodent-adapted filoviruses *in vivo* within ferrets

This aim is related to the second hypothesis, which is to investigate the pathogenicity of rodent-adapted filoviruses, namely MA-MARV, GPA-MARV, and GPA-EBOV *in vivo* within ferrets. This aim is related to the second hypothesis, as many of the mutations within these rodent-adapted viruses have been linked to the virus's ability to subvert the host immune response. The results from this aim are presented in *Section 5*.

# 2. Chapter 2. MATERIALS AND METHODS

## 2.1. Development and Characterization of Immortalized Ferret Cell Lines

### 2.1.1. Establishment of Primary Cell Culture

Male (n=1) and female (n=1) ferrets (*Mustela purtorius furo)* weighing 0.65-0.7 kg were purchased commercially from Marshall BioResources (New York, USA) and acclimatized for at least 10 days prior to euthanasia and necropsy. Lung, heart and spleen were harvested from each animal and stored on ice in pre-chilled processing media [Dulbecco's Phosphate Buffered Saline (DPBS) without calcium and magnesium (Cytiva, USA) supplemented with penicillin (100 U/mL), streptomycin (100 µg/mL) (Thermofisher Scientific, USA) and 2.5 µg/mL amphotericin B (Thermofisher Scientific, USA)]. Adipose and necrotic tissues were excised from the harvested tissues, which were then sliced finely (~2-3 mm) and washed twice with ice cold processing media to remove excess blood and cell debris.

Tissue pieces from the heart and lungs were digested enzymatically with pre-warmed 0.25% trypsin-EDTA (Thermofisher Scientific, USA) at 37°C for 30 min on an orbital shaker set to ~150-200 rpm. Following digestion, tubes were placed upright for 5 min to allow the tissue slices to settle, and the supernatant transferred through a 70-µm cell strainer into 2 mL heat-inactivated fetal bovine serum (HI-FBS) (VWR, USA). The resulting cell suspensions were subjected to centrifugation at 338 x *g* for 5 min, and the cell pellet was resuspended in 2 mL culture media [Dulbecco's Modified Eagle Medium (DMEM) High Glucose (Cytiva, USA) supplemented with penicillin (100 U/mL), streptomycin (100 µg/mL), 2.5 µg/mL amphotericin B and 10% HI-FBS]. The cell suspensions were transferred to T25 flasks and incubated at 37°C and 5% $CO_2$. The enzymatic digestion process was repeated two additional times, with cell suspensions transferred to the same T25 flask each time.

Tissue pieces from the spleen were transferred through a 70-µm cell strainer into culture media to yield a single cell suspension. The cell suspension was centrifuged at 338 x *g* for 5 min, after which the cell pellet was resuspended in ACK lysis buffer (Thermofisher Scientific, USA), incubated for 5 min at room temperature, and then centrifuged at 338 x *g* for 5 min. The resulting supernatant was discarded, and the process was repeated an additional 2-3 times to eliminate red blood cells. The final cell pellet was resuspended in culture media, transferred to a T25 flask, and incubated at 37°C and 5% $CO_2$.

### 2.1.2. Immortalization of Primary Ferret Cells

Primary ferret cells were passaged at least twice prior to immortalization. Cells were transduced (25-30% confluency) in the presence of 10 µg/mL polybrene with a lentivirus (multiplicity of infection [MOI] = 40) encoding the SV40 large T antigen as well as a neomycin resistance gene (Abm, USA). Cells were incubated for 48 h at 37°C and 5% $CO_2$, after which the virus inoculum was removed and cells were washed twice with DMEM. Cells were maintained in DMEM supplemented with 10% HI-FBS, and positively transduced cells were selected through multiple passages in the presence of the neomycin analogue Geneticin [G418] (Thermofisher Scientific, USA) at concentrations 1000 - 2000 µg/mL. Cells were incubated in the presence of G418 with selection media being changed every 3-4 days. Immortalized cells were cryopreserved in liquid nitrogen in 90% HI-FBS supplemented with 10% DMSO.

### 2.1.3. Characterization of Immortalized Ferret Cell Lines By 10X Genomics

Immortalized ferret spleen (*mpf*Spleen), heart (*mpf*Heart) and lung (*mpf*Lung) cells were characterized using the Chromium Next Gem Single Cell 3' Regent Kit v3.1 (10X Genomics, USA) according to the manufacturer's instructions. Briefly, *mpf*Spleen, *mpf*Heart and *mpf*Lung cells were thawed in a 37°C water batch from liquid nitrogen storage. Cell counts and viability

were determined using the Nexecelom cell counter (Nexcelom Bioscience, USA) and the acridine orange and propidium iodide. Cells were subsequently diluted to 1,000,000 cells/mL in PBS upon which GEM generation and barcoding, post GEM-RT cleanup, cDNA amplification and construction of 3' gene expression libraries were done according to the manufacturer's instructions for the Chromium Next Gem Single Cell 3' Regent Kit v3.1 (10X Genomics, USA). Prepare libraries were sequenced on a NextSeq 2000 (Illumina, USA) using the NextSeq 2000 P3 Reagents (100 Cycles) kit (Illumina, USA).

## 2.2. Evaluation of GP-mediated Entry Using VSV Pseudotypes

### 2.2.1. Cells and Viruses

Immortalized ferret spleen *(mpf*Spleen) cells were maintained in DMEM supplemented with 10% HI-FBS. Vero E6 cells (CRL-1586) were obtained from ATCC and maintained in DMEM supplemented with 10% HI-FBS and 1% L-glutamine. All cell lines were maintained in a humidified incubator at 37°C and 5% $CO_2$ and tested negative for mycoplasma contamination using the MycoAlert® Mycoplasma Detection Kit (Lonza, Switzerland).

VSV-EBOV, a recombinant VSV expressing GP from EBOV (variant Kikwit) and VSV-MARV, a recombinant VSV expressing GP from MARV (variant Angola) were previously rescued and used in this study for *in vitro* GP-permissibility studies at Passage (P)-2 and P3 respectively.

### 2.2.2. Infection of Immortalized Ferret Cells with VSV Pseudotypes

*mpf*Spleen and Vero E6 cells were seeded in 24-well plates at densities of 1.75 x $10^5$, and 2.20 x $10^5$ cells/well respectively to achieve ~90-95% confluency after 24 h. The following day, medium was aspirated, and the cells infected at a MOI of 0.1 with either VSV-EBOV or VSV-MARV in 100 µL DMEM. Infections were incubated at 37°C and 5% $CO_2$ for 1 h with rocking every 15 min. Following incubation, virus inoculums were aspirated, and cell monolayers washed

with 250 µL DMEM. After washing, 1 mL DMEM supplemented with 2% HI-FBS, 1% L-glutamine and 1% penicillin/streptomycin was added to each well and plates incubated at 37°C and 5% $CO_2$. Virus supernatants were harvested at 3, 6, 8 and 12 hours-post-infection (hpi) and total RNA extracted using the QIamp viral RNA minikit (Qiagen, USA) according to the manufacturer's instructions.

Viral RNA was quantified by reverse transcription quantitative PCR (RT-qPCR) using the Lightcycler 480 RNA Master Hydrolysis probes kit (Roche, USA) with primers and probes targeting VSV NP (Table 4). RT-qPCR reactions were done using a Quantstudio 3 Real-time PCR system (Applied Biosystems, USA) with the following cycling conditions: 63°C for 3 min, 95°C for 30 sec, followed by 45 cycles of 95°C for 15 sec, 60°C for 30 sec.

**Table 4.** RT-qPCR Primer and Probe Sequences for VSV

| Target | Forward Primer (5'-3') | Reverse Primer (3'-5') | Probe |
|---|---|---|---|
| VSV-NP | CGGAGGATTGACGACTAATGC | TCAAACCATCCGAGCCATTC | CY5-CCGCCACAAGGCAGAGATGTGGT |

## 2.3. Infection of Ferret Cell Lines with EBOV and MARV Viruses

### 2.3.1. Cells and Viruses

Immortalized ferret spleen *(mpf*Spleen), heart *(mpf*Heart) and lung (*mpf*Lung) cells were maintained in DMEM supplemented with 10% HI-FBS. Vero E6 cells (CRL-1586) were obtained from ATCC and maintained in DMEM supplemented with 10% HI-FBS and 1% L-glutamine. All cell lines were maintained in a humidified incubator at 37°C and 5% $CO_2$ and tested negative for mycoplasma contamination using the MycoAlert® Mycoplasma Detection Kit (Lonza, Switzerland).

MARV variant Musoke (Marburg virus - Musoke, Kenya, 1980; GenBank: DQ217792.2) was used at P2 and Ebola virus (Ebola virus/H.sapiens-wt/GIN/2014/Makona-C07; GenBank:

KT013257.3) used at P1. Sequence identities for both viruses were confirmed by Next-Generation Sequencing (NGS).

### 2.3.2. Next Generation Sequencing of Stock Viruses

Total RNA extracted from either whole blood or homogenized tissues were subjected to NGS to track virus evolution over time. Briefly, total RNA was extracted from whole blood and tissues as described above. Next, RNA was converted to cDNA using the SuperScript™ IV VILO™ Master Mix (Invitrogen, USA) with the following modifications to the manufactures protocol: Samples with CT values >22 were diluted 1:10 in nuclease free water otherwise samples were used neat. Following DNase treatment, reactions were immediately transferred on ice and not allowed to cool on the thermocycler. Reverse transcription reactions were completed using either a Proflex PCR system (Applied Biosystems, USA) or SimpliAmp Thermal Cycler (Applied Biosystems, USA) with the following modified thermocycling conditions: 25°C for 10 min, 37°C for 10 min, 50°C for 10 min, 55°C for 10 min, 65°C for 10 min and 85°C for 5 min. Next cDNA were subjected to PCR amplification using the Phusion U Multiplex PCR Master Mix (Thermofisher Scientific, USA) with the following thermocycling conditions: 98°C for 30 sec followed by 30 cycles of 98°C for 10 sec, 65°C for 30 sec and 72°C for 5 min. Amplicon sequencing of GPA-MARV was done using primers designed with primalscheme [358] using Lake Victoria marburgvirus - Angola2005 strain Ang0754 (GenBank: DQ447659.1) as the reference sequence. Primers were designed according to the default parameters defined by primalscheme with amplicon sizes of 800 bp and overlap of 200 bp. PCR amplicons from each pool were purified using RNAClean XP (Beckman Coulter, USA) according to the manufactures instructions and subsequently quantified on a Qubit Flex Fluorometer (Invitrogen, USA) using the 1X dsDNA BR Assay Kit (Invitrogen, USA). PCR amplicons from both pools were combined at equimolar

concentrations and library construction done using the Nextera XT DNA Library Preparation Kit (Illumina, USA) as per the manufactures protocol. Sequencing was done on a NextSeq2000 sequencer using a NextSeq 1000/2000 P1 Reagent Kit v3 (300 cycles) (Illumina, USA).

### 2.3.3. Growth Kinetics on Ferret Cell Lines

Prior to infection, *mpf*Spleen, *mpf*Heart, *mpf*Lung and Vero E6 cells were seeded in 24-well plates at densities of 1.75 x $10^5$, 3.25 x $10^5$, 1.5 x $10^5$, 2.2 x $10^5$ cells/well respectively in the aforementioned media to achieve a confluency of ~85-90% after 24 h. The following day, media was aspirated, and the cells infected at an MOI of 0.1 with either MARV Musoke or EBOV Makona C07 in 250 µL DMEM. Infections were incubated at 37°C and 5% $CO_2$ for 1 h with rocking every 15 min to allow for virus adsorption. After 1 h, virus inoculum was removed and replaced with 1 mL DMEM supplemented with 1% FBS, 1% penicillin/streptomycin (ferret cells) or DMEM supplemented with 1% HI-FBS, 1% L-glutamine and 1% penicillin/streptomycin (Vero E6 cells). Supernatants were harvested at 3, 7 and 14 days-post-infection (dpi) for virus quantification.

### 2.3.4. Quantification of viral RNA by RT-qPCR

Total RNA was extracted from cell culture supernatant using the QIamp viral RNA minikit (Qiagen, USA) according to the manufacturer's instructions Levels of viral RNA were quantified by RT-qPCR using the TaqPath™ 1-Step Multiplex Master Mix (Applied Biosystems, USA) according to the manufacturer's protocol using primers and probes targeting either EBOV L or MARV L (Table 5). RT-qPCR reactions were done using a Quantstudio 5 Real-time PCR system (Applied Biosystems, USA) with the following thermocycling conditions: 25°C for 2 min, 53°C for 10 min and 95°C for 2 min, followed by 40 cycles of 95°C for 3 sec, 60°C for 30 sec.

**Table 5.** RT-qPCR Primer and Probe Sequences for EBOV/MARV

| Target | Forward Primer (5'-3') | Reverse Primer (3'-5') | Probe |
|---|---|---|---|
| MARV L | GCAAAAGCATTCCCTAGTAACATGA<br>GCGAAGGCATTCCCTAGTAATATGA | CACCCCTCACTATRGCGTTYTC<br>CACCTCTTACTATGGCATTCTC | FAM-<br>TGGCACCAYAATTCAGCAAGCATAGG |
| EBOV L | CAGCCAGCAATTTCTTCCAT | TTTCGGTTGCTGTTTCTGTG | FAM-ATCATTGGCGTACTGGAGGAGCAG<br>FAM-TCATTGGCGTACTGGAGGAGCAGG |

### 2.3.5. Quantification of Infectious Virus by $TCID_{50}$

Vero E6 cells were seeded in 96-well plates at a cell density of 2.0 x $10^4$ cells/well to achieve a confluency of 90-95% after 24 h. The following day, medium was aspirated and replaced with DMEM supplemented with 1% HI-FBS, 1% L-glutamine and 1% penicillin/streptomycin added to each well. Cell culture supernatant (40 µL) was diluted in 360 µL of DMEM supplemented with 1% HI-FBS, 1% L-glutamine and 1% penicillin/streptomycin and serially diluted 10-fold ($10^{-1}$-$10^{-8}$). Diluted samples (100 µL) were added to the Vero E6 cells and incubated at 37°C and 5% $CO_2$ for 14 days, at which time cytopathic effects (CPE) were observed. The median tissue culture infectious dose ($TCID_{50}$) reported as $TCID_{50}$/mL were calculated using the Reed–Muench method.

## 2.4. Infection of Ferrets with EBOV-mGP

### 2.4.1. Viruses

MARV variant Angola 325 was used at P2 and Ebola virus (Ebola virus/H.sapiens-wt/GIN/2014/Makona-C07; GenBank: KT013257.3) at P1 for *in vivo* ferret challenged. Recombinant EBOV expressing MARV-GP in place of EBOV-GP (EBOV-mGP) was rescued according to the methods described in *Section 2.4.2* and a P2 working stock used in this study for *in vivo* ferret challenge.

### 2.4.2. Rescue of Recombinant Chimeric EBOV-mGP

The full-length cDNA clone of the EBOV-mGP chimeric virus was constructed based on the previously described rgEBOV-C07 [344] by swapping the rgEBOV-C07 GP with MARV Angola GP (Genbank: KY047763.1). For this purpose, three PCR fragments were amplified using

primer pairs eGP-PmlI-IFF (5'-ACAGGATTGTGACACGTGTC-3')/ EbMARV-1R (5'-GTGGTTTTCATTGTGTTGTCGCCTCACAATATC-3'), EbMARV-2F (5'-CGACAACACAATGAAAACCACATGTCTCCTTA-3')/ EbMARV-2R (5'-CTGAAGAAAGA TTATCCAATATATTTAGTAAAAATACG-3') and EbMARV-3F (5'-ATATATTGGATAATCTTTCTTCAGAT TGTTTCACG-3')/eGP-SacI-IFR (5'-TTGT CGGGTTCTTGGAGCTC-3'), respectively, with the rgEBOV-C07 plasmid or MARV Angola cDNA as templates, and pieced together into one PCR fragment using overlapping PCR, which was then ligated into PmlI/SacI-digested rgEBOV-C07 vector to replace the PmlI-SacI fragment of EBOV using In-Fusion HD cloning plus kit (Takara Bio Inc, Japan). The rescue of infectious EBOV-mGP chimeric virus was performed as previously described for rgEBOV-C07 [344] using the same helper plasmids.

### 2.4.3. Ethics Statement

All animal work involving infectious filoviruses was conducted in the containment level-4 (CL-4) facility at the Canadian Science Center for Human and Animal Health (CSCHAH) of the Public Health Agency of Canada in Winnipeg, Canada. All experiments were reviewed and approved by the Animal Care Committee of the CSCHAH in accordance with guidelines from the Canadian Council on Animal Care. Animals were acclimatized for a minimum of 7 days prior to infection, given food and water ad libitum, and monitored twice daily. Environmental enrichment was provided throughout the study.

### 2.4.4. Animals

Male (n=5) and female (n=5) ferrets (*Mustela putorius furo)* ~ 5-6 months old and weighing approximately 0.65-0.7 kg were purchased from Marshall BioResources and implanted with an IPTT-300 temperature and ID transponder (BioMedic Data Systems Inc., USA). Following acclimatization, ferrets were randomly assigned into groups containing equal numbers of males

and females and inoculated with either EBOV-mGP (n=6), EBOV (n=2) or MARV (n=2) at a target dose of 1000 $TCID_{50}$ via the intramuscular (IM) route. Virus inoculums were prepared in DMEM and administered equally at two sites (250 µL/rear quadricep). Animals were monitored daily for clinical signs of disease including changes in body weight, temperature, physical activity, and food/water intake. Animals that reached the clinical scoring criteria for humane endpoint were euthanized. Whole blood and serum were collected at -1 (blood only), 3, 5, 7, 10 and 14 dpi, as well as at time of euthanasia, to evaluate virus loads. Oral and rectal swabs, as well as nasal washes were collected at the aforementioned time points. Tissues, including liver, spleen, kidney, heart, testes, ovaries, eyes and brain, were harvested at time of necropsy from all animals for downstream viral titration.

### 2.4.5. Quantification of Viral RNA by RT-qPCR

Total RNA was extracted from whole blood as well as oral/rectal swabs and nasal washes using the QIamp viral RNA minikit (Qiagen, USA) according to the manufacturer's instructions with the sole modification being that for whole blood a second AW1 wash was performed. Total RNA was extracted from 30 mg homogenized tissues using the RNeasy Kit, according to the manufacturer's instructions (Qiagen, USA). Levels of viral RNA were quantified by RT-qPCR as described in *Section 2.3.4*.

### 2.4.6. Quantification of Infectious Virus by $TCID_{50}$

Vero E6 cells were seeded in 96-well plates at a cell density of 2.0 x $10^4$ cells/well to achieve a confluency of 90-95% after 24 h. The following day, medium was aspirated and replaced with DMEM supplemented with 1% HI-FBS, 1% L-glutamine and 1% penicillin/streptomycin added to each well. Tissues (liver, spleen, kidney, heart, lung, testes and brain) were homogenized in 750 µL DMEM containing a 5 mm steel bead using the Bead Ruptor Elite (Omni International,

USA), and clarified by centrifugation. Whole blood or clarified tissue homogenate (40 µL) was diluted in 360 µL of DMEM supplemented with 1% HI-FBS, 1% L-glutamine and 1% penicillin/streptomycin and serially diluted 10-fold ($10^{-1}$-$10^{-8}$). Diluted samples (100 µL) were added to the Vero E6 cells and incubated at 37°C and 5% $CO_2$ for 14 days, at which time cytopathic effects (CPE) were observed. The median tissue culture infectious dose ($TCID_{50}$) reported as $TCID_{50}$/mL for blood and $TCID_{50}$/g were calculated using the Reed–Muench method.

## 2.5. *In vitro* Evaluation of Type I IFN Response Inhibitors on Filovirus Infected Ferret Cell Lines

### 2.5.1. Cells

Ferret cell lines namely ferret spleen *(mpf*Spleen), heart *(mpf*Heart) and lung (*mpf*Lung) cells and Vero E6 cells were cultured as described in *Section 2.3.1*. All cell lines were maintained in a humidified incubator at 37°C and 5% $CO_2$ and tested negative for mycoplasma contamination using the MycoAlert® Mycoplasma Detection Kit (Lonza, Switzerland).

### 2.5.2. Viruses

Recombinant MARV expressing the ZsGreen fluorophore (MARV-ZsG) was obtained from the Centers for Disease Control (CDC) [359] and used for the *in vitro* ruxolitonib pilot study at P2. EBOV-GFP, a recombinant EBOV variant Mayinga expressing green fluorescent protein (GFP) was rescued previously and used for the *in vitro* ruxolitonib pilot study at P2. MARV variant Angola 709 was propagated from a clinical blood sample collected during the 2004 Angola outbreak. Briefly, blood (P0) was used to inoculated Vero E6 cells at a 1:1000 dilution and the resulting P1 stock used for the growth kinetic assay on ferret cell lines. MARV variant Musoke described in *Section 2.3.1* was used for the growth kinetic assay on ferret cell lines and evaluating type I IFN response inhibitors *in vitro*. EBOV variant Makona-C07 described in *Section 2.3.1* was used for the growth kinetic assay on ferret cell lines. EBOV-mGP described in *Section 2.4.1* was

used for the growth kinetic assay on ferret cell lines. GPA-EBOV (variant Mayinga) and GPA-MARV (variant Angola) were established as described previously [360,361] and both used for the growth kinetic assay on ferret cell lines at P1. RAVV was used for the growth kinetic assay on ferret cell lines at P1. MA-EBOV (variant Makona-C07) and MA-MARV (variant Angola) were established as previously described and used for the growth kinetic assay on ferret cell line at P1 [256,260]. MA-MARV was established as described previously [260]. The virus stock of the aforementioned MA-MARV developed in our lab was found to be contaminated with mycoplasma prior to beginning the study. As such, a fresh stock was propagated and subsequently plaque purified. Virus sequence was confirmed by NGS and found to be 100% identical to MA-MARV (GenBank: KM261523.1) except for two reversions in GP namely amino acid mutation D422N (86.4% frequency) and nucleotide mutation T8378C (99.5% frequency). These reversions were considered negligible as they are present in the original homogenate from which KM261523.1 was derived and only appeared once the homogenate was propagated to generate a virus stock and thus represent cell culture adaptations.

### 2.5.3. Growth Kinetics of Various Filoviruses on Ferret Cell Lines

Prior to infection, *mpf*Spleen, *mpf*Heart, *mpf*Lung and Vero E6 cells were seeded in 24-well plates at densities of 0.6 x $10^5$, 1.4 x $10^5$, 1.5 x $10^5$, 1.2 x $10^5$ cells/well respectively in the aforementioned media to achieve a confluency of ~70-75% after 24 h. The following day, media was aspirated, and the cells infected at an MOI of 0.1 with the following viruses: EBOV (variant Makona-C07), MARV (variants Musoke and Angola 709), EBOV-mGP, MA-MARV (variant Angola), MA-EBOV (variant Makona-C07), GPA-MARV (variant Angola), GPA-EBOV (variant Mayinga), RAVV and SUDV (variants Gulu). Infections were performed as described in *Section 2.3.3* with supernatants harvested at 3, 5, 7, 10, 14 and 21 dpi for virus quantification.

### 2.5.4. Drugs

Ruxolitionib (Cat #tlrl-rux) and BX795 (Cat #tlrl-bx7) were obtained lyophilized from Invivogen (USA) and diluted in dimethyl sulfoxide (DMSO) to a stock concentration of 20 mM. TPCA-1 (Cat#S2824), CYT-387 (Cat#S2219), AZD1480 (Cat#S2162) and Tofacitinib (Cat#S2789) were obtained lyophilized from Selleckchem (USA) and diluted in DMSO to a stock concentration of 20 mM.

### 2.5.5. Ruxolitonib Pilot Study

Prior to infection, *mpf*Spleen cells were seeded in 96-well clear bottom black plates (Corning, USA) at a density of 6.25 x $10^4$ cells/well to achieve a confluency of ~90-95% after 24 h. The following day, media was aspirated, and 50 µL of 2-fold serially diluted ruxolitonib (40 µM-0.625 µM) in DMEM supplemented with 1% FBS, 1% penicillin/streptomycin added to each well in triplicate. No drug wells received 50 µL DMEM supplemented with 1% FBS, 1% penicillin/streptomycin. EBOV and MARV were serially diluted 10-fold (1:10, 1:100, 1:1,000) in DMEM supplemented with 1% FBS, 1% penicillin/streptomycin and 50 added to each well in triplicate. Infections were incubated at 37°C and 5% $CO_2$ for 7 days after which plates were fixed overnight with 10% buffered formalin. After 24 h, formalin was replaced with fresh formalin and heat-sealed in bags and the plates subsequently removed from CL4. Plates were left to fix for an additional 24 h in the fresh 10% buffered formalin.

#### 2.5.5.1. Immunofluorescence Assay and Plate Read

Plates were removed from the bags containing 10% buffered formalin and subsequently dunked in PBS to remove residual formalin. Plates were then washed 3 times for 5 min each wash with 150 µL wash buffer (PBS supplemented with 1% FBS) using a microplate washer. Upon washing, cell were permeabilized with 50 µL 0.25% triton X-100 diluted in PBS. Permeabilizations were incubated at R.T for 15 min followed by washing as described. Next, plates

were blocked for 30 min at R.T with 100 µL 20% (v/v) goat serum (Sigma-Aldrich, USA) diluted in PBS. Plates were washed as described and 50 µL primary antibodies diluted 1:200 in PBS supplemented with 1% FBS added to each respective well. Primary antibodies are as follows rabbit anti-MARV NP pAb (IBT, USA, Cat# 0303-012), mouse anti-MARV VP40 mAb (IBT, USA, Cat# 203-016) and rabbit anti-EBOV NP pAb (IBT, USA, Cat# 0301-012). Plates were incubated in the presence of antibody for 1 h at R.T followed by washing as described above. Next, 50 µL DAPI (Invitrogen, USA) was added to each well at a concentration of 300mM in PBS. Following incubation at R.T for 5 min plates were washed and 50 µL of secondary antibody (diluted 1:1,000 in PBS) namely goat anti-Rb IgG Alexa Fluor Plus 555 (Invitrogen, USA) and goat anti-Ms IgG Alexa Fluor Plus 647 (Invitrogen, USA). Plates were incubated in the dark for 1 h R.T followed by a final wash as described above except each wash being 10 min instead of 5 min. Stained plates were imaged using either and EVOS M5000 Imaging System (Thrermofisher scientific, USA) or using a Cytation 7 Cell Imaging Multimode Reader (Agilent, USA).

#### 2.5.6. Testing of Type I IFN Response Inhibitors on MARV Infected Ferret Cell Lines

Prior to infection, *mpf*Spleen, *mpf*Heart, *mpf*Lung and A549 cells were seeded in 24-well plates at densities of 0.6 x $10^5$, 1.4 x $10^5$, 1.5 x $10^5$, 0.75 x $10^5$ cells/well respectively in DMEM supplemented with 2% FBS and 1% penicillin/streptomycin to achieve a confluency of ~75-80% after 24 h. The following day, media was aspirated, and the cells infected at an MOI of 0.1 with either MARV Musoke in 250 µL DMEM. Infections were incubated at 37°C and 5% $CO_2$ for 1 h with rocking every 15 min to allow for virus adsorption. After 1 h, virus inoculum was removed and replaced with 1 mL DMEM supplemented with 2% FBS, 1% penicillin/streptomycin containing type I IFN response inhibitors namely ruxolitinib, TPCA-1, BX795, CYT-397, AZD1480 and Tofacitinib at concentrations of 5, 2.5 and 1.25 µM. Drug treatments were done in

triplicate with no drug and mock infected wells included as controls. Supernatants were harvested at 3,5, 7,10 and 14 days-post-infection (dpi) for virus quantification by RT-qPCR as described in *Section 2.3.4*.

## 2.6. Evaluate the Pathogenicity of Rodent-Adapted Filoviruses *In vivo* Within Ferrets

### 2.6.1. Viruses

GPA-EBOV (variant Mayinga) and GPA-MARV (variant Angola) were established as described previously [360,361]. MA-MARV was established as described previously [260]. The virus stock of the aforementioned MA-MARV developed in our lab was found to be contaminated with mycoplasma prior to beginning the study. As such, a fresh stock was propagated and subsequently plaque purified. Virus sequence was confirmed by NGS and found to be 100% identical to MA-MARV (GenBank: KM261523.1) except for two reversions in GP namely amino acid mutation D422N (86.4% frequency) and nucleotide mutation T8378C (99.5% frequency). These reversions were considered negligible as they are present in the original homogenate from which KM261523.1 was derived and only appeared once the homogenate was propagated to generate a virus stock and thus represent cell culture adaptations. All virus stocks used for animal infections were mycoplasma negative.

### 2.6.2. Ethics Statement

As described in *Section 2.4.3*

### 2.6.3. Animals

Male (n=3) and female (n=3) ferrets (Mustela putorius furo) ~ 5-6 months old and weighing approximately 0.65-0.7 kg were purchased from Marshall BioResources and implanted with an IPTT-300 temperature and ID transponder (BioMedic Data Systems Inc., USA). Following acclimatization, ferrets were randomly assigned into groups containing equal numbers of males

and females and inoculated with either GPA-EBOV (n=6), GPA-MARV EBOV (n=6) or MA-MARV (n=6) at a target dose of 1000 $TCID_{50}$ via the IM route. Virus inoculums were prepared in DMEM and administered equally at two sites (250 µL/rear quadricep). Animals were monitored daily for clinical signs of disease including changes in body weight, temperature, physical activity, and food/water intake. Animals that reached the clinical scoring criteria for humane endpoint were euthanized. Whole blood (EDTA), Lithium-Hep and serum were collected pre-infection (Pre) as well as at 3, 5, 7, 10, 14 and 21 days-post infection (dpi), and at time of euthanasia for downstream analysis. Oral, rectal and nasal swabs were collected at the aforementioned time points. Tissues, including liver, spleen, kidney, heart, testes, ovaries, eyes and brain, were harvested at time of necropsy from all animals for downstream analysis.

### 2.6.4. Hematology

Plasma biochemistries were evaluated using the VetScan VS2 blood analyzer (Abaxis, USA), according to the manufacturer's instructions using whole blood collected in lithium heparin tubes (BD, USA). Complete blood counts (CBC) were evaluated using the VetScan HM5 hematology system (Abaxis, USA), using whole blood collected in EDTA tubes (BD, USA). Blood gases from whole blood collected in lithium heparin tubes were analyzed using the i-STAT Alinity v (Abbott, USA) equipped with the i-STAT CG8+ cartridge (Abbott, USA) according to the manufacturer's instructions.

### 2.6.5. Quantification of viral RNA by RT-qPCR

Total RNA was extracted from whole blood as well as oral, rectal and nasal swabs as described in *Section 2.4.5* or on the KingFisher using the viral pathogens kit (Applied Biosystems, USA) according to the manufactures instructions. Total RNA was extracted from 30 mg homogenized tissues using the KingFisher as described above, with the exception that RNA was

eluted in 50 µL elution buffer. Levels of viral RNA were quantified by RT-qPCR as described in *Section 2.3.4*.

### 2.6.6. Quantification of Infectious Virus by $TCID_{50}$

As described in *Section 2.4.6* with the following modifications. Replacement of the media was the following day was done using DMEM supplemented with 2% HI-FBS, 1% L-glutamine and 1% penicillin/streptomycin. Additionally, tissues were homogenized in 1000 µL DMEM instead of 750 µL.

### 2.6.7. Next-Generation Sequencing of RNA Extracted From Blood and Tissues

Total RNA was extracted from either whole blood or homogenized tissues as described in *Section 2.4.5* were subjected to NGS to track virus evolution over time. NGS was performed as described in *Section 2.3.2*.

### 2.6.8. 12-Plex Ferret Cytokine Luminex Assay

Gamma irradiated serum from animals challenged with GPA-EBOV, GPA-MARV and MA-MARV were subjected to a Luminex Assay using the 12-plex ferret cytokine panel (Ampersand bio, USA) testing the following analytes IFNγ, IL-2, IL-4, IL-6, IL-8, IL-12p40, IL-12p70, IL-17, MIP-1β, MCP-1, TNFα and IP-10. Its important to note that specific lot used for this study had a recall due to the fact that the target for IFNγ was actually IFNα. As such, any data collected with respect to IFNγ actually reflects IFNα. The Luminex assay was performed according to the manufactures instructions with the sole modification being that serum was clarified by centrifugation prior to the assay. Luminex plates were read using the MAGPIX Luminex system (Invitrogen, USA) with data collection, interpretation and analysis done using the xPONENT software. Historical control sera from ferrets challenged with WT-EBOV (n=2) and WT-MARV (n=2) from a previously published study [362] were included to establish a baseline cytokine profile of ferrets challenged with wildtype filoviruses.

## 2.7. Evaluate the Pathogenicity of Taï Forest Virus *In vivo* Within Ferrets

### 2.7.1. Ethics Statement

As described in *Section 2.4.3*

### 2.7.2. Viruses

Taï Forest virus (TAFV) isolate Tai Forest virus/H.sapiens-tc/CIV/1994/Tai Forest-CDC807212 (GenBank: KU182910.1) was previously obtained from the Centers for Disease Control and Prevention (Atlanta, USA) with an unknown passage history. The virus used in this study was a P4 working stock previously passaged on Vero E6 cells at CSCHAH. Deep sequencing of the P4 working stock revealed the virus was 100% identical to the TAFV reference sequence (GenBank: KU182910.1). The stock virus was tested for mycoplasma contamination using the Microstart RESEARCH Mycoplasma Detection kit as per the manufacturer's instructions (Sartorius, Germany).

### 2.7.3. Animals

Male (n = 4) and female (n = 4) ferrets (Mustela putorius furo), ~14–16 weeks old and weighing approximately 0.6–0.75 kg, were purchased commercially from Marshall Bioresources (New York, USA). All animals were given anticoccidials, in addition to vaccines against distemper and rabies virus at time of purchase. Additionally, all animals were implanted with an IPTT-300 temperature and ID transponder (BioMedic Data Systems Inc., USA). All animals were housed in the CL-4 facility at CSCHAH within negative pressure caging units supplied with high-efficiency particulate air (HEPA)-filtered air.

Ferrets were randomly assigned into two groups (n = 4), each with an equal number of male and females, and challenged either intramuscularly (IM) or intranasally (IN) with TAFV at a target dose of 1000 $TCID_{50}$ (back titered to 200 $TCID_{50}$), diluted in plain DMEM High Glucose (Hyclone, USA) to a final volume of 500 µL. The inoculum was equally administered (250 µL/site)

at two sites (both rear quadriceps for IM and both nostrils for IN) to ensure consistent infection among animals. Animals were monitored daily for signs of disease, which included changes in body weight, temperature, physical activity, and food/water intake. Whole blood was collected at −1, 3, 5, 7, 10, 14, and dpi, and at the study endpoint on day 26 post-infection to evaluate plasma biochemistry and CBC. Tissues, including liver, spleen, kidney, and lung, were harvested at study endpoint (26 dpi) from one male and one female from each group (258F, 754M, 649F, and 835M) for downstream viral RNA analysis.

### 2.7.4. Hematology

Plasma biochemistries and complete blood counts were evaluated as described in *Section 2.6.4*

### 2.7.5. Quantification of viral RNA by RT-qPCR

Total RNA was extracted from blood using the QIamp viral RNA minikit and from homogenized tissue using the RNeasy Kit as described in *Section 2.4.5*. Viral RNA levels were determined via RT-qPCR using the Lightcycler 480 RNA Master Hydrolysis probes kit (Roche, USA) with two sets of primers and probes targeting either TAFV L or NP. All RT-qPCR reactions were performed using a Quantstudio 3 Real-time PCR system (Applied Biosystems, USA) with the following cycling conditions: 63 °C for 3 min, 95 °C for 30 s, followed by 45 cycles of 95 °C for 15 s, 60 °C for 30 s. Samples with cycle threshold (CT) values of ≤36 were considered positive, whereas samples with CT values >36 but <40 were considered equivocally positive. Any sample with a CT ≥40 was considered negative.

### 2.7.6. Generation and Purification of TAFV GP

A plasmid encoding human codon optimized TAFV GP1 possessing an S tag was transfected into Expi293 cells using the ExpiFectamine 293 Reagent (Life Technologies, USA),

according to the manufacturer's instructions. Cells were harvested four days post-transfection by centrifugation at 3000× g for 10 min. EDTA was added to the supernatant to a final concentration of 10 mM, and the supernatant was subsequently incubated with S-protein agarose beads (Novagen) overnight at 4 °C with gentle shaking. The beads were collected in a spin filter column with gravity flow. The column was washed three times with wash buffer (0.15 M NaCl, 20 mM Tris-HCl, 0.1% TritonX-100, pH 7.5) by centrifuging at 500 × *g* for 5 min and eluted with 0.1 M citric acid (pH 2.5). The eluate was immediately neutralized with 3 M Tris base, followed by dialysis against PBS. Protein was then concentrated using Amicon Ultra-15 centrifugal filter units, and the purified proteins quantified using the BCA protein assay kit (Thermo Fisher Scientific, USA), per the manufacturer's instructions.

### 2.7.7. Evaluation of Humoral Immune Response by ELISA

Plasma samples collected on −1, 14, 20, and 26 dpi were subjected to an enzyme-linked immunosorbent assay (ELISA) developed in-house to quantify TAFV GP-specific immunoglobulin G (IgG). Briefly, 96-well half-area high binding plates (Corning, USA) were coated overnight at 4 °C with 1 µg/mL TAFV GP (described above) diluted in 50 mM carbonate buffer (pH 9.6). The following day, plates were blocked for 1 h at 37 °C with 5% (w/v) skim milk (BD, USA) diluted in phosphate-buffered saline (PBS) containing 1% (v/v) Tween-20 (1% PBST). Plasma samples were serially diluted 10-fold in 1% (w/v) bovine-serum albumin (BSA) prepared in PBS (1% BSA) starting at a dilution of 1:400 for all samples except pre-bleed (−1 dpi), for which the initial dilution was 1:100. After blocking, the plates were gently blotted, 30 µL diluted plasma was added to wells in triplicate, and plates were incubated for 1 h at 37 °C. Plates were then washed 4 times with 150 µL wash buffer (0.1% PBST) using a microplate washer. After washing, plates were blotted to remove residual wash buffer and subsequently incubated for 1 h at

37 °C with 30 µL/well HRP-conjugated goat anti-ferret IgG secondary antibody (Bethyl laboratories, Montgomery, TX, USA) diluted 1:10,000 in 1% BSA. Plates were then washed as described and incubated in the dark with 50 µL/well TMB (Thermo Fisher Scientific, USA) for 30 min at room temperature. The optical density (OD) was recorded at 650 nm using the Synergy HTX plate reader (Bio-Tek, USA). The OD cut-off was defined as the average of the pre-bleeds (1/100 dilution) plus 3 standard deviations.

### 2.7.8. Data Analysis

Interpretation of all RT-qPCR data was undertaken using the Quantstudio Design and Analysis Software (Applied Biosystems, USA). All graphs and statistics were generated using GraphPad Prism 8.0. All illustrations were prepared using Biorender (BioRender.com). Statistical analysis for blood biochemistry and complete blood count were performed using a two-way ANOVA analysis with Tukey's multiple comparisons test, with individual variances computed for each comparison. p values are as follows >0.05 (ns), ≤0.05 (*), ≤0.01 (**), ≤0.001 (***), ≤0.0001 (****).

# 3. Chapter 3: The Inability of Marburg Virus to Cause Disease in Ferrets is Not Solely Linked to the Virus Glycoprotein

*The material in this section has been published previously in* Schiffman, Z. *et al.* The Inability of Marburg Virus to Cause Disease in Ferrets Is Not Solely Linked to the Virus Glycoprotein. *The Journal of Infectious Diseases* 228, S594–S603 (2023) [363] *and is unmodified except for formatting to match the style of this thesis.*

## 3.1. Background

The domestic ferret (*Mustela putorius furo*) has become increasingly popular in recent years as an animal model for characterizing filovirus pathogenesis and evaluating the efficacy of candidate vaccines and therapeutics [364]. Unlike rodent models, the ferret model provides the advantage of being susceptible to most wild-type filoviruses, eliminating the need for host adaptation [364]. Moreover, ferrets exhibit disease progression that closely recapitulates human filovirus disease (FVD). Indeed, ferrets have been shown to be highly susceptible to several ebolaviruses, namely Ebola virus (EBOV) [340,341,344,346], Sudan virus (SUDV) [340,342], Bundibugyo virus (BDBV) [340,341] and Reston virus (RESTV) [343], all of which are uniformly lethal among infected animals. In contrast, Taï Forest virus (TAFV) is non-lethal among ferrets [365]. Unlike most ebolaviruses, however, inoculation with marburgviruses, namely Marburg virus (MARV) and Ravn virus (RAVV), does not cause disease in ferrets [347,348]. Although MARV-challenged ferrets have been shown to seroconvert following inoculation, none of the animals became viremic at any time point nor were there any disturbances observed in blood biochemistry or cell counts [347,348].

The fact that ferrets are highly susceptible to lethal infection with certain ebolaviruses but not marburgviruses suggests that these viruses differ in their pathogenic mechanisms. It is likely that these differences can be attributed to variation in one or more aspects of the virus replication

cycle, such as attachment, entry, replication, transcription, immune evasion, or egress. To investigate why MARV is non-pathogenic in ferrets, we chose to focus on the role of the glycoprotein (GP). As the sole viral protein expressed on the virion surface, GP plays an essential role in attachment to the host cell as well as entry into the cytosol via interaction with Niemann-Pick C1 (NPC1) [366]. Given its essential role in viral entry, we hypothesized that the lack of susceptibility by ferrets to lethal MARV infection is due to a block in GP-mediated viral entry.

Despite our hypothesis, we demonstrate here that MARV GP is, in fact, capable of mediating entry into ferret cells and that authentic MARV is capable of replication within these cells, albeit to lower levels than those observed for EBOV. Finally, we demonstrate that recombinant EBOV expressing MARV GP in place of EBOV GP is uniformly lethal among ferrets, suggesting that the inability of MARV to cause lethal disease in ferrets is not solely mediated by GP.

## 3.2. Results: Ferret spleen Cells Are Permissible to MARV GP-mediated Entry

Given that viral attachment and entry are the earliest stages of the filovirus replication cycle, we first set out to investigate whether ferret spleen cells were permissible to MARV GP-mediated entry. Ferret spleen cells were inoculated at an MOI of 0.1 with either VSV-EBOV or VSV-MARV, and supernatant was harvested at 3, 6, 8 and 12 hpi to quantify levels of viral RNA. Viral RNA was detectable in the supernatant of ferret spleen cells infected with VSV-MARV at all time points, indicating that MARV GP is capable of mediating entry into these cells (Figure 8). The same results were observed in Vero E6 cells (Figure 8). Interestingly, levels of VSV-EBOV RNA were slightly but significantly higher than VSV-MARV in the supernatant of ferret spleen cells and Vero E6 cells at 3 hpi (Figure 8), suggesting that EBOV GP may be more efficient at mediating entry during early stages of infection. No significant difference among levels of viral

RNA could be seen beyond 12 hpi (data not shown), which was expected given the rapid replication kinetics of VSV.

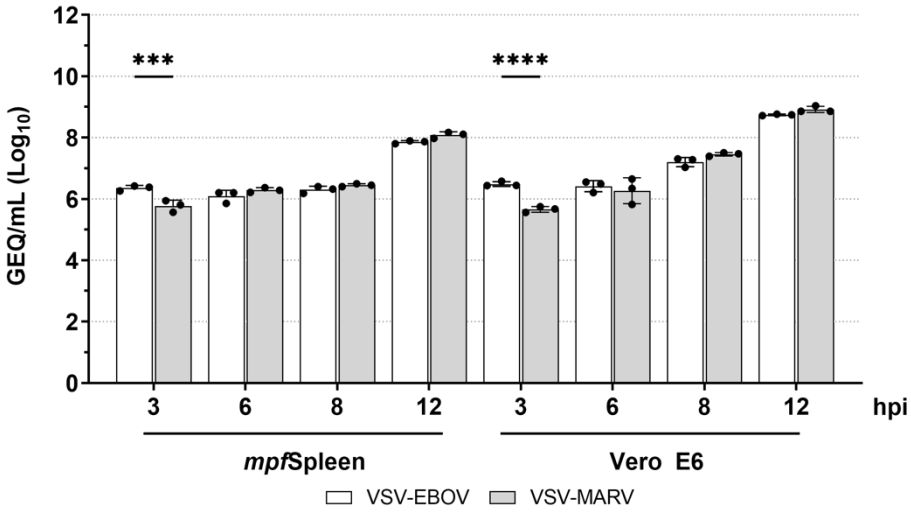


**Figure 8. Quantification of viral RNA in supernatant of cells inoculated with VSV pseudotypes.**
Ferret spleen (*mpf*Spleen) and Vero E6 cells were inoculated with either VSV-EBOV (white) or VSV-MARV (grey) at an MOI of 0.1 and levels of viral RNA quantified at 3-, 6-, 8- and 12-hours post-infection (hpi) in supernatant. Mean levels ± SD of viral RNA in genome equivalents per mL (GEQ/mL) are depicted as histograms, with the individual technical replicates depicted as black dots. Figure and caption obtained from [362]

## 3.3. Results: MARV is Capable of Replicating in Ferret Cells

Although ferret spleen cells were found to be permissible to MARV GP-mediated viral entry, we wanted to investigate whether ferret cells could support replication of authentic MARV. Ferret spleen, lung, and heart cells, along with Vero E6 cells, were inoculated at an MOI of 0.1 with MARV or EBOV, and levels of viral RNA and infectious virus were quantified in supernatant at 3, 7, and 14 dpi. Not surprisingly, peak levels of virus RNA and infectious virus were highest among Vero E6 cells, which are highly permissive to both EBOV and MARV. All ferret cell lines supported replication of EBOV, with levels of viral RNA reaching ~9 log10 genome equivalents (GEQ)/mL after 14 dpi (Figure 9A). Infectious EBOV could also be detected across all ferret cell lines, which showed an increase in titers from 3 to 14 dpi (Figure 9C). For MARV, viral RNA was

detected in all ferret cell lines at all time points, although the increases over time were modest, particularly for the spleen cells (Figure 9B). Indeed, with the exception of a single replicate at 3 dpi, no infectious MARV was recovered from the spleen cells, suggesting that this cell line does not support MARV replication (Figure 9D). In contrast, ferret lung cells showed significantly elevated levels of infectious MARV at 14 dpi relative to 3 dpi (Figure 9B). Despite ferret heart cells showing an increase in MARV viral RNA over time, the increase in infectious titers was much less pronounced (Figure 9D).

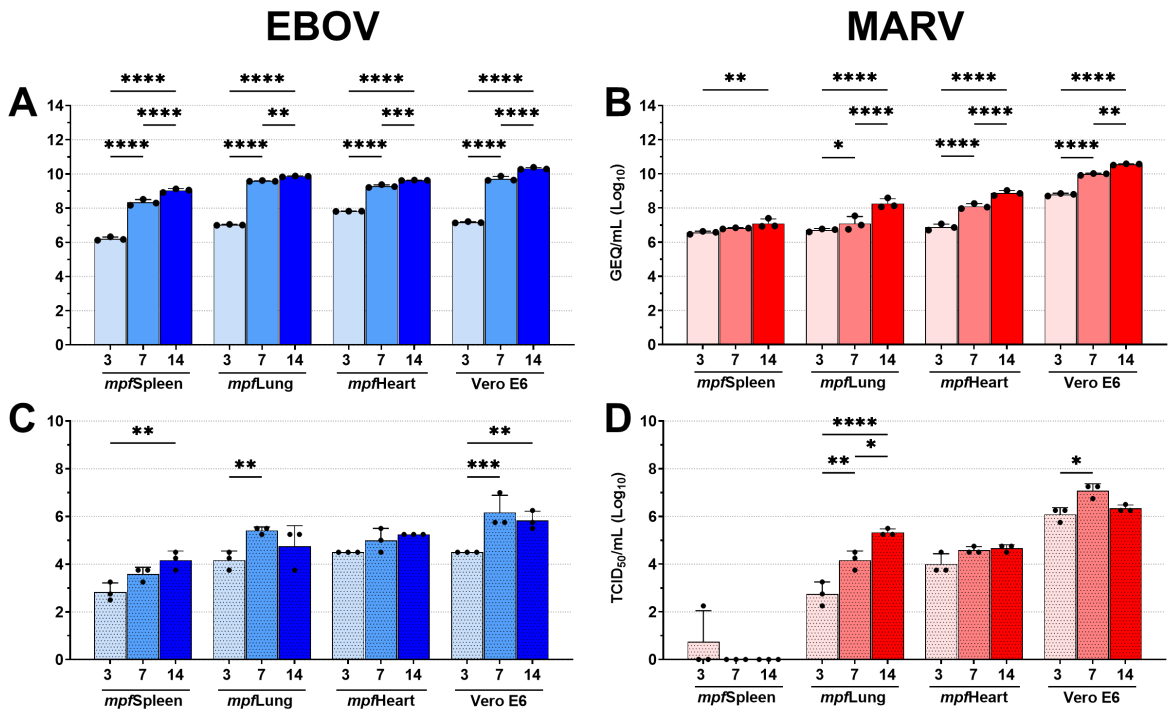


**Figure 9. Replication kinetics of EBOV and MARV in ferret cell lines.**

**A-D**, Ferret spleen (*mpf*Spleen), lung (*mpf*Lung), Heart (*mpf*Heart), and Vero E6 cells were inoculated with EBOV (**A, C**) or MARV (**B, D**) at an MOI of 0.1; virus RNA within the supernatant was quantified by RT-qPCR (**A, B**) and infectious virus within the supernatant was quantified by $TCID_{50}$ (**C, D**) at 3, 7, and 14 days post-infection (dpi). Mean levels ± SD of viral RNA in genome equivalents per mL (GEQ/mL) or mean tissue culture infectious dose per mL ($TCID_{50}$/mL) are depicted as histograms, with the individual technical replicates depicted as black dots. Figure and caption obtained from [362]

## 3.4. Results: EBOV-mGP is Uniformly Lethal Among Infected Ferrets

With our *in vitro* data confirming that MARV GP is capable of mediating entry into ferret cells and that authentic MARV can replicate (albeit modestly) in at least 2 different ferret cell lines, we next set out to evaluate the role of MARV GP in virus pathogenesis. To begin, we generated a recombinant EBOV-mGP. All ferret cell lines and Vero E6 cells were confirmed to support genome replication of EBOV-mGP *in vitro*, with levels of viral RNA reaching ~9 log10 GEQ/mL after 14 dpi (Figure 10). It is interesting to note that these levels were slightly albeit significantly lower than those observed for EBOV at 3, 7, and 14 dpi across all cell lines, suggesting that EBOV-mGP may have slower growth kinetics than EBOV.

To confirm the involvement of MARV GP *in vivo*, ferrets (n = 6) were inoculated with EBOV-mGP. A group of control ferrets were inoculated with EBOV (n = 2) or MARV (n = 2). The target inoculation dose was 1000 TCID50, and back titration revealed actual doses to be 734, 500, and 2180 TCID50 for EBOV-mGP, EBOV, and MARV, respectively. EBOV-mGP resulted in uniform lethality, with most animals (5 of 6) reaching the humane endpoint on 7 dpi and 1 animal found dead on 9 dpi (Figure 11A). By comparison, all control animals inoculated with EBOV reached the humane endpoint on 4 dpi (Figure 11A). Ferrets challenged with EBOV-mGP developed severe disease that paralleled what was observed in the EBOV-challenged ferrets, with all animals exhibiting weight loss, elevated temperatures (Figure 11B and C), decreased activity, and ruffled fur. A petechial rash, which represents a hallmark feature of FVD within the ferret model, was also observed among EBOV-mGP animals, consistent with what was observed in the EBOV-challenged control animals. Conversely, none of the animals inoculated with MARV succumbed to disease nor did they manifest any clinical signs of disease, with temperatures remaining within the normal range and a net gain in weight (Figure 11). Nonetheless, these 2 control animals seroconverted, with mean MARV GP-specific immunoglobulin G endpoint titers

of 1:800 at 14 dpi. To assess the progression of disease, blood samples, oral and rectal swabs, and nasal washes were collected from animals and subjected to RT-qPCR to quantify levels of viral RNA. Animals challenged with EBOV-mGP first exhibited virus RNA in the blood at 5 dpi, with a mean level of 3.10 log10 GEQ/mL that increased to 6.79 log10 GEQ/mL on 7 dpi (Figure 12A). A blood sample was not obtained from the single animal that succumbed to disease on 9 dpi. The swabs and nasal washes were all negative for virus RNA in EBOV-mGP infected animals at 3 and 5 dpi (Figure 12B-D). At 7 dpi, oral swabs from 3 of 6 animals exhibited low levels of viral RNA, with a mean level of 3.03 log10 GEQ/mL (Figure 12B).

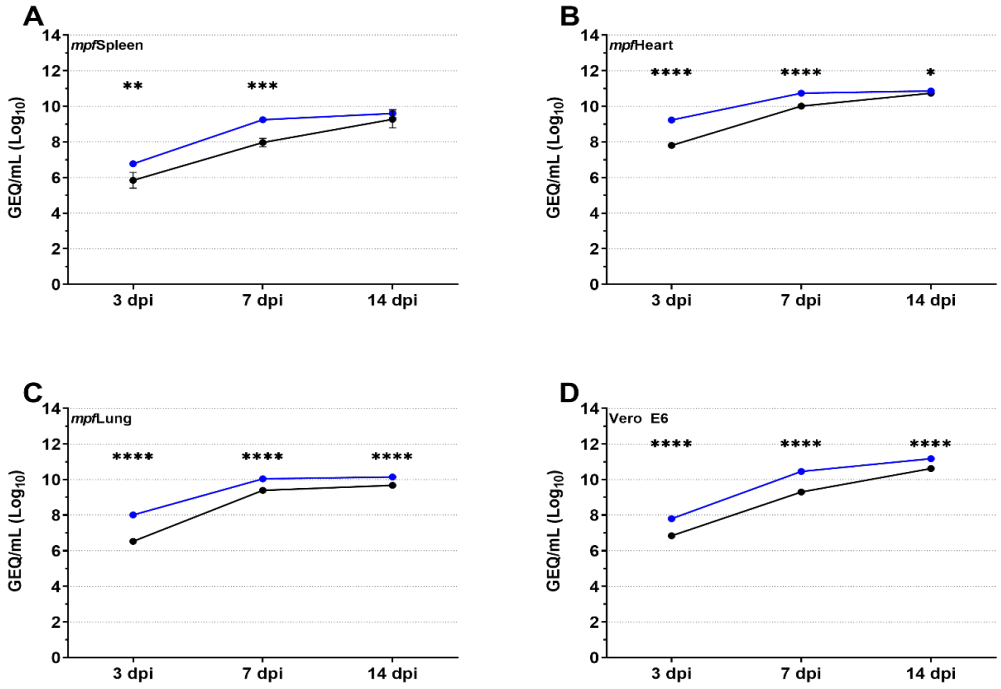


**Figure 10. Replication kinetics of EBOV-mGP and EBOV in ferret cell lines.**

(**A**), Ferret spleen (*mpf*Spleen), (**B**), Heart (*mpf*Heart), (**C**), lung (*mpf*Lung) and (**D**), Vero E6 cells were inoculated with EBOV (blue) or EBOV-mGP (black) at a MOI of 0.1; virus RNA within the supernatant was quantified by RT-qPCR at 3, 7, and 14 days post-infection (dpi). Mean levels ± SD of viral RNA in genome equivalents per mL (GEQ/mL). Error bars may be absent due to overlap with data points. Statistical analyses were performed using a two-way ANOVA Šidák's multiple comparisons test, with a single pooled variance computed for each comparison. P values are indicated as follows > 0.05 (ns), ≤ 0.05 (*), ≤ 0.01 (**), ≤ 0.001 (***) and ≤ 0.0001 (****). Figure and caption obtained from [362]

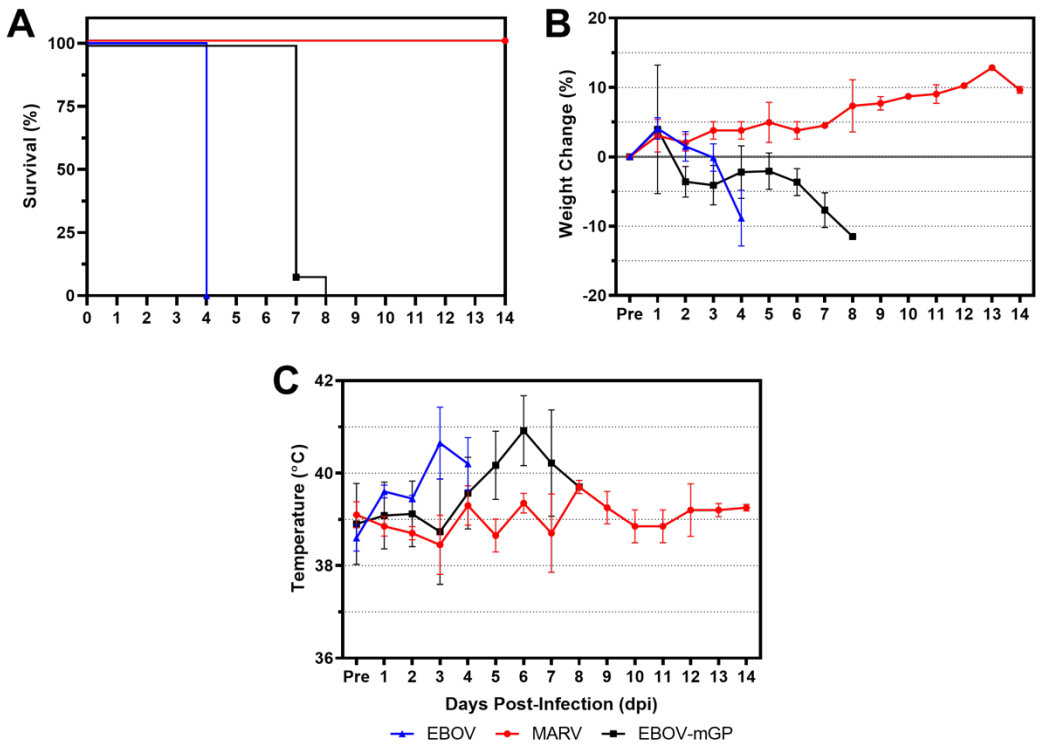


**Figure 11. Clinical parameters of infected ferrets.**

(**A**), survival curves, (**B**), percent weight change, (**C**), temperature. Data shown as group means with error bars reflecting standard deviation. Pre, pre-infection. Figure and caption obtained from [362]

Similarly, rectal swabs from 4 of 6 animals were positive at 7 dpi, with a mean viral RNA level of 3.51 log10 GEQ/mL, whereas RNA was detected in the nasal washes of only a single animal at a level of 3.41 log10 GEQ/mL (Figure 12C and D). Oral swabs (2.54 log10 GEQ/mL), rectal swabs (6.28 log10 GEQ/mL), and nasal washes (2.54 log10 GEQ/mL) were all positive for viral RNA in the single animal found dead on 9 dpi (Figure 12B and D). By comparison, the control animals challenged with EBOV had very high levels of virus RNA in the blood, with a mean level of 7.79 log10 GEQ/mL at 3 dpi that increased to 9.95 log10 GEQ/mL a day later at the time of euthanasia (Figure 12A). Swabs and nasal washes were all negative at 3 dpi but positive at 4 dpi, with mean values of 4.14, 6.00, and 3.25 log10 GEQ/mL, respectively (Figure 12B and D). As

expected, no virus RNA was detected at any time point in any sample from the control animals challenged with MARV.

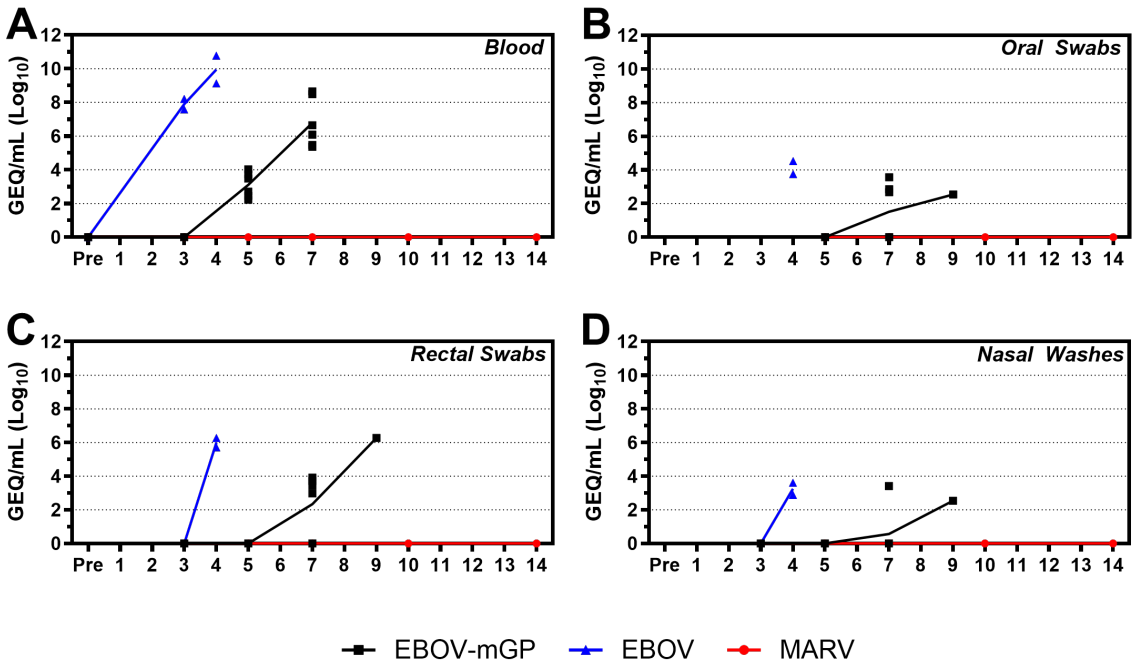


**Figure 12. Viral RNA levels in blood, oral/rectal swabs and nasal washes of infected ferrets.**
(**A**), whole blood (**B**), oral swabs, (**C**), rectal swabs and (**D**), nasal washes were collected from each animal at 3, 5, 7, 10 and 14 days post-infection (dpi) as well as at time of euthanasia to evaluate viremia and viral shedding by RT-qPCR. Results are depicted in genome equivalents per mL (GEQ/mL) for each animal (indicated by a square, triangle, or circle), with mean values depicted by a line. Figure and caption obtained from [362]

Tissues harvested at time of euthanasia, including liver, spleen, kidney, heart, lung, testes, ovaries, brain, and eye, were assessed for the presence of viral RNA and infectious virus to evaluate viral dissemination. All tissues from animals infected with EBOV-mGP or EBOV were positive for both viral RNA and infectious virus (Figure 13). In most cases, RNA and virus levels were higher among the EBOV-challenged control animals than among those challenged with EBOV-mGP, with the highest overall levels of virus observed in the liver and spleen (Figure 13A). Ovaries and eyes were not evaluated for the presence of infectious virus due to insufficient tissue

material. All tissues collected from MARV-inoculated animals were negative for both viral RNA and infectious virus (Figure 13).

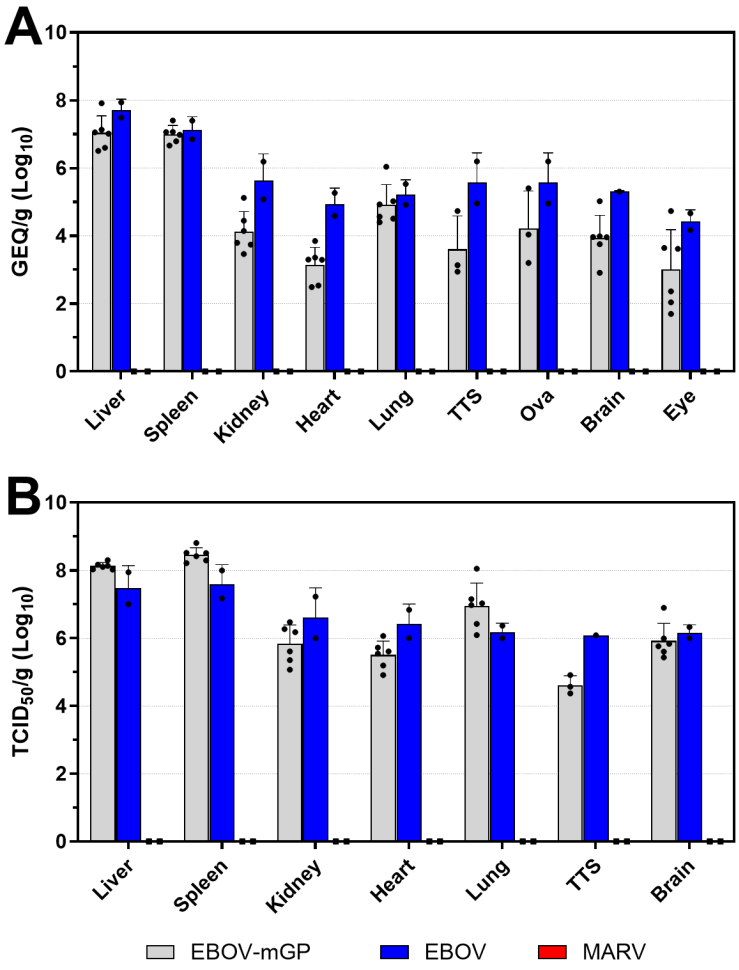


**Figure 13. Viral load in tissues of infected ferrets.**

(**A, B**), Liver, spleen, kidney, heart, lung, testes (TTS), ovaries (Ova), eyes and brain samples were harvested at time of necropsy; virus RNA was quantified by RT-qPCR (**A**) and infectious virus was quantified by $TCID_{50}$ (**B**). Mean levels ± SD of viral RNA in genome equivalents per gram (GEQ/g) or mean tissue culture infectious dose per gram ($TCID_{50}$/g) are depicted as histograms, with data from each animal depicted as black dots. Figure and caption obtained from [362]

## 3.5. Discussion: Key Findings, Significance, and Limitations

Despite the ferret being uniformly susceptible to infection with several different ebolaviruses namely, EBOV, SUDV, BDBV, and RESTV repeated studies have demonstrated that the same is not true for the closely related marburgviruses, MARV and RAVV. This is surprising given that ebolaviruses and marburgviruses cause severe, often fatal, disease in both humans and nonhuman primates that is at least superficially similar. Given the key role that MARV and EBOV GP plays in the virus replication cycle, we sought to investigate MARV GP as a potential contributing factor to the absence of MARV pathogenesis in the ferret.

Using pseudotyped recombinant VSVs, ferret spleen cells were found to be permissible to EBOV GP-mediated entry. This was not unexpected given that ferrets are highly susceptible to infection with EBOV, and it therefore follows that ferret cells should be permissible to VSV pseudotyped with EBOV GP. It is interesting to note that the ferret spleen cells were also found to support entry of VSV-MARV, suggesting that MARV GP is capable of not only interacting with host cell attachment factors but also mediating entry into the host cell, presumably via binding to ferret NPC1, which shares ~90% identity with human NPC1 (Figure 14). It is notable that at only 3 hpi, we did observe VSV-EBOV RNA levels that were slightly but significantly higher than VSV-MARV RNA levels in both ferret spleen cells and Vero E6 cells. It is possible that this is due to a difference in the efficiencies with which these two GPs interact with potential host cells, and it is tempting to speculate that a less efficient MARV GP could, in part, contribute to the lack of disease observed in ferrets. Indeed, this interpretation is in line with previous work demonstrating that filovirus GPs differ in their ability to mediate entry into cell lines of various species based on a differential ability to engage diverse host-cell entry factors [367]. Nevertheless, we also cannot rule out the possibility that the difference in viral RNA levels we observed was an artifact linked to residual input virus. In the future, it will be of particular interest to directly

evaluate the differences in binding efficiencies of various filovirus GPs to ferret NPC1 as well as host-cell attachment factors.




**Figure 14. Alignment of ferret and human NPC1 Domain C.**

NPC-1 luminal domain C (NPC1-C) has been shown previously to be responsible for binding to cathepsin-cleaved Ebola virus GP [368]. The amino acid sequences of NPC1-C (red box) for the ferret (NCBI Reference Sequence No. XP_004742895.2) and human (NCBI Reference Sequence No. NP_000262.2) proteins were aligned, and analysis revealed ~90% identity between the two proteins within NPC1-C. Moreover, the NPC1-C residues that have been determined to interact directly with Ebola virus GP (highlighted in red) are 100% identical between ferret and human NPC1 [369]. The above alignment was performed using Clustal Omega and NCBI BLASTp [370,371]. Asterisks (*) indicate identical amino acids; a colon (:) indicates two different amino acids with strongly conserved properties; and a period (.) indicates two different amino acids with weakly conserved properties. The values on the right indicate the amino acid number of the last residue in each line of the alignment. Figure and caption obtained from [362]

Although VSV pseudotyped with MARV GP was capable of entering and replicating in ferret spleen cells, the same cells did not seem to support replication of authentic MARV. We observed a modest increase in MARV RNA over the course of a 14-day infection in ferret spleen cells, yet essentially no infectious virus was detected. These results were even more striking given that ferret lung cells had nearly identical levels of virus RNA (particularly at 3 and 7 dpi) but also supported the production of infectious MARV. Like the lung cells, the ferret heart cells also supported MARV replication and the production of infectious virus, suggesting that the block in virus replication was exclusive to the spleen cells. The fact that the spleen cells were permissive

to MARV GP-mediated entry and supported modest genome replication/transcription despite not producing infectious MARV suggests that a block exists later in the virus replication cycle, perhaps affecting virus immune evasion or virion egress. Whether our observations in the ferret spleen cells are linked to the absence of disease caused by MARV in ferrets is unclear and will require additional investigation. However, it is also worth noting that, in general, MARV replicated more poorly in all three ferret cell lines than did EBOV, which is in line with *in vivo* observations and may suggest that the reasons for the differences in ferret pathogenesis between EBOV and MARV are multifactorial.

All ferrets infected with EBOV-mGP succumbed to disease, providing unequivocal evidence that MARV GP is capable of mediating entry into ferret cells. It is interesting to note, however, that the onset of viremia in EBOV-mGP-challenged animals was delayed compared with the EBOV-challenged animals, and peak levels of EBOV-mGP RNA were also much lower. Similar trends were observed in the oral/rectal swabs and nasal washes, which showed consistently lower and later RNA levels among animals challenged with EBOV-mGP than those challenged with EBOV. Furthermore, the majority of tissue samples taken from EBOV-mGP-challenged animals showed levels of virus RNA and infectious virus that were lower than what was observed in EBOV-challenged animals. In addition, the delays observed *in vivo* reflected the *in vitro* growth properties of EBOV-mGP, which exhibited slower replication kinetics compared with EBOV. Thus, although MARV GP may not be the sole factor responsible for the lack of disease in MARV-challenged ferrets, these data support the possibility that it is a contributing factor.

It is important to note that our study has a few key limitations. In general, dissecting the ferret host response to filovirus infection is difficult, both *in vitro* and *in vivo*, primarily because of a lack of commercially available reagents. For our *in vitro* analyses, we recognize that the ferret

cells we used in this study—although derived from ferrets—have yet to be fully characterized. A better understanding of these cell lines would improve our ability to make specific conclusions about our data, but work to characterize the cell lines in depths is ongoing. For our *in vivo* analyses, we currently lack the tools and reagents to perform a more comprehensive analysis of the host response to infection, but we hope that continued work in the ferret model, by us and others, will improve the capabilities of the field.

Taken together, our *in vitro* and *in vivo* data provide insight into the role that MARV GP plays in the context of a ferret infection. First, it is evident that MARV GP is capable of mediating entry into ferret cells. This ultimately indicates that ferret cells support all stages of filovirus GP-mediated entry including attachment, uptake, cleavage of GP via cysteine proteases, binding with NPC1 and subsequent fusion with the host cell endosomal membrane. Second, MARV infection appears to be hindered—at least to some degree—in ferret cells, a conclusion supported both by the cell-type specific restriction of MARV and the delayed kinetics of EBOV-mGP infection in ferrets. Third, the absence of disease among MARV-challenged ferrets cannot be exclusively linked to GP. Therefore, if GP is not the only factor involved in the absence of disease in ferrets, what other factors may play a role? Based on our data, we speculate that the most obvious factors are related to innate immune evasion or virion egress. In particular, both EBOV and MARV inhibit the JAK-STAT signaling pathway, which is responsible for upregulating the expression of numerous antiviral proteins in response to type I interferons; however, each virus uses a distinct inhibitory mechanism [115]. In the case of EBOV, VP24 blocks the nuclear import of STAT1, whereas in the case of MARV, VP40 blocks the upstream activation of JAK1. Perhaps the inability of MARV, but not EBOV, to cause disease in ferrets is linked to the mechanistic differences in the innate immune evasion tactics between these two viruses. Although the lack of ferret-specific

reagents complicates investigations into these cell signaling pathways, future investigations should focus on elucidating the role of MARV VP40 in viral pathogenesis within the ferret model.

Finally, as expected, all animals challenged with MARV survived the duration of the study with no observable signs of disease nor any detectable viremia. This is consistent with previous studies that have demonstrated that ferrets do not develop disease regardless of MARV challenge route, variant, and dose [347,347]. Recent evidence has demonstrated that filoviruses can persist in immune privileged niches [170], and as such we investigated ovaries/testes, eyes, and brain for the presence of MARV in case virus existed in these niches despite not being present in the blood, swabs, or tissues. No evidence of infectious MARV or MARV RNA was detected. These results confirm, again, that MARV is incapable of causing disease in ferrets, and they further suggest that ferrets may not even be susceptible to productive MARV infection.

Overall, these findings provide additional insight into the critical differences between the pathogenic mechanisms of EBOV and MARV. Future investigations into these differences could prove useful for identifying novel therapeutic targets as well as advancing our understanding of filovirus biology.

# 4. Chapter 4: Inhibitors of The Interferon Response Enhance Marburg Virus Replication Within Ferret Cell Lines to Varying Degrees

*This section is comprised of unpublished data.*

## 4.1. Background

As described in *Section 1.4.3* and *Section 1.5.1*, the host innate immune response, particularly the type I IFN response (IFN-α and IFN-β), plays a pivotal role in combatting filovirus infection by triggering a plethora of antiviral signalling pathways establishing an antiviral state and restricting viral replication. This type I IFN response can be divided into two components, namely; 1) production of type I IFNs upon recognition of viral RNAs by the cytoplasmic RNA helicases RIG-I and MDA5 (Figure 15) and 2) activation of antiviral signalling pathways, particularly the JAK/STAT signalling pathway, by type I IFNs ultimately triggering the expression of ISGs essential for inducing an antiviral state induce an antiviral state, rendering cells refractory to viral infection (Figure 16).

As described in *Section 1.5.1* both EBOV and MARV encode VP35, which functions as an antagonist of the innate immune response and is critical for inhibiting the production of type I IFNs (Figure 15). While both EBOV and MARV, through the activity of VP35, inhibit the production of type I IFNs, they also encode proteins, namely VP24 and VP40, which act to inhibit downstream signalling of ISGs via inhibition of the JAK/STAT pathway, albeit through different mechanisms. (Figure 16). In particular, this subversion is mediated by VP24 in the case of EBOV, which acts as a competitive inhibitor of pSTAT1. In contrast, in the case of MARV, this subversion is mediated by VP40, which blocks the activation and function of JAK1 [115].

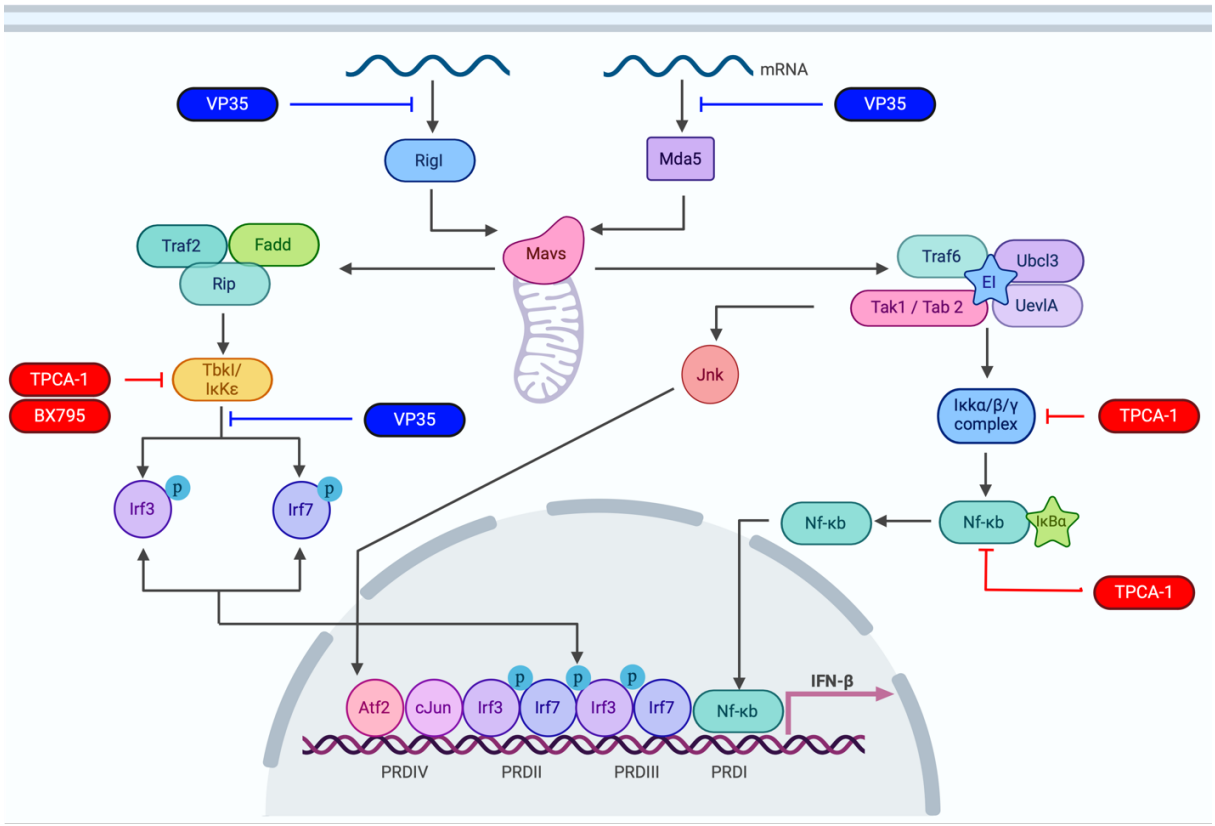


**Figure 15. Depiction of the Type I IFN production pathway and the targets of various drug inhibitors.**
RIG-I and MDA5 are cytoplasmic RNA helicases that detect viral RNAs and induce IFN-response. Upon recognition of 5'triphosphates and dsRNA, RIG-1 and MDA5 become activated and, in turn, activate serine/threonine kinases, namely TANK-binding kinase 1 (TBK1) and IκB kinase-ε (IKKε). Upon activation, TBK1 and IKKε phosphorylate IFN regulatory factor (IRF)-3 and IRF7, transcription factors which, upon accumulation, engage IFN-stimulated response elements (ISREs), triggering the expression of type I IFNs. Filovirus VP35 (denoted in blue) via its C-terminal IFN inhibitory domain (IID), forms a novel fold that recognizes and binds dsRNA intermediates in a sequence-independent manner. This, in turn, prevents the recognition of dsRNA intermediates by RIG-I and MDA-5, ultimately preventing the detection of the pathogen-associated molecular patterns (PAMPs). Highlighted in red are drugs which inhibit the production of type I IFN. Particularly, TPCA-1 targets IKB, STAT3 and NFκβ where BX795 targets TBK1 and IKKε. Figure created on Biorender.com

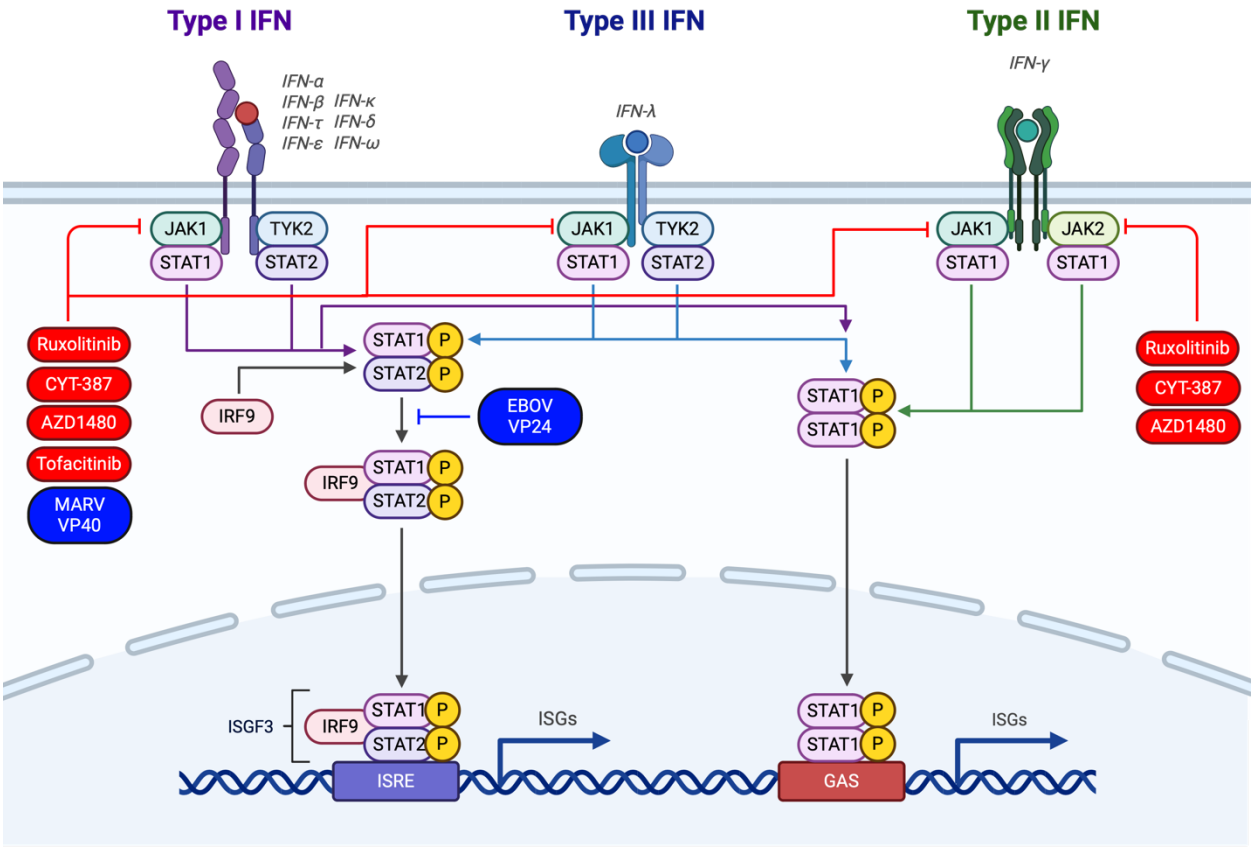


**Figure 16. Depiction of Type I, II and III IFN signaling via the JAK/STAT pathway and the targets of various drug inhibitors.**

Type I, II and III IFNs bind their respective extracellular receptors triggering a signaling cascade via the JAK/STAT pathway ultimately resulting in the expression of a plethora of interferon sensitive genes (ISGs). These ISGs, among which there are >500, result in the expression of a plethora of proteins whose effector functions aim to combat infection through various mechanisms. In the case of EBOV, VP24 competitively binds the pSTAT1 binding site of karyopherin alpha (KPNA), ultimately impairing the nuclear entry of pSTAT1 into the nucleus. As a result of this competitive inhibition, pSTAT1 translocation to the nucleus is impeded, preventing binding to ISG promoters effectively preventing their expression. MARV VP24 (blue) does not bind KPNAs or significantly alter IFN-induced gene expression. Instead, inhibition of IFN signalling by MARV is mediated by VP40 (blue), which blocks the activation and function of JAK1. Drug denoted in red target different aspects of the JAK/STAT pathway. Tofacitinib targets JAK1/JAK3, CYT-387 targets JAK1/JAK2, ruxolitinib targets JAK1/JAK2 and AZD1480 targets JAK1, JAK2 and STAT3. Figure created on Biorender.com

The results presented in *Section 3.3* demonstrate that while MARV is capable of replicating within ferret cells, replication is attenuated compared to EBOV (Figure 9). As such, it is hypothesized that this lack of susceptibility by ferrets to lethal infection with orthomarburgviruses but not orthoebolaviruses is the result of mechanistic differences in the innate immune evasion tactics of these two viruses. To investigate this hypothesis, we first investigated the replication kinetics of various MARV variants on ferret cells including GPA-MARV as well as RAVV to determine if this attenuated replication is variant specific. In tandem, we investigated the replication kinetics of EBOV, MA-EBOV and GPA-EBOV on ferret cells to determine if this replicative advantage is conserved across EBOVs with different genotypes. Additionally, we investigated the replication kinetics of SUDV on ferret cells to determine if this replicative advantage is unique to EBOV.

Next, we set out to investigate whether inhibition of the type I IFN response could promote the replication of MARV in ferret cells. More specifically, the contribution that IFN production has on viral replication was evaluated independently using two drugs namely TPCA-1 which targets IKB, STAT3 and NFKB as well as BX795 which targets TBK1 and IKKε (Figure 15). Lastly, the contribution that IFN signaling has via the JAK/STAT pathway was investigated using drugs targeting various aspects of the JAK/STAT pathway, namely tofacitinib which targets JAK1/JAK3, CYT-387 which targets JAK1/JAK2, ruxolitinib which targets JAK1/JAK2 and AZD1480 which targets JAK1, JAK2 and STAT3 (Figure 16).

## 4.2. Results: *Orthoebolaviruses* Replicate Efficiently Within Ferret Cell Lines Whereas Replication of *Orthomarburgviruses* is Modest

The results summarized in *Section 3.3* demonstrated that MARV Musoke could replicate within ferret cells; however, replication was attenuated compared to EBOV (Figure 9). Furthermore, while *mpf*Heart and *mpf*Lung demonstrate significantly elevated levels of viral RNA at 14 dpi compared to 3 dpi, these increases were only mildly significant among *mpf*Spleen cells (Figure 9). To investigate whether this moderate replication was variant-specific, ferret cells (*mpf*Spleen, *mpf*Heart and *mpf*Lung) were inoculated with MARV variants Musoke and Angola 709 as well as GPA-MARV and RAVN.

*mpf*Heart cells supported the replication of MARV Musoke, MARV Angola 709 and RAVV and demonstrated the most robust replication kinetics among all ferret cell lines (Figure 17). More specifically, levels of viral RNA were significantly elevated at 21 dpi relative to 3 dpi with peak levels of 9.76, 8.55 and 8.31 log10 GEQ/mL for MARV Musoke, MARV Angola 709 and RAVV respectively (Figure 17 A, B and D). These peak levels represent an increase of 2.66, 2.98 and 1.81 log10 GEQ/mL from 3dpi for MARV Musoke, MARV Angola 709 and RAVV, respectively (Figure 17 A, B and D). Although all time points were significantly elevated relative to 3 dpi for MARV Musoke and RAVV, only time points beyond 7 dpi were significantly elevated for MARV Angola 709 (Figure 17 A, B and D). By comparison, levels of viral RNA peaked at 21 dpi for MARV Musoke, MARV Angola 709 and RAVV in Vero E6 cells with mean levels of 10.41, 10.37 and 9.10 log10 GEQ/mL (Figure 17 A, B and D). Although peak levels in Vero E6 cells were higher than those observed among *mpf*Heart cells, increases relative to 3 dpi were more modest, with increases only 1.34, 2.20 and 1.10 log10 GEQ/mL for MARV Musoke, MARV Angola 709 and RAVV respectively. GPA-MARV is the sole *orthomarburgvirus* that did not

replicate in *mpf*Heart cells with no significant change in levels of viral RNA throughout 21 dpi (Figure 17C).

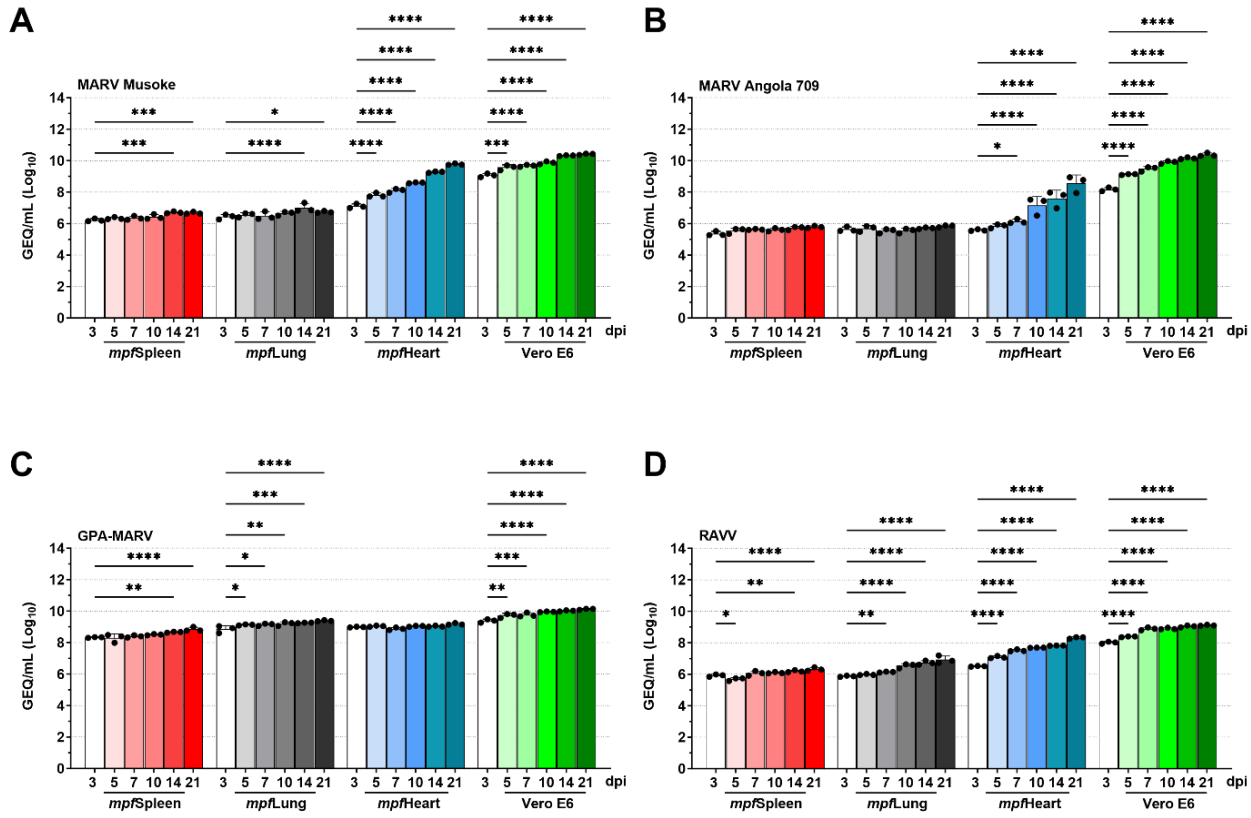


**Figure 17. Genome replication kinetics of orthomarburgviruses in ferret cell lines**

Ferret spleen (*mpf*Spleen), lung (*mpf*Lung), heart (*mpf*Heart), and Vero E6 cells were inoculated with (**A**) MARV Musoke, (**B**) MARV Angola 709, (**C**) GPA-MARV or (**D**) RAVV at an MOI of 0.1 and virus RNA within the supernatant was quantified by RT-qPCR at 3, 5, 7, 10, 14 and 21-days post-infection (dpi). Mean levels ± SD of viral RNA in genome equivalents per mL (GEQ/mL) are depicted as histograms, with the individual technical replicates depicted as black dots. Statistical analyses were performed using a two-way ANOVA Tukey's multiple comparisons test, with a single pooled variance computed for each comparison. P values are indicated as follows 0.1234 (ns), 0.0332 (*), 0.0021 (**), 0.0002 (***) and < 0.0001 (****). Statistics only shown relative to 3 dpi, all other comparisons have been omitted for clarity.

In the case of *mpf*Lung cells, replication of all orthomarburgviruses was limited except for RAVV, which demonstrated the best replication kinetics. With respect to RAVV, peak levels of 6.92 log10 GEQ/mL at 21 dpi were significantly higher than 5.87 log10 GEQ/mL observed at 3

dpi, corresponding to an increase of 1.05 log10 GEQ/mL (Figure 17D). Although statistically significant, increases in viral RNA between 3 and 21 dpi were minimal for MARV Musoke and GPA-MARV, with 0.30 and 0.53 log10 GEQ/mL increases, respectively (Figure 17A and C). Interestingly, MARV Angola 709 could not replicate within *mpf*Lung cells with no significant change in RNA levels throughout 21 dpi (Figure 17B).

Lastly, *mpf*Spleen cells support minimal replication of all tested orthomarburgviruses. Among the viruses, GPA-MARV showed the most significant increase in viral RNA from 3 to 21 dpi of only 0.49 log10 GEQ/mL (Figure 17C). Despite its significance, this increase is minimal, indicating poor replication of GPA-MARV in *mpf*Spleen cells. Despite its significance, similar findings were observed for RAVV, which only demonstrated an increase of 0.40 log10 GEQ/mL from 3 to 21 dpi (Figure 17D). Interestingly, MARV Angola 709 demonstrated an increase of 0.43 log10 GEQ/mL from 3 to 21 dpi; however, this increase was not statistically significant (Figure 17B). Lastly, MARV Musoke demonstrated significant increases of 0.45 log10 GEQ/mL from 3-21 dpi (Figure 17A). Taken together, replication kinetics of orthomarburgviruses was minimal in *mpf*Spleen cells with increases in levels of viral RNA ranging from 0.40 to 0.49 log10 GEQ/mL from 3 to 21 dpi (Figure 17).

With respect to infectious virus, *mpf*Heart cells are the sole cell line which demonstrated increasing titers of infectious virus throughout 21 dpi with the exception of GPA-MARV which showed decreasing titers as early as 3 dpi (Figure 18). In contrast, peak infectious titres for Vero E6 cells infected with MARV Musoke were reached by 5 dpi whereas peak titers for MARV Angola 709, GPA-MARV and RAVV were reached by 7 dpi (Figure 18). Following peak, a decrease in titers can be observed which most likely correlates with CPE development and decrease of viable cells for infection (Figure 18). With respect to MARV Angola 709, no infectious virus

could be detected for both *mpf*Spleen and *mpf*Lung at any timepoint (Figure 18B). The lack of infectious virus is agreement with the fact that both cell lines did not appear to support replication of MARV Angola 709 (Figure 17B). Likewise, infectious virus could not be detected among *mpf*Spleen cells infected with MARV Musoke at any timepoint or RAVV except for 14 dpi and one replicate at 3dpi (Figure 18A and D). *mpf*Lung cells inoculated with RAVV demonstrate no observable increase in infectious titers between 3 and 7 dpi, however titers increased by 10 dpi and remained elevated throughout 21 dpi (Figure 18D). In contrast, *mpf*Lung cells infected with MARV Musoke were only positive for infectious virus at 10 and 14 dpi (Figure 18A). Infectious titers for all cell lines inoculated with GPA-MARV demonstrated a decreasing trend for all timepoints beyond 3 dpi (Figure 18C), which likely reflect the minimal of replication observed with respect to genome equivalents (Figure 17C).

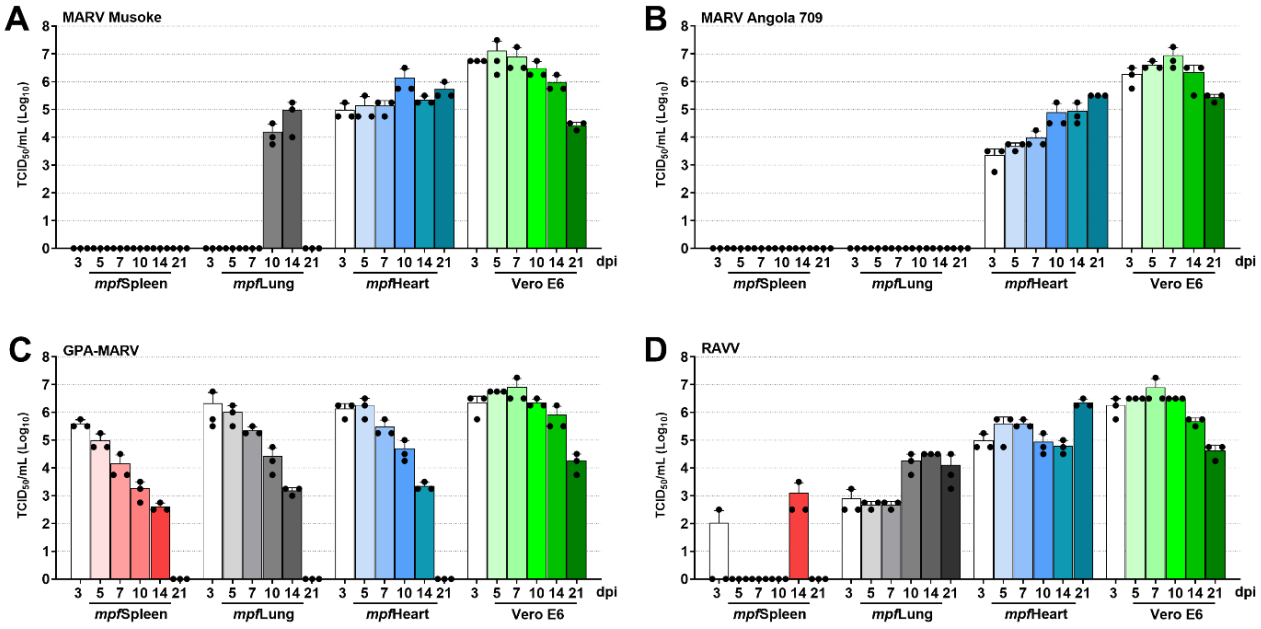


**Figure 18. Infectious virus replication kinetics of Orthomarburgviruses on ferret cell lines**

Ferret spleen (*mpf*Spleen), lung (*mpf*Lung), heart (*mpf*Heart), and Vero E6 cells were inoculated with (**A**) MARV Musoke, (**B**) MARV Angola 709, (**C**) GPA-MARV or (**D**) RAVV at an MOI of 0.1 and infectious virus within the supernatant was quantified by $TCID_{50}$ at 3, 5, 7, 10, 14 and 21-days post-infection (dpi). Mean tissue culture infectious dose per mL (TCID50/mL) are depicted as histograms, with the individual technical replicates depicted as black dots.

Analysis of orthomarburgvirus replication kinetics demonstrated relatively high levels of viral RNA at 3 dpi ranging from ~6-8 log10 GEQ/mL (Figure 17). These high levels were concerning given that peak levels of viral RNA ranged from 8-10 log10 GEQ/mL and an increase of ~2 log10 GEQ/mL from those observed at 3 dpi (Figure 17). To address these high levels, we investigated the influence that washing the cells post virus adsorption had on initial levels of viral RNA. The rational for investigation was that washing the cells post virus adsorption could potentially remove any residual virus not bound to cellular attachment factors. This would ultimately reduce the amount of initial input virus allowing for more refine growth curves demonstrating exponential growth extending the time frame required to reach peak viral levels. It can be observed that washing Vero E6 cells post-inoculation with MARV Angola 709 resulted in significantly lower levels of viral RNA at 0 and 1 dpi, with the significance decreasing by 2 dpi (Figure 19). Beyond 2 dpi, washing cells post-infection had no significant impact on levels of viral RNA compared to those which were not washed (Figure 19).

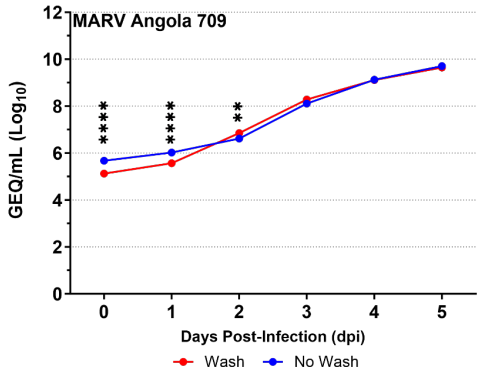


**Figure 19. Impact that washing cells post virus adsorption has on replication kinetics.**

Vero E6 cells were infected with MARV Angola 709 at a MOI of 0.1 and left to adsorb for 1 hr after which cells were either washed (red) or not washed (blue) prior to the addition of maintenance media. Virus RNA within the supernatant was quantified by RT-qPCR at 0,1, 2-, 3-, 4- and 5-days post-infection (dpi). Mean levels ± SD of viral RNA in genome equivalents per mL (GEQ/mL) are depicted as a line, with the individual technical replicates depicted as dots. Statistical analyses were performed using a two-way ANOVA Šidák's multiple comparisons test, with a single pooled variance computed for each comparison. P values are indicated as follows 0.1234 (ns), 0.0332 (*), 0.0021 (**), 0.0002 (***) and < 0.0001 (****).

In tandem, ferret cells were inoculated with EBOV, MA-EBOV and GPA-EBOV to determine if this replicative advantage observed in *Section 3.3* is conserved across EBOVs with different genotypes. Consistent with previous findings, ferret cells, namely *mpf*Spleen, *mpf*Heart and *mpf*Lung, supported the replication of all tested orthoebolaviruses. Replication kinetics were remarkably consistent among EBOV, MA-EBOV, GPA-EBOV and EBOV-mGP with levels of viral RNA at 3 dpi of ~6 log10 GEQ/mL, which peaked at 21 dpi at ~10-11 log10 GEQ/mL (Figure 20). Levels of viral RNA were significantly elevated (****) for all time points relative to 3 dpi (Figure 20). No major differences in peak levels could be observed between Vero E6 cells and the tested ferret cell lines, suggesting similar replication efficiencies.

Lastly, these ferret cells were also inoculated with SUDV to determine if this replicative advantage is unique to EBOV. As expected, the replication kinetics of SUDV mirrored what was observed among ferret cells infected with various orthoebolaviruses with all time points significantly elevated relative to 3 dpi (Figure 20E). Given that the genome replication kinetics revealed exponential growth representative of what was seen in *Section 3.3* investigations into infectious titers by $TCID_{50}$ were deemed not necessary as they are expected to mirror what has been shown previously.

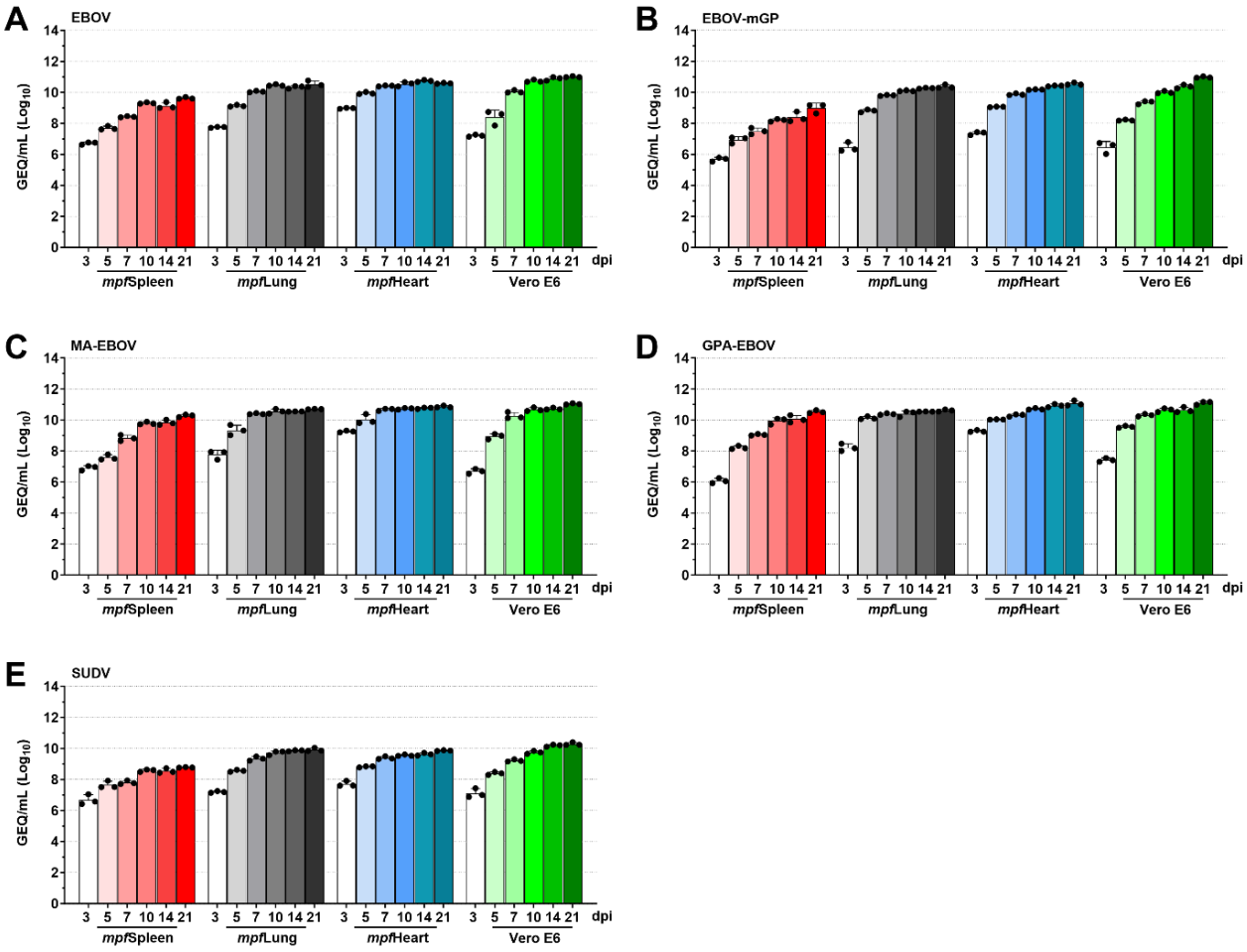


**Figure 20. Replication Kinetics of Orthoebolaviruses on ferret cell lines**

Ferret spleen (*mpf*Spleen), lung (*mpf*Lung), heart (*mpf*Heart), and Vero E6 cells were inoculated with (**A**) EBOV, (**B**) EBOV-mGP, (**C**) MA-EBOV, (**D**) GPA-EBOV and (**E**) SUDV at an MOI of 0.1 and virus RNA within the supernatant was quantified by RT-qPCR at 3, 5, 7, 10, 14 and 21-days post-infection (dpi). Mean levels ± SD of viral RNA in genome equivalents per mL (GEQ/mL) are depicted as histograms, with the individual technical replicates depicted as black dots. Statistical analyses were performed using a two-way ANOVA Tukey's multiple comparisons test, with a single pooled variance computed for each comparison. P values are indicated as follows 0.1234 (ns), 0.0332 (*), 0.0021 (**), 0.0002 (***) and < 0.0001 (****). Note statistics have been omitted from the graphs for ease of viewing, however all comparisons relative to 3 dpi were **** regardless of virus.

## 4.3. Results: Ruxolitinib Enhances Replication of EBOV-GFP

Ruxolitinib is a small molecule which acts as an inhibitor of type I IFN signalling via the JAK/STAT pathway by targeting JAK1/JAK2 (Figure 16). As a result, ruxolitinib closely resembles the activity of MARV VP40 and EBOV VP24, which act as inhibitors of the type I IFN response by interfering with signalling via the JAK/STAT pathway.

As such, for a pilot study, *mpf*Spleen cells were inoculated with either EBOV-GFP or MARV-ZsG expressing a fluorescent reporter followed by treatment with ruxolitinib to investigate the impact that inhibiting type I IFN signalling has on viral replication. For this, *mpf*Spleen cells were infected with a 1:1000 dilution of either virus followed by treatment with two-fold serial dilutions of ruxolitinib at concentrations ranging from 40 µM to 0.625µM, including no drug controls. Measurement of fluorescence intensity in tandem with imaging via an inverted fluorescent microscope revealed that high concentrations of ruxolitinib at 40 µM were cytotoxic to the cells (Figure 21A). Treatment of cells with ruxolitinib at concentrations ranging from 10-0.625 µM resulted in an increase in fluoresce intensity with values ranging from 30-35 relative fluoresce units (RFU) compared to only 17 RFU for the no drug control wells (Figure 21). To further quantify the impact of drug treatment on viral replication, EBOV-GFP infected cells treated with 2.5 µM ruxolitinib were further analyzed using a Cytation multimode plate reader. Remarkably, treatment with 2.5µM ruxolitinib resulted in 71% viral infectivity compared to only 22% among infected cells that received no drug treatment (Figure 22). These data from the pilot study demonstrate that treatment with ruxolitinib can promote viral infection among ferret cells. Unfortunately, fluorescence intensity among MARV-ZsG infected *mpf*Spleen cells was too weak for quantification using a plate reader. Furthermore, ZsG reporter activity appeared to be localized to inclusion bodies, a feature thought to be due to the fact that ZsG is expressed as a fusion protein with NP, and these inclusion bodies resulting from incomplete cleavage of ZsG from NP.

Additionally, ZsG expression appeared to be localized to cell clusters thought to be virus induced syncytia; however, DAPI staining revealed that these clusters were composed of distinct cells (Figure 23). Nonetheless, syncytia cannot be ruled out without further investigation. Given these issues with the recombinant MARV-ZsG virus, all further investigations in subsequent aims into the impact of inhibitors of the IFN response were done using wild-type MARV with quantification by RT-qPCR.

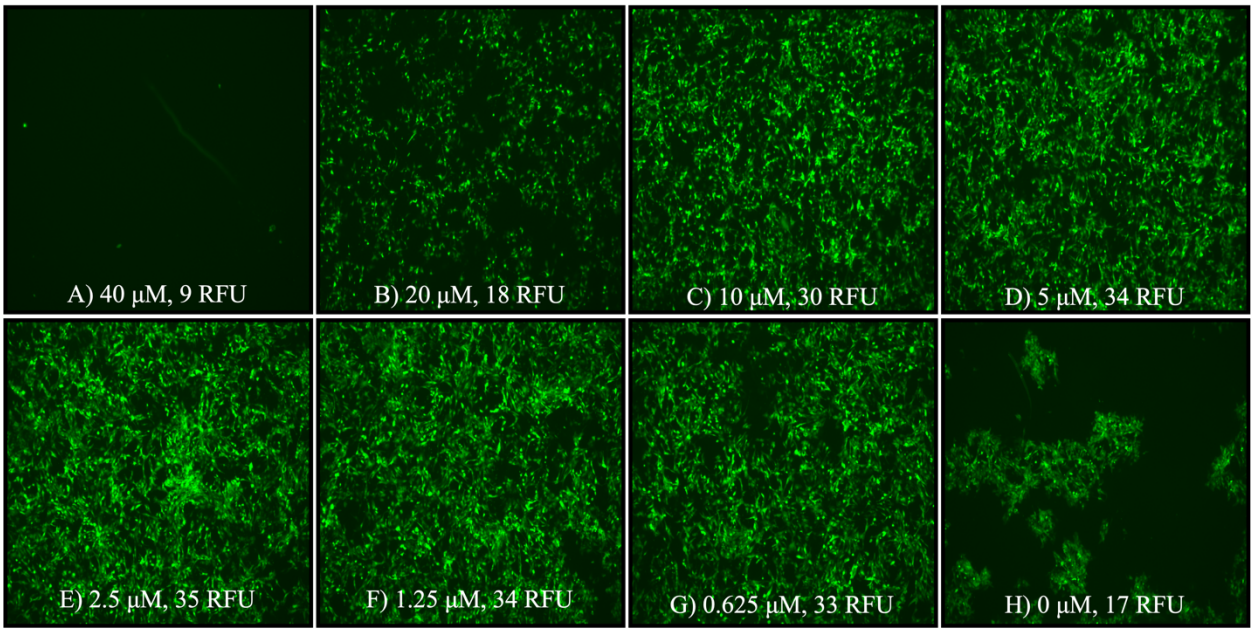


**Figure 21. Treatment of *mpf*Spleen cells with ruxolitinib enhances replication of EBOV-GFP**

*mpf*Spleen cells were infected with a 1:100 dilution of EBOV-GFP followed by treatment with ruxolitinib at concentrations of (**A**) 40 µM, (**B**) 20 µM, (**C**) 10 µM, (**D**) 5 µM, (**E**) 2.5 µM, (**F**) 1.25 µM, (**G**) 0.625 µM and (**H**) 0 µM. Cells were fixed in 10% buffered formalin at 7 days post-infection (dpi) and fluorescence intensity measured using a plate reader. Representative images were capture using an inverted fluorescence microscope at 4X magnification. Fluorescence intensity reported as relative fluorescence units (RFU).

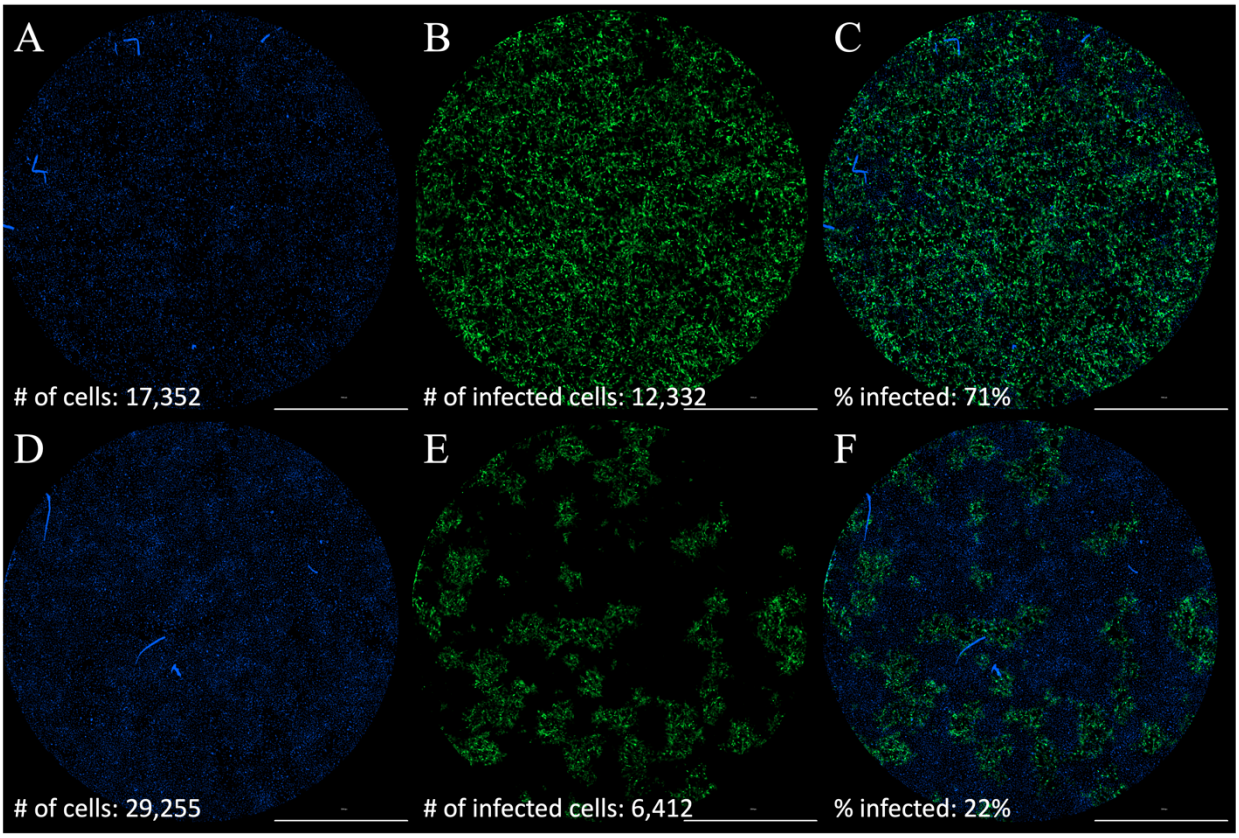


**Figure 22. Quantification of EBOV-GFP infected *mpf*Spleen cell populations in the presence of 2.5 µM ruxolitinib**

Ferret spleen (*mpf*Spleen) cells were infected with a 1:100 dilution of EBOV-GFP followed by treatment with (**A-C**) ruxolitinib at a concentration of 2.5 µM. (**D-F**) Mock treated cells received no ruxolitinib. Cells were fixed in 10% buffered formalin at 7 days post-infection (dpi) and nuclei stained with DAPI. Imagining was done using a Cytation 7 plate reader at 4X magnification for (**A, D**) DAPI and (**B , E**) GFP. Individual cell counts were determined according DAPI and infected cells according to GFP using the Gen5 software. (**C, F**) DAPI and GFP Images were stitched together using the Gen5 software and percent (%) infected cells calculated according to cells expressing DAPI alone vs those expressing both DAPI and GFP. Notes images are representative, and all infections/treatments were conducted in triplicate.

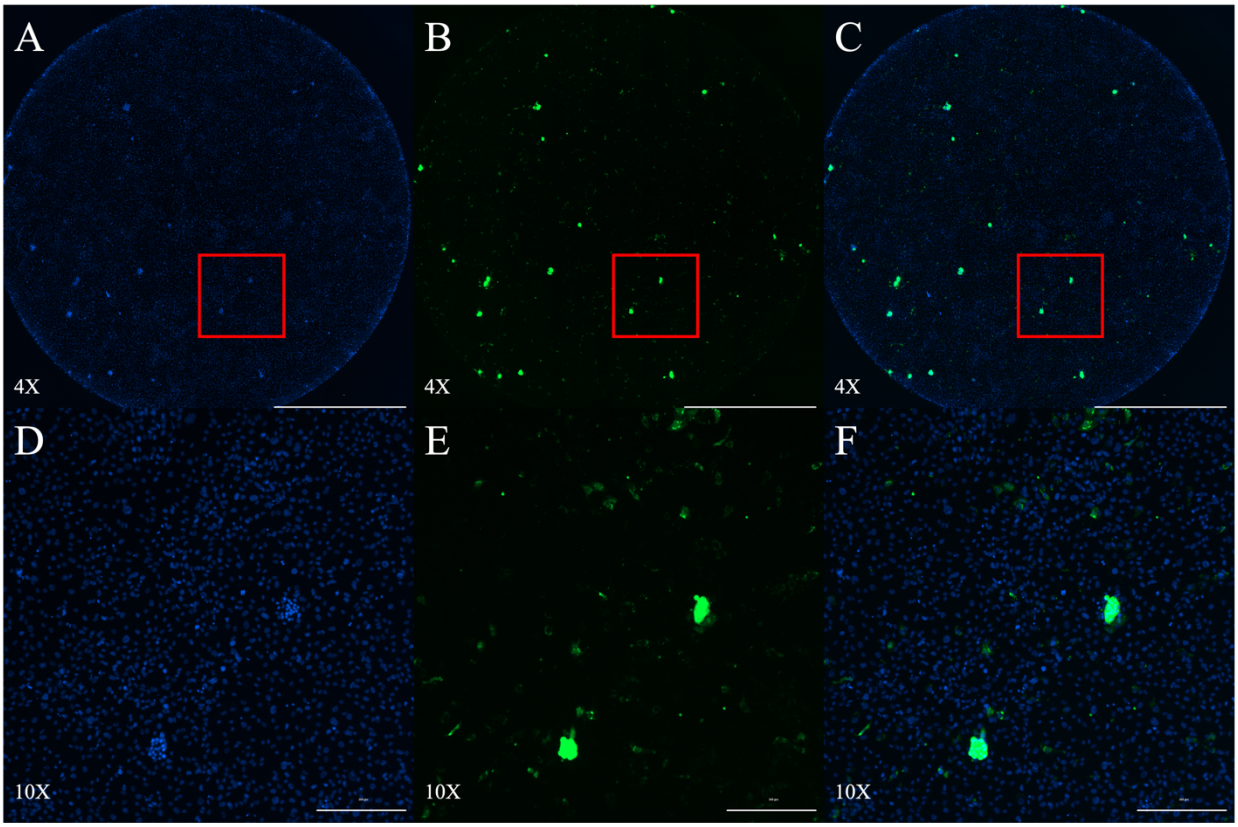


**Figure 23.Quantification of MARV-ZsG infected *mpf*Spleen cell populations in the presence of ruxolitinib**
Ferret spleen (*mpf*Spleen) cells were infected with a 1:100 dilution of MARV-ZsG followed by treatment with (**A-C**) 10 µM ruxolitinib. Cells were fixed in 10% buffered formalin at 7 days post-infection (dpi) and nuclei stained with DAPI. Imagining was done using a Cytation 7 plate reader at (**A-C**) 4X and (**D-F**) 10X magnification for (**A. D**) DAPI and (**B, E**) GFP. Individual cell counts were determined according DAPI and infected cells according to GFP using the Gen5 software. (**C, F**) DAPI and GFP Images were stitched together using the Gen5 software and percent (%) infected cells calculated according to cells expressing DAPI alone vs those expressing both DAPI and GFP. Notes images are representative, and all infections/treatments were conducted in triplicate. Red box represents region imaged at 10X magnification.

## 4.4. Results: Inhibitors of Type I IFN Production Do Not Enhance Replication of MARV in Ferret Cells

The proof of concept study described in *Section 4.3* demonstrated that interference of the type 1 IFN response via inhibition of JAK/STAT signalling using ruxolitinib enhanced viral replication of EBOV within *mpf*Spleen cells (Figure 21 and Figure 22). Here in this aim, two drugs, namely TPCA-1 and BX795, were investigated for their ability to promote replication of MARV

Musoke within ferret cell lines. For this, ferret cells, namely *mpf*Spleen, *mpf*Heart and *mpf*Lung, as well as A549 cells, were inoculated with MARV Musoke at a MOI of 0.1for 1 hr, after which the virus inoculum was removed and drugs added at concentrations of 5, 2.5 and 1.25 µM.

Replication of MARV Musoke within *mpf*Spleen cells was unaffected by either drug, with no significant change in levels of viral RNA between drug-treated cells and those that received no drug at any time point (Figure 24A and Figure 25A). These findings are consistent with the replication kinetics observed in *Section 4.2,* whereby levels of viral RNA hovered around 6 log10 GEQ/mL throughout 21 dpi (Figure 17). Similar findings were observed among *mpf*Heart cells, which also demonstrated negligible increases in viral RNA throughout 14 dpi for both TPCA-1 and BX795 (Figure 24B and Figure 25B). While not significant, levels of viral RNA among *mpf*Heart cells treated with 2.5 µM TPCA-1 trended toward significance with increasing levels of viral RNA observable at 10 dpi relative to the other drug concentrations (Figure 24B). In contrast, treatment of *mpf*Heart cells appeared to worsen and inhibit replication of MARV Musoke, with all drug-treated cells demonstrating significantly lower levels of viral RNA compared to no drug control wells at 10 dpi and 14 dpi, respectively (Figure 25B). No drug control wells for *mpf*Heart cells mirrored what was observed in *Section 4.2* (Figure 17A). Results observed for *mpf*Lung cells treated with TCPA-1 or BX795 were nearly identical, with no significant change in levels of viral RNA throughout 14 dpi (Figure 24C and Figure 25C). Similarly, no drug control wells also demonstrated no change in levels of viral RNA throughout 14 dpi (Figure 24C and Figure 25C), a result that closely mirrors the replication kinetics observed in *Section 4.2* (Figure 17A). Interestingly, A549 cells responded very mildly to treatment with TPCA-1. Despite not being significant, the levels of viral RNA among cells treated with 5 and 2.5µM TPCA-1 were slightly greater than the no drug control wells at 14 dpi (Figure 24D). In contrast, levels of viral RNA

among A549 cells treated with BX795 demonstrate increasing levels at 2.5 and 1.25 µM throughout 14 dpi; however, at no point were levels of drug-treated cells greater or equal to those observed among no drug control wells (Figure 25D).

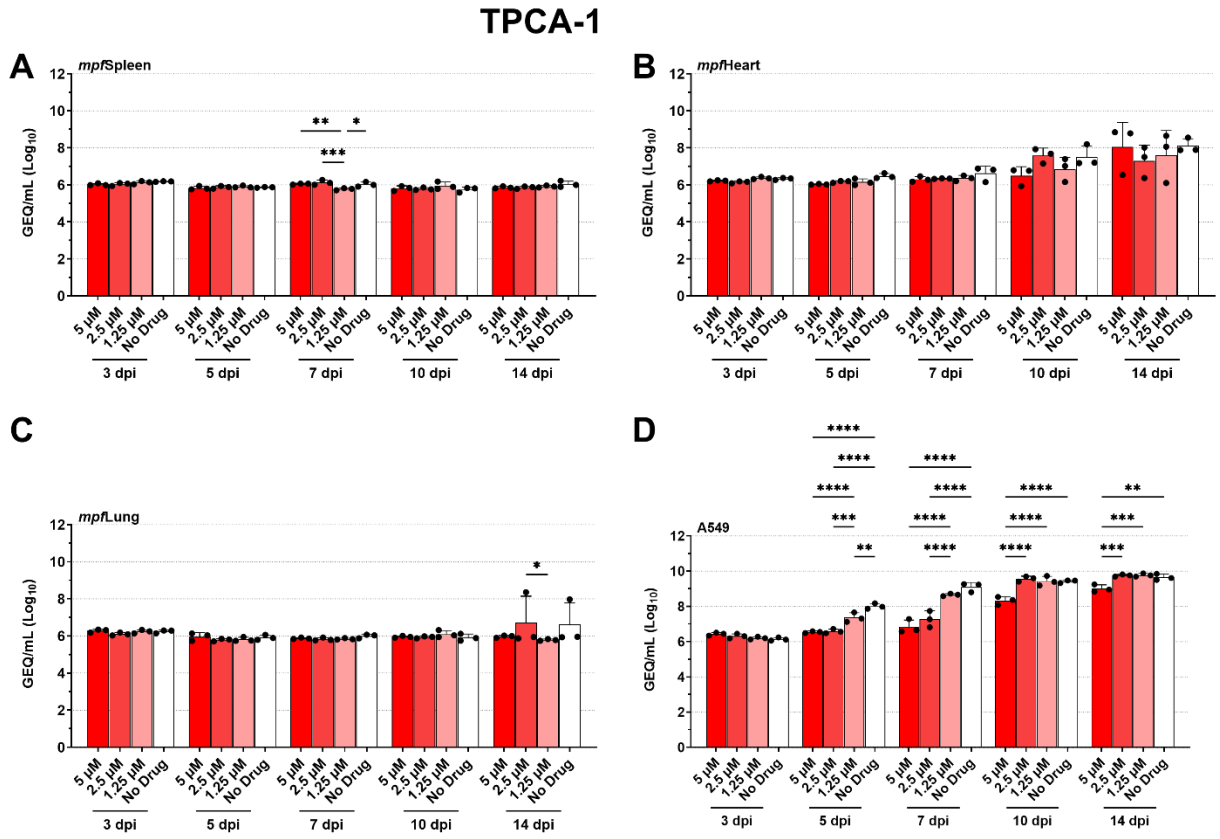


**Figure 24. Impact of TPCA-1 treatment on replication of MARV in ferret cell lines**

(**A**) Ferret spleen (*mpf*Spleen), (**B**) heart (*mpf*Heart), (**C**) lung (*mpf*Lung) and (**D**) A549 cells were inoculated with MARV Musoke at an MOI of 0.01 followed by treatment with TPCA-1 at concentrations of 5, 2.5 and 1.25 µM. No drug control wells received only media. Virus RNA within the supernatant was quantified by RT-qPCR at 3, 5, 7, 10, and 14 days post-infection (dpi). Mean levels ± SD of viral RNA in genome equivalents per mL (GEQ/mL) are depicted as histograms, with the individual technical replicates depicted as black dots. Statistical analyses were performed using a two-way ANOVA Tukey's multiple comparisons test, with a single pooled variance computed for each comparison. P values are indicated as follows 0.1234 (ns), 0.0332 (*), 0.0021 (**), 0.0002 (***) and < 0.0001 (****).

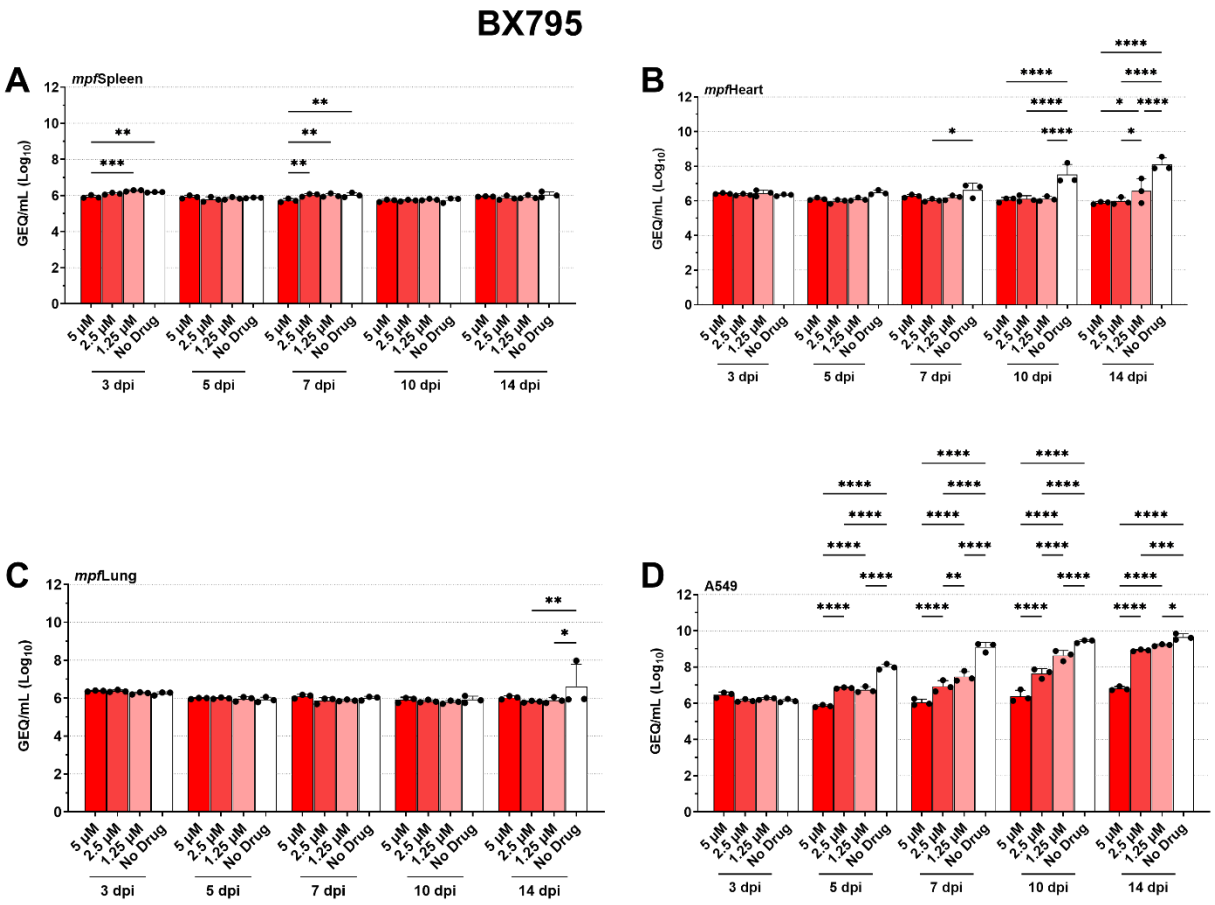


**Figure 25.** Impact of BX795 treatment on replication of MARV in ferret cell lines

(**A**) Ferret spleen (*mpf*Spleen), (**B**) heart (*mpf*Heart), (**C**) lung (*mpf*Lung) and (**D**) A549 cells were inoculated with MARV Musoke at an MOI of 0.01 followed by treatment with BX795 at concentrations of 5, 2.5 and 1.25 µM. No drug control wells received only media. Virus RNA within the supernatant was quantified by RT-qPCR at 3, 5, 7, 10, and 14 days post-infection (dpi). Mean levels ± SD of viral RNA in genome equivalents per mL (GEQ/mL) are depicted as histograms, with the individual technical replicates depicted as black dots. Statistical analyses were performed using a two-way ANOVA Tukey's multiple comparisons test, with a single pooled variance computed for each comparison. P values are indicated as follows 0.1234 (ns), 0.0332 (*), 0.0021 (**), 0.0002 (***) and < 0.0001 (****).

## 4.5. Results: Select Inhibitors of Type I IFN Signaling Enhance Replication of MARV In Ferret Cells

The results from the pilot study in *Section 4.3* demonstrated that treatment of EBOV-GFP-infected *mpf*Spleen cells with ruxolitinib enhanced viral replication relative to no drug control cells (Figure 22). With these data, we set out to investigate how interference of the type 1 IFN response

via inhibition of JAK/STAT signalling affects the replication of MARV Musoke within ferret cell lines. To explore this, four drugs, namely ruxolitinib, tofacitinib, AZD1480 and CYT-387, were evaluated for their ability to enhance viral replication of MARV Musoke in ferret cell lines.

Consistent with previous data, infection of *mpf*Spleen cells with MARV Musoke resulted in no change in levels of viral RNA throughout 14 dpi regardless of treatment with ruxolitinib (Figure 26A). In contrast, ruxolitinib enhanced replication of MARV Musoke within *mpf*Heart with increased levels of viral RNA relative to no drug control cells observable as early as 7 dpi (Figure 26B). Although non-significant, levels of viral RNA were 0.73 and 0.48 log10 GEQ/mL greater at 7 dpi among *mpf*Heart cells treated with 5 µM and 2.5 µM ruxolitinib respectively, compared to no drug control wells (Figure 26B). These differences reached significance at 10 dpi with 5 µM and 2.5 µM treated *mpf*Heart cells demonstrating levels of viral RNA 1.28 and 1.75 log10 GEQ/mL greater than those observed among no drug control wells (Figure 26B). Interestingly, *mpf*Heart cells treated with 1.25 µM ruxolitinib exhibited significantly lower levels of viral RNA at 10 dpi relative to no drug control wells (Figure 26B). Levels of viral RNA among *mpf*Heart cells were significantly elevated at 14 dpi relative to no drug control cells for all concentrations of ruxolitinib, with the greatest difference of 2.27 log10 GEQ/mL observed at a ruxolitinib concentration of 5 µM (Figure 26B). *mpf*Lung cells showed no differences in levels of viral RNA among treated cells compared to no drug control wells between 3-10 dpi except for 2.5 µM at 5 dpi, which was within the range of control wells (Figure 26C). The sole significant difference was observed at 14 dpi, whereby levels of viral RNA were significantly higher among *mpf*Lung cells treated with 5 µM ruxolitinib compared to no drug control wells (Figure 26C). Lastly, A549 control cells demonstrated trends similar to those observed among *mpf*Heart cells, although these differences were more modest (Figure 26D). Levels of viral RNA were significantly

elevated among A549 cells treated with 1.25 µM at 5 dpi relative to no drug control cells (Figure 26D). While levels among 2.5 µM treated cells at 7 dpi were elevated relative to no drug cells, this increase was insignificant (Figure 26D). Additionally, levels of viral RNA were elevated for all ruxolitinib concentrations at 10 dpi relative to no control wells; however, only 5 µM reached significance. The same could be observed at 14 dpi, with both 5 µM and 2.5 µM significantly elevated compared to no drug control wells (Figure 26D).

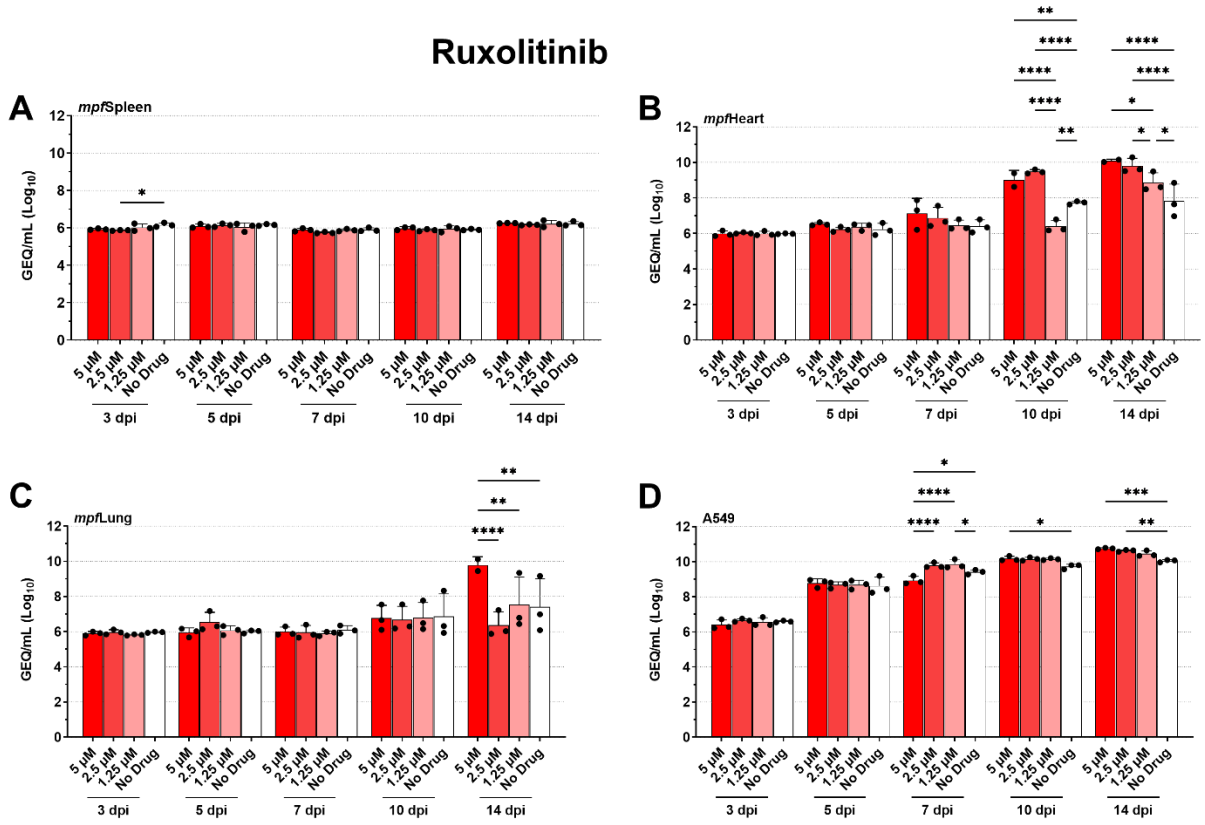


**Figure 26. Impact of ruxolitinib treatment on replication of MARV in ferret cell lines**

(**A**) Ferret spleen (*mpf*Spleen), (**B**) heart (*mpf*Heart), (**C**) lung (*mpf*Lung) and (**D**) A549 cells were inoculated with MARV Musoke at an MOI of 0.01 followed by treatment with ruxolitinib at concentrations of 5, 2.5 and 1.25 µM. No drug control wells received only media. Virus RNA within the supernatant was quantified by RT-qPCR at 3, 5, 7, 10, and 14 days post-infection (dpi). Mean levels ± SD of viral RNA in genome equivalents per mL (GEQ/mL) are depicted as histograms, with the individual technical replicates depicted as black dots. Statistical analyses were performed using a two-way ANOVA Tukey's multiple comparisons test, with a single pooled variance computed for each comparison. P values are indicated as follows 0.1234 (ns), 0.0332 (*), 0.0021 (**), 0.0002 (***) and < 0.0001 (****).

Consistent with previous data, infection of *mpf*Spleen cells with MARV Musoke resulted in no change in levels of viral RNA throughout 14 dpi regardless of treatment with tofacitinib (Figure 27A). *mpf*Heart cells demonstrate elevated levels of viral RNA as early as 7 dpi among cells treated with 5 µM tofacitinib relative to no drug control wells, although insignificant (Figure 27B). Levels of viral RNA among *mpf*Heart cells treated with tofacitinib were significantly elevated for all concentrations at 10 dpi relative to no drug control wells, with the greatest difference of 1.36 log10 GEQ/mL observed among 5 µM treated cells (Figure 27B). The same could be observed at 14 dpi, whereby all concentrations were significantly elevated relative to no drug control wells (Figure 27B).

In contrast, *mpf*Lung cells showed no change in levels of viral RNA throughout 14 dpi regardless of treatment with tofacitinib (Figure 27C). Among A549 cells, levels of viral RNA were only significantly elevated for tofacitinib-treated cells starting at 10 dpi for all concentrations compared to no drug control wells (Figure 27D). These significant differences were retained at 14 dpi for A549 cells treated with 5 µM and 1.25 µM tofacitinib (Figure 27D).

Consistent with previous data, infection of *mpf*Spleen or *mpf*Lung cells with MARV Musoke resulted in no change in levels of viral RNA throughout 14 dpi regardless of treatment with AZD1480 (Figure 28A, C). With respect to *mpf*Heart cells, elevated levels of viral RNA among cells treated with 5 µM and 2.5 µM AZD1480 relative to no drug control wells could be observed as early as 7 dpi (Figure 28B). While insignificant, levels of viral RNA at 7 dpi were 0.73 and 0.16 log10 GEQ/mL greater than no drug control wells at AZD1480 concretions of 5 µM and 2.5 µM (Figure 28B). All three ADZ1480 concentrations demonstrated elevated levels of viral RNA at 10 dpi compared to *mpf*Heart cells that received no drug with significance only observable at concentrations of 2.5 µM and 1.25 µM (Figure 28B). Surprisingly, levels of viral RNA plateaued

and were within range of no drug control cells for *mpf*Heart cells treated with AZD1480 at all concentrations (Figure 28B). Unlike the other drugs, A549 cells did not respond to treatment with ADZ1480 with no significant differences in levels of viral RNA between treated cells and control cells except for 1.25µM at 14 dpi, which was slightly but significantly elevated relative to no drug controls (Figure 28D).

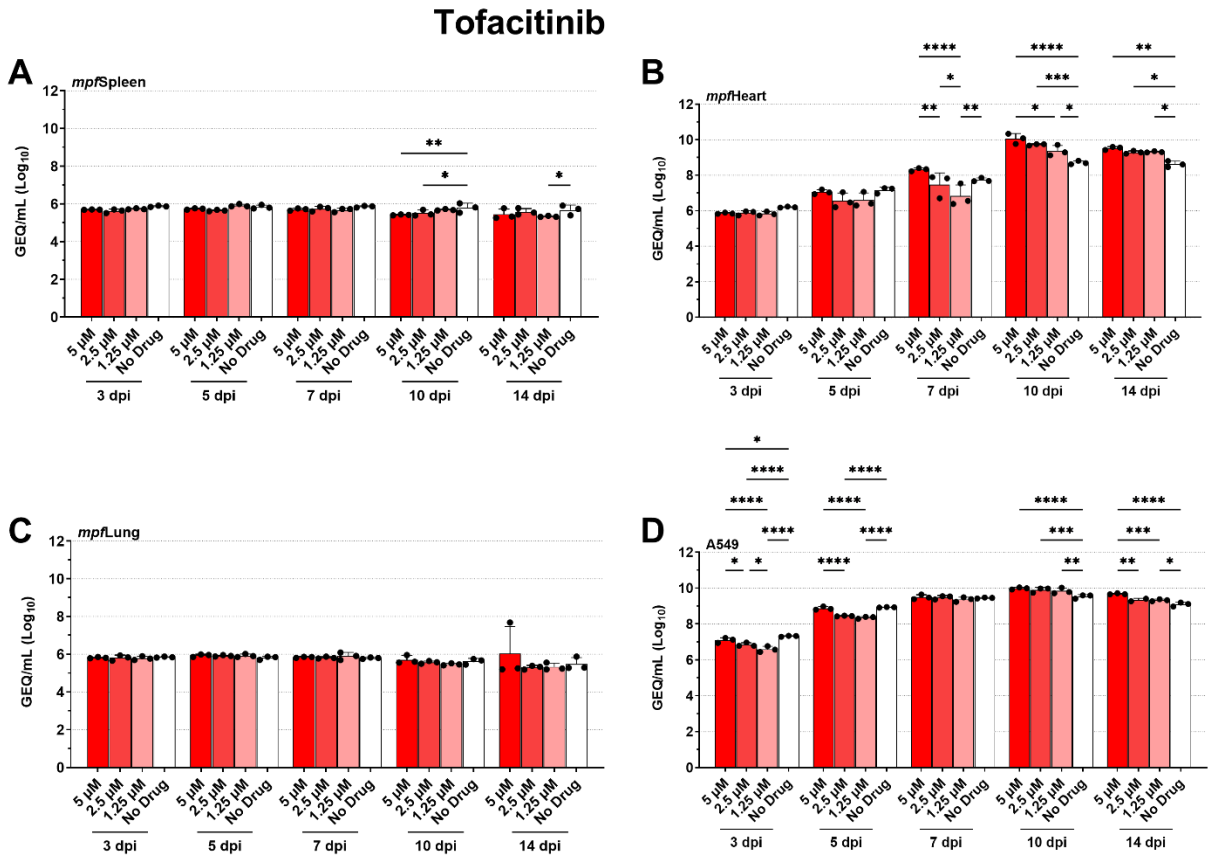


**Figure 27. Impact of tofacitinib treatment on replication of MARV in ferret cell lines**

(**A**) Ferret spleen (*mpf*Spleen), (**B**) heart (*mpf*Heart), (**C**) lung (*mpf*Lung) and (**D**) A549 cells were inoculated with MARV Musoke at an MOI of 0.01 followed by treatment with tofacitinib at concentrations of 5, 2.5 and 1.25 µM. No drug control wells received only media. Virus RNA within the supernatant was quantified by RT-qPCR at 3, 5, 7, 10, and 14 days post-infection (dpi). Mean levels ± SD of viral RNA in genome equivalents per mL (GEQ/mL) are depicted as histograms, with the individual technical replicates depicted as black dots. Statistical analyses were performed using a two-way ANOVA Tukey's multiple comparisons test, with a single pooled variance computed for each comparison. P values are indicated as follows 0.1234 (ns), 0.0332 (*), 0.0021 (**), 0.0002 (***) and < 0.0001 (****).

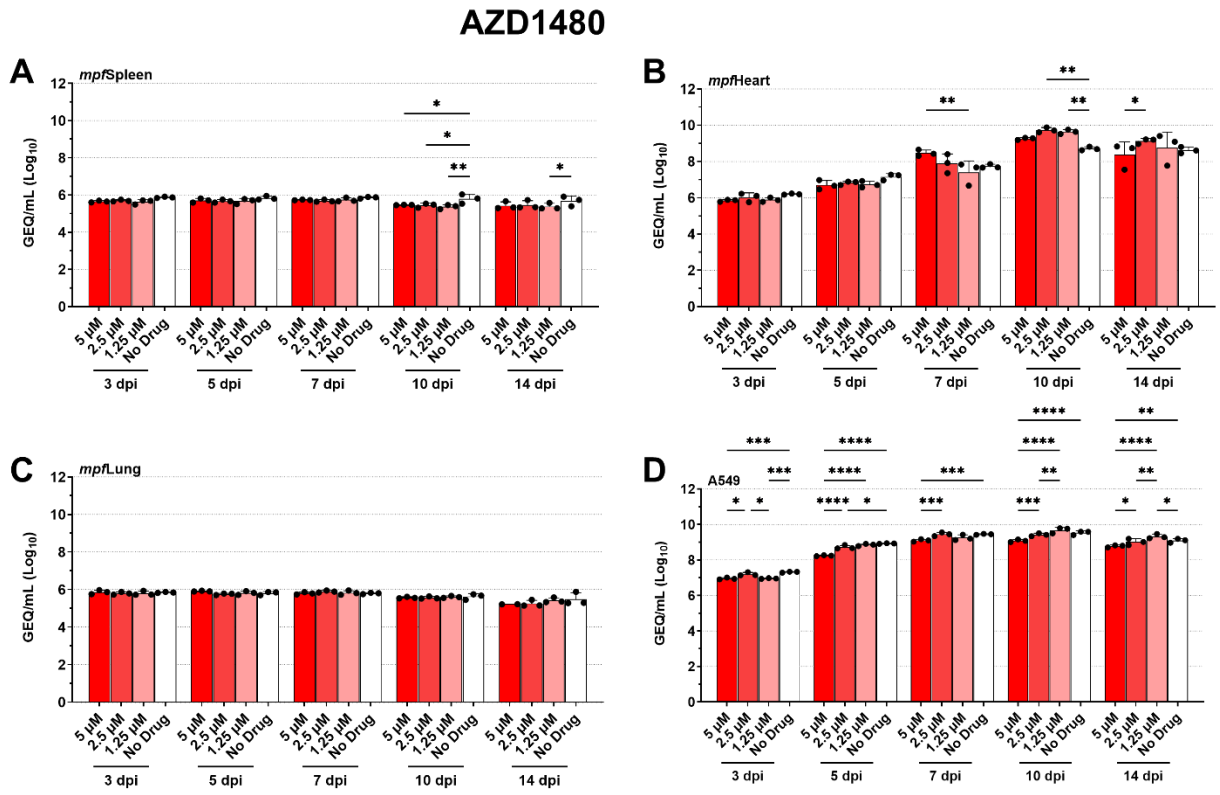


**Figure 28. Impact of AZD1480 treatment on replication of MARV in ferret cell lines**

(**A**) Ferret spleen (*mpf*Spleen), (**B**) heart (*mpf*Heart), (**C**) lung (*mpf*Lung) and (**D**) A549 cells were inoculated with MARV Musoke at an MOI of 0.01 followed by treatment with AZD1480 at concentrations of 5, 2.5 and 1.25 µM. No drug control wells received only media. Virus RNA within the supernatant was quantified by RT-qPCR at 3, 5, 7, 10, and 14 days post-infection (dpi). Mean levels ± SD of viral RNA in genome equivalents per mL (GEQ/mL) are depicted as histograms, with the individual technical replicates depicted as black dots. Statistical analyses were performed using a two-way ANOVA Tukey's multiple comparisons test, with a single pooled variance computed for each comparison. P values are indicated as follows 0.1234 (ns), 0.0332 (*), 0.0021 (**), 0.0002 (***) and < 0.0001 (****).

Consistent with previous data, infection of *mpf*Spleen cells with MARV Musoke resulted in no change in levels of viral RNA throughout 7 dpi regardless of treatment with CYT-387 (Figure 29A). Additionally, no data could be gathered for *mpf*Spleen cells beyond 7 dpi due to cytotoxicity induced by CYT-387 due to prolonged exposure to the drug. No drug wells were not harvested, given that data was reproduced in the previous drug studies and deemed not necessary (Figure 29A). *Mpf*Heart cells treated with CYT-387 showed no significant impacts until 10 dpi, whereby

2.5 μM treated cells were insignificantly elevated relative to no drug control wells (Figure 29B). Significance was only achieved at 14 dpi whereby *mpf*Heart cells treated with 2.5 μM CYT-387 demonstrated elevated levels relative to no drug control wells (Figure 29B). Similarly, *mpf*Lung cells showed no significant change in levels of viral RNA throughout 10 dpi regardless of treatment with CYT-387 (Figure 29C). While insignificant, levels of viral RNA among *mpf*Lung cells treated with CYT-387 at concentrations of 2.5 μM and 1.25 μM were elevated at 14 dpi relative to no drug control wells (Figure 29C). Treatment of A549 cells with CYT-387 appeared to worsen replication, with levels of viral RNA decreased relative to no drug control wells throughout 7 dpi (Figure 29D). Similar to *mpf*Heart cells, CYT-387 treatment of A549 cells beyond 7 dpi was cytotoxic (Figure 29D).

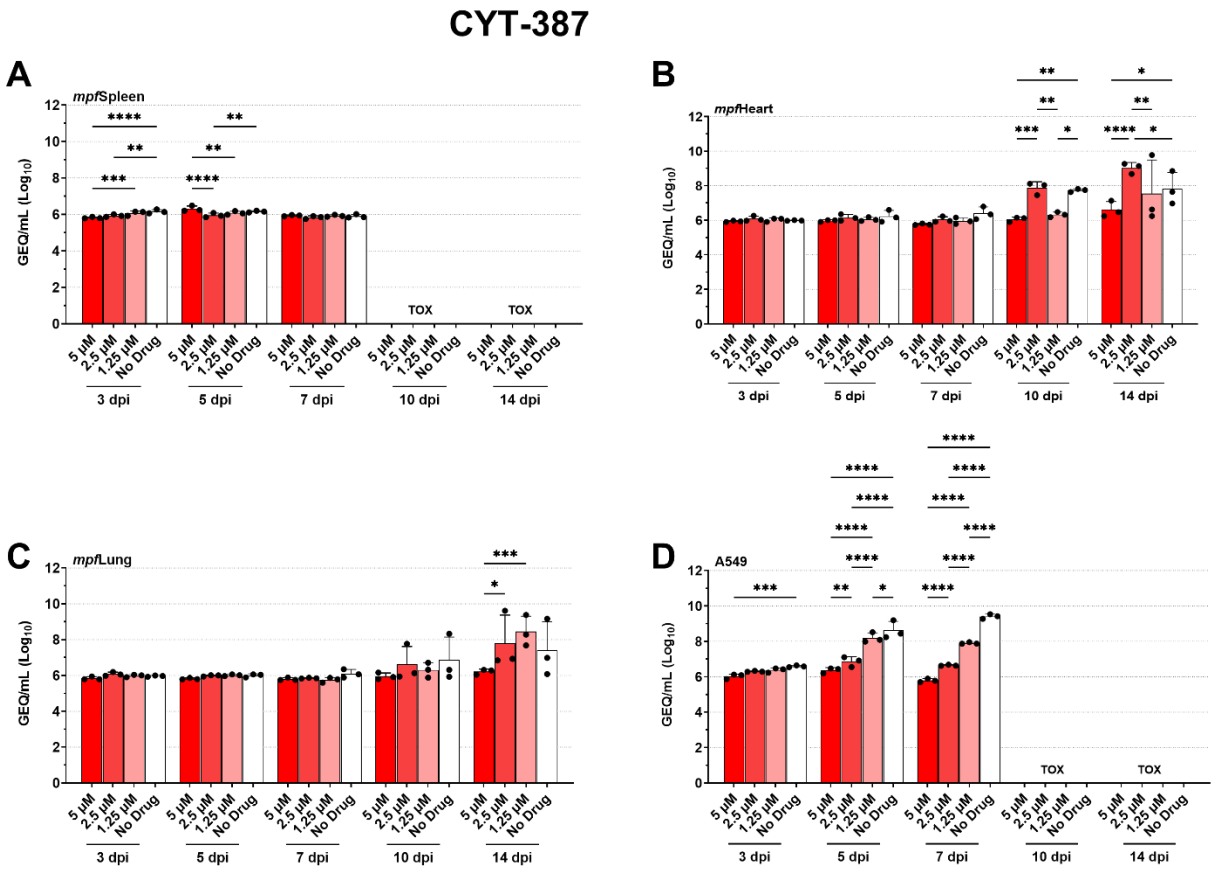


**Figure 29. Impact of CYT-387 treatment on replication of MARV in ferret cell lines**

(**A**) Ferret spleen (*mpf*Spleen), (**B**) heart (*mpf*Heart), (**C**) lung (*mpf*Lung) and (**D**) A549 cells were inoculated with MARV Musoke at an MOI of 0.01 followed by treatment with CTY-387 at concentrations of 5, 2.5 and 1.25 µM. No drug control wells received only media. Virus RNA within the supernatant was quantified by RT-qPCR at 3, 5, 7, 10, and 14 days post-infection (dpi). Mean levels ± SD of viral RNA in genome equivalents per mL (GEQ/mL) are depicted as histograms, with the individual technical replicates depicted as black dots. Statistical analyses were performed using a two-way ANOVA Tukey's multiple comparisons test, with a single pooled variance computed for each comparison. P values are indicated as follows 0.1234 (ns), 0.0332 (*), 0.0021 (**), 0.0002 (***) and < 0.0001 (****). TOX indicates drug treatment was cytotoxic.

## 4.6. Discussion: Key Findings, Significance, and Limitations

The previous chapter's results demonstrated that MARV-GP could mediate entry into ferret cells and that replication of WT-MARV was attenuated compared to that of EBOV. Furthermore, the *in vivo* study showed that a recombinant chimeric EBOV expressing MARV GP in place of EBOV GP was uniformly lethal among ferrets. These data suggest that MARV GP is likely not

the sole factor responsible for the lack of disease among MARV-infected ferrets but is possibly a contributing factor. This decreased efficiency in MARV GP-mediated viral entry and attenuated replication kinetics within ferret cells render MARV at a disadvantage when infecting ferrets.

Nonetheless, whether this attenuated replication observed among MARV-infected ferret cell lines was variant-specific remained unclear. As such, in this chapter, we first investigated whether different MARV variants and RAVV were capable of replicating within ferret cell lines. Amid the ferret cell lines, *mpf*Heart cells supported replication of MARV variants Musoke and Angola 709 and RAVV with no replication observed for GPA-MARV. Levels of viral RNA among the variants capable of replicating within *mpf*Heart cells paralleled what was observed among Vero E6 cells within 1-2 log10 GEQ/mL. Furthermore, peak levels of viral RNA were about 2 log10 GEQ/mL greater among MARV Musoke infected *mpf*Heart cells compared to MARV Angola 709 and RAVV, suggesting potential replicative advantages that are variant or species specific. By comparison, *mpf*Lung cells supported RAVV replication and minimal GPA-MARV replication, with no replication observed for MARV Musoke and MARV Angola 709. No replication for any Orthomarburgvirus could be seen among *mpf*Spleen cells, which is consistent with previous findings that these cells are refractory to infection. Moreover, infectious virus could only be recovered among *mpf*Heart cells for all tested orthomarburgviruses compared to *mpf*Lung cells, which only yielded infectious virus for RAVV. No infectious virus could be recovered for *mpf*Spleen cells infected with MARV Musoke or MARV Angola 709. In most cases, peak levels of infectious virus were reached around 7-10 dpi, followed by a decrease at 14 and 21 dpi, reflecting CPE and lack of cells for infection. Together, these data suggest that the attenuated replication kinetics of MARV within ferret cell lines is not variant nor species-specific. This ultimately suggests that the block in replication is at the cellular level and is thought to be linked

to MARV's innate immune evasion tactics. While this is the 'lowest hanging fruit,' it is likely that innate immune evasion tactics are not the sole factors accounting for this lack of disease. Instead, it is probable that many subtle differences related to one or more stages of the viral life cycle, including assembly and budding, could account for this lack of disease among MARV-challenged ferrets in synergy with innate immune evasion tactics. While differences in innate immune evasion tactics represent the most likely reason for this lack of disease among MARV-challenged ferrets, further investigation into all stages of the MARV life cycle is required to fully elucidate the root causes responsible for this lack of disease. Moreover, the block may also be species-specific, whereby specific MARV viral proteins may be less able to interact with their ferret cellular counterparts, including yet-identified receptors, further contributing to the lack of disease among MARV-challenged ferrets.

In contrast, orthoebolaviruses, namely EBOV and EBOV-mGP, and the rodent-adapted orthoebolaviruses, namely MA-EBOV and GPA-EBOV, were all capable of replicating efficiently in ferret cells. These data indicate the replication of EBOV is not variant-specific and that the hindrance observed for MARV does not apply to orthoebolaviruses. Moreover, SUDV could replicate to titres nearly identical to those seen for EBOV, indicating that no block in replication occurs at the species level for orthoebolaviruses.

With the finding that the blockage most likely lays at the cellular level, we next set out to investigate the contribution that the host type I IFN response has on the attenuated replication of MARV within ferret cells. Indeed both EBOV and MARV encode VP35, which functions as an antagonist of the innate immune response and is critical for inhibiting the production of type I IFN. While both EBOV and MARV, through the activity of VP35, inhibit the production of type I IFNs, they also encode proteins, namely VP24 and VP40, which act to inhibit downstream signalling of

ISGs via inhibition of the JAK/STAT pathway, albeit through different mechanisms. In particular, this subversion is mediated by VP24 in the case of EBOV, which acts as a competitive inhibitor of pSTAT1. In contrast, in the case of MARV, this subversion is mediated by VP40, which blocks the activation and function of JAK1. As such, hypothesized that this lack of susceptibility by ferrets to lethal infection with orthomarburgviruses but not orthoebolaviruses is the result of mechanistic differences in the innate immune evasion tactics of these two viruses.

To investigate this, ferret cells were infected with both EBOV and MARV and then treated with ruxolitinib, an inhibitor of type I IFN signalling via the JAK/STAT pathway. The results of the pilot study demonstrated that inhibition of type I IFN signalling increased the infectivity of ferret cells to EBOV by 48%. Unfortunately, the weak fluorophore activity of the ZsG reporter within the MARV-ZsG construct did not allow for quantification using a plate reader. Nonetheless, this proof-of-concept study showed that inhibition of type I IFN signalling via the JAK/STAT pathway enhanced the replication of EBOV within ferret cells.

With these results, we next set out to further investigate the contribution that each component of the type I IFN response, namely the production of type I IFN and type I IFN signalling via the JAK/STAT pathway, has on the replication of MARV. For this, a total of 6 drugs were screened, two targeting type I IFN production and four targeting type I IFN signalling via the JAK/STAT pathway. The drugs targeting type I IFN production, namely TPCA-1 and BX795, are intended to mimic the activity of filovirus VP35, whereas the four drugs targeting type I IFN signalling via the JAK/STAT pathway, namely ruxolitinib, tofacitinib, AZD148 and CYT-387 were intended to mimic the activity of EBOV VP24 and MARV VP40. Treatment of infected ferret cells with inhibitors of type I IFN production, namely TPCA-1 and BX795, had no impact on the replication of MARV Musoke. More specifically, no change in levels of viral RNA relative to no drug control

wells could be observed at any timepoint throughout 14 dpi. Similar findings were observed among A549 control cells. These data ultimately suggest that the block in viral replication is likely not linked to the production of type I IFN and the inefficiency of MARV VP35, particularly within ferret cells. By comparison, treatment of ferret cells with type I IFN signalling inhibitors demonstrated increased levels of viral replication relative to no drug control wells. Among the ferret cells, *mpf*Heart cells showed the best response to ruxolitinib and tofacitinib, with more modest increases observed for AZD1480 and CYT-387. In contrast, *mpf*Spleen cells and *mpf*Lung cells, to a certain extent, showed no change in levels of viral RNA regardless of treatment, further emphasizing that these cell lines are refractory to infection with MARV. Given that viral replication of MARV increased following treatment of ferret cell lines with inhibitors targeting JAK/STAT signalling, it indicates that the block in replication lies at the level of type I IFN signalling. More specifically, with these drugs mimicking the activity of MARV VP40, an increase following treatment suggests that MARV VP40 may be ineffective at subverting type I IFN signalling and potentially account for the lack of diseases among MARV-infected ferrets.

In short, these data suggest that the lack of disease among MARV-infected ferrets is likely due to the inability of MARV VP40 to subvert type I IFN signalling via the JAK/STAT pathway. However, it is important to note that the effect these drugs have on cellular replication is not known. These drugs may influence cellular replication kinetics, which might impact viral replication. Future investigations should focus on the quantification of ISG expression to evaluate drug treatment's impact on the ISGs triggered following infection and how they differ from untreated cells. Furthermore, it would be of particular interest to engineer KO ferrets deficient in type I IFN signalling to elucidate whether the abolishment of downstream signalling promotes infection and disease among MARV-infected ferrets.

# 5. Chapter 5: Rodent-Adapted Orthomarburgviruses Are Lethal in Ferrets

## 5.1. Background

The domestic ferret (*Mustela putorious furo*) has gained attention in recent years as an animal model for characterizing filovirus pathogenesis and evaluating the efficacy of candidate vaccines and countermeasures [314]. Indeed, ferrets share many similar anatomical, metabolic and physiological features with humans, which have long made them appealing animal models for infectious disease research [315]. Unlike immunocompetent rodent models, ferrets offer the advantage of being susceptible to most wild-type filoviruses, eliminating the need for host adaptation [314]. Additionally, ferrets recapitulate many hallmark features of human FVD, most notably petechial rash and internal hemorrhaging. Ferrets have been shown to be highly susceptible to several orthoebolaviruses, namely EBOV [340,341,344,346,362], SUDV [340,342], BDBV [340,341] and RESTV [343], all of which are uniformly lethal among infected animals. TAFV is non-lethal among ferrets, resulting in asymptomatic infection [365]. In contrast to most orthoebolaviruses, infection with orthomarburgviruses, namely MARV and RAVV, does not cause disease in ferrets regardless of challenge variant, dose and route [347,348,362]. While these animals do seroconvert following inoculation, none become viremic at any time point, nor are there any significant deviations from baseline plasma biochemistry and complete blood count [347,348,362].

The fact that ferrets are uniformly susceptible to infection with most orthoebolaviruses but not orthomarburgviruses suggests that these viruses differ fundamentally in their pathogenic mechanisms. Recently our lab set out to investigate the contribution that MARV GP may have toward the lack of disease among inoculated ferrets [362]. Our results demonstrated that while ferret cell lines are permissible to MARV GP-mediated viral entry, replication of authentic MARV

is attenuated compared to authentic EBOV [362]. Nonetheless, we demonstrated that ferrets are uniformly susceptible to infection with a chimeric EBOV (EBOV-mGP) expressing MARV GP in place of EBOV GP [362]. This ultimately provides unequivocal evidence that the lack of disease among MARV-inoculated ferrets is not the result of a block in GP-mediated entry and speculate that it is related to innate immune evasion or virion egress [362].

Drawing parallels to rodents, WT-EBOV and WT-MARV are non-lethal in immunocompetent rodent models, including mice and guinea pigs [248,264,275,372,373]. Serial passaging of these viruses within their respective rodents ultimately resulted in the development of uniformly lethal host-adapted viruses after several generations, namely mouse-adapted (MA)-EBOV[250,256], MA-MARV[258,260], guinea-pig adapted (GPA)-EBOV[273,276] and GPA-MARV [271,361] (See *Section 1.6*). Innate immune evasion tactics have proven to be critical determinants of filovirus pathogenesis. Molecular characterization of MA-EBOV and GPA-EBOV has revealed that adaptations within genes critical for innate immune evasion (VP35 and VP24) are instrumental in achieving uniform lethality within these rodents.[248,276] This is further emphasized by the fact that WT-EBOV is uniformly lethal in immunocompromised IFNAR$^{-/-}$ mice [373]. Unfortunately, characterization into the molecular determinants of disease for MA-MARV and GPA-MARV has yet to be completed. Nonetheless, with mutations present in genes critical for immune evasion (VP35 and VP40), it is not unreasonable to speculate that these adaptations play an important role towards the lethality of these viruses.

Here, we set out to investigate the pathogenicity of GPA-MARV and MA-MARV within ferrets in an attempt to establish a uniformly lethal model. More specifically, given that many of the mutations within these viruses are located in genes critical for IFN evasion, we set out to investigate whether these adapted viruses could result in lethality among ferrets. Our results

demonstrate that GPA-MARV is uniformly lethal among infected ferrets, with all animals succumbing to disease 10 days post-infection. In contrast, MA-MARV is only partially lethal among infected ferrets, with 33% of animals reaching scoring criteria for human endpoints at 8-9 dpi. This represents the first report of a uniformly lethal ferret MARV model. Lethally infected animals all demonstrated clinical signs of disease characteristic of FVD in ferrets, including petechial rash among GPA-MARV infected animals but not MA-MARV-challenged animals. All animals developed high viremia with dissemination to all tested tissues and exhibited hematological parameters characteristic of EVD within ferrets, including elevated ALT and thrombocytopenia, observed among GPA- and MA-MARV-challenged animals. Lastly, animals demonstrated a dysregulated immune response and corresponding 'cytokine storm', a hallmark feature of FVD in NHPs and humans.

## 5.2. Results: GPA-MARV is Uniformly Lethal in Ferrets

With the lack of lethal orthomarburgvirus ferret models, we set out to investigate in this study the pathogenicity of rodent-adapted MARVs, namely GPA-MARV and MA-MARV, in an attempt to establish a uniformly lethal ferret model.

Remarkably, GPA-MARV resulted in uniform lethality among infected ferrets, with all animals succumbing to disease at 10 dpi (Figure 30A). These animals were clinically normal and only began manifesting clinical signs of disease characteristic of FVD beginning at 7-8 dpi, which coincided with weight loss and an increase in body temperature ~40-41°C (Figure 30B-C). Beyond 8 dpi, clinical manifestations of disease progressed rapidly, with the most notable signs of disease being significantly decreased activity and food/water intake and hunched posture with ruffled fur. Moreover, 2/6 animals demonstrated a petechial rash observable roughly 24-48 h before euthanasia (Figure 31B).

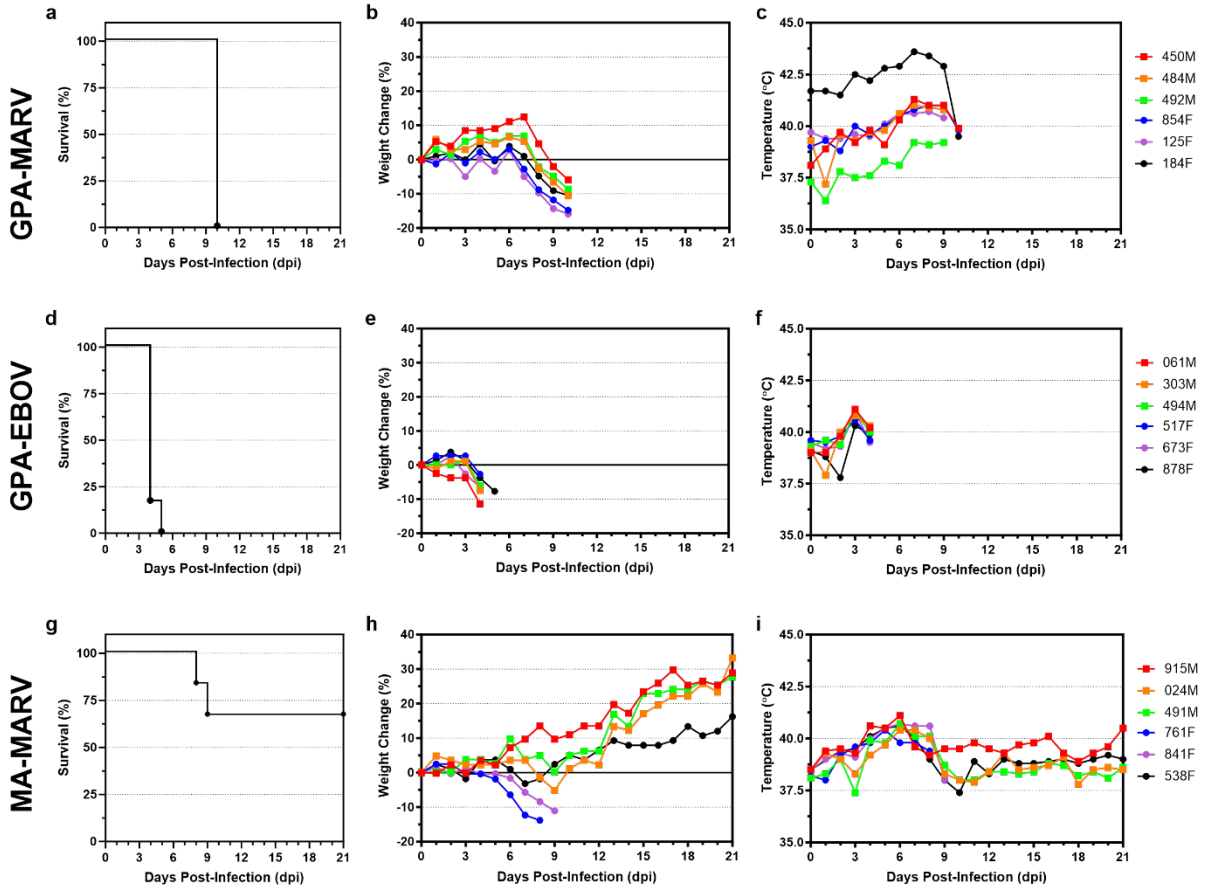


**Figure 30. Clinical parameters of ferrets inoculated with rodent-adapted filoviruses.**

Clinical parameters of ferrets inoculated with (**A-C**) GPA-MARV, (**D-F**) GPA-EBOV and (**G-I**) MA-MARV. (**A, D and G**) Kaplan-Meier survival curves, (**B, E and H**) percent weight change, (**C, F and I**) microchip scan temperature.

By comparison, GPA-EBOV-challenged animals all succumbed to disease with uniform lethality achieved by 5 dpi (Figure 30D). These animals only began manifesting clinical signs of disease roughly 24-48 h prior to euthanasia, coinciding with weight loss and an increase in temperature (Figure 30E-F) These most significant sign of disease was a maculopapular rash which rapidly progressed 24 h prior to death (Figure 31A). Interestingly, MA-MARV only resulted in partial lethality among infected ferrets, with 33% (2/6) animals meeting clinical scoring criteria for humane endpoint on days 8 and 9 post-infection (Figure 30G). Only MA-MARV animals that succumbed to disease exhibited clinical signs of disease, with these clinical signs being far less

severe than those observed for GPA-MARV. Weight loss was observable for the two lethal animals beginning at 3 dpi and gradually progressed till time of euthanasia, with temperatures staying within normal range or very mildly elevated (Figure 30 H-I). None of these MA-MARV-challenged animals developed a rash at any point (Figure 31C). With respect to gross pathology, internal hemorrhaging is absent among GPA-EBOV and MA-MARV challenged animals but prominent among GPA-MARV challenged animals (Figure 31 D-F). Its important to note that apparent hemorrhaging in the abdominal cavity among GPA-MARV challenged animals may actually be the result of cardia puncture during euthanasia. As such, hemorrhaging could only be confirmed by histology. Interestingly, pale live with mottling could be observed among GPA-EBOV challenged animals exclusively (Figure 31D)

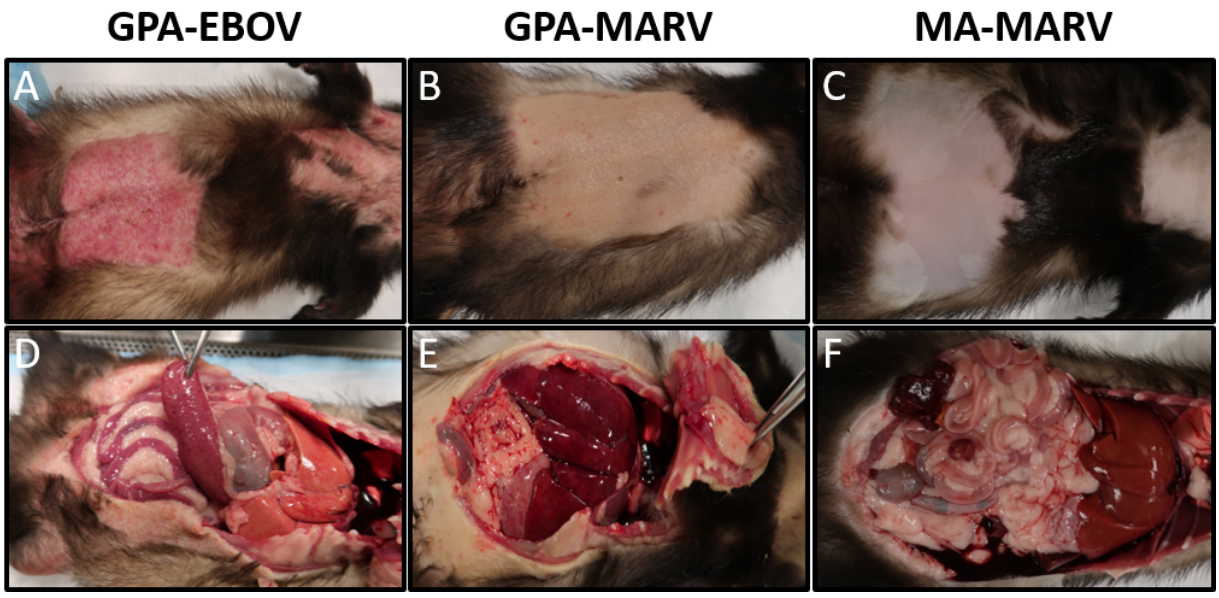


**Figure 31. Rash and gross pathology observed among ferrets infected with rodent-adapted filoviruses**

Representative images of rashes observed at terminal timepoint. (**A**) maculopapular rash among GPA-EBOV challenged ferrets, (**B**) petechial rash among GPA-MARV challenged ferrets and (**C**) no rash among MA-MARV challenged ferrets. Representative gross pathology images at terminal timepoint among (**D**) GPA-EBOV, (**E**) GPA-MARV and (**F**) MA-MARV challenged ferrets.

## 5.3. Results: GPA-MARV Infected Ferrets Support High Levels of Viral Replication

With respect to viral replication, all animals infected with GPA-MARV became viremic as of 5 dpi with low levels of viral RNA detectable within the blood (~3.40 $Log_{10}$ GEQ/mL) (Figure 32A). Levels of viral RNA increased moderately by ~2.20 $Log_{10}$ GEQ/mL by 7 dpi with terminal levels of ~9.07 $Log_{10}$ GEQ/mL at time of euthanasia (Figure 32A). With respect to viral shedding, oral, rectal and nasal swabs were weakly positive from 5-7 dpi and increased to ~5.97, 7.78, 6.38 $Log_{10}$ GEQ/mL at time of euthanasia, respectively (Figure 33 A-C). Tissues were uniformly positive for viral RNA at time of euthanasia, with liver, spleen and lymph nodes being most positive with mean levels of 7.73, 7.14 and 7.03 $Log_{10}$ GEQ/g, respectively (Figure 32B). To a certain extent, levels of infectious virus in the blood and tissues closely paralleled that observed for viral RNA (Figure 32 C-D). Swabs were weakly positive for infectious virus (data not shown).

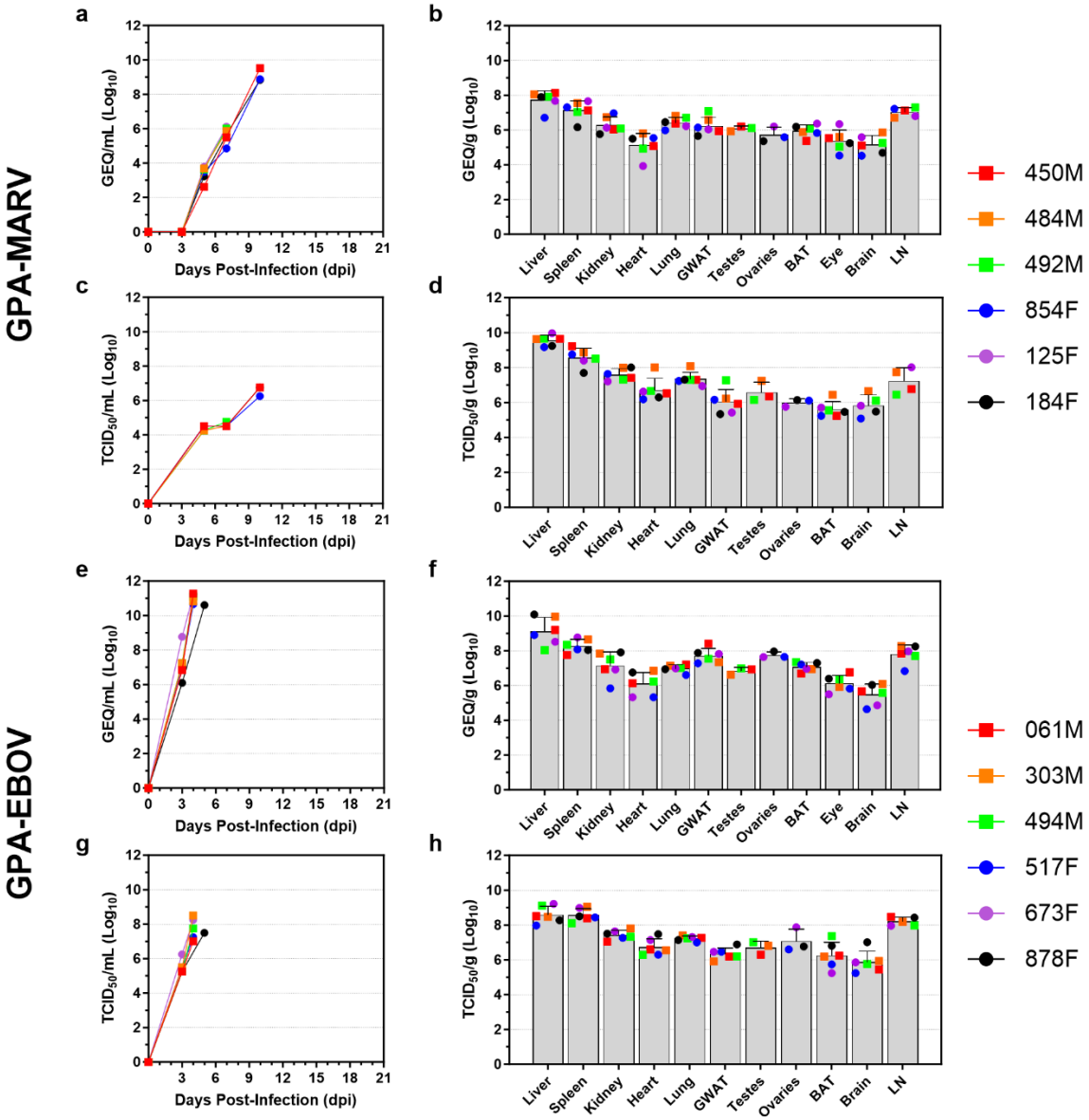


**Figure 32. Viral load in blood and tissues of ferrets infected with Guinea pig adapted filoviruses.**

Whole blood (**A, C, E, G**) was collected from each animal at 3, 5, 7, 10, 14 and 21 days post-infection (dpi) and at the time of euthanasia, while tissues (liver, spleen, kidney, heart, lung, gonadal white adipose tissue (GWAT), testes, ovaries, brown adipose tissue (BAT), eye, brain, and lymph node (LN)) were collected upon necropsy to evaluate viral loads among animals challenged with GPA-MARV (**A-D**) and GPA-EBOV (**E-H**). Virus RNA was quantified by RT-qPCR (**A, B, E, F**) and infectious virus was quantified by $TCID_{50}$ (**C, D, G, H**). Results are depicted in genome equivalents per mL (GEQ/mL) for each animal (indicated by a square for males and circle for females) or mean tissue culture infectious dose per mL ($TCID_{50}$/mL) or per g ($TCID_{50}$/g) depicted as histograms, with data from each animal depicted as dots.

By comparison, replication kinetics for GPA-EBOV challenged animals were more rapid with all animals positive for viral RNA within blood at 3 dpi with mean levels of 7.72 $Log_{10}$ GEQ/mL, which increased to 10.95 $Log_{10}$ GEQ/mL at time of euthanasia at 4 dpi (Figure 32E). Similar to GPA-MARV, tissues were uniformly positive for viral RNA at time of euthanasia with liver, spleen and lymph nodes being most positive with mean levels of 9.12, 8.27 and 7.81 $Log_{10}$ GEQ/g, respectively (Figure 32F). Overall levels of viral RNA at time of euthanasia were ~ 2 $Log_{10}$ GEQ/mL greater among GPA-EBOV-challenged animals compared to GPA-MARV. Levels of infectious virus in the blood and tissues of GPA-EBOV-challenged animals closely paralleled that observed for viral RNA (Figure 32 G-H). Oral, rectal and nasal swabs were uniformly positive for viral RNA at time of euthanasia (Figure 33 D-F).

In contrast, MA-MARV-challenged animals only became viremic at 5 dpi with mean levels of viral RNA in the blood of 4.85 $Log_{10}$ GEQ/mL (Figure 34A). Levels of viral RNA increased very little within blood at 7 dpi with mean levels of ~5.61 $Log_{10}$ GEQ/mL and after 7 dpi, began to decrease with all surviving animals negative for viral RNA at 14 and 21 dpi (Figure 34A). Animals that succumbed to disease had mean viral RNA levels of 6.03 $Log_{10}$ GEQ/mL at time of euthanasia (Figure 34A). Swabs were mostly negative throughout the duration of the study, with the most positives being found in oral swabs at 7 dpi (Figure 33 G-I). The two animals that succumbed to disease at 8 and 9 dpi were uniformly positive for viral RNA across all tested tissues; however, levels were considerably lower than those observed for GPA-MARV (Figure 34B). By comparison, the spleen was the only tissue weakly positive for viral RNA among all surviving animals at time of euthanasia at 21 dpi (Figure 34C).

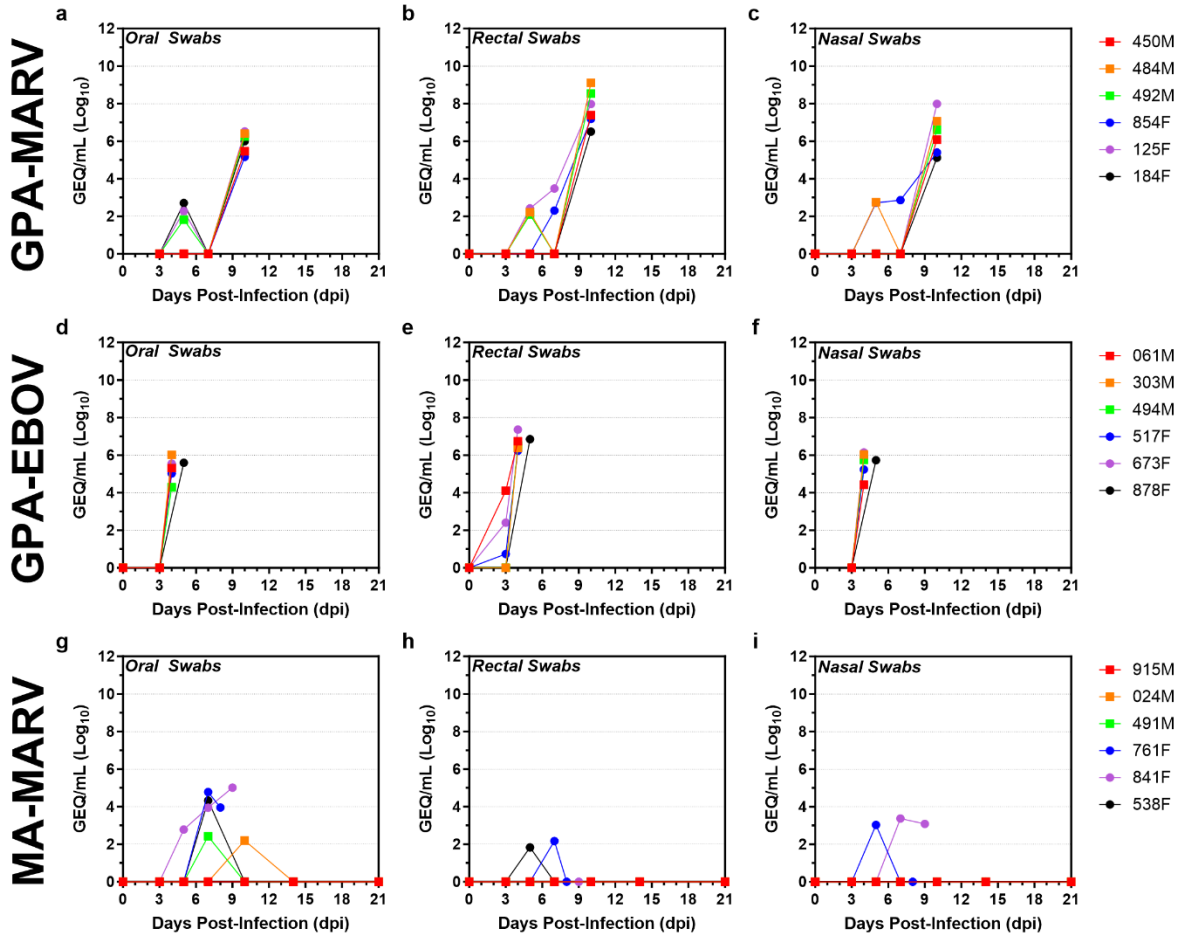


**Figure 33. Levels of viral RNA in oral, rectal and nasal swabs of ferrets infected with Guinea pig adapted filoviruses.**

(**A, D, G**) oral, (**B, E, H**) rectal and (**C, F, I**) nasal swabs were collected from each animal challenged with (**A-C**) GPA-MARV, (**D-E**) GPA-EBOV or (**G-I**) MA-MARV at 3, 5, 7, 10, 14 and 21 days post-infection (dpi) as well as at time of euthanasia to evaluate viral shedding by RT-qPCR. Results are depicted in genome equivalents per mL (GEQ/mL) for each animal (indicated by a square for males and circle for females.

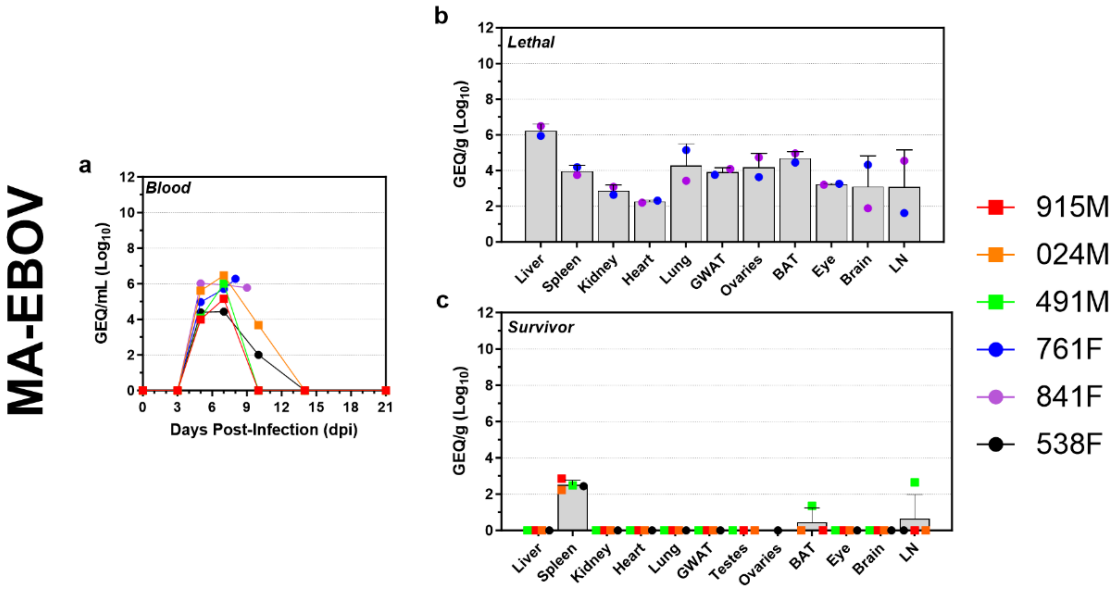


**Figure 34. Viral load in blood and tissues of ferrets infected with MA-MARV.**

(**A**) Whole blood were collected from each animal challenged with MA-MARV at 3, 5, 7, 10, 14 and 21 days post-infection (dpi) as well as at time of euthanasia to evaluate viremia. Virus RNA in the blood was quantified by RT-qPCR and results depicted in genome equivalents per mL (GEQ/mL) for each animal (indicated by a square for males and circle for females). Liver, spleen, kidney, heart, lung, gonadal white adipose tissue (GWAT), testes, ovaries , eyes, brain and lymph nodes (LN) samples were harvested at time of necropsy from (**B**) animals lethally infected with MA-MARV and (**C**) survivors of MA-MARV challenge. Results are depicted in genome equivalents per gram (GEQ/g) for each animal (indicated by a square for males and circle for females) depicted as histograms, with data from each animal depicted as dots.

## 5.4. Results: GPA-MARV Causes Deviations in Baseline Hematology Characteristic of FVD

In terms of biochemistry GPA-MARV challenged animals demonstrated deviations characteristic of FVD. More specifically, all females showed mildly elevated levels of ALT as early as 3 dpi with levels remaining mildly elevated until time of euthanasia (Figure 35A). Interestingly, ALT levels for males remained within normal range throughout 7 dpi (Figure 35A). ALT levels for all animals euthanized at 10 dpi (450M, 854F and 184F) reached the upper limit of quantification (ULOQ) of 2000 U/L (Figure 35A). Unfortunately, 3/6 animals (484M, 492M and 125F) were found dead the morning of 10 dpi, and as such no hematology is available for these

animals. Levels for ALP, TBIL and BUN were all relatively stable throughout 7 dpi but were elevated at 10 dpi for 450M, 854F and 184F (Figure 35B-D). Remaining analytes namely, ALB, AMY, $Ca^{2+}$, PHOS, CRE, GLU, $Na^{+}$, $K^{+}$, TP and GLOB were mostly unremarkable except AMY, PHOS and $K^{+}$ which was elevated for a single animal (184F) at time of euthanasia at 10 dpi (Figure 36). Similarly, levels of ALT for all animals challenged with GPA-EBOV reached the ULOQ at time of euthanasia at 4 dpi (Figure 35E). Likewise, levels for ALP, TBIL and BUN were all elevated at time of euthanasia (Figure 35 F-H). Unlike GPA-MARV levels of PHOS, CRE, $K^{+}$ and GLOB were all elevated among GPA-EBOV challenged animals at time of euthanasia (Figure 36). With respect to MA-MARV, levels of ALT for animals that succumbed to disease namely 761F and 841F were elevated as early as 3 dpi and continued to increase reaching the ULOQ at time of euthanasia at 8 and 9 dpi respectively (Figure 35I). ALT levels for surviving animals peaked at 7 dpi, all of which were elevated relative to baseline pre-bleed (Figure 35I). Beyond 7 dpi, ALT levels gradually normalized to baseline for all surviving animals at 21 dpi apart from 024M whose levels were mildly elevated (Figure 35I). Levels of ALP and BUN remained mostly within normal range throughout 21 dpi (Figure 35J and L). Interestingly, TBIL levels were within normal range for males but elevated for females throughout the duration of the study (Figure 35K). Also of note, GLOB levels increased for all animals as early as 3 dpi and peaked at 7 dpi before returning to baseline at 21 dpi (Figure 36). Regarding CBC, GPA-MARV and GPA-EBOV challenged animals all demonstrated lymphopenia at time of euthanasia with the exception of 878F for GPA-EBOV (Figure 35 N, R). All GPA-MARV challenged animals demonstrated thrombocytopenia at time of euthanasia unlike GPA-EBOV challenged animals whose PLT were within normal range up till time of death (Figure 35 P, T). It's important to note that in some instances PLT values are reported as 0 x $10^{9}$ cells/L and is likely not a true representation of the actual value and is reported as 0 x

$10^9$ cells/L due to the value being lower than the detection limit of the equipment. Lastly, all MA-MARV challenged animals demonstrated thrombocytopenia which peaked at 7 dpi and gradually returned to mostly normal levels by study endpoint at 21 dpi (Figure 35X). Remaining CBC analytes were unremarkable for all viruses (Figure 37).

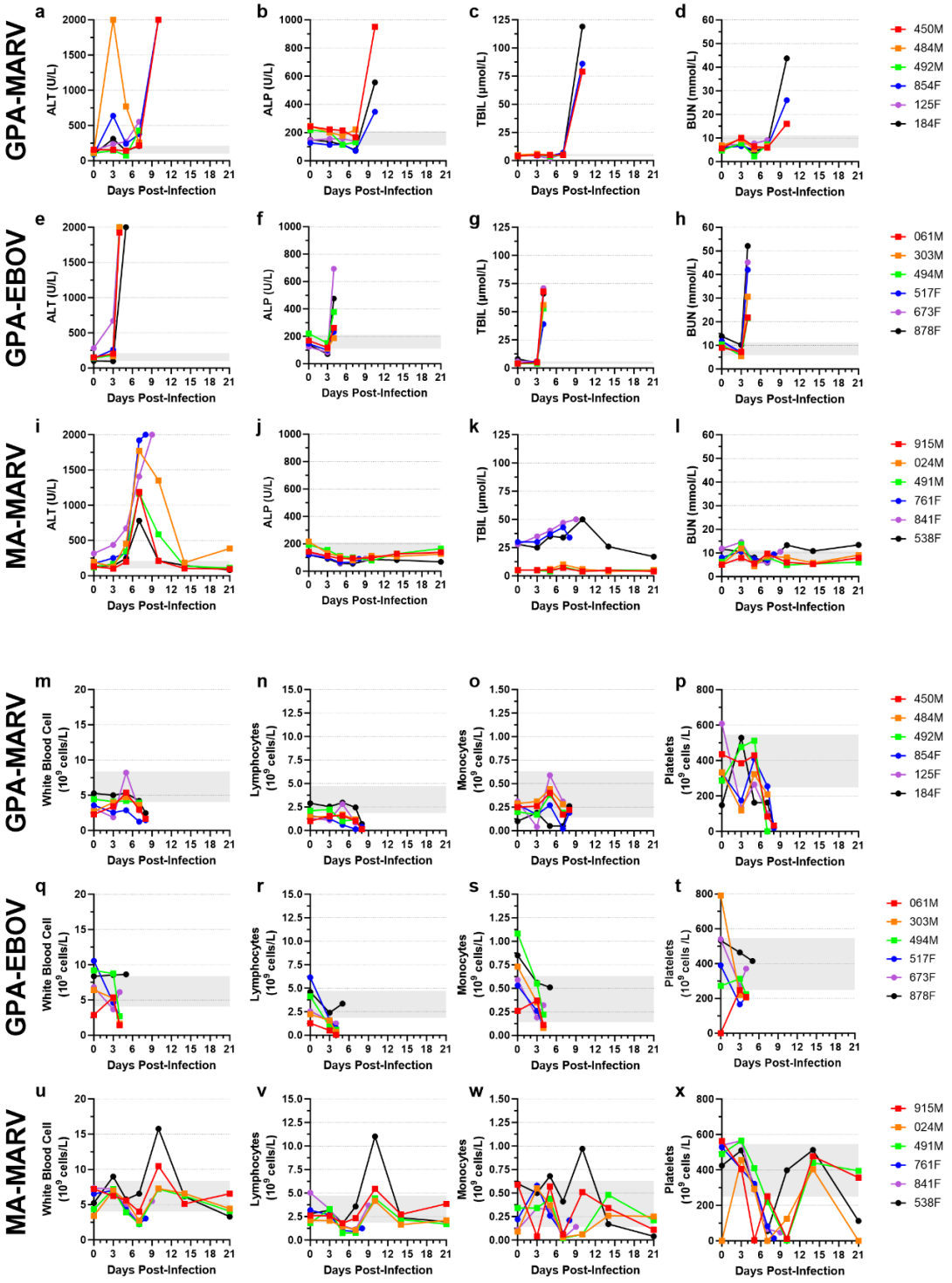


**Figure 35. Select biochemistries and blood counts of rodent adapted filovirus infected ferrets.**

Whole blood was collected from each animal on days 0, 3, 5, 7, 10, 14 and 21 days post-infection (dpi) as well as at time of euthanasia to evaluate (**A-L**) serum biochemistry and (**M-X**) complete blood counts. Biochemistry analytes measured are as follows (**A, E, I**) alanine aminotransferase [ALT]; (**B, F, J**) alkaline phosphatase [ALP]; (**C, G, K**)

total bilirubin [TBIL] and (**D, H, L**) blood urea nitrogen [BUN]. Complete blood count analytes measured are as follows: (**M, Q, U**) white blood cells [WBC]; (**N, R, V**) lymphocytes [LYM]; (**O, S, W**) monocytes [MON]; (**P, T, X**) platelets [PLT]. Individual animal IDs and sex (F/M) are indicated in the key.

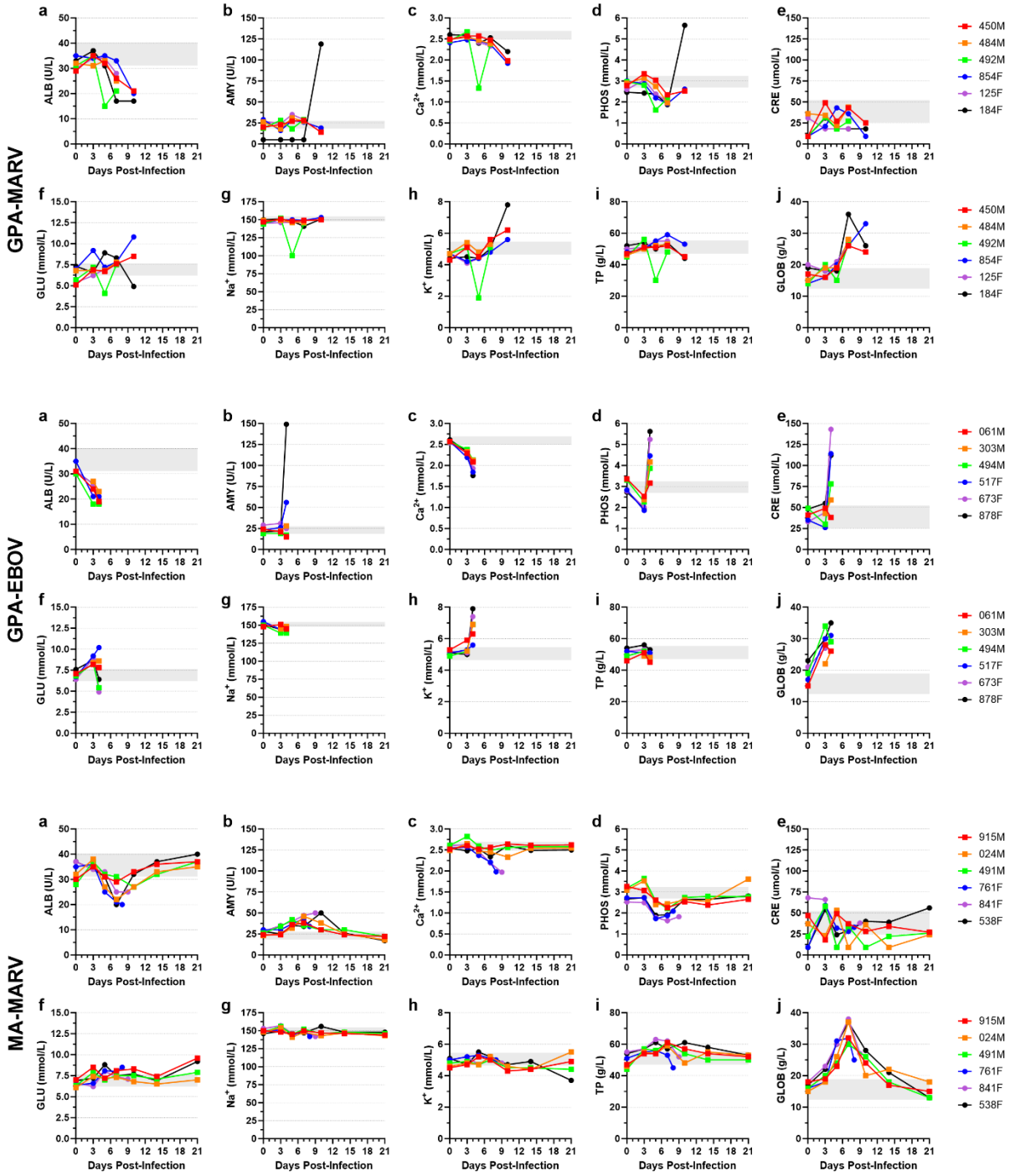


**Figure 36. Serum biochemistry of ferrets challenged with rodent-adapted filoviruses.**

Whole blood was collected from each animal on days 0, 3, 5, 7, 10, 14 and 21 days post-infection (dpi) as well as at time of euthanasia to evaluate serum biochemistry. Biochemistry analytes measured are as follows (**A**) albumin [ALB]; (**B**) amylase [AMY]; (**C**) calcium [$Ca^{2+}$]; (**D**) phosphorous [PHOS]; (**E**) creatinine [CRE]; (**F**) blood glucose [GLU]; (**G**) sodium [$Na^{+}$]; (**H**) potassium [$K^{+}$]; (**I**) total protein [TP]; (**J**) globulin [GLOB]. Individual animal IDs and sex (F/M) are indicated in the key.

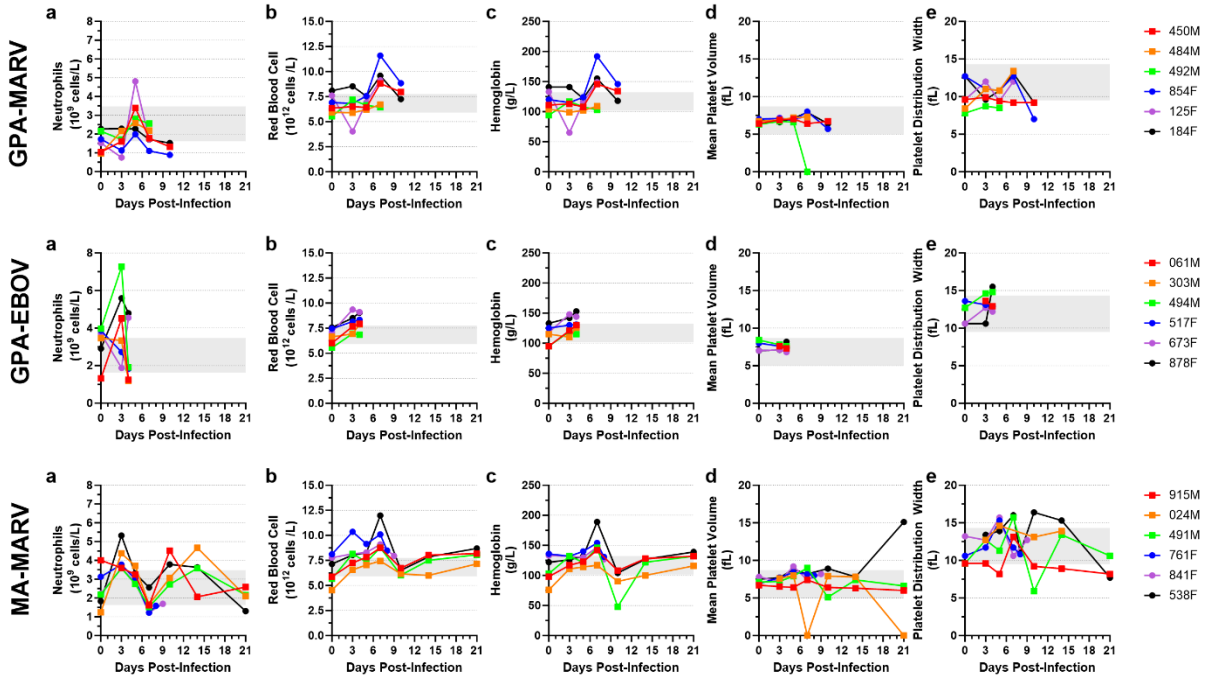


**Figure 37. Hematology of ferrets challenged with rodent-adapted filoviruses.**

Whole blood was collected from each animal on days 0, 3, 5, 7, 10, 14 and 21 days post-infection (dpi) as well as at time of euthanasia to evaluate complete blood counts. Selected complete blood count analytes measured are as follows (**A**) neutrophils [NEU]; (**B**) red blood cell [RBC]; (**C**) Hemoglobin [HGB]; (**D**) mean platelet volume [MPV]; (**E**) platelet distribution width [PDW]. Individual animal IDs and sex (F/M) are indicated in the key. Note: Mean platelet volumes of 0 are believed aberrant results.

## 5.5. Results: Infected Ferrets Demonstrate a Cytokine Storm Characteristic Of FVD

Sera from infected ferrets were subjected to a 12-plex ferret cytokine panel to investigate changes in the cytokines profile that occur as a result of infection. Animals infected with GPA-MARV, GPA-EBOV and MA-MARV all demonstrated deviations in cytokine levels from pre-challenged levels, albeit to various magnitudes. More specifically, GPA-MARV-challenged animals demonstrated elevated levels of proinflammatory cytokines, namely IFN-α and IL-8, as early as 3 dpi (Figure 38 A,C). Proinflammatory cytokines, namely IL-6 and MCP-1, became elevated at 5 dpi relative to pre-challenge control sera and continued to increase until time of euthanasia (Figure 38B and Figure 39F). Increases were most drastic for MCP-10, with mean

levels of ~70,000 pg at time of euthanasia at 10 dpi compared to only ~420 pg observed among historical control animals at 10 dpi (Figure 39F). IP-10 showed minimal increases in levels at 7 dpi; however, levels were elevated among all animals euthanized at 10 dpi at >75,000 pg (Figure 38D). By comparison, levels of IP-10 among historical control animals challenged with WT-MARV never exceeded 12,000 pg throughout 14 dpi (Figure 38D). Cytokine levels for TNF-α, IL-12P70, IL-12p40, IL-17, IL-2, IL-4 and MIP-1β showed considerable fluctuation throughout the course of disease with no discernable trends (Figure 38 and Figure 39). Nonetheless, all cytokines mentioned above were elevated relative to historical control animals challenged with WT-MARV. Interestingly, animal 492M showed consistently elevated levels of TNF-α, IL-12P70, IL-12p40, IL-17 and IL-2 relative to all other animals challenged with GPA-MARV (Figure 38 and Figure 39).

Concerning GPA-EBOV, trends observed for IL-6 and IL-8 were similar to those observed for GPA-MARV, such that they were elevated at terminal timepoint relative to pre-challenge samples (Figure 38 G-H). Remarkably, levels at terminal timepoint for IL-8 were ~2,500 pg greater than those observed among GPA-MARV-challenged animals (Figure 38H). IP-10 was also elevated at terminal timepoint among GPA-EBOV challenged animals, although to levels lower than those observed for GPA-MARV. Unlike GPA-MARV, levels of IL-12p40 were elevated for all animals challenged with GPA-EBOV at terminal timepoint (Figure 39I). The remaining cytokines, IFNα, TNFα, IL-12p70, IL-17, IL-2, IL-4 and MIP-1β, showed fluctuations throughout the disease course with no discernable trends (Figure 38 and Figure 39). Nonetheless, trends observed for GPA-EBOV closely paralleled those observed among historical control animals challenged with WT-EBOV.

Lastly, trends observed for MA-MARV-challenged animals deviated from those observed among GPA-MARV-challenged animals. More specifically, the elevated levels observed IFN-α, IL-6, and MCP-1 among GPA-MARV challenged animals were absent among MA-MARV challenged animals (Figure 38 K,L and Figure 39T). Nonetheless, slight increases can be seen among these analytes around 5-7 dpi; however, these levels normalized shortly after at 10 dpi (Figure 38 K,L and Figure 39T). Interestingly, levels of IL-8 show an increase at 10 dpi, coinciding with disease onset and clinical scoring, followed by a decrease at 14 dpi only to return to elevated levels at time of euthanasia at 21 dpi (Figure 38N). For unknown reasons, levels of IL-17 and IL-4 were elevated throughout the study compared to animals of the same challenge group (Figure 39 Q, S). The remaining analytes, namely TNF-α, IP-10, IL-12p70, IL-12p40, IL-2, MCP-1 and MIP-1β showed fluctuations with peaks observed around 7 dpi, however, with no discernable trends (Figure 38 and Figure 39).

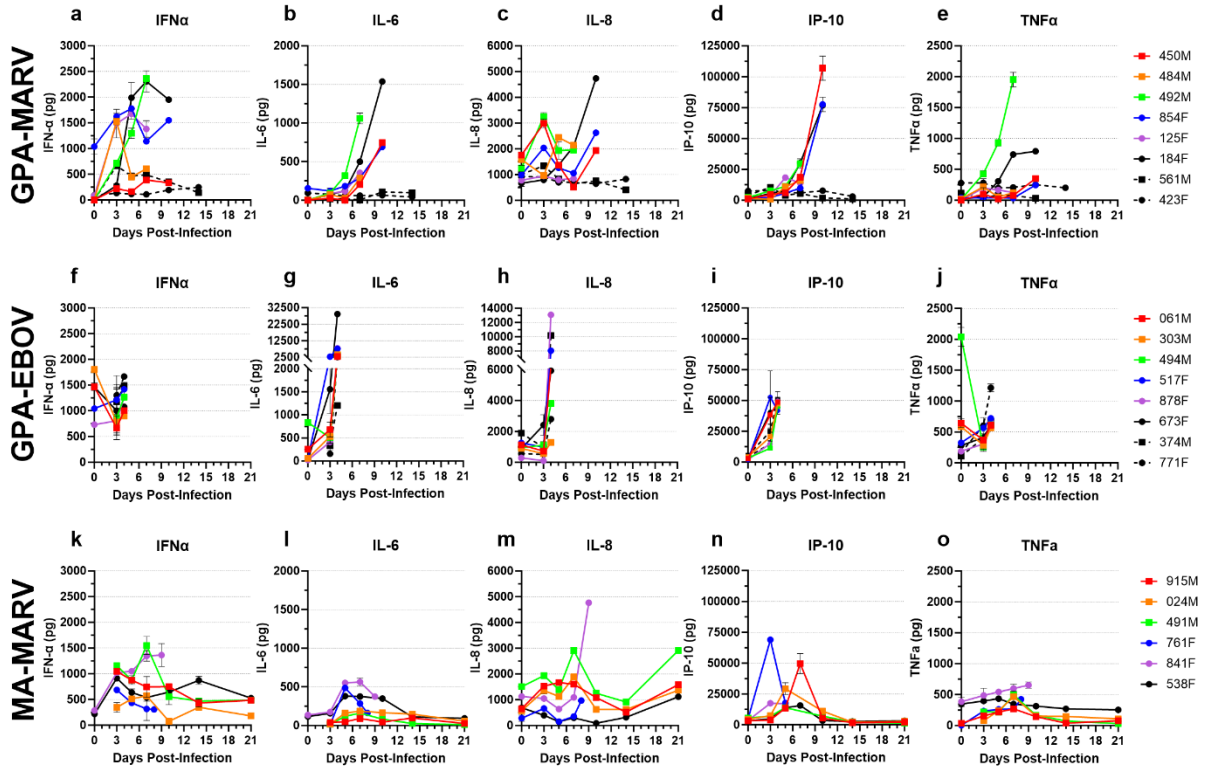


**Figure 38. The cytokine/chemokine response in ferrets challenged with rodent-adapted filoviruses .**

Serum was collected from each animal challenged with (**A-E**) GPA-MARV, (**F-J**) GPA-EBOV or (**K-O**) MA-MARV at 0, 3, 5, 7, 10, 14 and 21 days post-infection (dpi) as well as at time of euthanasia to evaluate cytokine/chemokine profiles using a 12-plex ferret Luminex assay. Analytes measured are as follows: (**A, F, K**) Interferon-alpha [IFNα]; (**B, G, L**) interleukin-6 [IL-6]; (**C, H, M**) interleukin-8 [IL-8]; (**D, I, N**) Interferon gamma-induced protein 10 [IP-10]; (**E, J, O**) Tumor necrosis factor alpha [TNFα]. Individual animal IDs and sex (F/M) are indicated in the key.

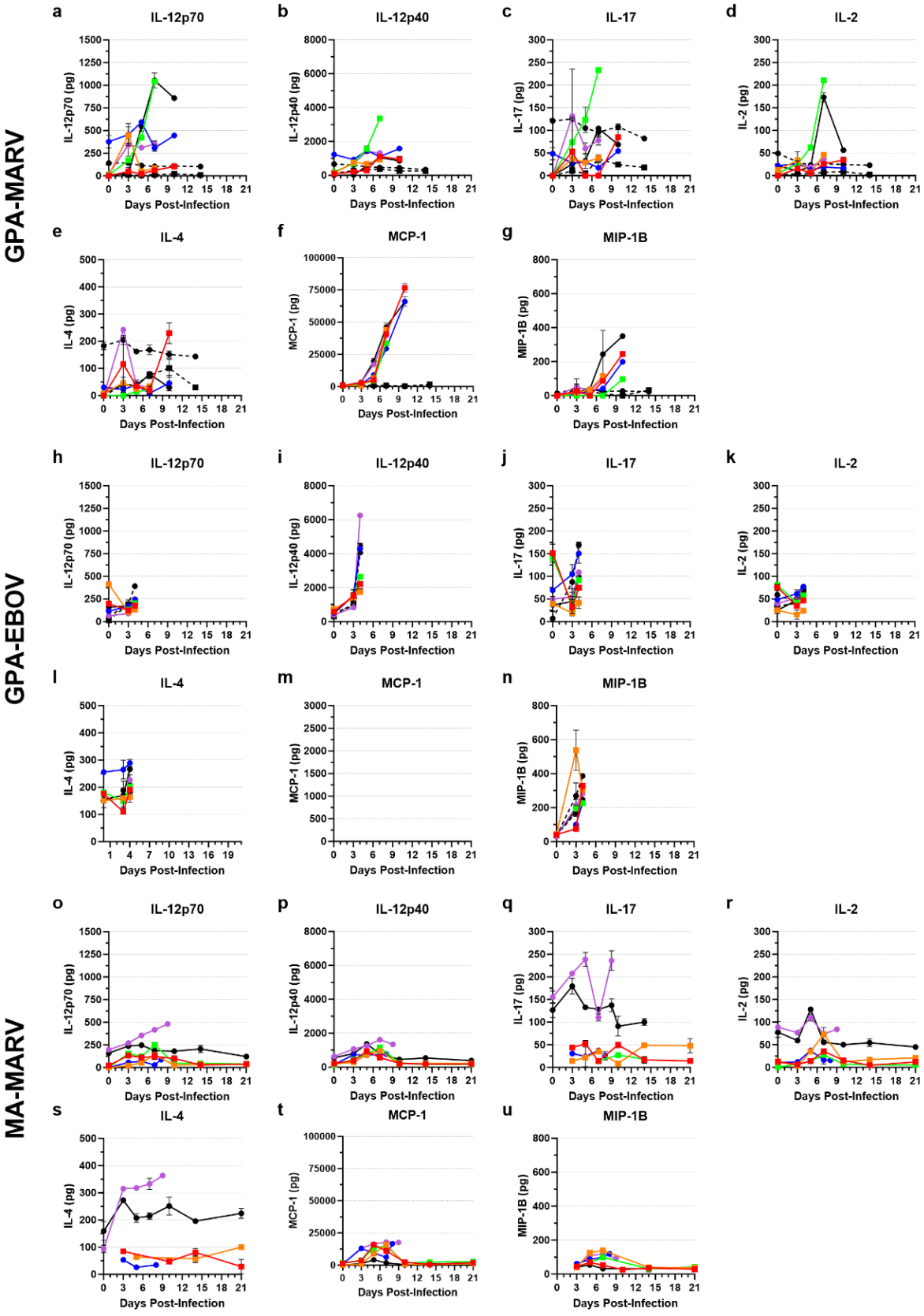
GPA-MARV
GPA-EBOV
MA-MARV
a
IL-12p70
IL-12p70 (pg)
b
IL-12p40
IL-12p40 (pg)
c
IL-17
IL-17 (pg)
d
IL-2
IL-2 (pg)
e
IL-4
IL-4 (pg)
f
MCP-1
MCP-1 (pg)
g
MIP-1B
MIP-1B (pg)
h
IL-12p70
IL-12p70 (pg)
i
IL-12p40
IL-12p40 (pg)
j
IL-17
IL-17 (pg)
k
IL-2
IL-2 (pg)
l
IL-4
IL-4 (pg)
m
MCP-1
MCP-1 (pg)
n
MIP-1B
MIP-1B (pg)
o
IL-12p70
IL-12p70 (pg)
p
IL-12p40
IL-12p40 (pg)
q
IL-17
IL-17 (pg)
r
IL-2
IL-2 (pg)
s
IL-4
IL-4 (pg)
t
MCP-1
MCP-1 (pg)
u
MIP-1B
MIP-1B (pg)
Days Post-Infection

**Figure 39. The cytokine/chemokine response in ferrets challenged with rodent-adapted filoviruses (Extended.)** Serum was collected from each animal challenged with (**A-G**) GPA-MARV, (**H-N**) GPA-EBOV or (**O-U**) MA-MARV at 0, 3, 5, 7, 10, 14 and 21 days post-infection (dpi) as well as at time of euthanasia to evaluate cytokine/chemokine profiles using a 12-plex ferret Luminex assay. Analytes measured are as follows: (**A, H, O**) interleukin-12 p70 [IL-12p70]; (**B, I, P**) interleukin-12 p40 [IL-12p40]; (**C, J, Q**) interleukin-17 [IL-17]; (**D, K, R**) interleukin-2 [IL-2]; (**E, I, S**) interleukin-4 [IL-4]; (**F, M, T**) monocyte chemoattractant protein-1 [MCP-1]; (**G, N, U**) macrophage inflammatory protein-1 beta [MIP-1B]. Individual animal IDs and sex (F/M) are indicated in the key.

## 5.6. Results: Several Mutations Reach Consensus Threshold Following Challenge With GPA-MARV

To track virus evolution, whole blood collected at 3, 5, 7 and at time of euthanasia along with tissues were subjected to NGS. In total, 28 mutations were identified within the blood and tissues of ferrets challenged with GPA-MARV, among which eight were located within coding regions (Table 6). All mutations within coding regions except a single mutation in VP35 (A2931T) were non-synonymous including one in NP (T1562C:F287L), two in VP35 (T3033C:L30S and T3044C:Y34H), three in VP40 (A4735T:K56N, G4802A:G79S and G5117A:D184N) and one in VP24 (A10402G:I66V) (Figure 40 and Figure 41). Each of these non-synonymous mutations was present within the virus challenge stock at frequencies below 25%; however, all reached consensus threshold frequency of ≥ 50%, with the majority of these mutations being present at a frequency ≥ 75%. The remaining 20 mutations were silent and located within intergenic regions, including 19 between VP35 and VP40 (T4114C, T4116C, T4121C, T4122C, T4129C, T4130C, T4148C, T4153C, T4154C, T4157C, T4171C, T4182C, T4201C, T4236C, T4273C, T4274C, T4324C, T4325C, T4326C) and one between GP and VP30 (G8309A) (Figure 40 and Figure 41). In addition to these mutations, several random mutations were also present in the blood and tissues of select animals; however, many mutations were unique to a single animal with no discernible trends observable.

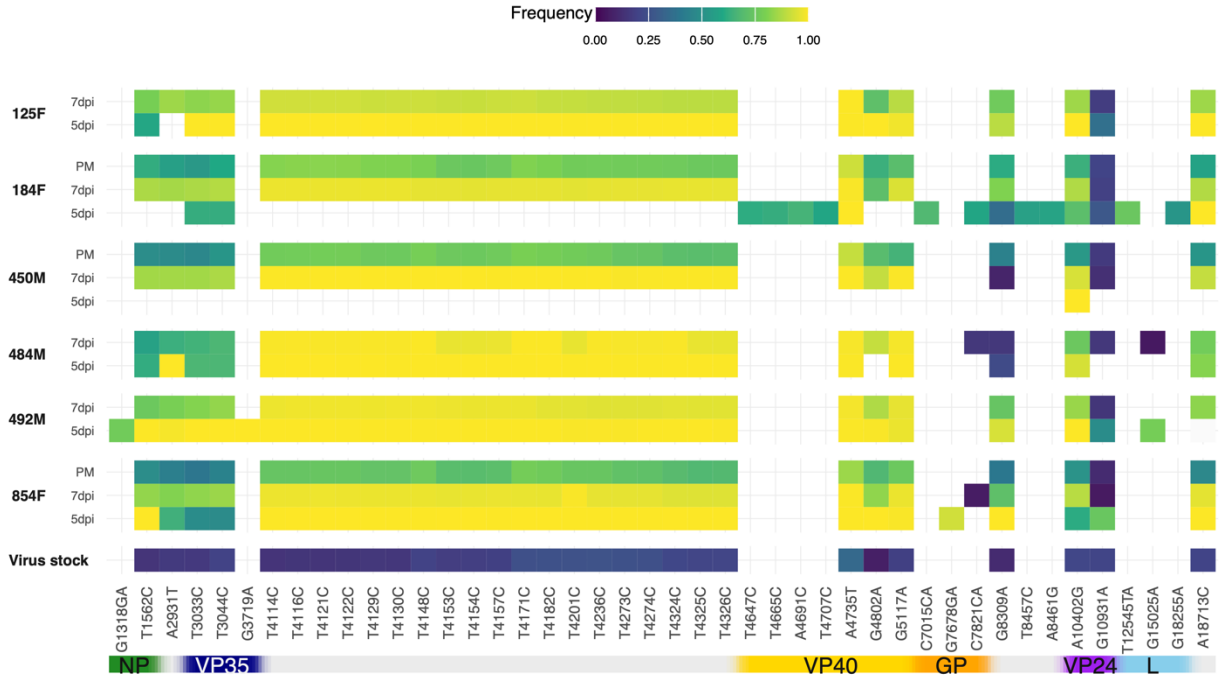


**Figure 40. Heatmap depicting mutations that meet consensus threshold in the blood of ferrets challenged with GPA-MARV**

Whole blood was collected from ferrets challenged with GPA-MARV at 3, 5 and 7 days post-infection (dpi) as well as at time of euthanasia to track virus evolution overtime by Next-Generation Sequencing (NGS). Only mutations with a frequency of ≥ 50% that meet consensus are depicted within the heatmap. Virus stock corresponds to the GPA-MARV stock used for virus challenge. Mutations are denoted according to original base, position and mutant base. Note: no data available for blood at 3 dpi due to lack of viremia as well as PM for animals 492M, 125F and 484M due to lack of blood. Abbreviations: PM (postmortem), adenine (A), guanine (G), thymine (T), cytosine (C), nucleoprotein (NP), viral protein (VP), glycoprotein (GP), RNA-dependent RNA polymerase (L).

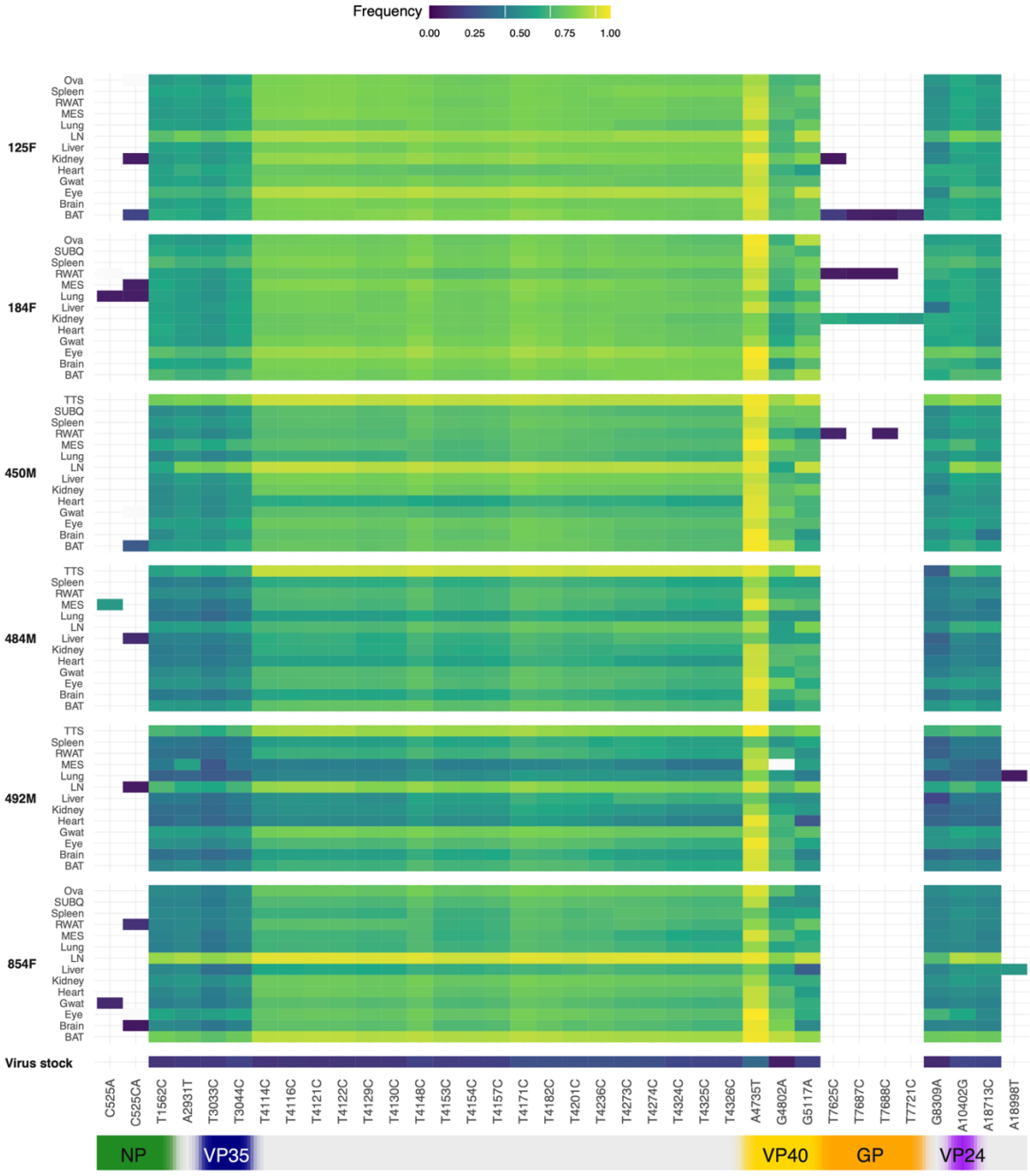


**Figure 41. Mutations that meet consensus threshold within tissues.**

Tissues were collected from ferrets challenged with GPA-MARV at time of euthanasia to evaluate virus evolution across tissue by Next-Generation Sequencing (NGS). Only mutations with a frequency of ≥ 50% that meet consensus are depicted within the heatmap. Virus stock corresponds to the GPA-MARV stock used for virus challenge. Mutations are denoted according to original base, position and mutant base. Abbreviations: Ovaries (Ova), testes (TTS), subcutaneous white adipose (SUBQ), retroperitoneal white adipose (RWAT), mesenteric white adipose (MES), gonadal white adpipose (GWAT), lymphonode (LN), brown adipose tissue (BAT), adenine (A), guanine (G), thymine (T), cytosine (C), nucleoprotein (NP), viral protein (VP), glycoprotein (GP), RNA-dependent RNA polymerase (L).

**Table 6.** Summary of consensus mutations present in blood and tissues of GPA-MARV challenged ferrets

| Location | SNP | Mutation type | SNP effect |
|---|---|---|---|
| NP | T1562C | Missense | F287L |
| VP35 | A2931T | Silent | - |
| | T3033C | Missense | L30S |
| | T3044C | Missense | Y34H |
| IR VP35:VP40 | T4114C | - | - |
| | T4116C | - | - |
| | T4121C | - | - |
| | T4122C | - | - |
| | T4129C | - | - |
| | T4130C | - | - |
| | T4148C | - | - |
| | T4153C | - | - |
| | T4154C | - | - |
| | T4157C | - | - |
| | T4171C | - | - |
| | T4182C | - | - |
| | T4201C | - | - |
| | T4236C | - | - |
| | T4273C | - | - |
| | T4274C | - | - |
| | T4324C | - | - |
| | T4325C | - | - |
| | T4326C | - | - |
| VP40 | A4735T | Missense | K56N |
| | G4802A | Missense | G79S |
| | G5117A | Missense | D184N |
| IR GP:VP30 | G8309A | - | - |
| VP24 | A10402G | Missense | I66V |

## 5.7. Discussion: Key Findings, Significance, and Limitations

Studies have repeatedly demonstrated that ferrets are uniformly susceptible to infection with several orthoebolaviruses, namely, EBOV, SUDV, BDBV, and RESTV, yet otherwise refractory to infection with closely related orthomarburgviruses, MARV and RAVV. This is surprising given that orthoebolaviruses and orthomarburgviruses cause severe, often fatal, disease in both humans and NHPs that are at least superficially similar. Furthermore, studies from our lab

recently demonstrated that the absence of disease among MARV-challenged ferrets cannot be exclusively linked to GP. Nonetheless, the efficiency by which MARV-GP mediates entry into ferret cells is poor compared to that of EBOV, potentially contributing to the lack of disease among MARV-challenged ferrets. As such, GP likely represents only one of many factors contributing to the absence of disease in ferrets. Based on our data, we speculate that factors related to innate immune evasion likely contribute to the lack of disease among MARV-challenged ferrets. Indeed, the results presented in *Section 4* demonstrated that inhibition of type I IFN production had no impact on the replication of MARV within ferret cells. In contrast, inhibition of type I IFN signalling via the JAK/STAT pathway enhanced the replication of MARV within ferret cells. Here, we set out to investigate the pathogenicity of GPA-MARV and MA-MARV within ferrets in an attempt to establish a uniformly lethal model. More specifically, given that many of the mutations within these viruses are located in genes critical for IFN evasion, namely VP35 and VP40, we set out to investigate whether these adapted viruses could result in lethality among ferrets.

Remarkably, ferrets were found to be uniformly susceptible to infection with GPA-MARV but only partially susceptible to infection with MA-MARV. Surprisingly, animals challenged with MA-MARV met the criteria for human endpoint roughly 1-2 days prior to GPA-MARV. While manifestations of disease were similar, the onset of clinical signs of disease occurred approximately 1 day prior among MA-MARV compared to GPA-MARV. Interestingly, GPA-MARV but not MA-MARV challenged animals developed a petechial rash characteristic of what is observed in NHPs. Importantly, the rash observed among GPA-MARV differed from that observed among GPA-EBOV-challenged animals. More specifically, GPA-MARV-challenged animals developed a petechial rash, whereas GPA-EBOV animals developed a maculopapular rash, which blanched upon applying pressure. Although disease manifestations were identical for

all viruses, weight loss was more prominent among females challenged with GPA-MARV and MA-MARV. These findings are consistent with our previous observations, suggesting females are more sensitive to infection than males. Lastly, gross pathology differed among all viruses. GPA-MARV-challenged animals demonstrated signs of internal hemorrhaging with necrosis observed on the spleen, liver, intestines and stomach. Hemorrhaging was not apparent among GPA-EBOV of MA-MARV-challenged animals. Adipose tissues were also far less prominent in the abdominal cavity of GPA-MARV-challenged animals than in MA-MARV and GPA-EBOV.

Hematological findings were similar among GPA-MARV and GPA-EBOV challenged animals, including elevated levels of ALT, ALP, TBIL and BUN, indicating liver and kidney dysfunction consistent with observations in NHPs. While levels of ALT spiked around 7-8 dpi for MA-MARV-challenged animals, levels normalized among survivors, which was consistent with the resolution of the disease. Interestingly, levels of ALP, TBIL, and BUN did not change throughout the course of the study, which is indicative of a very mild disease. Additionally, GPA-MARV-challenged animals exhibited thrombocytopenia, a previously unseen phenomenon among EBOV-challenged animals. This could also be observed among MA-MARV-challenged animals; however, PLT levels normalized among surviving animals. These coagulation abnormalities represent a hallmark feature of FVD and are frequently seen in NHPs, but this represents the first instance seen in ferrets challenged with orthomarburgviruses.

The onset of viremia was delayed among MA-MARV and GPA-MARV-challenged animals, with viral RNA only being detectable at 5 dpi compared to 3 dpi for GPA-EBOV. While levels of viral RNA continued to increase until the time of euthanasia for GPA-MARV, levels peaked at 7 dpi for MA-MARV and cleared among survivors by 14 dpi. Furthermore, terminal levels were 9.8 $\log_{10}$ GEQ/mL for GPA-MARV compared to only ~6.2 $\log_{10}$ GEQ/mL for MA-

MARV among lethally infected animals. These lower levels of viremia among MA-MARV-challenged animals correlate to mild disease. Nonetheless, GPA-MARV and MA-MARV had considerably lower levels of viral RNA than GPA-EBOV, which peaked at ~11 $\log_{10}$ GEQ/mL. These differences in levels of viral RNA likely correlated to the reduced efficiency of GP-mediated entry and attenuated replication kinetics of orthomarburgviruses observed *in vitro* within ferret cell lines. Despite this, levels of viral RNA among tissues at terminal timepoint were roughly similar among GPA-MARV and GPA-EBOV but approximately 2 $\log_{10}$ GEQ/mL lower for animals lethally infected with MA-MARV.

A strong cytokine response can be observed among GPA-MARV and GPA-EBOV-challenged animals characterized by elevated levels of notable proinflammatory cytokines, namely IL-6, IL-8, and IP-10. Surprisingly, levels of IL-6 and IL-8 among GPA-EBOV greatly exceeded those observed among GPA-MARV challenged animals at terminal timepoint despite euthanasia occurring 6 days prior. Nonetheless, the strong cytokine response observed among GPA-MARV and GPA-EBOV challenged was essentially absent among MA-MARV challenged animals. More specifically, the elevated levels observed for IFN-α, IL-6, and MCP-1 among GPA-MARV-challenged animals were absent among MA-MARV-challenged animals. Slight increases can be seen among these analytes around 5-7 dpi; however, these levels normalized shortly after at 10 dpi. These cytokine data observed among GPA-MARV and GPA-EBOV-challenged animals are consistent with what has been observed in NHPs. In contrast, this minimal cytokine response observed among MA-MARV-challenged animals correlates with the lack of lethal decrease among most animals.

Finally, NGS was conducted to track virus evolution among GPA-MARV-challenged animals. Sequencing revealed 28 mutations present in both the tissues and blood of ferrets

challenged with GPA-MARV, of which eight were located within coding regions. Seven of these eight mutations within coding regions were non-synonymous, resulting in changes to the amino acid sequence. Four of these missense mutations, namely L30S and Y34H in VP35 and G79S and D184N in VP40 have previously been identified in other mouse-adapted orthomarburgviruses. More specifically, L30S and Y34H are present within MA-MARV$_{Angola}$ [260], however, their function has yet to be elucidated, but it is reasonable to speculate that they contribute to the viruses' ability to function as an antagonist of IFN induction. The G79S mutation within VP40 has previously been identified in both MA-MARV$_{Ci67}$ [259] and MA-MARV$_{Angola}$ [260] and has been found to enhance VP40s ability to function as an antagonist of type I IFN signalling [261]. Similarly, the D184N mutation within VP40 has also previously been identified in MA-MARV$_{Ci67,}$ MA-RAVV [259] and MA-MARV$_{Angola}$ [260] and has been found to have no impact on MARVs ability to subvert to the host IFN response but rather impact virion assembly and budding [269]. The remaining missense mutations, namely F287L in NP, K56N in VP40 and I66V in VP24, have not previously been identified but likely contribute to the pathogenesis of GPA-MARV in some unknown manner. Unfortunately, given the low viral load among MA-MARV-challenged animals with high CTs, NGS was not feasible.

While this represents the first instance of a lethal orthomarburgvirus ferret model, it is nonetheless surprising that MA-MARV is only partially lethal in ferrets despite containing a total of 8 non-synonymous mutations in genes critical for immune evasion. Among the eight mutations, two in VP35 namely L30S and Y34H and six in VP40 namely L27S, L33P, N42H, L47S, G79S and D184N. Among these mutations, G79S has been shown to counter the IFN response, whereas D184N has been shown to contribute to VP40s role as a viral matrix protein and have no effect on the ability of VP40 to inhibit the IFN response in guineapig or human cells [261,269]. In contrast,

GPA-MARV contains three mutations, namely N56K in VP35 and V66I and L216S in GP, potentially contributing to the lethality in ferrets. The role of these mutations has yet to be elucidated. Still, it is reasonable to speculate that the N56K mutation in VP35 may enhance the subversion of ferret IFN production [258], whereas V66I and L216S in GP could potentially enhance the viruses' ability to mediate entry into ferret cells.

All in all, this represents the first report of a lethal ferret model for orthomarburgviruses. The GPA-MARV ferret model draws many parallels many hallmark features to those observed in NHPs, including petechial rash, thrombocytopenia and dysregulated immune response characterized by an overzealous 'cytokine storm'. Moreover, the disease window of 10 days compared to only 4 days for EBOV makes this lethal model for countermeasure evaluation in particular small molecules and drugs. While attempts were made to compare and contrast the host transcriptome among lethal and non-lethally infected animals, poor RNA quality made such analysis difficult, marking a limitation to this study. The adaptations within the GPA-MARV virus genome are directly responsible for the lethality observed among GPA-MARV-challenged ferrets. As such, future investigations should focus on elucidating the molecular determinants of disease using reverse genetics. Furthermore, it would be of interest to further characterize the ferret type I IFN response to infection with WT-MARV and contrast this response to that observed among GPA-MARV-infected ferrets.

# 6. Chapter 6: Final Discussion, Conclusions and Future Directions

## 6.1. Summary of Key Findings

The domestic ferret (*Mustela putorius furo*) is a small carnivore belonging to the Mustelidae family, members of which can be found across the globe in a number of highly diverse ecosystems ranging from arctic tundra to tropical rainforests [315]. These animals share many anatomical, metabolic, and physiological features with humans, which has long made them appealing models for infectious disease research. Indeed, the ferret has become an increasingly popular animal model for characterizing filovirus pathogenesis and evaluating the efficacy of candidate vaccines and therapeutics [364]. These intermediate-sized animals are of a higher sentient order than rodents and exhibit disease progression that more closely recapitulates human filovirus disease (FVD). Multiple studies have demonstrated that ferrets are highly susceptible to several orthoebolaviruses, namely Ebola virus (EBOV) [340,341,344,346], Sudan virus (SUDV) [340,342], Bundibugyo virus (BDBV) [340,341] and Reston virus (RESTV) [343], all of which are uniformly lethal among infected animals. In contrast, Taï Forest virus (TAFV) is non-lethal among ferrets [365]. Unlike most orthoebolaviruses, however, inoculation with orthomarburgviruses, namely Marburg virus (MARV) and Ravn virus (RAVV), does not cause disease in ferrets [347,348]. Although MARV-challenged ferrets have been shown to seroconvert following inoculation, none of the animals became viremic at any time point, nor were there any disturbances observed in blood biochemistry or cell counts [347,348].

The fact that ferrets are highly susceptible to lethal infection with certain orthoebolaviruses but not orthomarburgviruses suggests that these viruses differ in their pathogenic mechanisms. It is likely that these differences can be attributed to variations in one or more aspects of the virus replication cycle, such as attachment, entry, replication, transcription, immune evasion, or egress. Accordingly, the primary focus of this thesis is to elucidate the cellular and molecular mechanisms

that govern filovirus pathogenesis within ferrets with emphasis on Marburg virus. The ultimate goal of this thesis is to provide insight into potential mechanisms accounting for the lack of disease among ferrets infected with orthomarburgviruses.

Overall, this thesis explored two main hypotheses. Firstly, it was hypothesized that this lack of susceptibility by ferrets to lethal infection with orthomarburgviruses but not orthoebolaviruses is due to a block in GP-mediated viral entry, which functions to either interfere or inhibit viral entry and/or replication. Secondly, it was hypothesized that this lack of susceptibility by ferrets to lethal infection with orthomarburgviruses but not orthoebolaviruses is the result of mechanistic differences in the innate immune evasion tactics of these two viruses.

To address the first hypothesis, the aim of *Chapter 3* was to investigate the role of GP-mediated entry towards infectivity of ferret cell lines *in vitro* and viral pathogenesis *in vivo*. Given the lack of commercially available ferret cell lines, immortalized ferret cell lines derived from the spleen, lung and heart were established for this project to be used as an *in vitro* ferret cell model. These ferret cell lines were evaluated for their permissibility to GP-mediated viral entry using VSV pseudotyped with either MARV or EBOV-GP. The results demonstrate that while these ferret cell lines are permissible to both EBOV and MARV GP-mediated entry, the efficiencies differ. More specifically, EBOV-GP is more efficient at mediating entry into ferret cells than MARV-GP, particularly during the early stages of infection. Furthermore, these ferret cell lines were shown to support replication of WT-MARV, albeit replication was attenuated compared to that observed for EBOV. Not only was a delay in replication observed, but peak titers observed for EBOV greatly exceeded what was seen for MARV. Furthermore, spleen cells demonstrated no replication of MARV, suggesting that these cells are refractory to infection. This is surprising given that the spleen represents a prominent target of filoviruses and, thus, among all the ferret cell lines, was

expected to support the greatest replication for MARV. Nonetheless, these data suggest EBOV has the advantage over MARV with respect to entry and replication kinetics. Indeed, it is probable that this reduced efficiency in GP-mediated entry and attenuated replication of MARV within ferret cells may provide the host's innate response with an advantage to counter infection.

The results from *Chapter 3* also demonstrated that ferrets are uniformly susceptible to infection with EBOV-mGP, providing unequivocal evidence that MARV-GP is capable of mediating entry into ferret cells. It is interesting to note, however, that the onset of viremia in EBOV-mGP-challenged animals was delayed compared with the EBOV-challenged animals, and peak levels of EBOV-mGP RNA were also much lower. Similar trends were observed in the oral/rectal swabs and nasal washes, which showed consistently lower and later RNA levels among animals challenged with EBOV-mGP than those challenged with EBOV. Furthermore, the majority of tissue samples taken from EBOV-mGP-challenged animals showed levels of virus RNA and infectious virus that were lower than what was observed in EBOV-challenged animals. In addition, the delays observed *in vivo* reflected the *in vitro* growth properties of EBOV-mGP, which exhibited slower replication kinetics compared with EBOV. Thus, although MARV-GP may not be the sole factor responsible for the lack of disease in MARV-challenged ferrets, these data support the possibility that it is a contributing factor. More specifically, MARV-GP likely interacts with ferret cellular host-attachment factors and possibly the intracellular receptor NPC1 with reduced efficiency compared to EBOV-GP, contributing to differences among disease outcomes of these two filoviruses in ferrets.

With the conclusion that GP is not the sole factor responsible for the lack of disease in MARV-challenged ferrets, we next set out in *Chapter 4* to investigate the contribution that the host type I IFN response may have towards the replication of MARV in ferret cells. The aim of *Chapter*

4 was to examine whether inhibitors of the type I IFN response, including production and signalling via the JAK/STAT pathway, promote replication of MARV *in vitro* within ferret cell lines. The results from this chapter demonstrated that inhibition of type I IFN production had a negligible impact on the replication of MARV within ferret cells. This was also the case among A549 control cells treated with drugs inhibiting type I IFN production. In contrast, inhibition of type I IFN signalling via the JAK/STAT pathway enhanced MARV replication within select ferret cell lines. Among the drugs, ruxolitinib, an inhibitor of JAK1/JAK2 activity, strongly promoted the replication of MARV within *mpf*Heart cells. The increases in viral replication at timepoints beyond 10 dpi were significant compared to no drug control wells. Similar results were also observed for JAK/STAT signalling inhibitors, namely tofacitinib, AZD1480 and CYT-387. Interestingly, the *mpf*Heart cells responded the best to drug treatments, where no changes in levels of replication can be seen in *mpf*Spleen cells. Similarly, only ruxolitinib and CYT-387 significantly improved the replication of MARV in the presence of drug compared to no drug control wells. Taken together, the results from this chapter emphasize that type I IFN production has a negligible impact on viral replication, diminishing the role that MARV VP35 may play towards the replication of MARV in ferret cells. It is important to note, however, that levels of IFN were never quantified due to a lack of available reagents, and this conclusion is drawn exclusively based on the fact that inhibitors of type I IFN production did not enhance viral replication of MARV within ferret cells. In contrast, type I IFN signalling via the JAK/STAT pathway appears to have a more significant role in regulating the replication of MARV in ferret cells. As such, MARV VP40 plays an essential role in subverting type I IFN signalling via the JAK/STAT pathway and, thus, is reasonable to speculate that the lack of disease among MARV-challenged ferrets could potentially be attributed to the inefficiency of VP40 at subverting type I IFN signalling.

Despite these results, the findings from *Chapter 4* have limitations. Firstly, there are more than 200 ISEs that have the potential for upregulation in response to type I IFN, the majority of which have yet to be characterized. Little is known about which ISEs play an important role in the host's innate immune response. As such, investigating the impact that drug treatments have on ISE expression would be analogous to a needle in a haystack and identifying the ISEs responsible for inhibiting MARV replication would be extremely difficult. In the future, it would be ideal to conduct 10X genomics on cells following drug treatment to identify how the single-cell transcriptome is altered in the presence of drug. Unfortunately, such an experiment is cost-prohibitive given the extremely high cost associated with 10X genomics. Furthermore, transcriptomics does not accurately reflect protein expression. As such an additional experiment for future investigation would be to conduct a proteomic analysis to infer how the ferret proteasome changes in response to infection. Another limitation is that the exact mechanism of action of the drugs tested is not entirely known. Indeed, these drugs are known to inhibit various aspects of the JAK/STAT pathway. However, their off-target effects are not entirely known. Notably, the influence these drugs have on cellular replication is not known and, as a result, may influence cellular replication kinetics, which in turn may have a negative impact on viral replication. A future direction of this study would be to rescue MARV chimeric viruses where VP40 and VP24 are swapped independently and in concert with the homologous genes from EBOV. This would ultimately allow for further elucidation of the role that VP40 plays in the replication of MARV in ferret cells and highlight the role that EBOV VP24 may have at enhanced replication. Unfortunately, difficulties associated with the rescue of MARV have hampered such investigations.

With the conclusion that the lack of disease among MARV-challenged ferrets is most likely the result of MARVs inability to subvert the ferret type I IFN response, we next set out in *Chapter 5,* to investigate the pathogenesis of rodent-adapted filoviruses, namely GPA-MARV, GPA-EBOV and MA-MARV within ferrets. These viruses contain mutations in genes critical for innate immune evasion tactics. As such, the aim of *Chapter 5* was to investigate whether these adapted orthomarburgviruses containing critical mutations could result in lethality. While the molecular characterization of every mutation present within MA-MARV and GPA-MARV has yet to be completed, several are present within genes critical of immune evasion (VP35 and VP40). As such, it was reasonable to speculate that these adaptations play an important role in the lethality of these viruses. Indeed, molecular characterization of MA-EBOV and GPA-EBOV has revealed that adaptations within genes critical for innate immune evasion (VP35 and VP24) are instrumental in achieving uniform lethality within these rodents [248,276].

Remarkably, GPA-MARV challenge resulted in uniform lethality, whereas inoculation with MA-MARV resulted in only partial lethality with 33% of animals succumbing to disease. Interestingly, the onset of disease and lethality among MA-MARV-challenged animals occurred roughly 1-2 days prior to GPA-MARV. While disease manifestations were nearly identical among GPA-MARV and MA-MARV-challenged animals, only animals challenged with GPA-MARV developed a what looked like a petechial rash. This rash differed from what was observed among GPA-EBOV-challenged animals, which demonstrated more maculopapular in nature that appeared more raised and blanched upon applying pressure. Unfortunately, this study did not investigate coagulation factors due to the lack of species-specific reagents. Such an investigation into coagulation factors would've provided additional insight into why a petechial rash was observable among GPA-MARV-challenged ferrets and not MA-MARV-challenged animals despite both

challenge groups exhibiting thrombocytopenia. Additionally, weight loss was more prominent among females challenged with GPA-MARV and MA-MARV, a phenomenon consistent with previous observations made in our lab. This suggests that females are likely more sensitive to infection with filoviruses than males, indicating potential sex bias. This sex bias was not seen among GPA-EBOV-challenged animals, likely due to the rapid onset of disease and lethality. Gross pathology differed among all viruses. Notably, GPA-MARV-challenged animals demonstrated signs of internal hemorrhaging that were not apparent among GPA-EBOV of MA-MARV-challenged animals. Adipose tissues were also far less prominent in the abdominal cavity of GPA-MARV-challenged animals than in MA-MARV and GPA-EBOV. These differences in gross pathology could potentially reflect variations among the tissue tropisms of each virus.

Hematological parameters were similar among GPA-MARV and GPA-EBOV-challenged animals but deviated among MA-MARV-challenged animals. Notably, GPA-MARV and GPA-EBOV challenge demonstrated elevated levels of ALT, ALP, TBIL and BUN, indicating liver and kidney dysfunction. By comparison, ALP, TBIL, and BUN levels did not change throughout the study, where ALT spiked around 7-8 dpi, which normalized among survivors consistent with the resolution of the disease. Additionally, GPA-MARV-challenged animals exhibited thrombocytopenia, a previously unseen phenomenon among EBOV-challenged animals. This could also be observed among MA-MARV-challenged animals; however, PLT levels normalized among surviving animals. These coagulation abnormalities represent a hallmark feature of FVD and are frequently seen in NHPs, but this represents the first instance seen in ferrets challenged with orthomarburgviruses. The absence of thrombocytopenia among GPA-EBOV-challenged animals could potentially explain the lack of internal hemorrhaging observed among GPA-challenged animals. Future studies should focus on conducting coagulation testing for parameters

such as PT and PTT, among others, to fully characterize the coagulation abnormalities that result from filovirus infection.

A strong cytokine response can be observed among GPA-MARV and GPA-EBOV-challenged animals characterized by elevated levels of notable proinflammatory cytokines, namely IL-6, IL-8, and IP-10. Surprisingly, levels of IL-6 and IL-8 among GPA-EBOV greatly exceeded those observed among GPA-MARV challenged animals at terminal timepoint despite GPA-EBOV challenged animals being euthanized 6 days prior to those challenged with GPA-MARV. Nonetheless, the strong cytokine response observed among GPA-MARV and GPA-EBOV challenged was essentially absent among MA-MARV challenged animals.

The onset of viremia was delayed among MA-MARV and GPA-MARV-challenged animals compared to GPA-EBOV. Overall, titers were lower among GPA-MARV and MA-MARV-challenged animals than GPA-EBOV. This can potentially reflect the more rapid replication kinetics of orthoebolaviruses compared to orthomarburgviruses. Moreover, these lower levels of viremia among MA-MARV-challenged animals correlate to mild disease. These differences in levels of viral RNA likely correlated to the reduced efficiency of GP-mediated entry and attenuated replication kinetics of orthomarburgviruses observed *in vitro* within ferret cell lines.

Taken together, this represents the first report of a lethal orthomarburgvirus ferret model with hallmark features of disease that closely parallel what is observed in humans. Furthermore, the extended disease window compared to that observed for many orthoebolaviruses make this ferret model appealing for countermeasure evaluations. A major limitation of this study is that coagulation parameters were not evaluated. Further characterization of coagulation abnormalities is required to fully elucidate the contribution to disease pathology. Although tissues were collected for pathology, the lack of available resources made such an analysis difficult. Histological

investigations would allow for visualization of the tissue structure, providing insight into any characteristic changes to the tissues resulting from filovirus infection. Additionally, future investigations should incorporate single-cell sequencing technologies to allow for comparative transcriptomics among lethally infected GPA-MARV ferrets relative to lethal and non-lethal MA-MARV challenged ferrets. Such an investigation would provide insight into critical differences in the transcriptome among lethal vs non-lethal outcomes following challenge with different rodent-adapted MARVs. This investigation could be complemented with proteomics, allowing for evaluations into differences among the proteome of lethally infected GPA-MARV ferrets relative to lethal and non-lethal MA-MARV challenged ferrets. Furthermore, a comparison between the transcriptome and proteome would allow for investigations into the degree of transcripts that are translated into protein, potentially highlighting another limiting aspect pertaining to the pathogenesis of various rodent-adapted MARVs within ferrets. Additional characterization should focus on quantifying the host innate immune response among GPA-MARV and MA-MARV challenged ferrets to fully elucidate the role that the host innate immune response, particularly IFN, plays in combatting infection.

## 6.2. Concluding Remarks

In conclusion, this thesis sets out to address a major gap in knowledge, which is why ferrets are uniformly susceptible to several Orthoebolaviruses yet refractory to infection with orthomarburgviruses despite being phylogenetically related. To address this knowledge gap, this thesis set out to investigate several key questions: 1) can orthomarburgviruses enter ferret cells, 2) can orthomarburgviruses replicate in ferret cells 3) can a chimeric EBOV expressing MARV-GP cause disease in ferrets 4) can inhibition of the host IFN response promote replication of orthomarburgviruses within ferret cells and 5) can rodent-adapted filoviruses cause disease in

ferrets. In short, MARV GP was determined to be capable of mediating entry into ferret cells, albeit with a lower efficiency than EBOV-GP. Likewise, WT-MARV was capable of replicating within ferret cells, although replication was attenuated compared to EBOV. Furthermore, chimeric EBOV-mGP containing MARV-GP in place of EBOV-GP was uniformly lethal among infected ferrets, although lethality was delayed compared to WT-EBOV. These findings indicate that the absence of disease among MARV-challenged ferrets cannot be exclusively linked to GP. As such, GP likely represents only one of many factors contributing to the absence of disease in ferrets. Based on these data, we next speculate that the lack of disease among MARV-challenged ferrets is likely related to innate immune evasion. With the finding that the block lies at the cellular level, we next set out to investigate the contribution of the host type I IFN response on the attenuated replication of MARV within ferret cells. Interestingly, the treatment of ferret cells with drugs that inhibited the production of type I IFN did not promote the replication of MARV. In contrast, treatment of ferret cells with drugs inhibiting type I IFN signalling via the JAK/STAT pathway positively impacted replication of MARV, resulting in significantly elevated levels of viral RNA compared to no drug controls. These data indicate that inhibition of type I IFN production analogous to the activity of VP35 did not have an impact on drug replication. As such, inhibition of type I IFN signalling via the JAK/STAT pathway analogous to VP40 significantly impacts MARV replication in ferret cells. Finally, the pathogenesis of rodent-adapted filoviruses, namely GPA-EBOV, GPA-MARV and MA-MARV were investigated within ferrets. Remarkably, GPA-MARV was uniformly lethal among challenged ferrets, whereas MA-MARV resulted in only partial lethality. Animals infected with GPA-MARV developed severe disease with hallmark features of FVD, including a petechial rash, thrombocytopenia, elevated biochemical parameters, viremia and viral shedding and dysregulated immune response characterized by a ‘cytokine storm.’

Disease among MA-MARV-challenged animals was mild, and unlike GPA-MARV, it did not cause petechial rash or any major perturbations in plasma biochemistry. Furthermore, viremia and viral shedding were minimal compared to GPA-MARV with a dampened 'cytokine storm' .

The data presented within this thesis expands on potential mechanisms for why MARV is non-lethal among ferrets. These data ultimately suggest that this lack of disease likely results from a combination of factors, including reduced efficiency of GP-mediated entry, attenuated replication kinetics and reduced efficiency at subverting type I IFN signalling. Nonetheless, these data provide critical insight into the pathogenesis of MARV within ferrets. Despite this, it is essential to note that the balance between lethal and non-lethal outcomes is likely influenced by an intricate coordination of many vital factors which remain to be elucidated. More specifically, many factors likely impact the outcome, including many aspects of the virus life cycle such as replication, assembly and budding, as well as the ability to counter the host immune response, the ability of viral proteins to interact with cellular host factors and the ability to disrupt the host kinome. Effectively, factors likely exist in a delicate balance whereby augmentations or disruptions to these factors and the systems they act upon can significantly impact disease outcomes. The data generated throughout this thesis provide some insight into the potential contribution of these factors; however, a complete exploration into all factors is required to provide a detailed picture of the differences accounting for disease outcomes.

In short, the data generated throughout this thesis contributes to the characterization of the ferret as a model for filoviruses with an emphasis on orthomarburgviruses. The intent of these data is to highlight the use of the ferret as an intermediate-size animal model of higher sentient order than rodents. With high costs and ethical considerations associated with using NHPs, ferrets represent a suitable preliminary animal model prior to investigations in these animals.

Indeed, the orthomarburgvirus ferret model represents a novel and unique addition to the filovirus field. This thesis describes three orthmarburgvirus ferret models of various disease outcomes, namely, lethal, partially lethal and non-lethal, providing a unique window into the differing states of orthomarburgvirus pathogenesis. In concert, the *in vitro* and *in vivo* studies combined with the molecular and immunological methods employed throughout this thesis aim to enhance the understanding of these differences and provide valuable perception into interactions between ferrets and orthomarburgviruses. These investigations not only lend insight into the pathogenesis of orthomarburgviruses but, using this model, could possibly be translated to humans and advance the understanding of why filovirus outcomes can vary among humans. Such investigations utilizing this model could then be exploited to improve the methodology and strategy used in developing medical countermeasures, particularly for orthomarburgviruses. These data may also provide an alternative perspective on how a filovirus may behave within a reservoir host. Further investigation into the parallels between ferrets and *Rousettus aegyptiacus* bats could lend valuable insight into viral pathogenesis and mechanisms essential for maintaining a virus within a population without causing lethal disease. This information can then be used to advance the understanding of potential factors critical for spill-over and re-emergence from reservoir hosts.

It is the hope that the data generated throughout this thesis will provide valuable insight into the use of the ferret as a model for filoviruses with an emphasis on orthomarburgviruses while taking into consideration the limitations associated with the model.

# 7. Chapter 7: References


1. Gordon Smith CE, Simpson DIH, Bowen ETW, Zlotnik I. FATAL HUMAN DISEASE FROM VERVET MONKEYS. The Lancet. **1967**; 290(7526):1119–1121.

2. Kissling RE, Robinson RQ, Murphy FA, Whitfield SG. Agent of Disease Contracted from Green Monkeys. Science. American Association for the Advancement of Science; **1968**; 160(3830):888–890.

3. Martini GA. Marburg Virus Disease. Clinical Syndrome. In: Martini GA, Siegert R, editors. Marburg Virus Disease [Internet]. Berlin, Heidelberg: Springer Berlin Heidelberg; 1971. p. 1–9. Available from: https://doi.org/10.1007/978-3-662-01593-3_1

4. Kunz C, Hofmann H, Kovac W, Stockinger L. [Biological and morphological characteristics of the "hemorrhagic fever" virus occurring in Germany]. Wien Klin Wochenschr. Austria; **1968**; 80(9):161-162 passim.

5. Siegert R, Shu HL, Slenczka HL, Peters D, Müller G. The aetiology of an unknown human infection transmitted by monkeys (preliminary communication). Ger Med Mon. Germany; **1968**; 13(1):1–2.

6. Slenczka W, Klenk HD. Forty Years of Marburg Virus. The Journal of Infectious Diseases. **2007**; 196(Supplement_2):S131–S135.

7. Brauburger K, Hume AJ, Mühlberger E, Olejnik J. Forty-Five Years of Marburg Virus Research. Viruses. **2012**; 4(10).

8. Biedenkopf N, Bukreyev A, Chandran K, et al. Renaming of genera Ebolavirus and Marburgvirus to Orthoebolavirus and Orthomarburgvirus, respectively, and introduction of binomial species names within family Filoviridae. Archives of Virology. **2023**; 168(8):220.

9. Kuhn JH, Amarasinghe GK, Basler CF, et al. ICTV Virus Taxonomy Profile: Filoviridae. Journal of General Virology. **2019**; 100(6):911–912.

10. Howley PM, Knipe DM. Fields Virology : Emerging viruses [Internet]. Seventh edition. Philadelphia, PA: Wolters Kluwer Health; 2021. Available from: http://ovidsp.ovid.com/ovidweb.cgi?T=JS&NEWS=n&CSC=Y&PAGE=booktext&D=books&AN=02181733$&XPATH=/PG(0)&EPUB=Y

11. Biedenkopf N, Bukreyev A, Chandran K, et al. ICTV Virus Taxonomy Profile: Filoviridae 2024 [Internet]. Journal of General Virology. Microbiology Society; 2024. Available from: https://www.microbiologyresearch.org/content/journal/jgv/10.1099/jgv.0.001955

12. Gear JS, Cassel GA, Gear AJ, et al. Outbreake of Marburg virus disease in Johannesburg. Br Med J. England; **1975**; 4(5995):489–493.

13. Smith DH, Johnson BK, Isaacson M, et al. Marburg-virus disease in Kenya. Lancet. England; **1982**; 1(8276):816–820.

14. Kuhn J, Calisher CH. Filoviruses: A Compendium of 40 Years of Epidemiological, Clinical, and Laboratory Studies [Internet]. Springer Vienna; 2008. Available from: https://books.google.ca/books?id=LaOue0F9Ns4C

15. Nikiforov V, Turovskii Y, Kalinin P, others. The laboratory case of Marburg hemorrhagic fever. Zurnal Mikrobiologii Epidemiologii Immunologii. **1994**; 3:104–6.

16. Bausch DG, Nichol ST, Muyembe-Tamfum JJ, et al. Marburg Hemorrhagic Fever Associated with Multiple Genetic Lineages of Virus. N Engl J Med. Massachusetts Medical Society; **2006**; 355(9):909–919.

17. Towner Jonathan S., Khristova Marina L., Sealy Tara K., et al. Marburgvirus Genomics and Association with a Large Hemorrhagic Fever Outbreak in Angola. Journal of Virology. American Society for Microbiology; **2006**; 80(13):6497–6516.

18. Imported case of Marburg hemorrhagic fever - Colorado, 2008. MMWR Morb Mortal Wkly Rep. United States; **2009**; 58(49):1377–1381.

19. Timen A, Koopmans MPG, Vossen ACTM, et al. Response to imported case of Marburg hemorrhagic fever, the Netherland. Emerg Infect Dis. United States; **2009**; 15(8):1171–1175.

20. Johnson ED, Johnson BK, Silverstein D, et al. Characterization of a new Marburg virus isolated from a 1987 fatal case in Kenya. Arch Virol Suppl. Austria; **1996**; 11:101–114.

21. Adjemian J, Farnon EC, Tschioko F, et al. Outbreak of Marburg Hemorrhagic Fever Among Miners in Kamwenge and Ibanda Districts, Uganda, 2007. The Journal of Infectious Diseases. **2011**; 204(suppl_3):S796–S799.

22. Conrad JL, Isaacson M, Smith EB, et al. Epidemiologic investigation of Marburg virus disease, Southern Africa, 1975. Am J Trop Med Hyg. United States; **1978**; 27(6):1210–1215.

23. Knust B, Schafer IJ, Wamala J, et al. Multidistrict Outbreak of Marburg Virus Disease—Uganda, 2012. The Journal of Infectious Diseases. **2015**; 212(suppl_2):S119–S128.

24. Nyakarahuka L, Ojwang J, Tumusiime A, et al. Isolated Case of Marburg Virus Disease, Kampala, Uganda, 2014. Emerg Infect Dis. United States; **2017**; 23(6):1001–1004.

25. Nyakarahuka L, Shoemaker TR, Balinandi S, et al. Marburg virus disease outbreak in Kween District Uganda, 2017: Epidemiological and laboratory findings. PLOS Neglected Tropical Diseases. Public Library of Science; **2019**; 13(3):e0007257.

26. Koundouno FR, Kafetzopoulou LE, Faye M, et al. Detection of Marburg Virus Disease in Guinea. N Engl J Med. Massachusetts Medical Society; **2022**; 386(26):2528–2530.

27. Sah R, Mohanty A, Reda A, Siddiq A, Mohapatra RK, Dhama K. Marburg virus re-emerged in 2022: recently detected in Ghana, another zoonotic pathogen coming up amid rising cases

of Monkeypox and ongoing COVID-19 pandemic- global health concerns and counteracting measures. Veterinary Quarterly. Taylor & Francis; **2022**; 42(1):167–171.

28. Marburg Virus Disease outbreak in Equatorial Guinea ends [Internet]. WHO | Regional Office for Africa. 2023 [cited 2024 Jan 23]. Available from: https://www.afro.who.int/countries/equatorial-guinea/news/marburg-virus-disease-outbreak-equatorial-guinea-ends

29. Manohar MPM, Lee VJ, Odunukwe EUC, et al. Advancements in Marburg (MARV) virus vaccine research with its recent Reemergence in Equatorial Guinea and Tanzania: a scoping review. Cureus. Cureus; **2023**; 15(7).

30. Johnson KM, Lange JV, Webb PA, Murphy FA. ISOLATION AND PARTIAL CHARACTERISATION OF A NEW VIRUS CAUSING ACUTE HÆMORRHAGIC FEVER IN ZAIRE. The Lancet. **1977**; 309(8011):569–571.

31. Richman DD, Cleveland PH, McCormick JB, Johnson KM. Antigenic Analysis of Strains of Ebola Virus: Identification of Two Ebola Virus Serotypes. The Journal of Infectious Diseases. **1983**; 147(2):268–271.

32. Jahrling PB, Geisbert TW, Johnson ED, Peters CJ, Dalgard DW, Hall WC. Preliminary report: isolation of Ebola virus from monkeys imported to USA. The Lancet. **1990**; 335(8688):502–505.

33. Centers for Disease Control. Update: evidence of filovirus infection in an animal caretaker in a research/service facility. MMWR Morb Mortal Wkly Rep. United States; **1990**; 39(17):296–297.

34. Miranda ME, White ME, Dayrit MM, Hayes CG, Ksiazek TG, Burans JP. Seroepidemiological study of filovirus related to Ebola in the Philippines. Lancet. England; **1991**; 337(8738):425–426.

35. World Health Organization. Ebola Reston in pigs and humans, Philippines. Weekly Epidemiological Record= Relevé épidémiologique hebdomadaire. **2009**; 84(07):49–50.

36. Le Guenno B, Formenty P, Wyers M, Gounon P, Walker F, Boesch C. Isolation and partial characterisation of a new strain of Ebola virus. The Lancet. **1995**; 345(8960):1271–1274.

37. Formenty P, Hatz C, Le Guenno B, Stoll A, Rogenmoser P, Widmer A. Human Infection Due to Ebola Virus, Subtype Côte d'Ivoire: Clinical and Biologic Presentation. The Journal of Infectious Diseases. **1999**; 179(Supplement_1):S48–S53.

38. Towner JS, Sealy TK, Khristova ML, et al. Newly Discovered Ebola Virus Associated with Hemorrhagic Fever Outbreak in Uganda. PLOS Pathogens. **2008**; 4(11):e1000212.

39. MacNeil A, Farnon EC, Morgan OW, et al. Filovirus Outbreak Detection and Surveillance: Lessons From Bundibugyo. The Journal of Infectious Diseases. **2011**; 204(suppl_3):S761–S767.

40. Heymann DL, Weisfeld JS, Webb PA, Johnson KM, Cairns T, Berquist H. Ebola Hemorrhagic Fever: Tandala, Zaire, 1977–1978. The Journal of Infectious Diseases. **1980**; 142(3):372–376.

41. Georges A-J, Leroy EM, Renaut AA, et al. Ebola Hemorrhagic Fever Outbreaks in Gabon, 1994–1997: Epidemiologic and Health Control Issues. The Journal of Infectious Diseases. **1999**; 179(Supplement_1):S65–S75.

42. Khan AS, Tshioko FK, Heymann DL, et al. The Reemergence of Ebola Hemorrhagic Fever, Democratic Republic of the Congo, 1995. The Journal of Infectious Diseases. **1999**; 179(Supplement_1):S76–S86.

43. World Health Organization. Weekly Epidemiological Record, 1996, vol. 71, 47 [full issue]. Weekly Epidemiological Record = Relevé épidémiologique hebdomadaire. **1996**; 71(47):353–360.

44. World Health Organization. Outbreak(s) of Ebola haemorrhagic fever, Congo and Gabon, October 2001-July 2002. Weekly Epidemiological Report. **2003**; 78(26):223–228.

45. World Health Organization. Ebola haemorrhagic fever in the Republic of the Congo - update 6 [Internet]. 2004 Jan. Report No.: 6. Available from: https://www.who.int/emergencies/disease-outbreak-news/item/2004_01_06-en

46. Formenty P, Libama F, Epelboin A, et al. Outbreak of Ebola hemorrhagic fever in the Republic of the Congo, 2003: a new strategy?. Med Trop (Mars). France; **2003**; 63(3):291–295.

47. Nkoghe D, Kone ML, Yada A, Leroy E. A limited outbreak of Ebola haemorrhagic fever in Etoumbi, Republic of Congo, 2005. Transactions of The Royal Society of Tropical Medicine and Hygiene. **2011**; 105(8):466–472.

48. World Health Organization. Ebola virus haemorrhagic fever, Democratic Republic of the Congo — update. Weekly Epidemiological Record = Relevé épidémiologique hebdomadaire. **2007**; 82(40):345–346.

49. World Health Organization. End of Ebola outbreak in the Democratic Republic of the Congo [Internet]. Disease Outbreak News. [cited 2024 Feb 27]. Available from: https://www.who.int/emergencies/disease-outbreak-news/item/2009_02_17-en

50. Bell B, Damon I, Jernigan D, et al. Overview, Control Strategies, and Lessons Learned in the CDC Response to the 2014–2016 Ebola Epidemic. MMWR Supplements. **2016**; 65:4–11.

51. World Health Organization. Ebola virus disease – Italy [Internet]. [cited 2024 Jun 3]. Available from: https://www.who.int/emergencies/disease-outbreak-news/item/13-may-2015-ebola-en

52. World Health Organization. Ebola virus disease – Spain [Internet]. [cited 2024 Jun 3]. Available from: https://www.who.int/emergencies/disease-outbreak-news/item/09-october-2014-ebola-en

53. Jacobs M, Rodger A, Bell DJ, et al. Late Ebola virus relapse causing meningoencephalitis: a case report. The Lancet. Elsevier; **2016**; 388(10043):498–503.

54. Maganga GD, Kapetshi J, Berthet N, et al. Ebola Virus Disease in the Democratic Republic of Congo. N Engl J Med. Massachusetts Medical Society; **2014**; 371(22):2083–2091.

55. Nsio J, Kapetshi J, Makiala S, et al. 2017 Outbreak of Ebola Virus Disease in Northern Democratic Republic of Congo. The Journal of Infectious Diseases. **2020**; 221(5):701–706.

56. World Health Organization. Ebola outbreak in the Democratic Republic of the Congo declared a Public Health Emergency of International Concern [Internet]. [cited 2024 Jun 3]. Available from: https://www.who.int/news/item/17-07-2019-ebola-outbreak-in-the-democratic-republic-of-the-congo-declared-a-public-health-emergency-of-international-concern

57. Mbala-Kingebeni P, Pratt CB, Wiley MR, et al. 2018 Ebola virus disease outbreak in Équateur Province, Democratic Republic of the Congo: a retrospective genomic characterisation. The Lancet Infectious Diseases. Elsevier; **2019**; 19(6):641–647.

58. Virological. Two Ebola virus variants circulating during the 2020 Equateur Province outbreak - Ebolavirus [Internet]. Virological. 2020 [cited 2024 Jun 3]. Available from: https://virological.org/t/two-ebola-virus-variants-circulating-during-the-2020-equateur-province-outbreak/538

59. Centers for Disease Control. Outbreak History [Internet]. Ebola. 2024 [cited 2024 Jun 3]. Available from: https://www.cdc.gov/ebola/outbreaks/index.html

60. Keita AK, Koundouno FR, Faye M, et al. Resurgence of Ebola virus in 2021 in Guinea suggests a new paradigm for outbreaks. Nature. **2021**; 597(7877):539–543.

61. Makoni M. Ebola outbreak in DR Congo. The Lancet. Elsevier; **2022**; 399(10337):1766.

62. World Health Organisation. Ebola haemorrhagic fever in Sudan, 1976. Bull World Health Organ. Switzerland; **1978**; 56(2):247–270.

63. Baron RC, McCormick JB, Zubeir OA. Ebola virus disease in southern Sudan: hospital dissemination and intrafamilial spread. Bull World Health Organ. Switzerland; **1983**; 61(6):997–1003.

64. Okware SI, Omaswa FG, Zaramba S, et al. An outbreak of Ebola in Uganda. Tropical Medicine & International Health. John Wiley & Sons, Ltd; **2002**; 7(12):1068–1075.

65. World Health Organization. Outbreak of Ebola haemorrhagic fever in Yambio, south Sudan, April - June 2004. Wkly Epidemiol Rec. Switzerland; **2005**; 80(43):370–375.

66. Shoemaker T, MacNeil A, Balinandi S, et al. Reemerging Sudan Ebola Virus Disease in Uganda, 2011. Emerging Infectious Disease journal. **2012**; 18(9):1480.

67. Albariño CG, Shoemaker T, Khristova ML, et al. Genomic analysis of filoviruses associated with four viral hemorrhagic fever outbreaks in Uganda and the Democratic Republic of the Congo in 2012. Virology. **2013**; 442(2):97–100.

68. Balinandi S, Whitmer S, Mulei S, et al. Molecular characterization of the 2022 Sudan virus disease outbreak in Uganda. J Virol. United States; **2023**; 97(10):e0059023.

69. Miranda MEG, Miranda NLJ. Reston ebolavirus in Humans and Animals in the Philippines: A Review. The Journal of Infectious Diseases. **2011**; 204(suppl_3):S757–S760.

70. Monath TP. Ecology of Marburg and Ebola Viruses: Speculations and Directions for Future Research. The Journal of Infectious Diseases. **1999**; 179(Supplement_1):S127–S138.

71. Peterson AT, Bauer JT, Mills JN. Ecologic and geographic distribution of filovirus disease. Emerg Infect Dis. United States; **2004**; 10(1):40–47.

72. Peterson AT, Lash RR, Carroll DS, Johnson KM. Geographic potential for outbreaks of Marburg hemorrhagic fever. Am J Trop Med Hyg. United States; **2006**; 75(1):9–15.

73. Breman JG, Johnson KM, Groen G van der, et al. A Search for Ebola Virus in Animals in the Democratic Republic of the Congo and Cameroon: Ecologic, Virologic, and Serologic Surveys, 1979–1980. The Journal of Infectious Diseases. **1999**; 179(Supplement_1):S139–S147.

74. Leirs H, Mills JN, Krebs JW, et al. Search for the Ebola Virus Reservoir in Kikwit, Democratic Republic of the Congo: Reflections on a Vertebrate Collection. The Journal of Infectious Diseases. **1999**; 179(Supplement_1):S155–S163.

75. Reiter P, Turell M, Coleman R, et al. Field Investigations of an Outbreak of Ebola Hemorrhagic Fever, Kikwit, Democratic Republic of the Congo, 1995: Arthropod Studies. The Journal of Infectious Diseases. **1999**; 179(Supplement_1):S148–S154.

76. Barnes M, Chughtai AA, Macintyre CR. Persistence of Ebola virus in various body fluids during convalescence: evidence and implications for disease transmission and control. Epidemiology and Infection. 2016/01/25 ed. Cambridge University Press; **2016**; 144(8):1652–1660.

77. Den Boon S, Marston BJ, Nyenswah TG, et al. Ebola Virus Infection Associated with Transmission from Survivors. Emerg Infect Dis. United States; **2019**; 25(2):249–255.

78. Leroy EM, Kumulungui B, Pourrut X, et al. Fruit bats as reservoirs of Ebola virus. Nature. **2005**; 438(7068):575–576.

79. Towner JS, Pourrut X, Albariño CG, et al. Marburg Virus Infection Detected in a Common African Bat. PLOS ONE. **2007**; 2(8):e764.

80. Swanepoel R, Smit SB, Rollin PE, et al. Studies of reservoir hosts for Marburg virus. Emerg Infect Dis. United States; **2007**; 13(12):1847–1851.

81. Towner JS, Amman BR, Sealy TK, et al. Isolation of Genetically Diverse Marburg Viruses from Egyptian Fruit Bats. PLOS Pathogens. **2009**; 5(7):e1000536.

82. Amman BR, Bird BH, Bakarr IA, et al. Isolation of Angola-like Marburg virus from Egyptian rousette bats from West Africa. Nature Communications. **2020**; 11(1):510.

83. Kuzmin IV, Niezgoda M, Franka R, et al. Marburg virus in fruit bat, Kenya. Emerg Infect Dis. United States; **2010**; 16(2):352–354.

84. Amman BR, Carroll SA, Reed ZD, et al. Seasonal Pulses of Marburg Virus Circulation in Juvenile Rousettus aegyptiacus Bats Coincide with Periods of Increased Risk of Human Infection. PLOS Pathogens. Public Library of Science; **2012**; 8(10):e1002877.

85. Negredo A, Palacios G, Vázquez-Morón S, et al. Discovery of an Ebolavirus-Like Filovirus in Europe. PLOS Pathogens. Public Library of Science; **2011**; 7(10):e1002304.

86. Maruyama Junki, Miyamoto Hiroko, Kajihara Masahiro, et al. Characterization of the Envelope Glycoprotein of a Novel Filovirus, Lloviu Virus. Journal of Virology. American Society for Microbiology; **2014**; 88(1):99–109.

87. Ramírez de Arellano E, Sanchez-Lockhart M, Perteguer MJ, et al. First Evidence of Antibodies Against Lloviu Virus in Schreiber's Bent-Winged Insectivorous Bats Demonstrate a Wide Circulation of the Virus in Spain. Viruses. Switzerland; **2019**; 11(4).

88. Kemenesi G, Kurucz K, Dallos B, et al. Re-emergence of Lloviu virus in Miniopterus schreibersii bats, Hungary, 2016. Emerging Microbes & Infections. Taylor & Francis; **2018**; 7(1):1–4.

89. Kemenesi G, Tóth GE, Mayora-Neto M, et al. Isolation of infectious Lloviu virus from Schreiber's bats in Hungary. Nature Communications. **2022**; 13(1):1706.

90. Tóth GE, Hume AJ, Suder EL, et al. Isolation and genome characterization of Lloviu virus from Italian Schreibers's bats. Scientific Reports. **2023**; 13(1):11310.

91. Goldstein T, Anthony SJ, Gbakima A, et al. The discovery of Bombali virus adds further support for bats as hosts of ebolaviruses. Nature Microbiology. **2018**; 3(10):1084–1089.

92. Forbes KM, Webala PW, Jääskeläinen AJ, et al. Bombali Virus in Mops condylurus Bat, Kenya. Emerg Infect Dis. **2019**; 25(5):955–957.

93. Karan LS, Makenov MT, Korneev MG, et al. Bombali Virus in Mops condylurus Bats, Guinea. Emerg Infect Dis. United States; **2019**; 25(9):1774–1775.

94. Yang X-L, Tan CW, Anderson DE, et al. Characterization of a filovirus (Měnglà virus) from Rousettus bats in China. Nature Microbiology. **2019**; 4(3):390–395.

95. Makenov MT, Le LAT, Stukolova OA, et al. Detection of Filoviruses in Bats in Vietnam. Viruses. **2023**; 15(9).

96. Olival KJ, Islam A, Yu M, et al. Ebola virus antibodies in fruit bats, bangladesh. Emerg Infect Dis. United States; **2013**; 19(2):270–273.

97. Hayman DTS, Yu M, Crameri G, et al. Ebola virus antibodies in fruit bats, Ghana, West Africa. Emerg Infect Dis. United States; **2012**; 18(7):1207–1209.

98. Hayman DTS, Emmerich P, Yu M, et al. Long-Term Survival of an Urban Fruit Bat Seropositive for Ebola and Lagos Bat Viruses. PLOS ONE. Public Library of Science; **2010**; 5(8):e11978.

99. Pourrut X, Souris M, Towner JS, et al. Large serological survey showing cocirculation of Ebola and Marburg viruses in Gabonese bat populations, and a high seroprevalence of both viruses in Rousettus aegyptiacus. BMC Infectious Diseases. **2009**; 9(1):159.

100. Olival KJ, Hayman DTS. Filoviruses in Bats: Current Knowledge and Future Directions. Viruses. **2014**; 6(4):1759–1788.

101. Caron A, Bourgarel M, Cappelle J, Liégeois F, De Nys HM, Roger F. Ebola Virus Maintenance: If Not (Only) Bats, What Else? Viruses. **2018**; 10(10).

102. Yuan J, Zhang Y, Li J, Zhang Y, Wang L-F, Shi Z. Serological evidence of ebolavirus infection in bats, China. Virology Journal. **2012**; 9(1):236.

103. Yang X-L, Zhang Y-Z, Jiang R-D, et al. Genetically Diverse Filoviruses in Rousettus and Eonycteris spp. Bats, China, 2009 and 2015. Emerg Infect Dis. United States; **2017**; 23(3):482–486.

104. Taniguchi S, Watanabe S, Masangkay JS, et al. Reston Ebolavirus antibodies in bats, the Philippines. Emerg Infect Dis. United States; **2011**; 17(8):1559–1560.

105. Kiley MP, Bowen ETW, Eddy GA, et al. Filoviridae: a Taxonomic Home for Marburg and Ebola Viruses ? Intervirology. **1982**; 18(1–2):24–32.

106. Geisbert TW, Jahrling PB. Differentiation of filoviruses by electron microscopy. Virus Research. **1995**; 39(2):129–150.

107. Bharat TAM, Riches JD, Kolesnikova L, et al. Cryo-Electron Tomography of Marburg Virus Particles and Their Morphogenesis within Infected Cells. PLOS Biology. Public Library of Science; **2011**; 9(11):e1001196.

108. Hume AJ, Mühlberger E. Distinct Genome Replication and Transcription Strategies within the Growing Filovirus Family. Journal of Molecular Biology. **2019**; 431(21):4290–4320.

109. Kirchdoerfer RN, Wasserman H, Amarasinghe GK, Saphire EO. Filovirus Structural Biology: The Molecules in the Machine. In: Mühlberger E, Hensley LL, Towner JS, editors.

Marburg- and Ebolaviruses: From Ecosystems to Molecules [Internet]. Cham: Springer International Publishing; 2017. p. 381–417. Available from: https://doi.org/10.1007/82_2017_16

110. Baseler L, Chertow DS, Johnson KM, Feldmann H, Morens DM. The Pathogenesis of Ebola Virus Disease. Annu Rev Pathol Mech Dis. **2017**; 12(1):387–418.

111. Mühlberger E. Filovirus replication and transcription. Future Virol. England; **2007**; 2(2):205–215.

112. Hu S, Noda T. Filovirus helical nucleocapsid structures. Microscopy. **2023**; 72(3):178–190.

113. Becker S, Rinne C, Hofsäß U, Klenk H-D, Mühlberger E. Interactions of Marburg Virus Nucleocapsid Proteins. Virology. **1998**; 249(2):406–417.

114. Groseth A, Charton JE, Sauerborn M, et al. The Ebola virus ribonucleoprotein complex: A novel VP30–L interaction identified. Virus Research. **2009**; 140(1):8–14.

115. Messaoudi I, Amarasinghe GK, Basler CF. Filovirus pathogenesis and immune evasion: insights from Ebola virus and Marburg virus. Nature reviews Microbiology. **2015**; 13(11):663–676.

116. Beniac DR, Melito PL, deVarennes SL, et al. The Organisation of Ebola Virus Reveals a Capacity for Extensive, Modular Polyploidy. PLOS ONE. Public Library of Science; **2012**; 7(1):e29608.

117. Bornholdt ZA, Noda T, Abelson DM, et al. Structural Rearrangement of Ebola Virus VP40 Begets Multiple Functions in the Virus Life Cycle. Cell. **2013**; 154(4):763–774.

118. Kolesnikova L, Ryabchikova E, Shestopalov A, Becker S. Basolateral Budding of Marburg Virus: VP40 Retargets Viral Glycoprotein GP to the Basolateral Surface. The Journal of Infectious Diseases. **2007**; 196(Supplement_2):S232–S236.

119. Hoenen T., Biedenkopf N., Zielecki F., et al. Oligomerization of Ebola Virus VP40 Is Essential for Particle Morphogenesis and Regulation of Viral Transcription. Journal of Virology. American Society for Microbiology; **2010**; 84(14):7053–7063.

120. Hoenen T, Jung S, Herwig A, Groseth A, Becker S. Both matrix proteins of Ebola virus contribute to the regulation of viral genome replication and transcription. Virology. **2010**; 403(1):56–66.

121. Valmas C, Grosch MN, Schümann M, et al. Marburg Virus Evades Interferon Responses by a Mechanism Distinct from Ebola Virus. PLOS Pathogens. Public Library of Science; **2010**; 6(1):e1000721.

122. Valmas C, Basler CF. Marburg Virus VP40 Antagonizes Interferon Signaling in a Species-Specific Manner. Journal of Virology. American Society for Microbiology; **2011**; 85(9):4309–4317.

123. Oda Shun-ichiro, Noda Takeshi, Wijesinghe Kaveesha J., et al. Crystal Structure of Marburg Virus VP40 Reveals a Broad, Basic Patch for Matrix Assembly and a Requirement of the N-Terminal Domain for Immunosuppression. Journal of Virology. American Society for Microbiology; **2016**; 90(4):1839–1848.

124. John Sinu P., Wang Tan, Steffen Scott, Longhi Sonia, Schmaljohn Connie S., Jonsson Colleen B. Ebola Virus VP30 Is an RNA Binding Protein. Journal of Virology. American Society for Microbiology; **2007**; 81(17):8967–8976.

125. Xu W, Luthra P, Wu C, et al. Ebola virus VP30 and nucleoprotein interactions modulate viral RNA synthesis. Nature Communications. **2017**; 8(1):15576.

126. Weik Michael, Modrof Jens, Klenk Hans-Dieter, Becker Stephan, Mühlberger Elke. Ebola Virus VP30-Mediated Transcription Is Regulated by RNA Secondary Structure Formation. Journal of Virology. American Society for Microbiology; **2002**; 76(17):8532–8539.

127. Martínez Miguel J., Biedenkopf Nadine, Volchkova Valentina, et al. Role of Ebola Virus VP30 in Transcription Reinitiation. Journal of Virology. American Society for Microbiology; **2008**; 82(24):12569–12573.

128. Mehedi M, Hoenen T, Robertson S, et al. Ebola Virus RNA Editing Depends on the Primary Editing Site Sequence and an Upstream Secondary Structure. PLOS Pathogens. Public Library of Science; **2013**; 9(10):e1003677.

129. Noda T, Halfmann P, Sagara H, Kawaoka Y. Regions in Ebola Virus VP24 That Are Important for Nucleocapsid Formation. The Journal of Infectious Diseases. **2007**; 196(Supplement_2):S247–S250.

130. Watanabe S, Noda T, Halfmann P, Jasenosky L, Kawaoka Y. Ebola Virus (EBOV) VP24 Inhibits Transcription and Replication of the EBOV Genome. The Journal of Infectious Diseases. **2007**; 196(Supplement_2):S284–S290.

131. Patrick RSt, Leung LW, Hartman AL, et al. Ebola Virus VP24 Binds Karyopherin α1 and Blocks STAT1 Nuclear Accumulation. Journal of Virology. American Society for Microbiology; **2006**; 80(11):5156–5167.

132. Sanchez A, Trappier SG, Mahy BW, Peters CJ, Nichol ST. The virion glycoproteins of Ebola viruses are encoded in two reading frames and are expressed through transcriptional editing. Proceedings of the National Academy of Sciences. Proceedings of the National Academy of Sciences; **1996**; 93(8):3602–3607.

133. Volchkov VE, Volchkova VA, Ströher U, et al. Proteolytic Processing of Marburg Virus Glycoprotein. Virology. **2000**; 268(1):1–6.

134. Jain S, Martynova E, Rizvanov A, Khaiboullina S, Baranwal M. Structural and Functional Aspects of Ebola Virus Proteins. Pathogens. **2021**; 10(10).

135. Volchkova VA, Dolnik O, Martinez MJ, Reynard O, Volchkov VE. RNA Editing of the GP Gene of Ebola Virus is an Important Pathogenicity Factor. The Journal of Infectious Diseases. **2015**; 212(suppl_2):S226–S233.

136. Volchkova VA, BECKER S, VOLCHKOVA VA, et al. GP mRNA of Ebola Virus Is Edited by the Ebola Virus Polymerase and by T7 and Vaccinia Virus Polymerases1. Virology. **1995**; 214(2):421–430.

137. Volchkova VA, Feldmann H, Klenk H-D, Volchkov VE. The Nonstructural Small Glycoprotein sGP of Ebola Virus Is Secreted as an Antiparallel-Orientated Homodimer. Virology. **1998**; 250(2):408–414.

138. Radoshitzky SR, Warfield KL, Chi Xiaoli, et al. Ebolavirus Δ-Peptide Immunoadhesins Inhibit Marburgvirus and Ebolavirus Cell Entry. Journal of Virology. American Society for Microbiology; **2011**; 85(17):8502–8513.

139. Mohan GS, Li W, Ye L, Compans RW, Yang C. Antigenic Subversion: A Novel Mechanism of Host Immune Evasion by Ebola Virus. PLOS Pathogens. Public Library of Science; **2012**; 8(12):e1003065.

140. Ito Hiroshi, Watanabe Shinji, Takada Ayato, Kawaoka Yoshihiro. Ebola Virus Glycoprotein: Proteolytic Processing, Acylation, Cell Tropism, and Detection of Neutralizing Antibodies. Journal of Virology. American Society for Microbiology; **2001**; 75(3):1576–1580.

141. Kuhn JH, Radoshitzky SR, Guth AC, et al. Conserved Receptor-binding Domains of Lake Victoria Marburgvirus and Zaire Ebolavirus Bind a Common Receptor*. J Biol Chem. **2006**; 281(23):15951–15958.

142. Malashkevich VN, Schneider BJ, McNally ML, Milhollen MA, Pang JX, Kim PS. Core structure of the envelope glycoprotein GP2 from Ebola virus at 1.9-Å resolution. Proceedings of the National Academy of Sciences. Proceedings of the National Academy of Sciences; **1999**; 96(6):2662–2667.

143. Mehedi Masfique, Falzarano Darryl, Seebach Jochen, et al. A New Ebola Virus Nonstructural Glycoprotein Expressed through RNA Editing. Journal of Virology. American Society for Microbiology; **2011**; 85(11):5406–5414.

144. Alvarez C P, Lasala Fátima, Carrillo Jaime, Muñiz Oscar, Corbí Angel L., Delgado Rafael. C-Type Lectins DC-SIGN and L-SIGN Mediate Cellular Entry by Ebola Virus in cis and in trans. Journal of Virology. American Society for Microbiology; **2002**; 76(13):6841–6844.

145. Andrea M, Gramberg Thomas, Simmons Graham, et al. DC-SIGN and DC-SIGNR Interact with the Glycoprotein of Marburg Virus and the S Protein of Severe Acute Respiratory Syndrome Coronavirus. Journal of Virology. American Society for Microbiology; **2004**; 78(21):12090–12095.

146. Gramberg T, Hofmann H, Möller P, et al. LSECtin interacts with filovirus glycoproteins and the spike protein of SARS coronavirus. Virology. **2005**; 340(2):224–236.

147. Becker S, Spiess M, Klenk HD. The asialoglycoprotein receptor is a potential liver-specific receptor for Marburg virus. J Gen Virol. England; **1995**; 76 ( Pt 2):393–399.

148. Ayato T, Fujioka Kouki, Tsuiji Makoto, et al. Human Macrophage C-Type Lectin Specific for Galactose and N-Acetylgalactosamine Promotes Filovirus Entry. Journal of Virology. American Society for Microbiology; **2004**; 78(6):2943–2947.

149. O'Hearn A, Wang Minxiu, Cheng Han, et al. Role of EXT1 and Glycosaminoglycans in the Early Stage of Filovirus Entry. Journal of Virology. American Society for Microbiology; **2015**; 89(10):5441–5449.

150. Kondratowicz AS, Lennemann NJ, Sinn PL, et al. T-cell immunoglobulin and mucin domain 1 (TIM-1) is a receptor for Zaire Ebolavirus and Lake Victoria Marburgvirus. Proceedings of the National Academy of Sciences. Proceedings of the National Academy of Sciences; **2011**; 108(20):8426–8431.

151. Brindley MA, Hunt CL, Kondratowicz AS, et al. Tyrosine kinase receptor Axl enhances entry of Zaire ebolavirus without direct interactions with the viral glycoprotein. Virology. **2011**; 415(2):83–94.

152. Saeed MF, Kolokoltsov AA, Albrecht T, Davey RA. Cellular Entry of Ebola Virus Involves Uptake by a Macropinocytosis-Like Mechanism and Subsequent Trafficking through Early and Late Endosomes. PLOS Pathogens. **2010**; 6(9):e1001110.

153. Nanbo A, Imai M, Watanabe S, et al. Ebolavirus Is Internalized into Host Cells via Macropinocytosis in a Viral Glycoprotein-Dependent Manner. PLOS Pathogens. Public Library of Science; **2010**; 6(9):e1001121.

154. Chandran K, Sullivan NJ, Felbor U, Whelan SP, Cunningham JM. Endosomal Proteolysis of the Ebola Virus Glycoprotein Is Necessary for Infection. Science. American Association for the Advancement of Science; **2005**; 308(5728):1643–1645.

155. Carette JE, Raaben M, Wong AC, et al. Ebola virus entry requires the cholesterol transporter Niemann–Pick C1. Nature. **2011**; 477(7364):340–343.

156. Misasi J, Chandran K, Yang J-Y, et al. Filoviruses Require Endosomal Cysteine Proteases for Entry but Exhibit Distinct Protease Preferences. J Virol. **2012**; 86(6):3284.

157. Gnirß K, Kühl A, Karsten C, et al. Cathepsins B and L activate Ebola but not Marburg virus glycoproteins for efficient entry into cell lines and macrophages independent of TMPRSS2 expression. Virology. **2012**; 424(1):3–10.

158. Marzi A, Reinheckel T, Feldmann H. Cathepsin B & L Are Not Required for Ebola Virus Replication. PLOS Neglected Tropical Diseases. **2012**; 6(12):e1923.

159. Mühlberger E, Trommer S, Funke C, Volchkov V, Klenk H-D, Becker S. Termini of All mRNA Species of Marburg Virus: Sequence and Secondary Structure. Virology. **1996**; 223(2):376–380.

160. Mühlberger E, Weik Michael, Volchkov Viktor E., Klenk Hans-Dieter, Becker Stephan. Comparison of the Transcription and Replication Strategies of Marburg Virus and Ebola Virus by Using Artificial Replication Systems. Journal of Virology. American Society for Microbiology; **1999**; 73(3):2333–2342.

161. Mühlberger, Lötfering Beate, Klenk Hans-Dieter, Becker Stephan. Three of the Four Nucleocapsid Proteins of Marburg Virus, NP, VP35, and L, Are Sufficient To Mediate Replication and Transcription of Marburg Virus-Specific Monocistronic Minigenomes. Journal of Virology. American Society for Microbiology; **1998**; 72(11):8756–8764.

162. Crary SM, Towner JS, Honig JE, Shoemaker TR, Nichol ST. Analysis of the role of predicted RNA secondary structures in Ebola virus replication. Virology. **2003**; 306(2):210–218.

163. Schudt G, Dolnik O, Kolesnikova L, Biedenkopf N, Herwig A, Becker S. Transport of Ebolavirus Nucleocapsids Is Dependent on Actin Polymerization: Live-Cell Imaging Analysis of Ebolavirus-Infected Cells. The Journal of Infectious Diseases. **2015**; 212(suppl_2):S160–S166.

164. Schudt G, Kolesnikova L, Dolnik O, Sodeik B, Becker S. Live-cell imaging of Marburg virus-infected cells uncovers actin-dependent transport of nucleocapsids over long distances. Proceedings of the National Academy of Sciences. Proceedings of the National Academy of Sciences; **2013**; 110(35):14402–14407.

165. Grikscheit K, Dolnik O, Takamatsu Y, Pereira AR, Becker S. Ebola Virus Nucleocapsid-Like Structures Utilize Arp2/3 Signaling for Intracellular Long-Distance Transport. Cells. **2020**; 9(7).

166. Dolnik O, Becker S. Assembly and transport of filovirus nucleocapsids. PLoS Pathog. **2022**; 18(7):e1010616.

167. Kuhn JH, Adachi T, Adhikari NKJ, et al. New filovirus disease classification and nomenclature. Nature Reviews Microbiology. **2019**; 17(5):261–263.

168. Jacob ST, Crozier I, Fischer WA, et al. Ebola virus disease. Nature Reviews Disease Primers. **2020**; 6(1):13.

169. Bausch DG, Towner JS, Dowell SF, et al. Assessment of the Risk of Ebola Virus Transmission from Bodily Fluids and Fomites. The Journal of Infectious Diseases. **2007**; 196(Supplement_2):S142–S147.

170. Schindell BG, Webb AL, Kindrachuk J. Persistence and Sexual Transmission of Filoviruses. Viruses. **2018**; 10(12):683.

171. Medina-Rivera M, Centeno-Tablante E, Finkelstein JL, et al. Presence of Ebola virus in breast milk and risk of mother-to-child transmission: synthesis of evidence. Annals of the New York Academy of Sciences. John Wiley & Sons, Ltd; **2021**; 1488(1):33–43.

172. Dowell SF, Mukunu R, Ksiazek TG, et al. Transmission of Ebola Hemorrhagic Fever: A Study of Risk Factors in Family Members, Kikwit, Democratic Republic of the Congo, 1995. The Journal of Infectious Diseases. **1999**; 179(Supplement_1):S87–S91.

173. Victory KR, Coronado F, Ifono SO, Soropogui T, Dahl BA. Ebola transmission linked to a single traditional funeral ceremony - Kissidougou, Guinea, December, 2014-January 2015. MMWR Morb Mortal Wkly Rep. United States; **2015**; 64(14):386–388.

174. European Food Safety Authority. An update on the risk of transmission of Ebola virus (EBOV) via the food chain. EFSA Journal. John Wiley & Sons, Ltd; **2014**; 12(11):3884.

175. Mate SE, Kugelman JR, Nyenswah TG, et al. Molecular Evidence of Sexual Transmission of Ebola Virus. N Engl J Med. **2015**; 373(25):2448–2454.

176. Martini GA, Schmidt HA. Spermatogene Übertragung des „Virus Marburg“. Klinische Wochenschrift. **1968**; 46(7):398–400.

177. Leroy EM, Epelboin A, Mondonge V, et al. Human Ebola Outbreak Resulting from Direct Exposure to Fruit Bats in Luebo, Democratic Republic of Congo, 2007. Vector-Borne and Zoonotic Diseases. Mary Ann Liebert, Inc., publishers; **2009**; 9(6):723–728.

178. Velásquez GE, Aibana O, Ling EJ, Diakite I, Mooring EQ, Murray MB. Time From Infection to Disease and Infectiousness for Ebola Virus Disease, a Systematic Review. Clinical Infectious Diseases. **2015**; 61(7):1135–1140.

179. Kortepeter MG, Bausch DG, Bray M. Basic Clinical and Laboratory Features of Filoviral Hemorrhagic Fever. The Journal of Infectious Diseases. **2011**; 204(suppl_3):S810–S816.

180. Geisbert TW, Young HA, Jahrling PB, et al. Pathogenesis of Ebola Hemorrhagic Fever in Primate Models: Evidence that Hemorrhage Is Not a Direct Effect of Virus-Induced Cytolysis of Endothelial Cells. The American Journal of Pathology. **2003**; 163(6):2371–2382.

181. Bray M, Geisbert TW. Ebola virus: The role of macrophages and dendritic cells in the pathogenesis of Ebola hemorrhagic fever. The International Journal of Biochemistry & Cell Biology. **2005**; 37(8):1560–1566.

182. Schnittler H-J, Feldmann H. Marburg and Ebola Hemorrhagic Fevers: Does the Primary Course of Infection Depend on the Accessibility of Organ-Specific Macrophages? Clinical Infectious Diseases. **1998**; 27(2):404–406.

183. Liu L, Wei Q, Nishiura K, et al. Spatiotemporal interplay of severe acute respiratory syndrome coronavirus and respiratory mucosal cells drives viral dissemination in rhesus macaques. Mucosal Immunology. Elsevier; **2016**; 9(4):1089–1101.

184. Cusi MG, Gandolfo C, Terrosi C, Gori Savellini G, Belmonte G, Miracco C. Toscana virus infects dendritic and endothelial cells opening the way for the central nervous system. Journal of NeuroVirology. **2016**; 22(3):307–315.

185. Mesman AW, Vries RD de, McQuaid S, Duprex WP, Swart RL de, Geijtenbeek TBH. A Prominent Role for DC-SIGN+ Dendritic Cells in Initiation and Dissemination of Measles Virus Infection in Non-Human Primates. PLOS ONE. Public Library of Science; **2012**; 7(12):e49573.

186. Wahl-Jensen Victoria, Kurz Sabine K., Hazelton Paul R., et al. Role of Ebola Virus Secreted Glycoproteins and Virus-Like Particles in Activation of Human Macrophages. Journal of Virology. American Society for Microbiology; **2005**; 79(4):2413–2419.

187. Ströher Ute, West Elmar, Bugany Harald, Klenk Hans-Dieter, Schnittler Hans-Joachim, Feldmann Heinz. Infection and Activation of Monocytes by Marburg and Ebola Viruses. Journal of Virology. American Society for Microbiology; **2001**; 75(22):11025–11033.

188. Rogers KJ, Maury W. The role of mononuclear phagocytes in Ebola virus infection. Journal of Leukocyte Biology. **2018**; 104(4):717–727.

189. Ebihara H, Rockx B, Marzi A, et al. Host Response Dynamics Following Lethal Infection of Rhesus Macaques With Zaire ebolavirus. The Journal of Infectious Diseases. **2011**; 204(suppl_3):S991–S999.

190. Hensley LE, Young HA, Jahrling PB, Geisbert TW. Proinflammatory response during Ebola virus infection of primate models: possible involvement of the tumor necrosis factor receptor superfamily. Immunology Letters. **2002**; 80(3):169–179.

191. Villinger F, Rollin PE, Brar SS, et al. Markedly Elevated Levels of Interferon (IFN)-γ, IFN-α, Interleukin (IL)-2, IL-10, and Tumor Necrosis Factor-α Associated with Fatal Ebola Virus Infection. The Journal of Infectious Diseases. **1999**; 179(Supplement_1):S188–S191.

192. Sanchez Anthony, Lukwiya Matthew, Bausch Daniel, et al. Analysis of Human Peripheral Blood Samples from Fatal and Nonfatal Cases of Ebola (Sudan) Hemorrhagic Fever: Cellular Responses, Virus Load, and Nitric Oxide Levels. Journal of Virology. American Society for Microbiology; **2004**; 78(19):10370–10377.

193. Wauquier N, Becquart P, Padilla C, Baize S, Leroy EM. Human Fatal Zaire Ebola Virus Infection Is Associated with an Aberrant Innate Immunity and with Massive Lymphocyte Apoptosis. PLOS Neglected Tropical Diseases. Public Library of Science; **2010**; 4(10):e837.

194. Zampieri CA, Sullivan NJ, Nabel GJ. Immunopathology of highly virulent pathogens: insights from Ebola virus. Nature Immunology. **2007**; 8(11):1159–1164.

195. Geisbert TW, Hensley LE, Gibb TR, Steele KE, Jaax NK, Jahrling PB. Apoptosis Induced In Vitro and In Vivo During Infection by Ebola and Marburg Viruses. Laboratory Investigation. Elsevier; **2000**; 80(2):171–186.

196. Hunt L, Gupta-Wright A, Simms V, et al. Clinical presentation, biochemical, and haematological parameters and their association with outcome in patients with Ebola virus disease: an observational cohort study. The Lancet Infectious Diseases. Elsevier; **2015**; 15(11):1292–1299.

197. Geisbert TW, Strong JE, Feldmann H. Considerations in the Use of Nonhuman Primate Models of Ebola Virus and Marburg Virus Infection. The Journal of Infectious Diseases. **2015**; 212(suppl_2):S91–S97.

198. Schieffelin JS, Shaffer JG, Goba A, et al. Clinical Illness and Outcomes in Patients with Ebola in Sierra Leone. N Engl J Med. Massachusetts Medical Society; **2014**; 371(22):2092–2100.

199. Martines RB, Ng DL, Greer PW, Rollin PE, Zaki SR. Tissue and cellular tropism, pathology and pathogenesis of Ebola and Marburg viruses. J Pathol. **2015**; 235(2):153–174.

200. Geisbert TW, Young HA, Jahrling PB, Davis KJ, Kagan E, Hensley LE. Mechanisms Underlying Coagulation Abnormalities in Ebola Hemorrhagic Fever: Overexpression of Tissue Factor in Primate Monocytes/Macrophages Is a Key Event. The Journal of Infectious Diseases. **2003**; 188(11):1618–1629.

201. Bixler SL, Goff AJ. The Role of Cytokines and Chemokines in Filovirus Infection. Viruses. **2015**; 7(10):5489–5507.

202. Basler CF. Innate immune evasion by filoviruses. Virology. **2015**; 479–480:122–130.

203. Escudero-Pérez B, Muñoz-Fontela C. Role of Type I Interferons on Filovirus Pathogenesis. Vaccines. **2019**; 7(1).

204. Schroder K, Hertzog PJ, Ravasi T, Hume DA. Interferon-γ: an overview of signals, mechanisms and functions. Journal of Leukocyte Biology. **2004**; 75(2):163–189.

205. Fernando L, Qiu X, Melito PL, et al. Immune Response to Marburg Virus Angola Infection in Nonhuman Primates. The Journal of Infectious Diseases. **2015**; 212(suppl_2):S234–S241.

206. Gupta M, MacNeil A, Reed ZD, Rollin PE, Spiropoulou CF. Serology and cytokine profiles in patients infected with the newly discovered Bundibugyo ebolavirus. Virology. **2012**; 423(2):119–124.

207. Connor John H., Yen Judy, Caballero Ignacio S., et al. Transcriptional Profiling of the Immune Response to Marburg Virus Infection. Journal of Virology. American Society for Microbiology; **2015**; 89(19):9865–9874.

208. Alves DA, Glynn AR, Steele KE, et al. Aerosol Exposure to the Angola Strain of Marburg Virus Causes Lethal Viral Hemorrhagic Fever in Cynomolgus Macaques. Vet Pathol. SAGE Publications Inc; **2010**; 47(5):831–851.

209. Lin Kenny L., Twenhafel Nancy A., Connor John H., et al. Temporal Characterization of Marburg Virus Angola Infection following Aerosol Challenge in Rhesus Macaques. Journal of Virology. American Society for Microbiology; **2015**; 89(19):9875–9885.

210. Hutchinson KL, Rollin PE. Cytokine and Chemokine Expression in Humans Infected with Sudan Ebola Virus. The Journal of Infectious Diseases. **2007**; 196(Supplement_2):S357–S363.

211. Leroy EM, Baize S, Debre P, Lansoud-Soukate J, Mavoungou E. Early immune responses accompanying human asymptomatic Ebola infections. Clinical and Experimental Immunology. **2001**; 124(3):453–460.

212. Fritz EA, Geisbert JB, Geisbert TW, Hensley LE, Reed DS. Cellular Immune Response to Marburg Virus Infection in Cynomolgus Macaques. Viral Immunology. Mary Ann Liebert, Inc., publishers; **2008**; 21(3):355–364.

213. Commins SP, Borish L, Steinke JW. Immunologic messenger molecules: Cytokines, interferons, and chemokines. Journal of Allergy and Clinical Immunology. Elsevier; **2010**; 125(2):S53–S72.

214. Rouse BT, Sehrawat S. Immunity and immunopathology to viruses: what decides the outcome? Nature Reviews Immunology. **2010**; 10(7):514–526.

215. Schoggins JW. Interferon-stimulated genes: roles in viral pathogenesis. Current Opinion in Virology. **2014**; 6:40–46.

216. Cárdenas Washington B., Loo Yueh-Ming, Gale Michael, et al. Ebola Virus VP35 Protein Binds Double-Stranded RNA and Inhibits Alpha/Beta Interferon Production Induced by RIG-I Signaling. Journal of Virology. American Society for Microbiology; **2006**; 80(11):5168–5178.

217. Hartman AL, Towner JS, Nichol ST. A C-terminal basic amino acid motif of Zaire ebolavirus VP35 is essential for type I interferon antagonism and displays high identity with the RNA-binding domain of another interferon antagonist, the NS1 protein of influenza A virus. Virology. **2004**; 328(2):177–184.

218. Basler CF, Wang X, Mühlberger E, et al. The Ebola virus VP35 protein functions as a type I IFN antagonist. Proceedings of the National Academy of Sciences. Proceedings of the National Academy of Sciences; **2000**; 97(22):12289–12294.

219. Feng Zongdi, Cerveny Melissa, Yan Zhipeng, He Bin. The VP35 Protein of Ebola Virus Inhibits the Antiviral Effect Mediated by Double-Stranded RNA-Dependent Protein Kinase PKR. Journal of Virology. American Society for Microbiology; **2007**; 81(1):182–192.

220. Schümann Michael, Gantke Thorsten, Mühlberger Elke. Ebola Virus VP35 Antagonizes PKR Activity through Its C-Terminal Interferon Inhibitory Domain. Journal of Virology. American Society for Microbiology; **2009**; 83(17):8993–8997.

221. Lubaki Ndongala M., Ilinykh Philipp, Pietzsch Colette, et al. The Lack of Maturation of Ebola Virus-Infected Dendritic Cells Results from the Cooperative Effect of at Least Two Viral Domains. Journal of Virology. American Society for Microbiology; **2013**; 87(13):7471–7485.

222. Raftery N, Stevenson NJ. Advances in anti-viral immune defence: revealing the importance of the IFN JAK/STAT pathway. Cell Mol Life Sci. **2017**; 74(14):2525–2535.

223. Mazewski C, Perez RE, Fish EN, Platanias LC. Type I Interferon (IFN)-Regulated Activation of Canonical and Non-Canonical Signaling Pathways. Front Immunol. **2020**; 11:606456.

224. Platanias LC. Mechanisms of type-I- and type-II-interferon-mediated signalling. Nature Reviews Immunology. **2005**; 5(5):375–386.

225. McBride KM, Reich NC. The ins and outs of STAT1 nuclear transport. Sci STKE. United States; **2003**; 2003(195):RE13.

226. Reid St. Patrick, Valmas Charalampos, Martinez Osvaldo, Sanchez Freddy Mauricio, Basler Christopher F. Ebola Virus VP24 Proteins Inhibit the Interaction of NPI-1 Subfamily Karyopherin α Proteins with Activated STAT1. Journal of Virology. American Society for Microbiology; **2007**; 81(24):13469–13477.

227. Ruibal P, Oestereich L, Lüdtke A, et al. Unique human immune signature of Ebola virus disease in Guinea. Nature. **2016**; 533(7601):100–104.

228. McElroy AK, Akondy RS, Davis CW, et al. Human Ebola virus infection results in substantial immune activation. Proceedings of the National Academy of Sciences. Proceedings of the National Academy of Sciences; **2015**; 112(15):4719–4724.

229. Ksiazek TG, Rollin PE, Williams AJ, et al. Clinical Virology of Ebola Hemorrhagic Fever (EHF): Virus, Virus Antigen, and IgG and IgM Antibody Findings among EHF Patients in Kikwit, Democratic Republic of the Congo, 1995. The Journal of Infectious Diseases. **1999**; 179(Supplement_1):S177–S187.

230. Kreuels B, Wichmann D, Emmerich P, et al. A Case of Severe Ebola Virus Infection Complicated by Gram-Negative Septicemia. N Engl J Med. Massachusetts Medical Society; **2014**; 371(25):2394–2401.

231. Baize S, Leroy EM, Georges-Courbot M-C, et al. Defective humoral responses and extensive intravascular apoptosis are associated with fatal outcome in Ebola virus-infected patients. Nature Medicine. **1999**; 5(4):423–426.

232. Paassen J van, Bauer MP, Arbous MS, et al. Acute liver failure, multiorgan failure, cerebral oedema, and activation of proangiogenic and antiangiogenic factors in a case of Marburg haemorrhagic fever. The Lancet Infectious Diseases. Elsevier; **2012**; 12(8):635–642.

233. Wolf T, Kann G, Becker S, et al. Severe Ebola virus disease with vascular leakage and multiorgan failure: treatment of a patient in intensive care. The Lancet. Elsevier; **2015**; 385(9976):1428–1435.

234. Bornholdt ZA, Turner HL, Murin CD, et al. Isolation of potent neutralizing antibodies from a survivor of the 2014 Ebola virus outbreak. Science (New York, NY). **2016**; 351(6277):1078–1083.

235. Misasi J, Gilman MSA, Kanekiyo M, et al. Structural and molecular basis for Ebola virus neutralization by protective human antibodies. Science. American Association for the Advancement of Science; **2016**; 351(6279):1343–1346.

236. Murin CD, Fusco ML, Bornholdt ZA, et al. Structures of protective antibodies reveal sites of vulnerability on Ebola virus. Proceedings of the National Academy of Sciences. Proceedings of the National Academy of Sciences; **2014**; 111(48):17182–17187.

237. Luczkowiak J, Arribas JR, Gómez S, et al. Specific neutralizing response in plasma from convalescent patients of Ebola Virus Disease against the West Africa Makona variant of Ebola virus. Virus Research. **2016**; 213:224–229.

238. Natesan Mohan, Jensen Stig M., Keasey Sarah L., et al. Human Survivors of Disease Outbreaks Caused by Ebola or Marburg Virus Exhibit Cross-Reactive and Long-Lived Antibody Responses. Clinical and Vaccine Immunology. American Society for Microbiology; **2016**; 23(8):717–724.

239. Stonier SW, Herbert AS, Kuehne AI, et al. Marburg virus survivor immune responses are Th1 skewed with limited neutralizing antibody responses. Journal of Experimental Medicine. **2017**; 214(9):2563–2572.

240. Flyak AI, Ilinykh PA, Murin CD, et al. Mechanism of Human Antibody-Mediated Neutralization of Marburg Virus. Cell. **2015**; 160(5):893–903.

241. Qiu X, Wong G, Audet J, et al. Reversion of advanced Ebola virus disease in nonhuman primates with ZMapp(TM). Nature. **2014**; 514(7520):47–53.

242. Corti D, Misasi J, Mulangu S, et al. Protective monotherapy against lethal Ebola virus infection by a potently neutralizing antibody. Science. **2016**; 351(6279):1339.

243. Pascal KE, Dudgeon D, Trefry JC, et al. Development of Clinical-Stage Human Monoclonal Antibodies That Treat Advanced Ebola Virus Disease in Nonhuman Primates. The Journal of Infectious Diseases. **2018**; :jiy285–jiy285.

244. Mire CE, Geisbert JB, Borisevich V, et al. Therapeutic treatment of Marburg and Ravn virus infection in nonhuman primates with a human monoclonal antibody. Science translational medicine. **2017**; 9(384):eaai8711.

245. Bray M. The role of the Type I interferon response in the resistance of mice to filovirus infection. J Gen Virol. England; **2001**; 82(Pt 6):1365–1373.

246. Gonchar NI, Pshenichnov VA, Pokhodiaev VA, Lopatov KL, Firsova IV. [The sensitivity of different experimental animals to the Marburg virus]. Vopr Virusol. Russia (Federation); **1991**; 36(5):435–437.

247. Warfield KL, Bradfute SB, Wells J, et al. Development and characterization of a mouse model for Marburg hemorrhagic fever. J Virol. United States; **2009**; 83(13):6404–6415.

248. Banadyga L, Dolan MA, Ebihara H. Rodent-Adapted Filoviruses and the Molecular Basis of Pathogenesis. Journal of Molecular Biology. **2016**; 428(17):3449–3466.

249. Siragam V, Wong G, Qiu X-G. Animal models for filovirus infections. Zool Res. **2018**; 39(1):15–24.

250. Bray M, Davis K, Geisbert T, Schmaljohn C, Huggins J. A Mouse Model for Evaluation of Prophylaxis and Therapy of Ebola Hemorrhagic Fever. The Journal of Infectious Diseases. **1998**; 178(3):651–661.

251. Mahanty S, Gupta M, Paragas J, Bray M, Ahmed R, Rollin PE. Protection from lethal infection is determined by innate immune responses in a mouse model of Ebola virus infection. Virology. **2003**; 312(2):415–424.

252. Gibb TR, Bray M, Geisbert TW, et al. Pathogenesis of Experimental Ebola Zaire Virus Infection in BALB/c Mice. Journal of Comparative Pathology. **2001**; 125(4):233–242.

253. Bray M, Hatfill S, Hensley L, Huggins JW. Haematological, Biochemical and Coagulation Changes in Mice, Guinea-pigs and Monkeys Infected with a Mouse-adapted Variant of Ebola Zaire Virus. Journal of Comparative Pathology. **2001**; 125(4):243–253.

254. Bradfute SB, Warfield KL, Bavari S. Functional CD8+ T Cell Responses in Lethal Ebola Virus Infection. The Journal of Immunology. **2008**; 180(6):4058–4066.

255. Bradfute SB, Warfield KL, Bray M. Mouse Models for Filovirus Infections. Viruses. **2012**; 4(9):1477–1508.

256. Chan M, Leung A, Griffin BD, et al. Generation and Characterization of a Mouse-Adapted Makona Variant of Ebola Virus. Viruses. **2019**; 11(11).

257. Ebihara H, Takada A, Kobasa D, et al. Molecular Determinants of Ebola Virus Virulence in Mice. PLOS Pathogens. Public Library of Science; **2006**; 2(7):e73.

258. Warfield KL, Alves DA, Bradfute SB, et al. Development of a model for marburgvirus based on severe-combined immunodeficiency mice. Virology Journal. **2007**; 4(1):108.

259. Lofts LL, Wells Jay B., Bavari Sina, Warfield Kelly L. Key Genomic Changes Necessary for an In Vivo Lethal Mouse Marburgvirus Variant Selection Process. Journal of Virology. American Society for Microbiology; **2011**; 85(8):3905–3917.

260. Qiu X, Wong Gary, Audet Jonathan, et al. Establishment and Characterization of a Lethal Mouse Model for the Angola Strain of Marburg Virus. Journal of Virology. American Society for Microbiology; **2014**; 88(21):12703–12714.

261. Feagins AR, Basler CF. Amino Acid Residue at Position 79 of Marburg Virus VP40 Confers Interferon Antagonism in Mouse Cells. The Journal of Infectious Diseases. **2015**; 212(suppl_2):S219–S225.

262. Lever MS, Piercy TJ, Steward JA, et al. Lethality and pathogenesis of airborne infection with filoviruses in A129 α/β −/− interferon receptor-deficient mice. Journal of Medical Microbiology. Microbiology Society; 2012. p. 8–15.

263. Raymond J, Bradfute S, Bray M. Filovirus Infection of STAT-1 Knockout Mice. The Journal of Infectious Diseases. **2011**; 204(suppl_3):S986–S990.

264. Simpson DI, Zlotnik I, Rutter DA. Vervet monkey disease. Experiment infection of guinea pigs and monkeys with the causative agent. Br J Exp Pathol. England; **1968**; 49(5):458–464.

265. Ebihara H, Zivcec M, Gardner D, et al. A Syrian Golden Hamster Model Recapitulating Ebola Hemorrhagic Fever. The Journal of Infectious Diseases. **2013**; 207(2):306–318.

266. Marzi A, Banadyga L, Haddock E, et al. A hamster model for Marburg virus infection accurately recapitulates Marburg hemorrhagic fever. Scientific Reports. **2016**; 6(1):39214.

267. Simpson DI. Vervent monkey disease. Transmission to the hamster. Br J Exp Pathol. England; **1969**; 50(4):389–392.

268. Lofts LL, Ibrahim MS, Negley DL, Hevey MC, Schmaljohn AL. Genomic Differences between Guinea Pig Lethal and Nonlethal Marburg Virus Variants. The Journal of Infectious Diseases. **2007**; 196(Supplement_2):S305–S312.

269. Koehler A, Kolesnikova Larissa, Welzel Ulla, Schudt Gordian, Herwig Astrid, Becker Stephan. A Single Amino Acid Change in the Marburg Virus Matrix Protein VP40 Provides a Replicative Advantage in a Species-Specific Manner. Journal of Virology. American Society for Microbiology; **2016**; 90(3):1444–1454.

270. Cross RW, Fenton KA, Foster SL, Geisbert JB, Geisbert TW. Modelling Marburg Virus Disease in Syrian Golden Hamsters: Contrasted Virulence Between Angola and Ci67 Strains. J Infect Dis. **2023**; 228(Supplement_7):S559–S570.

271. Cross RW, Fenton KA, Geisbert JB, Ebihara H, Mire CE, Geisbert TW. Comparison of the Pathogenesis of the Angola and Ravn Strains of Marburg Virus in the Outbred Guinea Pig Model. The Journal of Infectious Diseases. **2015**; 212(suppl_2):S258–S270.

272. Atkins C, Miao J, Kalveram B, et al. Natural History and Pathogenesis of Wild-Type Marburg Virus Infection in STAT2 Knockout Hamsters. The Journal of Infectious Diseases. **2018**; 218(suppl_5):S438–S447.

273. Connolly BM, Steele KE, Davis KJ, et al. Pathogenesis of Experimental Ebola Virus Infection in Guinea Pigs. The Journal of Infectious Diseases. **1999**; 179(Supplement_1):S203–S217.

274. Klenk HD, Feldmann H. Ebola and Marburg Viruses: Molecular and Cellular Biology [Internet]. Horizon Bioscience; 2004. Available from: https://books.google.ca/books?id=EV_mFgnyPoMC

275. Ryabchikova E, Kolesnikova L, Smolina M, et al. Ebola virus infection in guinea pigs: presumable role of granulomatous inflammation in pathogenesis. Archives of Virology. **1996**; 141(5):909–921.

276. Volchkov VE, Chepurnov AA, Volchkova VA, Ternovoj VA, Klenk H-D. Molecular Characterization of Guinea Pig-Adapted Variants of Ebola Virus. Virology. **2000**; 277(1):147–155.

277. Subbotina E, Dadaeva A, Kachko A, Chepurnov A. Genetic factors of Ebola virus virulence in guinea pigs. Virus Research. **2010**; 153(1):121–133.

278. Cross RW, Fenton KA, Geisbert JB, Mire CE, Geisbert TW. Modeling the Disease Course of Zaire ebolavirus Infection in the Outbred Guinea Pig. The Journal of Infectious Diseases. **2015**; 212(suppl_2):S305–S315.

279. Chepurnov AA, Zubavichene NM, Dadaeva AA. Elaboration of laboratory strains of Ebola virus and study of pathophysiological reactions of animals inoculated with these strains. Acta Tropica. **2003**; 87(3):321–329.

280. Bowen ETW, Platt GS, Simpson DIH, McArdell LB, Raymond RT. Ebola haemorrhagic fever: experimental infection of monkeys. Transactions of The Royal Society of Tropical Medicine and Hygiene. **1978**; 72(2):188–191.

281. Ellis DS, Bowen ET, Simpson DI, Stamford S. Ebola virus: a comparison, at ultrastructural level, of the behaviour of the Sudan and Zaire strains in monkeys. Br J Exp Pathol. England; **1978**; 59(6):584–593.

282. Ryabchikova EI, Kolesnikova LV, Luchko SV. An Analysis of Features of Pathogenesis in Two Animal Models of Ebola Virus Infection. The Journal of Infectious Diseases. **1999**; 179(Supplement_1):S199–S202.

283. Wong G, Qiu X, La Vega M-A de, et al. Pathogenicity Comparison Between the Kikwit and Makona Ebola Virus Variants in Rhesus Macaques. The Journal of Infectious Diseases. **2016**; 214(suppl_3):S281–S289.

284. Fisher-Hoch SP, Brammer TL, Trappier SG, et al. Pathogenic Potential of Filoviruses: Role of Geographic Origin of Primate Host and Virus Strain. The Journal of Infectious Diseases. **1992**; 166(4):753–763.

285. Jaax NK, Davis KJ, Geisbert TJ, et al. Lethal experimental infection of rhesus monkeys with Ebola-Zaire (Mayinga) virus by the oral and conjunctival route of exposure. Arch Pathol Lab Med. United States; **1996**; 120(2):140–155.

286. Jahrling PB, Geisbert TW, Jaax NK, Hanes MA, Ksiazek TG, Peters CJ. Experimental infection of cynomolgus macaques with Ebola-Reston filoviruses from the 1989-1990 U.S. epizootic. Arch Virol Suppl. Austria; **1996**; 11:115–134.

287. Geisbert TW, Daddario-DiCaprio KM, Geisbert JB, et al. Marburg Virus Angola Infection of Rhesus Macaques: Pathogenesis and Treatment with Recombinant Nematode Anticoagulant Protein c2. The Journal of Infectious Diseases. **2007**; 196(Supplement_2):S372–S381.

288. Hensley LE, Alves DA, Geisbert JB, et al. Pathogenesis of Marburg Hemorrhagic Fever in Cynomolgus Macaques. The Journal of Infectious Diseases. **2011**; 204(suppl_3):S1021–S1031.

289. Simpson DIH. Marburg agent disease: In monkeys. Transactions of The Royal Society of Tropical Medicine and Hygiene. **1969**; 63(3):303–309.

290. Murphy FA, Simpson DI, Whitfield SG, Zlotnik I, Carter GB. Marburg virus infection in monkeys. Ultrastructural studies. Lab Invest. United States; **1971**; 24(4):279–291.

291. Spiridonov VA, Bazhutin NB, Belanov EF, et al. [Changes in the blood serum aminotransferase activity in the experimental infection of Cercopithecus aethiops monkeys with the Marburg virus]. Vopr Virusol. Russia (Federation); **1992**; 37(3):156–157.

292. Carrion R, Ro Y, Hoosien K, et al. A small nonhuman primate model for filovirus-induced disease. Virology. **2011**; 420(2):117–124.

293. Smither SJ, Nelson M, Eastaugh L, Nunez A, Salguero FJ, Lever MS. Experimental Respiratory Infection of Marmosets (Callithrix jacchus) With Ebola Virus Kikwit. The Journal of Infectious Diseases. **2015**; 212(suppl_2):S336–S345.

294. Smither SJ, Nelson M, Eastaugh L, et al. Experimental respiratory Marburg virus haemorrhagic fever infection in the common marmoset (Callithrix jacchus). International Journal of Experimental Pathology. John Wiley & Sons, Ltd; **2013**; 94(2):156–168.

295. Mikhaĭlov VV, Borisevich IV, Chernikova NK, Potryvaeva NV, Krasnianskiĭ VP. [The evaluation in hamadryas baboons of the possibility for the specific prevention of Ebola fever]. Vopr Virusol. Russia (Federation); **1994**; 39(2):82–84.

296. Chupurnov AA, Chernukhin IV, Ternovoĭ VA, et al. [Attempts to develop a vaccine against Ebola fever]. Vopr Virusol. Russia (Federation); **1995**; 40(6):257–260.

297. Ryabchikova EI, Kolesnikova LV, Netesov SV. Animal pathology of filoviral infections. Curr Top Microbiol Immunol. Germany; **1999**; 235:145–173.

298. Kudoyarova-Zubavichene NM, Sergeyev NN, Chepurnov AA, Netesov SV. Preparation and Use of Hyperimmune Serum for Prophylaxis and Therapy of Ebola Virus Infections. The Journal of Infectious Diseases. **1999**; 179(Supplement_1):S218–S223.

299. Alfson Kendra J., Avena Laura E., Beadles Michael W., et al. Particle-to-PFU Ratio of Ebola Virus Influences Disease Course and Survival in Cynomolgus Macaques. Journal of Virology. American Society for Microbiology; **2015**; 89(13):6773–6781.

300. Sullivan NJ, Geisbert TW, Geisbert JB, et al. Accelerated vaccination for Ebola virus haemorrhagic fever in non-human primates. Nature. **2003**; 424(6949):681–684.

301. Geisbert TW, Hensley LE, Larsen T, et al. Pathogenesis of Ebola Hemorrhagic Fever in Cynomolgus Macaques: Evidence that Dendritic Cells Are Early and Sustained Targets of Infection. The American Journal of Pathology. **2003**; 163(6):2347–2370.

302. Mire CE, Geisbert JB, Agans KN, Deer DJ, Fenton KA, Geisbert TW. Oral and Conjunctival Exposure of Nonhuman Primates to Low Doses of Ebola Makona Virus. The Journal of Infectious Diseases. **2016**; 214(suppl_3):S263–S267.

303. Johnson Dylan M., Brasel Trevor, Massey Shane, et al. Characterization of Ebola Virus Mucosal Challenge Routes in Cynomolgus Macaques. Journal of Virology. American Society for Microbiology; **2023**; 97(5):e01888-22.

304. Twenhafel NA, Mattix ME, Johnson JC, et al. Pathology of Experimental Aerosol Zaire Ebolavirus Infection in Rhesus Macaques. Vet Pathol. SAGE Publications Inc; **2013**; 50(3):514–529.

305. Johnson E, Jaax N, White J, Jahrling P. Lethal experimental infections of rhesus monkeys by aerosolized Ebola virus. Int J Exp Pathol. England; **1995**; 76(4):227–236.

306. Reed DS, Lackemeyer MG, Garza NL, Sullivan LJ, Nichols DK. Aerosol exposure to Zaire ebolavirus in three nonhuman primate species: differences in disease course and clinical pathology. Microbes and Infection. **2011**; 13(11):930–936.

307. Ebihara H, Rockx B, Marzi A, et al. Host Response Dynamics Following Lethal Infection of Rhesus Macaques With Zaire ebolavirus. The Journal of Infectious Diseases. **2011**; 204(suppl_3):S991–S999.

308. Geisbert TW, Hensley LE, Jahrling PB, et al. Treatment of Ebola virus infection with a recombinant inhibitor of factor VIIa/tissue factor: a study in rhesus monkeys. The Lancet. Elsevier; **2003**; 362(9400):1953–1958.

309. Niemuth NA, Fallacara D, Triplett CA, et al. Natural history of disease in cynomolgus monkeys exposed to Ebola virus Kikwit strain demonstrates the reliability of this non-human primate model for Ebola virus disease. PLOS ONE. Public Library of Science; **2021**; 16(7):e0252874.

310. Alfson KJ, Goez-Gazi Y, Gazi M, et al. Development of a Well-Characterized Cynomolgus Macaque Model of Marburg Virus Disease for Support of Vaccine and Therapy Development. Vaccines. **2022**; 10(8).

311. Comer JE, Brasel T, Massey S, et al. Natural History of Marburg Virus Infection to Support Medical Countermeasure Development. Viruses. **2022**; 14(10).

312. Zumbrun EE, Garvey CB, Wells JB, et al. Characterization of the Cynomolgus Macaque Model of Marburg Virus Disease and Assessment of Timing for Therapeutic Treatment Testing. Viruses. **2023**; 15(12).

313. Nicholas VV, Rosenke R, Feldmann F, et al. Distinct Biological Phenotypes of Marburg and Ravn Virus Infection in Macaques. The Journal of Infectious Diseases. **2018**; 218(suppl_5):S458–S465.

314. Schiffman Z, Liu G, Cao W, et al. The Ferret as a Model for Filovirus Pathogenesis and Countermeasure Evaluation. ILAR Journal. **2020**; 61(1):62–71.

315. Fox JG. Taxonomy, History, and Use. Biology and Diseases of the Ferret [Internet]. John Wiley & Sons, Ltd; 2014. p. 1–22. Available from: https://onlinelibrary.wiley.com/doi/abs/10.1002/9781118782699.ch1

316. THOMSON APD. A History of the Ferret. Journal of the History of Medicine and Allied Sciences. **1951**; VI(Autumn):471–480.

317. Smith W, Andrewes CH, Laidlaw PP. A Virus Obtained from Influenza Patients. Lancet. **1933**; :66–8.

318. Oh DY, Hurt AC. Using the Ferret as an Animal Model for Investigating Influenza Antiviral Effectiveness. Front Microbiol. **2016**; 7:80–80.

319. Prince GA, Porter DD. The pathogenesis of respiratory syncytial virus infection in infant ferrets. Am J Pathol. **1976**; 82(2):339–352.

320. Stittelaar KJ, Waal L de, Amerongen G van, et al. Ferrets as a Novel Animal Model for Studying Human Respiratory Syncytial Virus Infections in Immunocompetent and Immunocompromised Hosts. Viruses. **2016**; 8(6).

321. Martina BEE, Haagmans BL, Kuiken T, et al. SARS virus infection of cats and ferrets. Nature. **2003**; 425(6961):915–915.

322. Brand JMA van den, Haagmans BL, Leijten L, et al. Pathology of Experimental SARS Coronavirus Infection in Cats and Ferrets. Vet Pathol. **2008**; 45(4):551–562.

323. Chu Y-K, Ali GD, Jia F, et al. The SARS-CoV ferret model in an infection–challenge study. Virology. **2008**; 374(1):151–163.

324. Kim Y-I, Kim S-G, Kim S-M, et al. Infection and Rapid Transmission of SARS-CoV-2 in Ferrets. Cell Host & Microbe. **2020**; 27(5):704-709.e2.

325. Shi J, Wen Z, Zhong G, et al. Susceptibility of ferrets, cats, dogs, and other domesticated animals to SARS–coronavirus 2. Science. **2020**; 368(6494):1016.

326. Pillet S, Svitek N, Messling V von. Ferrets as a model for morbillivirus pathogenesis, complications, and vaccines. Curr Top Microbiol Immunol. **2009**; 330:73–87.

327. Raj VS, Smits SL, Provacia LB, et al. Adenosine Deaminase Acts as a Natural Antagonist for Dipeptidyl Peptidase 4-Mediated Entry of the Middle East Respiratory Syndrome Coronavirus. J Virol. **2014**; 88(3):1834.

328. Niezgoda M, Briggs DJ, Shaddock J, Dreesen DW, Rupprecht CE. Pathogenesis of experimentally induced rabies in domestic ferrets. Am J Vet Res. **1997**; 58(11):1327–1331.

329. Niezgoda M, Briggs DJ, Shaddock J, Rupprecht CE. Viral excretion in domestic ferrets (Mustela putorius furo) inoculated with a raccoon rabies isolate. Am J Vet Res. **1998**; 59(12):1629–1632.

330. Hamir AN, Niezgoda M, Rupprecht CE. Recovery from and Clearance of Rabies Virus in a Domestic Ferret. Journal of the American Association for Laboratory Animal Science. **2011**; 50(2):248–251.

331. Marsh GA, Virtue ER, Smith I, et al. Recombinant Hendra viruses expressing a reporter gene retain pathogenicity in ferrets. Virology Journal. **2013**; 10(1):95.

332. Pallister J, Middleton D, Wang L-F, et al. A recombinant Hendra virus G glycoprotein-based subunit vaccine protects ferrets from lethal Hendra virus challenge. Vaccine. **2011**; 29(34):5623–5630.

333. Pallister J, Middleton D, Crameri G, et al. Chloroquine Administration Does Not Prevent Nipah Virus Infection and Disease in Ferrets. J Virol. **2009**; 83(22):11979.

334. Xu P, Huang Z, Gao X, et al. Infection of Mice, Ferrets, and Rhesus Macaques with a Clinical Mumps Virus Isolate. J Virol. **2013**; 87(14):8158.

335. Parker L, Gilliland SM, Minor P, Schepelmann S. Assessment of the ferret as an in vivo model for mumps virus infection. Journal of General Virology,. **2013**; 94(6):1200–1205.

336. Gordon I, Pavri K, Cohen SM. Response of Ferrets to Mumps Virus. J Immunol. **1956**; 76(4):328.

337. Capraro GA, Johnson JB, Kock ND, Parks GD. Virus growth and antibody responses following respiratory tract infection of ferrets and mice with WT and P/V mutants of the paramyxovirus Simian Virus 5. Virology. **2008**; 376(2):416–428.

338. Durchfeld B, Baumgärtner W, Krakowka S. Intranasal Infection of Ferrets (Mustela putorius furo) with Canine Parainfluenza Virus. Journal of Veterinary Medicine, Series B. **1991**; 38(1-10):505–512.

339. Enkirch T, Messling V von. Ferret models of viral pathogenesis. Virology. **2015**; 479–480:259–270.

340. Cross RW, Mire CE, Borisevich V, Geisbert JB, Fenton KA, Geisbert TW. The Domestic Ferret (Mustela putorius furo) as a Lethal Infection Model for 3 Species of Ebolavirus. The Journal of Infectious Diseases. **2016**; 214(4):565–569.

341. Kozak R, He S, Kroeker A, et al. Ferrets Infected with Bundibugyo Virus or Ebola Virus Recapitulate Important Aspects of Human Filovirus Disease. J Virol. **2016**; 90(20):9209–9223.

342. Kroeker A, He S, La Vega M-A de, Wong G, Embury-Hyatt C, Qiu X. Characterization of Sudan Ebolavirus infection in ferrets. Oncotarget. **2017**; 8(28):46262–46272.

343. Yan F, He S, Banadyga L, et al. Characterization of Reston virus infection in ferrets. Antiviral Research. **2019**; 165:1–10.

344. Wong G, Leung A, He S, et al. The Makona Variant of Ebola Virus Is Highly Lethal to Immunocompromised Mice and Immunocompetent Ferrets. The Journal of Infectious Diseases. **2018**; :jiy141–jiy141.

345. de La Vega Marc-Antoine, Soule Geoff, Tran Kaylie N., et al. Modeling Ebola Virus Transmission Using Ferrets. mSphere. American Society for Microbiology; **2018**; 3(5):10.1128/msphere.00309-18.

346. Cross RW, Speranza E, Borisevich V, et al. Comparative Transcriptomics in Ebola Makona-Infected Ferrets, Nonhuman Primates, and Humans. The Journal of Infectious Diseases. **2018**; 218(suppl_5):S486–S495.

347. Cross RW, Mire CE, Agans KN, Borisevich V, Fenton KA, Geisbert TW. Marburg and Ravn Viruses Fail to Cause Disease in the Domestic Ferret (Mustela putorius furo). The Journal of Infectious Diseases. **2018**; :jiy268–jiy268.

348. Wong G, Zhang Z, He S, et al. Marburg and Ravn Virus Infections Do Not Cause Observable Disease in Ferrets. The Journal of Infectious Diseases. **2018**; :jiy245–jiy245.

349. Cross RW, Mire CE, Feldmann H, Geisbert TW. Post-exposure treatments for Ebola and Marburg virus infections. Nature Reviews Drug Discovery. **2018**; 17(6):413–434.

350. Mulangu Sabue, Dodd Lori E., Davey Richard T., et al. A Randomized, Controlled Trial of Ebola Virus Disease Therapeutics. New England Journal of Medicine. Massachusetts Medical Society; **2019**; 381(24):2293–2303.

351. Wec AZ, Herbert AS, Murin CD, et al. Antibodies from a Human Survivor Define Sites of Vulnerability for Broad Protection against Ebolaviruses. Cell. **2017**; 169(5):878-890.e15.

352. Zhao X, Howell KA, He S, et al. Immunization-elicited Broadly Protective Antibody Reveals Ebolavirus Fusion Loop as a Site of Vulnerability. Cell. **2017**; 169(5):891-904.e15.

353. Gilchuk P, Kuzmina N, Ilinykh PA, et al. Multifunctional Pan-ebolavirus Antibody Recognizes a Site of Broad Vulnerability on the Ebolavirus Glycoprotein. Immunity. **2018**; 49(2):363-374.e10.

354. Flyak AI, Kuzmina N, Murin CD, et al. Broadly neutralizing antibodies from human survivors target a conserved site in the Ebola virus glycoprotein HR2–MPER region. Nature Microbiology. **2018**; 3(6):670–677.

355. Bornholdt ZA, Herbert AS, Mire CE, et al. A Two-Antibody Pan-Ebolavirus Cocktail Confers Broad Therapeutic Protection in Ferrets and Nonhuman Primates. Cell Host & Microbe. Elsevier; **2019**; 25(1):49-58.e5.

356. Wec AZ, Bornholdt ZA, He S, et al. Development of a Human Antibody Cocktail that Deploys Multiple Functions to Confer Pan-Ebolavirus Protection. Cell Host & Microbe. Elsevier; **2019**; 25(1):39-48.e5.

357. Kimble J. Brian, Malherbe Delphine C., Meyer Michelle, et al. Antibody-Mediated Protective Mechanisms Induced by a Trivalent Parainfluenza Virus-Vectored Ebolavirus Vaccine. Journal of Virology. American Society for Microbiology; **2019**; 93(4):10.1128/jvi.01845-18.

358. Quick J, Grubaugh ND, Pullan ST, et al. Multiplex PCR method for MinION and Illumina sequencing of Zika and other virus genomes directly from clinical samples. Nature Protocols. **2017**; 12(6):1261–1276.

359. Albariño CG, Wiggleton Guerrero L, Chakrabarti AK, Nichol ST. Transcriptional analysis of viral mRNAs reveals common transcription patterns in cells infected by five different filoviruses. PLOS ONE. Public Library of Science; **2018**; 13(8):e0201827.

360. Connolly BM, Steele KE, Davis KJ, et al. Pathogenesis of Experimental Ebola Virus Infection in Guinea Pigs. The Journal of Infectious Diseases. **1999**; 179(Supplement_1):S203–S217.

361. Wong G, Cao W-G, He S-H, et al. Development and characterization of a guinea pig model for Marburg virus. Zoöl Res. **2018**; 39(1):32–41.

362. Schiffman Z, Garnett L, Tran KN, et al. The inability of Marburg virus to cause disease in ferrets is not solely linked to the virus glycoprotein. The Journal of Infectious Diseases. **2023**; :jiad206.

363. Schiffman Z, Garnett L, Tran KN, et al. The Inability of Marburg Virus to Cause Disease in Ferrets Is Not Solely Linked to the Virus Glycoprotein. The Journal of Infectious Diseases. **2023**; 228(Supplement_7):S594–S603.

364. Schiffman Z, Liu G, Cao W, et al. The Ferret as a Model for Filovirus Pathogenesis and Countermeasure Evaluation. ILAR Journal [Internet]. **2021** [cited 2021 Dec 5]; (ilab011). Available from: https://doi.org/10.1093/ilar/ilab011

365. Schiffman Z, Yan F, He S, et al. Taï Forest Virus Does Not Cause Lethal Disease in Ferrets. Microorganisms. **2021**; 9(2).

366. Miller EH, Chandran K. Filovirus entry into cells – new insights. Current Opinion in Virology. **2012**; 2(2):206–214.

367. Hoffmann M, González Hernández M, Berger E, Marzi A, Pöhlmann S. The Glycoproteins of All Filovirus Species Use the Same Host Factors for Entry into Bat and Human Cells but Entry Efficiency Is Species Dependent. PLOS ONE. Public Library of Science; **2016**; 11(2):e0149651.

368. Miller EH, Obernosterer G, Raaben M, et al. Ebola virus entry requires the host-programmed recognition of an intracellular receptor. The EMBO Journal. John Wiley & Sons, Ltd; **2012**; 31(8):1947–1960.

369. Wang H, Shi Y, Song J, et al. Ebola Viral Glycoprotein Bound to Its Endosomal Receptor Niemann-Pick C1. Cell. Elsevier; **2016**; 164(1):258–268.

370. Sievers F, Wilm A, Dineen D, et al. Fast, scalable generation of high-quality protein multiple sequence alignments using Clustal Omega. Molecular Systems Biology. John Wiley & Sons, Ltd; **2011**; 7(1):539.

371. Goujon M, McWilliam H, Li W, et al. A new bioinformatics analysis tools framework at EMBL–EBI. Nucleic Acids Research. **2010**; 38(suppl_2):W695–W699.

372. Warfield Kelly L., Bradfute Steven B., Wells Jay, et al. Development and Characterization of a Mouse Model for Marburg Hemorrhagic Fever. Journal of Virology. American Society for Microbiology; **2009**; 83(13):6404–6415.

373. Bray M. The role of the Type I interferon response in the resistance of mice to filovirus infection. Journal of General Virology. Microbiology Society; 2001. p. 1365–1373.

374. Schiffman Z, Yan F, He S, et al. Taï Forest Virus Does Not Cause Lethal Disease in Ferrets. Microorganisms. **2021**; 9(2).

375. Forbes KM, Webala PW, Jääskeläinen AJ, et al. Bombali Virus in Mops condylurus Bat, Kenya. Emerg Infect Dis. **2019**; 25(5):955–957.

376. Martell HJ, Masterson SG, McGreig JE, Michaelis M, Wass MN. Is the Bombali virus pathogenic in humans? Bioinformatics. **2019**; 35(19):3553–3558.

377. Banadyga L, Wong G, Qiu X. Small Animal Models for Evaluating Filovirus Countermeasures. ACS Infect Dis. **2018**; 4(5):673–685.

378. Siragam V, Wong G, Qiu X-G. Animal models for filovirus infections. Zool Res. **2018**; 39(1):15–24.

379. Yamaoka S, Banadyga L, Bray M, Ebihara H. Small Animal Models for Studying Filovirus Pathogenesis. In: Mühlberger E, Hensley LL, Towner JS, editors. Marburg- and Ebolaviruses: From Ecosystems to Molecules [Internet]. Cham: Springer International Publishing; 2017. p. 195–227. Available from: https://doi.org/10.1007/82_2017_9

380. Banadyga L, Schiffman Z, He S, Qiu X. Virus inoculation and treatment regimens for evaluating anti-filovirus monoclonal antibody efficacy in vivo. Biosafety and Health. **2019**; 1(1):6–13.

381. Burk R, Bollinger L, Johnson JC, et al. Neglected filoviruses. FEMS Microbiol Rev. **2016**; 40(4):494–519.

382. Nakayama E, Saijo M. Animal models for Ebola and Marburg virus infections. Frontiers in Microbiology. **2013**; 4:267.

383. Cross RW, Fenton KA, Geisbert TW. Small animal models of filovirus disease: recent advances and future directions. null. **2018**; 13(11):1027–1040.

384. Carroll Serena A., Towner Jonathan S., Sealy Tara K., et al. Molecular Evolution of Viruses of the Family Filoviridae Based on 97 Whole-Genome Sequences. Journal of Virology. American Society for Microbiology; **2013**; 87(5):2608–2616.

385. Brannan JM, Froude JW, Prugar LI, et al. Interferon α/β Receptor–Deficient Mice as a Model for Ebola Virus Disease. The Journal of Infectious Diseases. **2015**; 212(suppl_2):S282–S294.

386. Geisbert TW, Geisbert JB, Leung A, et al. Single-Injection Vaccine Protects Nonhuman Primates against Infection with Marburg Virus and Three Species of Ebola Virus. Journal of Virology. **2009**; 83(14):7296–7304.

387. Shifflett K, Marzi A. Marburg virus pathogenesis – differences and similarities in humans and animal models. Virology Journal. **2019**; 16(1):165.

# 8. Appendix 1: Taï Forest Virus Does Not Cause Lethal Disease in Ferrets

*The material in this section has been published previously in Schiffman, Z. et al. Taï Forest Virus Does Not Cause Lethal Disease in Ferrets. Microorganisms **9**, (2021). [374] and is unmodified except for formatting to match the style of this thesis. These data are being included as an appendix as they don't fit into the narrative of this Ph.D thesis. However, this manuscript and the data within represent work done throughout graduate studies.*

## 8.1. Background

Filoviruses are zoonotic, negative-sense, single-stranded RNA viruses belonging to the family *Filoviridae* of the order *Mononegavirales.* These viruses are the causative agent of Filovirus Disease (FVD), a form of viral hemorrhagic fever affecting both humans and nonhuman primates (NHPs), often with high case-fatality rates [110,115]. While the family *Filoviridae* encompasses a total of six distinct genera, only members of the *Ebolavirus* and *Marburgvirus* genera are known to be capable of causing disease in humans [168]. Among the ebolaviruses, Ebola virus (EBOV), Sudan virus (SUDV) and Bundibugyo virus (BDBV) are considered the most pathogenic, having been responsible for a number of sporadic outbreaks since 1976, with overall case fatality rates ranging from 33-53% depending on the virus [168]. In contrast, Reston virus (RESTV) does not cause disease in humans but does cause serious, often lethal disease in NHPs, specifically cynomolgus macaques (*Macaca fascicularis*) [69]. While studies have demonstrated that the glycoprotein (GP) of the recently identified Bombali virus (BOMV) is capable of mediating entry into human cells, it is not yet known whether BOMV can cause disease in humans [91,375,376]. Lastly, there has been only a single reported case of Taï Forest virus (TAFV) in humans, which occurred in 1994 in Côte-d'Ivoire when a 34-year-old veterinarian became ill after performing an autopsy on a wild chimpanzee found in the Taï Forest [36–38]. The patient initially presented with

non-specific symptoms including fever, nausea, vomiting, diarrhea, rash and abdominal pain that were later linked to TAFV, a novel ebolavirus. The patient ultimately made a full recovery, and since then no additional human cases of TAFV infection have been reported [36].

Animal models represent a critical tool for studying filovirus pathogenesis, with a number of models, including immunocompetent and immunocompromised mice, guinea pigs, hamsters and NHPs, having been developed for most ebolaviruses [377–382]. While, TAFV infections have previously been evaluated in NHPs (*Macaca fascicularis*), immunodeficient mice (IFN-α/βR$^{-/-}$) and Egyptian fruit bats (*Rousettus Aegypticus*) [381], there still remains no well characterized animal model for studying TAFV pathogenesis. This is likely due to the fact that TAFV has yet to cause any significant outbreaks, and by extension can be regarded as a low public health risk and therefore a low research priority.

The domestic ferret (*Mustela putorius furo*) has become increasingly popular as a small animal model for evaluating filovirus transmission and pathogenesis as well as efficacy of candidate countermeasures [383]. The main advantage to the ferret as a model for filoviruses is that, unlike the majority of rodent models, ferrets are susceptible to most wild type filoviruses without the need for host-adaptation, and they exhibit disease progression that closely parallels what is observed in humans and NHPs [383]. Interestingly, infection in ferrets with EBOV [340,341], SUDV [342], BDBV [341] and RESTV [343] results in uniform lethality, whereas infection with marburgviruses, namely Marburg virus (MARV) and Ravn virus (RAVV), does not result in disease [347,348].

With the lack of available animal models for TAFV, and the success of the ferret as a lethal model for a number of ebolaviruses, we set out to evaluate the suitability of ferrets as a small animal model for evaluating TAFV pathogenesis. A well characterized animal model for TAFV

could provide additional insight into the pathogenesis of TAFV and, by extension, ebolaviruses and filoviruses in general. Moreover, having an animal model for TAFV would also prove useful for the evaluation of cross-reactive or pan-filovirus therapeutics and vaccines.

## 8.2. Results: Ferrets Did Not Develop Lethal Disease Following TAFV Infection

To investigate the susceptibility of ferrets to infection with TAFV, animals were divided into two groups with equal numbers of males and females and infected either IM or IN with TAFV at a target dose of 1000 $TCID_{50}$. All animals survived challenge with TAFV regardless of challenge route (Figure 42A). Interestingly, however, all animals within the IN, but not IM, group demonstrated mild to moderate weight loss at some point prior to 9 dpi, with weight loss most pronounced in animals 835M and 827M at 4 and 5 dpi, respectively (Figure 42B). None of the animals in either group exhibited body temperature perturbations outside of the normal range (Figure 42C), nor did any of the animals demonstrate reduced physical activity or food/water intake throughout the duration of the study.

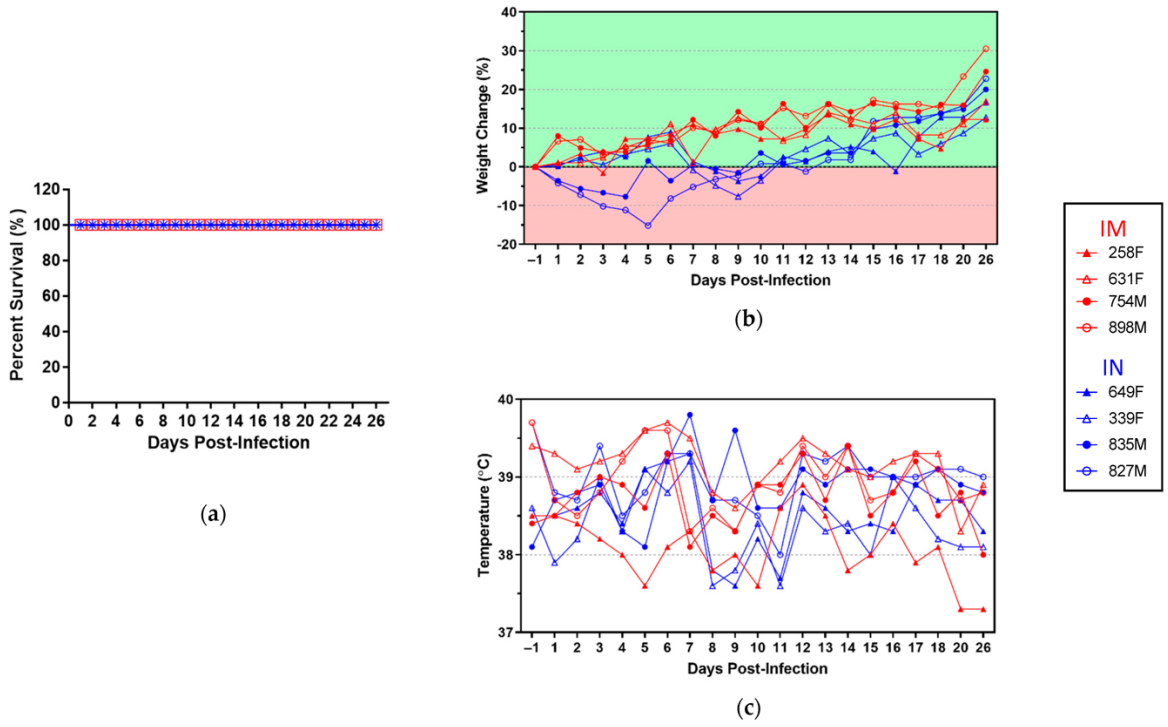


**Figure 42.Clinical parameters of TAFV-infected ferrets.**

Survival curves (**a**), percent weight loss (**b**) and temperature (**c**) for each animal over the duration of the study. Individual animal IDs and sex (F/M) are indicated in the key.

## 8.3.Results: Transient Viremia Early After Infection

To evaluate viral RNA levels from the blood, total RNA samples was subjected to RT-qPCR using two primer/probe sets targeting either TAFV nucleoprotein (NP) or polymerase (L). All animals challenged via the IN route were weakly positive (CT <36) for NP and/or L at 7 dpi (Table 7). In contrast, only two animals within the IM group were weakly positive, namely 898M at 5 dpi for NP and 631F at 7 dpi for L (Table 7). Several blood samples from both the IM and IN groups were equivocally positive at 3, 7 and 10 dpi (CT > 36 but <40), potentially indicative of extremely low levels of viral RNA. None of the animals had detectable viral RNA in blood at 3, 14, 20 and 26 dpi (Table 7). At study endpoint (26 dpi), tissues from four animals (two each from the IM and IN groups) were also assessed for viral RNA using the same RT-qPCR methodology (Table 7). The spleen was uniformly positive or equivocally positive for viral RNA in all four

animals, whereas the liver and kidney were uniformly negative. The lung samples were similarly negative, except for the sample from 649F, which was considered to be equivocally positive.

**Table 7.** Viral RNA load in blood of ferrets infected with TAFV

| Intramuscular (IM) | | | | Intranasal (IN) | | | |
|---|---|---|---|---|---|---|---|
| **Animal ID** | **Day Post-Infection** | **CT** | | **Animal ID** | **Day Post-Infection** | **CT** | |
| | | **L** | **NP** | | | **L** | **NP** |
| 258F | 3 | - | - | 339F | 3 | - | - |
| | 5 | (36.90) | - | | 5 | - | - |
| | 7 | - | (38.93) | | 7 | **35.48** | **35.80** |
| | 10 | - | - | | 10 | - | - |
| | 14 | - | - | | 14 | - | - |
| | 20 | - | - | | 20 | - | - |
| | 26 | - | - | | 26 | - | - |
| 631F | 3 | - | - | 649F | 3 | - | - |
| | 5 | (38.61) | (36.18) | | 5 | (36.06) | (36.91) |
| | 7 | **35.30** | (37.42) | | 7 | **35.57** | **35.34** |
| | 10 | - | - | | 10 | (37.24) | (39.04) |
| | 14 | - | - | | 14 | - | - |
| | 20 | - | - | | 20 | - | - |
| | 26 | - | - | | 26 | - | - |
| 898M | 3 | - | - | 827M | 3 | - | - |
| | 5 | (39.71) | **34.94** | | 5 | - | - |
| | 7 | - | (37.00) | | 7 | **35.62** | **34.78** |
| | 10 | - | - | | 10 | - | - |
| | 14 | - | - | | 14 | - | - |
| | 20 | - | - | | 20 | - | - |
| | 26 | - | - | | 26 | - | - |
| 754M | 3 | - | - | 835M | 3 | - | - |
| | 5 | (39.88) | (37.04) | | 5 | - | (39.28) |
| | 7 | - | - | | 7 | (36.40) | **34.24** |
| | 10 | - | - | | 10 | - | - |
| | 14 | - | - | | 14 | - | - |
| | 20 | - | - | | 20 | - | - |
| | 26 | - | - | | 26 | - | - |

Positive samples (CT<36) denoted in bold letters, equivocally positive samples (CT>36<40) denoted in parentheses and negative samples denoted by "-". CT, cycle threshold; L, target L gene of TAFV; NP, target nucleoprotein of TAFV.

**Table 8.**Viral RNA load in tissues of ferrets (tissues) infected with TAFV

| Route | Animal ID | Tissue | CT | |
|---|---|---|---|---|
| | | | L | NP |
| Intramuscular (IM) | 258F | Liver | - | - |
| | | Lung | - | - |
| | | Spleen | **35.98** | (38.25) |
| | | Kidney | - | - |
| | 754M | Liver | - | - |
| | | Lung | - | - |
| | | Spleen | (37.70) | - |
| | | Kidney | - | - |
| Intranasal (IN) | 649F | Liver | - | - |
| | | Lung | (37.75) | (38.71) |
| | | Spleen | **33.47** | **34.70** |
| | | Kidney | - | - |
| | 835M | Liver | - | - |
| | | Lung | - | - |
| | | Spleen | (36.17) | (36.48) |
| | | Kidney | - | - |

Positive samples (CT<36) denoted in bold letters, equivocally positive samples (CT>36<40) denoted in parentheses and negative samples denoted by "-".CT, cycle threshold; L, target L gene of TAFV; NP, target nucleoprotein of TAFV.

## 8.4.Results: No Major Perturbations in Hematology or biochemistry

Analysis of blood biochemistry and cell counts was performed at all time-points to further characterize TAFV pathogenesis and the impact on both the circulatory and immune systems. All animals displayed relatively normal blood biochemistries, with values for all parameters within normal physiological ranges (Figure 43). Overall, none of the biochemical parameters evaluated were statistically different between the two groups, with the exception of glucose (GLU), which was significantly lower at 3 dpi in the IM group compared to the IN group.

Analysis of blood cell counts also revealed no major perturbations, although a few notable trends were observed (Figure 44). Animal 835M was found to have elevated white blood cells (WBC) at 10 dpi, reflecting an increase in both lymphocytes (LYM) and neutrophils (NEU) at the same time point, and animal 649F showed a distinct peak in monocytes (MON) at 14 dpi. While no significant differences were observed between the IM and IN groups for many of the parameters measured, a significant decrease in lymphocytes (LYM) was observed in the IN group at 7 dpi, suggesting possible lymphopenia. Moreover, animals within the IM group demonstrated overall

lower MON and NEU counts as compared to those within the IN group. Red blood cell (RBC) counts were also significantly lower at 3 and 26 dpi, as was hemoglobin (HB) at 26 dpi, in the IM group compared to the IN group.

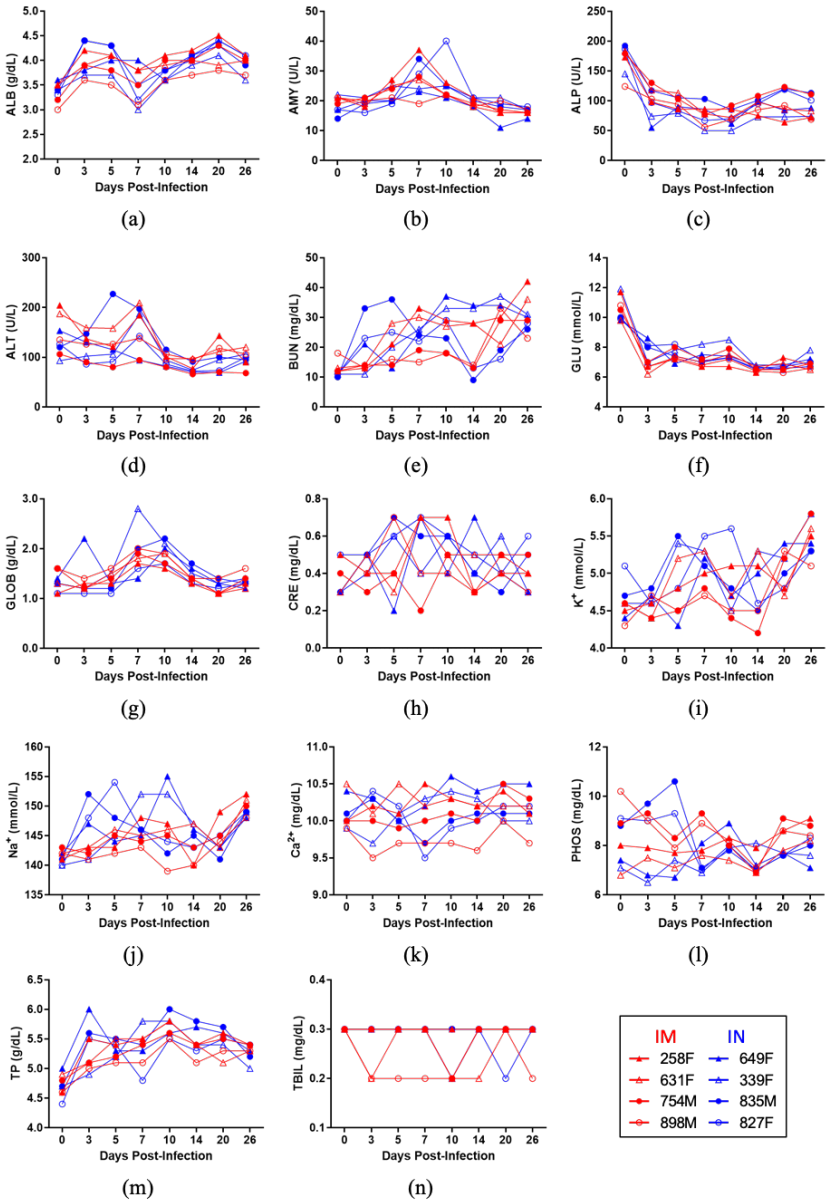


**Figure 43.Biochemical parameters of TAFV-infected ferrets.**

Whole blood was collected from each animal on days 0, 3, 5, 7, 10, 14, 20 and 26 post-infection, and the concentrations of the following analytes measured: (**a**) albumin (ALB); (**b**) amylase (AMY); (**c**) alkaline phosphatase (ALP); (**d**) alanine aminotransferase (ALT); (**e**) blood urea nitrogen (BUN); (**f**) blood glucose (GLU); (**g**) globulin (GLOB); (**h**) creatinine (CRE); (**i**) potassium ($K^+$); (**j**) sodium ($Na^+$); (**k**) calcium ($Ca^{2+}$); (**l**) phosphorus (PHOS); (**m**) total protein (TP); (**n**) total bilirubin (TBIL). Individual animal IDs and sex (F/M) are indicated in the key.

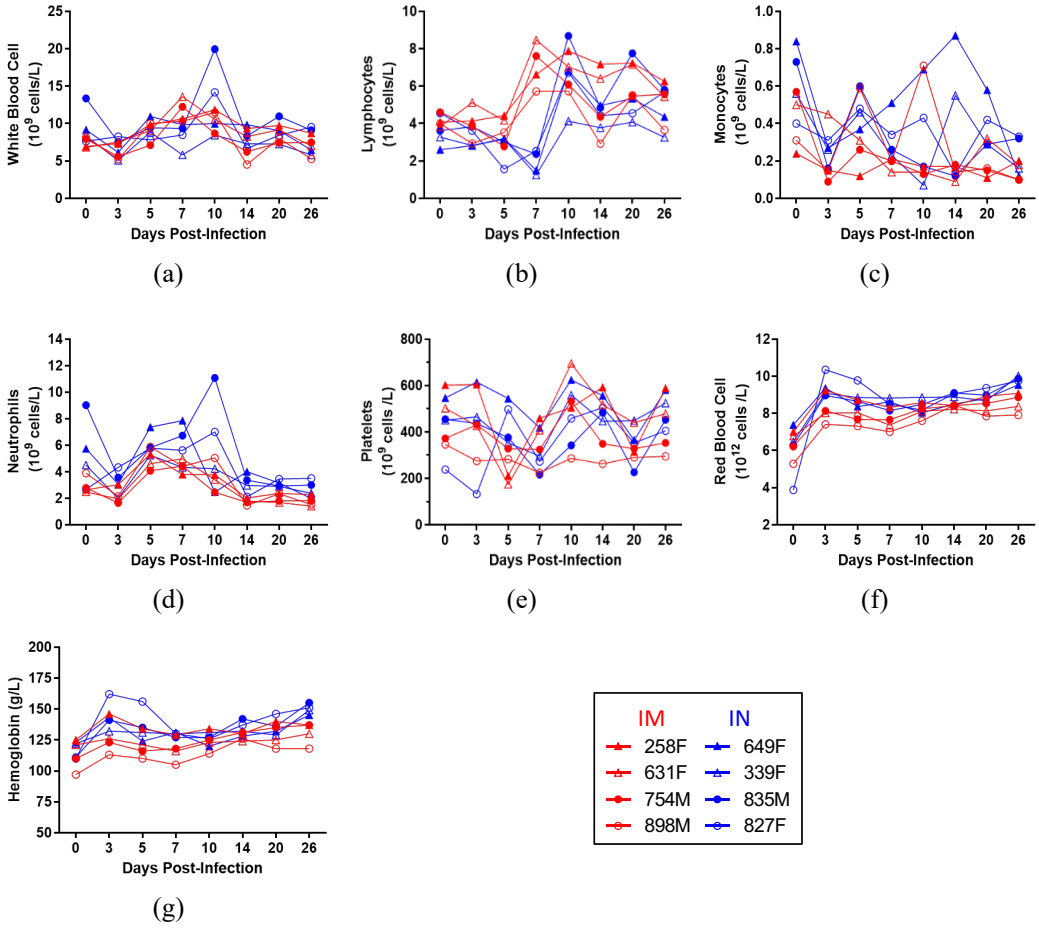


**Figure 44.Complete blood counts of TAFV-infected ferrets**

Whole blood was collected from each animal on days 0, 3, 5, 7, 10, 14, 20 and 26 post-infection and the concentrations of the following analytes measured: (**a**) white blood cells (WBC); (**b**) lymphocytes (LYM); (**c**) monocytes (MON); (**d**) neutrophils (NEU); (**e**) platelets (PLT); (**f**) red blood cells (RBC) and (**g**) hemoglobin (HB). Individual animal IDs and sex (F/M) are indicated in the key.

## 8.5. Results: High Titers of TAFV GP-Specific IgG Detectable as Early as 14 dpi

To evaluate the humoral immune response mounted after challenge with TAFV, plasma samples collected at −1, 14, 20, and 26 dpi were subjected to an indirect ELISA to quantify titers of TAFV GP-specific IgG. In contrast to the pre-challenge (−1 dpi) plasma samples, which were uniformly negative , all post-infection samples exhibited high GP-specific IgG titers, indicating that all animals seroconverted and mounted a humoral immune response against TAFV GP (Figure

45). Overall, the mean TAFV GP-specific IgG titers trended higher in IN-challenged animals than in IM-challenged animals, and the difference was significant at 20 dpi (Figure 45). These data suggest that animals infected via the IN route mounted a more pronounced humoral immune response compared to those infected via the IM route.

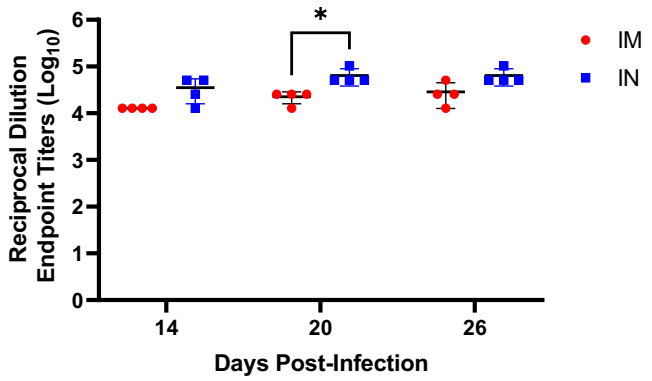


**Figure 45. Endpoint Titers of TAFV GP-specific IgG**

Endpoint titers of TAFV GP-specific IgG. Plasma samples were collected from each animal at 14, 20, and 26 dpi and subjected to ELISA to quantify total amounts of circulating TAFV GP-specific IgG. Values reported represent lowest reciprocal dilution (Log10) above the cut-off. IM, intramuscular inoculation; IN, intranasal inoculation. * indicates a p-value ≤ 0.05.

## 8.6. Discussion: Key Findings, Significance, and Limitations

Although the ferret has long been considered an exceptional model for influenza viruses [339], it has more recently been shown to be an appealing animal model for evaluating ebolavirus pathogenesis. Indeed, the ferret is highly susceptible to lethal infection with EBOV, SUDV, BDBV, and RESTV, and displays many of the clinical hallmarks associated with disease in humans and NHPs [340–343]. Nevertheless, we demonstrate here that TAFV—another ebolavirus most closely related to BDBV [384]—did not produce lethal disease in ferrets, regardless of whether the animals were challenged via the IM or IN route.

Despite the fact that no animal developed severe disease in response to TAFV inoculation, our data suggest most animals experienced a productive infection that may have led to mild signs

of disease. In particular, animals inoculated via the IN route showed more consistent signs of disease than those inoculated via the IM route. All IN-inoculated animals demonstrated mild to moderate weight loss early post-infection, with a few animals (835M, 827M, and 339F) losing as much as ~5–15% their starting weight. Although weight loss is one of the key indicators of Ebola virus disease (EVD) in ferrets, it is typically accompanied by other signs, such as elevated temperature, rash, reduced physical activity and/or changes in food/water intake [341–343], none of which were observed at any point in this study. Thus, while the weight loss observed here is thought to be virus-induced, we cannot exclude a role for other factors, such as stress. In contrast to the IN-inoculated animals, however, none of the animals within the IM group exhibited substantial weight loss at any point during the study. These data suggest that, unlike the IM-inoculated animals, the IN-inoculated animals experienced a mild form of disease, and they are consistent with the analysis of viral RNA loads.

Although the CT values were relatively high in general, all animals were weakly positive or equivocally positive for viral RNA in the blood around 5–10 dpi, suggesting limited virus replication and viremia. Moreover, low levels of viral RNA were also detected in some tissues, particularly the spleen, further indicating virus dissemination. Interestingly, only IN-inoculated animals showed uniformly positive RT-qPCR results at 7 dpi, whereas almost all IM-inoculated animals showed equivocally positive results, if any. Indeed, the CT values observed in IN-inoculated animals were more numerous and lower in magnitude than those from IM-inoculated animals, suggesting a higher viral burden in the former group.

Despite limited weight loss and low levels of viral replication, none of the animals in either group demonstrated any major perturbations in blood biochemistry outside of their normal range, indicating that little damage was sustained by organs, such as the liver and spleen. Blood cells

counts were similarly unremarkable, with the exception of the lymphocyte count. IN-inoculated animals demonstrated significantly lower lymphocyte counts at 7 dpi when compared to IM challenged animals, indicating possible lymphopenia, a common feature of EVD [110]. Although it is difficult to draw any concrete conclusions from these data, it is once again interesting to note that the apparent lymphopenia in the IN-inoculated animals is consistent with their slightly higher viral burden and increased weight loss.

As expected, all animals were found to have high titers of TAFV GP-specific IgG as early as 14 dpi, regardless of inoculation route, indicating that all animals mounted a humoral immune response. Nevertheless, the mean endpoint titers were higher among IN-inoculated animals than among IM-inoculated, suggesting that animals infected via the IN route may have elicited a more pronounced humoral immune response. In the future, it would be interesting to further characterize both the humoral and cell-mediated immune responses to TAFV infection in an effort to gain further insight into whether the absence of lethal disease is the result of a robust immune response. Unfortunately, the lack of commercially available reagents, particularly for immunology, makes such a characterization difficult. In addition, with such high titers of TAFV GP-specific IgG, it would also be interesting to evaluate whether these antibodies exhibit any neutralizing activity, because high neutralizing titers could be a hallmark feature of TAFV infections and critical for preventing lethal disease in both humans and animal models.

Taken together, our findings indicate that although ferrets inoculated with TAFV did not succumb to the virus, they appeared to develop a productive infection with mild signs of disease and a robust immune response, particularly when inoculated via the IN route. These results stand in contrast to those obtained with EBOV, SUDV, BDBV, and RESTV, which cause a serious and uniformly lethal disease in ferrets [341–343]. It is unclear why TAFV did not result in lethal

disease, although it could be related to the overall pathogenicity of the virus, which is assumed to be low, based on a single non-fatal case in humans and limited experiments in mice and NHPs. Indeed, despite being partially susceptible to EBOV and SUDV, immunodeficient mice (IFN-α/βR-/-) are resistant to disease caused by TAFV [385] Similarly, TAFV was shown to be only partially lethal in cynomolgus macaques, with 3/5 (60%) animals succumbing to disease at 12–14 dpi following inoculation with 1000 PFU [386]. It is worth nothing, however, that MARV and RAVV, which both cause lethal disease in humans and NHPs [387], do not cause disease in ferrets [347,348], similar to TAFV. Conversely, RESTV, which does not cause lethal disease in humans, does so in ferrets [343]. Thus, filovirus pathogenesis may be more complicated than can be accounted for in the ferret model, and more work is required to understand the degree to which these animals do (or do not) recapitulate filovirus disease processes. An important caveat to this interpretation—and a limitation to our study—is that back titration of our TAFV inoculum revealed a dose of 200 TCID50, rather than the target dose of 1000 TCID50. Although doses of 200 TCID50 or less proved lethal for EBOV [341,344] and BDBV [341] in ferrets, it cannot be ruled out that a higher dose of TAFV would result in more serious disease and/or lethality in this animal.

Importantly, following the completion of this study, mycoplasma DNA was detected in our stock preparation of TAFV, suggesting mycoplasma contamination. Nevertheless, we did not observe any signs of respiratory disease or pathology that could be related to mycoplasma infection in the ferrets involved in this study, and we find it unlikely that this mycoplasma contamination could influence the pathogenicity of TAFV in these animals.

The ferret remains a relatively new animal model for studying filovirus pathogenesis and its translatability to humans is unclear. Not only does this work to establish a ferret model of TAFV

add to the complexity of our understanding of this model system, but it may also help shed some light on a relatively understudied filovirus. Because it is likely that TAFV continues to circulate in an unknown reservoir host, another human spillover event—or potentially an outbreak—remains a consistent threat [381]. This threat, in addition to our relative ignorance of the virus's biology, further emphasizes the need for continual research on TAFV.

# 9. Appendix 2: Characterization of Immortalized Ferret Cell Lines By 10X Genomics

Given the lack of commercially available ferret cell lines, immortalized ferret cell lines derived from the spleen, heart and lung were established in this thesis project to be used as an *in vitro* ferret cell model. Each cell line, namely *mpf*Heart, *mpf*Lung and *mpf*Spleen, was subjected to single-cell sequencing using the 10X Genomics platform to characterize the cell populations composing these cell lines. Analysis of immortalized *mpf*Spleen revealed these cell lines are composed prominently of mesenchymal stem cells (MSC) followed by smooth muscle cells and fibroblasts, respectively (Figure 46). No immune cell types, including macrophages or dendritic cells, could be detected among *mpf*Spleen cell populations. Similarly, *mpf*Heart cells have like cell populations composed mainly of MSC, smooth muscle cells and fibroblasts, which, unlike *mpf*Spleen cells, are present nearly equal amounts (Figure 47). Finally, *mpf*Lung cells had similar compositions to *mpf*Spleen cells, with MSC being the most prominent cell type, followed by fibroblasts and smooth muscle cells (Figure 48). These data demonstrate that all three ferret cell lines, namely, *mpf*Spllen, *mpf*Lung and *mpf*Heart, had roughly similar cell compositions consisting predominantly of MSC, fibroblasts and smooth muscle cells. These data identify the cell populations within the ferret cell lines and confirm that they are, in fact, of ferret origin, eliminating any possibility of contamination with cells from another organism.

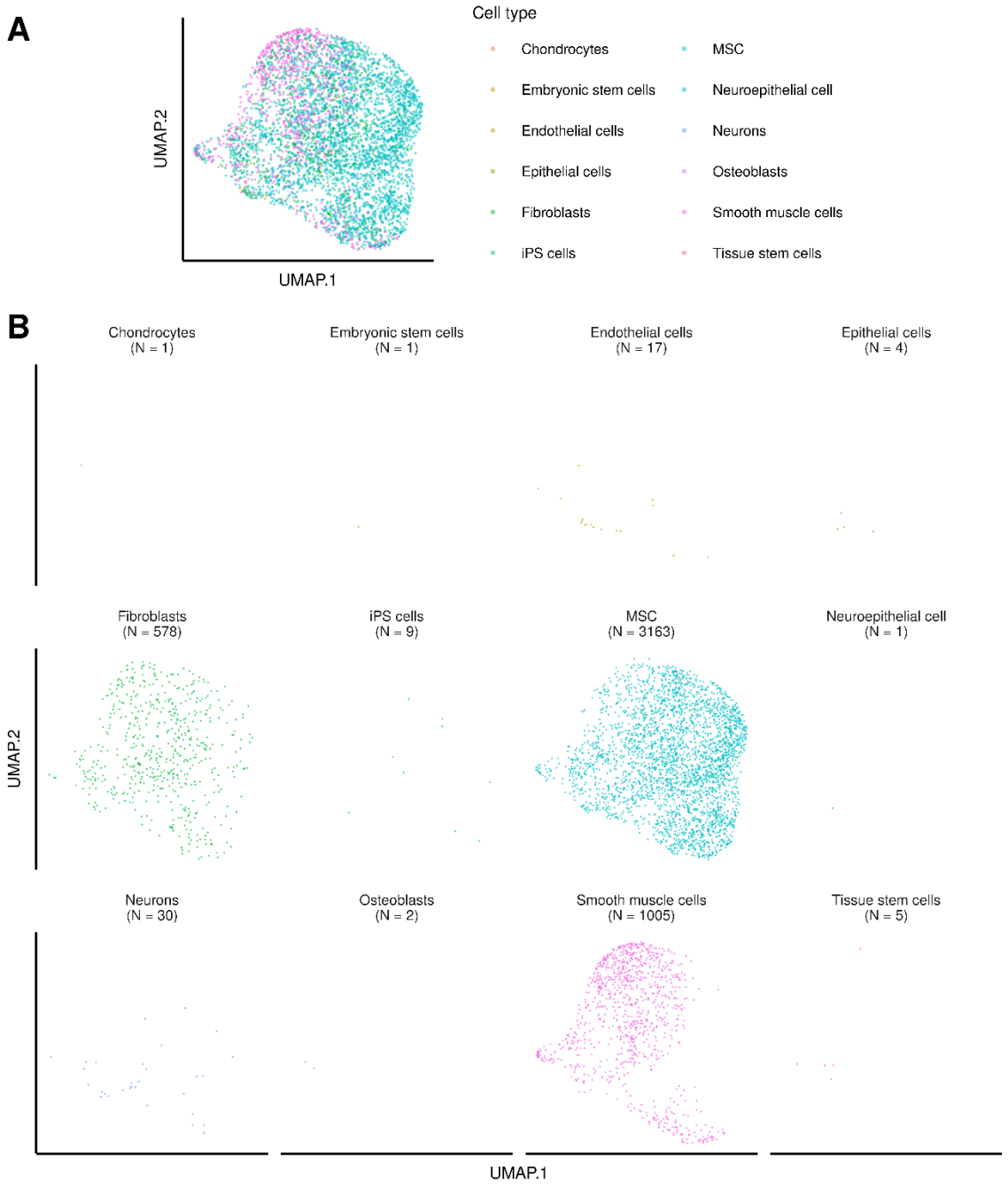


**Figure 46. UMAP of immortalized ferret spleen cells (*mpf*Spleen)**

Ferret spleen cells (*mpf*Spleen) were subjected to single cells sequencing using 10X Genomics to identify cell populations present within *mpf*Spleen cells. (**A**) UMAP depiction summarizing all cell types present in *mpf*Spleen cells and (**B**) breakdown of the global UMAP into composing cell types highlighting the number of cells present within each cluster.

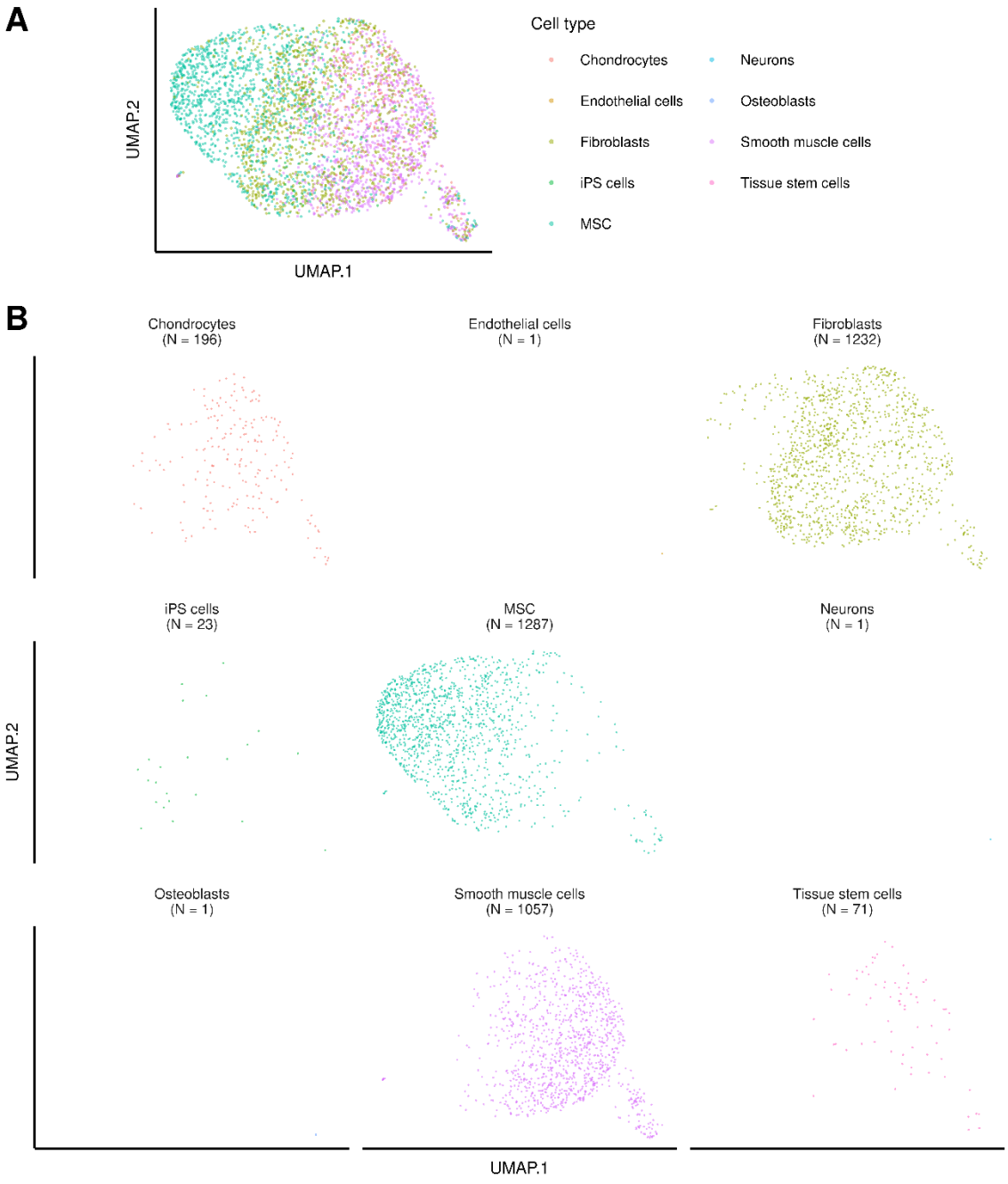


**Figure 47. UMAP of immortalized ferret heart cells (*mpf*Heart)**

Ferret heart cells (*mpf*Heart) were subjected to single cells sequencing using 10X Genomics to identify cell populations present within *mpf*Heart cells. (**A**) UMAP depiction summarizing all cell types present in *mpf*Heart cells and (**B**) breakdown of the global UMAP into composing cell types highlighting the number of cells present within each cluster.

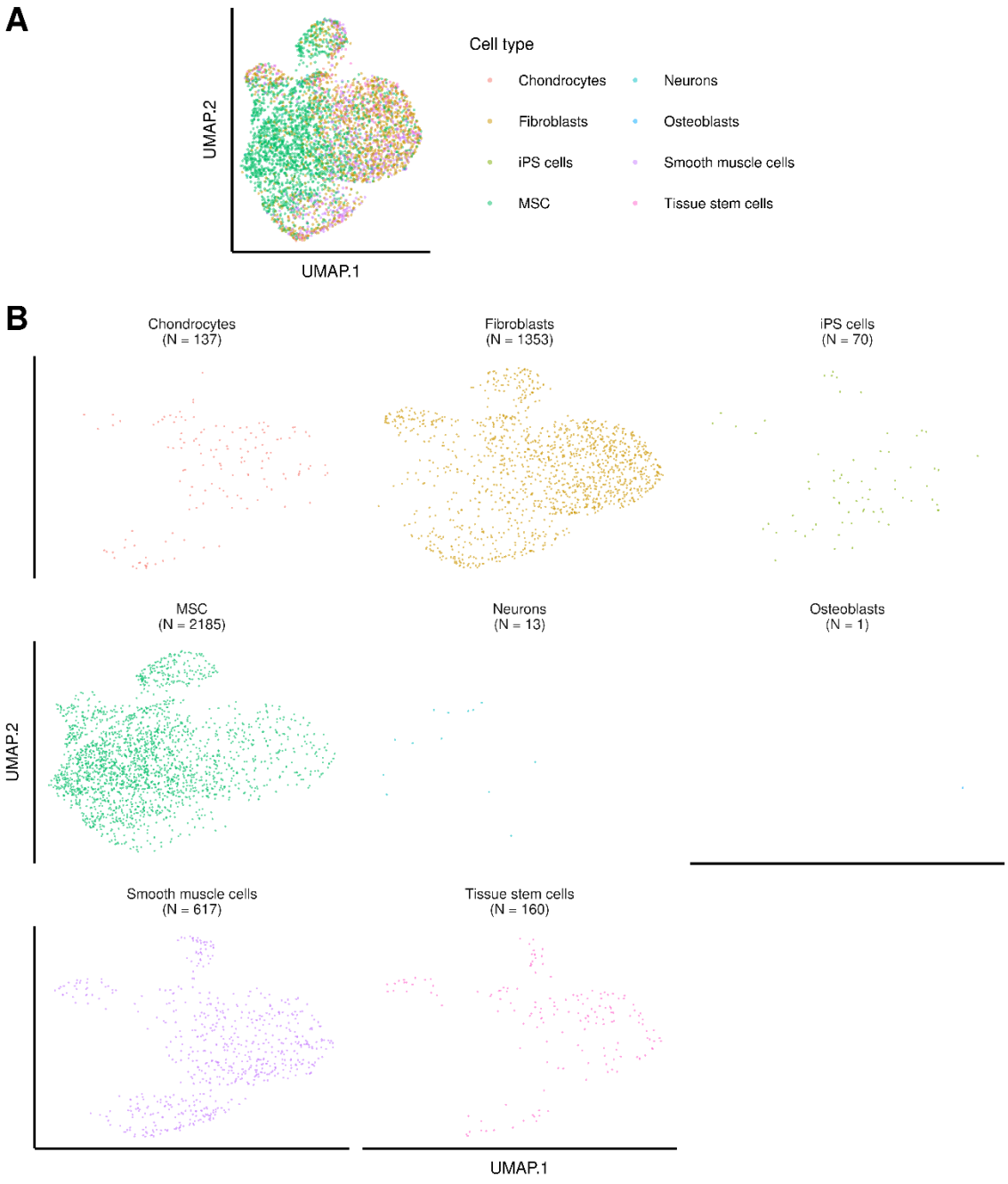


**Figure 48. UMAP of immortalized ferret lung cells (*mpf*Lung)**

Ferret lung cells (*mpf*Lung) were subjected to single cells sequencing using 10X Genomics to identify cell populations present within *mpf*Lung cells. (**A**) UMAP depiction summarizing all cell types present in *mpf*Lung cells and (**B**) breakdown of the global UMAP into composing cell types highlighting the number of cells present within each cluster.